Biogeomorphology of salt marshes

Understanding the decadal salt marsh dynamics for flood defense

PIM WILLEMSEN

Biogeomorphology of salt marshes

Understanding the decadal salt marsh dynamics for flood defense

PIM WILHELMUS JOHANNES MARIA WILLEMSEN

Biogeomorphology of salt marshes

Understanding the decadal salt marsh dynamics for flood defense

DISSERTATION

to obtain
the degree of doctor at the Universiteit Twente,
on the authority of the rector magnificus,
prof. dr. ir. A. Veldkamp,
on account of the decision of the Doctorate Board
to be publicly defended
on Friday 22 January 2021 at 12.45 hours

by

Pim Wilhelmus Johannes Maria Willemsen

born on the 7th of April, 1991
in Zevenaar, The Netherlands

This dissertation has been approved by:

Supervisors
prof. dr. ir. S.J.M.H. Hulscher
prof. dr. ir. T.J. Bouma

Co-supervisor
dr. B.W. Borsje

The presented research in this thesis is carried out at the department of Water Engineering and Management (WEM), Civil Engineering, Faculty of Engineering Technology (ET) University of Twente, The Netherlands; and the department of Estuarine & Delta Systems (EDS), Royal Netherlands Institute for Sea Research, The Netherlands.

This work is part of the research program BE SAFE (Bio-Engineering for Safety using vegetated foreshores), which is (partly) financed by the Dutch Research Council (NWO) (grant 850.13.010).

Cover design Michel Wolf; *photography* Pim Willemsen
Lay-out Proefschriftenbalie, Michel Wolf
Printed by Ipskamp Printing

ISBN 978-90-365-5112-0
DOI 10.3990/1.9789036551120

Graduation Committee

Chair / secretary	Prof.dr.ir. H.F.J.M. Koopman
Supervisors	Prof.dr.ir. S.J.M.H. Hulscher Prof.dr.ir. T.J. Bouma
Co-supervisor	Dr. B.W. Borsje
Committee Members	Prof.dr. S.J.M.H. Hulscher Prof. dr. T.J. Bouma Dr.ir. B.W. Borsje Prof.dr. K.M. Wijnberg Dr.ir. J.J. van der Werf Prof. dr. ir. S.N. Jonkman Prof. dr. S. Temmerman Dr. A. D'Alpaos

Preface

Het schrijven van een dankwoord, hier heb ik gedurende het hele onderzoekstraject mijn bedenkingen bij gehad. Je doet toch immers je inhoudelijke werk, “gewoon” zoals je zou moeten doen, net zoals de mensen om je heen. Dus waarom is het presenteren van het inhoudelijke werk niet voldoende? Nu ik kan terugkijken op zo’n 5 jaar onderzoek, ben ik me er terdege van bewust dat steun van anderen onmisbaar is in een dergelijk onderzoekstraject: zowel discussies om de diepgang van het onderzoek te garanderen, als alle fijne mensen om me heen die gezelligheid en ontspanning verzorgen, zodat ik me niet volledig verlies in het onderzoek. Dankzij jullie allemaal zijn de afgelopen 5 jaar op alle vlakken een succes geworden en is de weg vrij voor nog veel meer interessant onderzoek! Op zondagochtend, met een kop koffie (bijna onmisbaar tijdens het werk) op de bank in de najaarszon wil ik dan ook iedereen hartelijk danken.

Bas, Tjeerd en Suzanne, de misschien wel perfecte mix van begeleiders. Tijdens mijn afstuderen was ik heel stellig in hetgeen ik wilde gaan doen na de studie: een dynamisch onderzoek met zowel veld- als modelcomponenten. Een combinatie die ik tijdens het afstuderen als uitdagend, prettig en interessant ervaarde. Al tijdens mijn afstudeeronderzoek lag er zo’n PhD positie klaar en heb ik deze positie met beide handen aan kunnen pakken. Alle drie, bedankt voor deze mogelijkheid: de start van m’n promotie.

Bas, al sinds het afstudeeronderzoek in de mangroves van Singapore weet je me te enthousiasmeren. Ondanks dat we bij vrijwel ieder PhD manuscript tegenslag hebben gehad, heeft dit door jouw motivatie keer op keer geresulteerd in een manuscript met een sterkere inhoud. Het heeft me ook altijd verbaasd hoe snel je tijd wist vrij te maken voor leuke leerzame discussies en kritische feedback. Ondanks alle andere werkzaamheden die je uitvoerde. Daarnaast stond je altijd klaar voor een gesprek over allerlei zaken, waaronder het verkrijgen van een duidelijke toekomstvisie. Ten slotte, hebben we zelfs mooie buitenlandse verhalen weten over te houden aan onze reizen naar Boston, waar onze Nederlandse stijl van fietsen niet volledig geaccepteerd werd. In mijn optiek liep de samenwerking altijd erg gemakkelijk en op een hele prettige manier, daar kan ik je niet genoeg voor bedanken! Je was een fantastische begeleider, dank daarvoor.

Tjeerd, je vroeg altijd door en streefde naar de beste boodschap uit ieder stukje onderzoek. Dat heeft me enerzijds geleerd om nog kritischer te kijken naar het onderzoek en niet te ongeduldig te zijn, anderzijds om eerst zelf een goede boodschap te formuleren, alvorens feedback te vragen. Ook heb je me laten zien hoe je nuance in teksten aan kan brengen om resultaten op een juiste manier te beschrijven. Daarnaast

heb ik je mogen leren kennen als persoon die op persoonlijk vlak sterk betrokken is. Dat leidde onder andere tot gesprekken met adviezen over de toekomst en heeft ervoor gezorgd dat ik voor mezelf een duidelijk beeld heb van het vervolg na m'n promotie. Het was geweldig je als promotor te hebben. Bedankt voor de samenwerking die hopelijk nog lang voortgezet kan worden.

Suzanne, bedankt voor de altijd constructieve feedback. Het schaven aan het doel van de manuscripten heeft iedere keer weer geleid tot betere inzichten in het onderzoek. Daarnaast heb je er altijd voor gezorgd dat ik m'n focus op mijn eigen onderzoek kon houden Ondanks, dat ik in mijn enthousiasme en stroom aan ideeën vaak extra onderzoek uit wilde voeren, of nieuwe afstudeerders wilde begeleiden. Uiteindelijk heeft dit geleidt tot een, in mijn ogen, complete thesis. Hartelijk dank!

It was an honor to join the multidisciplinary BE SAFE team, that was already fully up to speed when I joined. Nevertheless, thanks to all team members I felt highly welcome. Moreover, I am happy I was able to collaborate on papers with Zhenchang and Vincent, and work with Stephanie at Deltares. By combining all different represented disciplines in the team, the study into Bio-Engineering for SAfety using vegetated foreshores became rather complete. Thank you all for working together, and hopefully we can continue working together on promising Building with Nature topics in the future!

I would like to thank all colleagues from the WEM department at the University of Twente. Doors were always open to discuss both science and nonsense. Thank you for the nice talks at the coffee machine, walks, soccer matches with SouthWEMton and all other activities. Also thanks to Anke, Joke, Dorette and Monique, who knew where to get answers on many organizational questions. A special thanks to Erik, who might have infected me with doing fieldwork during my Master thesis research in Singapore. Although you mainly encouraged doing fieldwork in the tropical climate, I am very happy we now have also conducted fieldwork in the temperate climate. Our fieldtrip to Singapore with Hunter and Marijn was intense, but much fun. I am looking forward to continue working together in Twente on mangroves and salt marshes! Mannen van W211, wat hebben we samen plezier gehad de afgelopen jaren. Ons kantoor werd veelvuldig gevonden om even slap te ouwehoeren. Ondanks dat hebben we ook inhoudelijk veel van elkaar kunnen leren. Koen, hoeveel slechte grappen je vertelt, ze toveren toch bijna altijd een glimlach op eenieders gezicht. Michiel, jouw open mind zorgt dat je volgens mij met iedereen op kan schieten. Echter, heeft het ook vaak ongemakkelijke momenten opgeleverd, waar we smakelijk om gelachen hebben. Ik ben blij dat we gezamenlijk San Francisco hebben mogen verkennen en wat geleerd hebben over wateroverlast in de stad. Ten slotte Johan, Perth en Granada zijn reizen om niet te vergeten en hier zullen we veelvuldig over uit blijven wijden. Maar ook dichterbij was hotel Damveld

een prettige plek om te verblijven. Gelukkig hebben we een gedeelde interesse voor biogeomorfologie op onze kamer. Bedankt voor de ervaringen afgelopen jaren, gelukkig kunnen we dit voortzetten!

Thanks to my NIOZ colleges. Although I haven't been much around in Yerseke, it was wonderful working for this institute. Thank you Jeroen and Lennart for the support with the SED and ASED sensors!

The interest for doing fieldwork was also fueled by the researchers from the Mangrove Lab at the National University of Singapore. Dan Friess, thank you for showing me around in the field, this made me think about pursuing a PhD in the field. Wei Kit and Dan Richards, also many thanks for your help and the nice time when visiting Singapore again. Pierre, we started to know each other already during my Master thesis research in Singapore and I am happy we had the change to meet again in Vietnam and San Francisco. Conducting fieldwork in Vietnam was probably the biggest fieldwork adventure in the past 5 years. Thank you very much!

Also many thanks to the colleagues from Deltares I have been working with. First of all, Ankie thank you for giving me the opportunity to work at Deltares during my PhD. Combining knowledge and experience both at Deltares and the University of Twente made the past 5 years much more interesting. Being able to use fieldwork knowledge in more applied projects such as the Slibmotor and Marconi gave a lot of energy. Jill, thanks for the adventures up to the hips in the mud at the Slibmotor. Also all other Slibmotor team members, thank you for working together. The Marconi project, was one of a kind. Being able to see a marsh grow from almost nothing was impressive. Marinka, Martin, Petra, Laura, Bente, Luca, Kelly thank you for collaborating on this project. This project already resulted in a lot of knowledge, hopefully to be shared in much scientific output! I was very happy to be able to really combine state-of-the-art model possibilities at Deltares with my PhD research. Jasper and Peter, thank you for giving me the opportunity to work with Delft3D – Flexible Mesh coupled with a vegetation growth module. Also thanks to the people from DSC for the technological development. Bob, a special thanks to you for endlessly discussing model errors and potential improvements. Although it seemed sometimes that it would never work, the result is here.

Obtaining knowledge is only valuable, when being able to share it. That has been done by working together in inspiring Master thesis projects. Creative ideas of many students have resulted in interesting Master theses, and sometimes even scientific publications. I am grateful to have worked with Jules, Uwe, Marc, Daan, Anja, Stijn, Jesse, Marijn and Shawnee. Thank you for your creative ideas and insights.

Beste KaterZzz, Stoere mannen (Ivo, Robert, Stefan, Martijn, Dirk, Joost, Jeroen, Sjoerd), Integralis en slagwerkers van Crescendo (o.a. Teun, John en Frans), bedankt voor het verzorgen van de soms broodnodige ontspanning. Zware discussies kunnen prima afgewisseld worden met slap geouwehoer. Er lijkt soms wel een parallel te zitten tussen transities in muzikale patronen en in het intergetijde gebied. Muziek maken en gezelligheid zorgt ervoor dat je je gedachten gemakkelijk kan verzetten en de volgende dag weer met frisse ideeën het onderzoek kan oppakken. Jullie zijn allemaal fantastische mensen, bedankt voor de afgelopen 5 jaar.

De afgelopen 5 jaar is familie onmisbaar geweest. Jullie stonden altijd klaar als het echt nodig was: een plotse verhuizing op het moment dat ik in Kuala Lumpur op het vliegveld stond, tot het hele proces na een auto ongeluk. Maar ook alle ondersteuning tijdens het herstel van m'n hartproblemen: het bed stond al in de woonkamer, voordat ik terug was uit het ziekenhuis. Er werden meer autoritjes gemaakt dan een gemiddeld taxi bedrijf en er was altijd ruimte voor een kop koffie, toen ik weer een paar kilometer kon lopen. Anique en Jean-Michel en natuurlijk ook Lynn en Zoë, bij jullie in Twente kunnen we altijd terecht, voor gezelligheid, maar ook voor allerlei adviezen. Dank daarvoor! Noud, één van de belangrijkste bijzaken waar we de afgelopen jaren achter zijn gekomen: je kan je misschien wel het beste ontspannen met een goede BBQ en een biertje. Bedankt, en dat er nog veel mogen volgen! Martin en Antoinette, jullie zijn fantastische schoonouders die altijd tijd en ruimte hebben voor alles wat we nodig hebben, bedankt! Oma, wat ben jij een prachtig persoon, met een wereldse blik. Ik ben dankbaar dat je dit allemaal mee kan maken. Nanda, je bent de beste zus die ik me kan wensen. De afgelopen 5 jaar hebben we heel veel serieuze, maar ook gezellige gesprekken over onder andere werk gehad, wat altijd weer tot interessante inzichten leidt. Je hebt me altijd ondersteund. Hartelijk dank! Ten slotte pap en mam, jullie staan altijd klaar. Van praktische zaken als veldwerk materialen tot een luisterend oor en zorgtaken in de tijd dat het niet zo goed ging. Besef goed dat jullie me de mogelijkheden hebben gegeven om te komen waar ik nu ben. Ik ben daar ontzettend dankbaar voor.

Lieve Dagmar, jij bent een uniek persoon in mijn leven. Je geeft me de ruimte om alles wat ik graag wil te kunnen doen. En dat is behoorlijk wat. Samen maken we fantastische dingen mee, van simpele momenten om te genieten door alleen bij elkaar te zijn, lekker te koken, te sporten en te klussen, tot prachtige reizen. Je bent ongelooflijk intelligent en uniek in het bij elkaar brengen van mensen, zowel op sociaal vlak als tijdens je promotie en werk. Je promotie heb je ruim binnen 4 jaar afgerond, waardoor ik altijd om advies kon vragen. Je bent ook een ontzettend zorgzaam persoon: naast het afronden van je PhD, heb je me maandenlang ondersteund gedurende het herstel van pericarditis. Ongelooflijk hoe je alles voor elkaar hebt gekregen in die tijd. Een dag heeft maar 24 uur en je moet toch uitgerust zijn om ook zelf fatsoenlijke stukken tekst op papier te zetten.

Gelukkig zijn we nu beiden helemaal gezond. We hebben een mooi, compleet plekje. Ik ben blij dat we ons leven binnenkort met 3 personen mee kunnen maken. Ik kijk dan ook erg uit naar 23 mei. Dagmar, bedankt voor alles, ik hou van jou. En, doordat je jouw promotie zo razendsnel doorlopen hebt, kan ik nu zeggen: Jij bent de allerbeste!

Summary

The coastal zone is the most densely populated area globally and economic activity is high. 70% of the world's megacities (with more than 1.6 million inhabitants) is located in this area, and the population is still growing. However, coastal protection is a prerequisite to work and live in this area, especially with predicted sea level rise and extreme storms becoming more frequent and severe. Salt marshes can contribute to coastal protection by having the ability to adapt to a changing environment. They are able to (1) trap sediment and vertically grow with sea level rise, (2) stabilize the bed with the roots of the vegetation, thereby decreasing the erodibility of the coastal area, and (3) attenuate waves due to the bed and vegetation roughness, and decrease the wave energy for the landward area. Salt marshes are able to adapt to their environment, whereas conventional infrastructure like dikes and seawalls remain fixed over time. So by combining conventional coastal infrastructure and ecosystems in nature based flood defenses (NBFD), coastal protection becomes more sustainable.

The protective capacity of NBFD including salt marshes, depends on the extent (i.e. the size) of the ecosystem. However, the effectiveness of NBFD, over the design period equal to conventional coastal protection infrastructure (e.g. 50 years), and the predictability of their coastal defense function remains rather unknown, since a long-term understanding of ecosystem dynamics (e.g. the variable extent) both in space and time lacks. As a consequence, local implementation of NBFD is hampered. To apply salt marshes, the natural dynamics and thereby the extent of the marsh system should be mapped, understood and quantified. Although previous studies identified the processes driving the lateral dynamics (i.e. cross-shore) of the salt marsh, the variability of the cross-shore marsh width did not receive much attention so far in scientific literature and is not yet quantified. It is key to know for a particular location how far a marsh can grow seaward before it will start retreating landward. However, little is known about the amplitude over which the salt marsh can expand and retreat. Hence, this study aims: (1) to provide a generic understanding of the fundamental biophysical parameters determining the lateral location of the salt marsh edge, and (2) to apply this knowledge to determine the contribution of foreshores to coastal protection over a decadal timescale. Based on the research objective, the key question of this thesis is: What is the long-term (50 year) variability of the location of the salt marsh edge and what is the corresponding variability of the wave attenuating capacity of salt marshes?

In Chapter 2, the variability of the foreshore width, consisting of a bare tidal flat and vegetated salt marsh was assessed. A dataset over a period of 65 years, including bathymetrical data available approximately once every one or two years, was used to

obtain 36 profiles covering six salt marshes in the Westerschelde estuary. The variability of the width of the tidal flat and salt marsh was quantified. Thereafter, the wave attenuation was simulated using the Simulating WAves Nearshore (SWAN) model under daily conditions with and without vegetation and under extreme conditions (i.e. events statistically occurring once every 10,000 years). The spatial variability of the width of the full foreshore and the width of the vegetated salt marsh was much larger than the temporal variability. The temporal change of the salt marsh width did not follow the change of the width of the entire foreshore, suggesting a changing shape of the foreshore. A contribution to the wave attenuating capacity was observed for all foreshores, both under daily and extreme conditions, thereby decreasing the wave load at the landward dike. Wave attenuation at the bare tidal flat was small and rather independent of the width, whereas a relation was found between the wave attenuation and width of the vegetated salt marsh: the longer the salt marsh, the larger the wave attenuation.

Insights in the parameters confining the location of the marsh edge (i.e. boundary between tidal flat and salt marsh) were obtained in Chapter 3. A unique data set was collected, containing measurements of daily bed level changes (i.e., integrative result of physical forcing and sediment properties) at six intertidal transects in the North Sea area. Moreover, various biophysical parameters were measured, such as sediment characteristics, waves, inundation time, and chlorophyll-*a* levels. Seasonal patterns in bed level change were observed at the tidal flat, but were absent in the marsh. Those differences might be driven by the seasonal presence of diatoms at the tidal flat (approximated by chlorophyll-*a* levels) and year-round presence of vegetation in the salt marsh. Measurements of the wave height showed a decreasing wave height from the seaward side of the tidal flat to the landward side of the salt marsh. A direct relation between bed level change and wave height was not found, possibly due to the more gradual decrease of wave height over the profile, whereas the bed level change abruptly decreases at the salt marsh edge. A combination of the different parameters implies that bed level change and inundation period near the marsh edge give an indication of the development of the marsh edge by controlling plant growth. The location of the lower marsh edge is restricted by two interacting factors: inundation time and bed level change. For vegetation establishment to withstand longer inundation stress, which slows down plant growth, more stable bed levels are required so that plants are not heavily disturbed. Conversely, to withstand more dynamic bed levels that disturbs plant growth, lower inundation stress is needed, so that plants grow fast enough to recover from the stress. The results suggest that bed level change is important in determining the position of the marsh edge.

In Chapter 4, the dynamic extent of the salt marsh was assessed by a state-of-the-art biogeomorphological model. The influence of the magnitude of homogeneous forcing and

sediment availability on salt marsh development was simulated over a decadal timescale. Salt marsh development was simulated by modelling online-coupled hydrodynamics (tides and waves), morphodynamics and vegetation growth using the numerical Delft3D – Flexible Mesh model, coupled with a vegetation growth module in Python. Salt marsh development under mild nearshore wave conditions (significant wave height of 0.00m, 0.05m, 0.10m and 0.15m), typical for rather low-energy environments in estuaries, was computed over a 50-year period. The sediment availability was varied (10mg/L, 25mg/L and 50mg/L) for average waves that were observed in the field (0.10m). The simulated temporal variability of the salt marsh edge, affected by the magnitude of wave conditions only, corresponded well to the variability observed in the field. In the model, the salt marsh extended seaward at small wave forcing (Hs = 0.00m and Hs = 0.05m), but retreated landwards at higher wave forcing (Hs = 0.10m and Hs = 0.15m). Nevertheless, the salt marsh was able to switch from a retreating extent towards an expanding extent, with increasing sediment availability. The results imply a large sensitivity of the lateral movement of the salt marsh edge to small changes in wave height and sediment availability, enabling even to transform from a retreating to an expanding marsh.

The influence of high waves on the development of artificial marshes was assessed in Chapter 5. The effect of short-term high wave forcing (hours to days) on the long-term (years to decades) development of salt marshes, and the sensitivity of this for the rate by which plants stabilize their own environment in different stages of development (i.e. pioneer marsh, established marsh and mature marsh), was explored. The numerical online-coupled Delft3D – Flexible Mesh model used in Chapter 4 was extended in Chapter 5 to include the growing strength of the vegetation and salt marsh substrate with the time vegetation is present. A spatio-temporal variable critical bed shear stress was used to increase the bed substrate strength. The resilience of the developing artificial marsh was assessed by imposing short-term high waves (significant wave height of 1.0m, 2.0m and 3.0m) on artificial marshes developed for a period of 2 to 20 years. A clear marsh edge was observed after a development period of 5 years and the vegetation and bed substrate was almost fully developed after 10 years of development. The cross-shore marsh width and vegetation cover largely changed over the first 5 years of development under influence of high waves. Nevertheless, after a development period of 10 years or more, the decrease of the salt marsh extent remained small, indicating an almost completely decreased vulnerability to short-term high waves. Although the wave attenuating capacity was relatively large after 2 years of development already, the waves hampered the vegetation growth and thereby the development of the salt marsh approximately over the first 5 year. So additional protective measures are (temporarily) needed to enable the artificial marsh to establish for over the initial 5 years of development. Once the salt marsh is established after 5 to 10 years, it can withstand large waves , without additional measures. However, the sensitivity to large waves increases after 15 years of development. So measures to

keep the marsh stability and ecosystem services intact after 15 years (mature marsh), such as marsh rejuvenation, might be necessary.

It can be generally concluded that the extent of the salt marsh is affected by processes on a range of temporal and spatial scales: on a large scale the extent of the salt marsh is affected by geographical boundaries surrounding the salt marsh and tidal flat, such as seaward channels and landward dikes. On a smaller scale, the location of the lower marsh edge is restricted by two interacting factors: inundation time and bed level change. For vegetation establishment to withstand longer inundation stress, which slows down plant growth, more stable bed levels are required so that plants are not disturbed. Vice versa, to withstand more dynamic bed levels that disturb plant growth, lower inundation stress is required, so that plants grow fast enough to recover from the stress. Moreover, the seaward growth and landward retreat of the marsh edge is driven by the magnitude of long-term (decades) daily mild wave conditions and sediment availability. Periods of small waves and/or large sediment availability enable the marsh to grow seaward, whereas periods of larger waves and/or small sediment availability result in a retreating marsh edge. On a timescale of days, short-term high wave conditions affect the establishment of the salt marsh and result in a retreat of the lowest elevated location where vegetation can grow. Finally, the contribution of salt marshes to coastal protection was highlighted in this thesis. Both artificial marshes and existing salt marshes contribute to the wave attenuation under a range of hydrodynamic conditions. Generally, the larger the cross-shore width of the salt marsh and the denser the vegetation, the larger the wave attenuation. However, delicate changes of hydrodynamic and morphodynamic parameters among which inundation time and bed level change, result in a changing marsh width, thereby affecting the wave attenuating capacity

Samenvatting

De kustzone is wereldwijd het meest dichtbevolkte gebied en de economische activiteit is aanzienlijk. 70% van de megasteden (met meer dan 1,6 miljoen inwoners) bevindt zich in dit gebied, en de populatie blijft groeien. Echter, om te leven en werken in dit gebied is bescherming tegen overstromingen essentieel, met name gezien de te verwachten zeespiegelstijging en het mogelijk vaker voorkomen van extreme stormen. Kwelders, oftewel begroeide vooroevers, kunnen bijdragen aan kustbescherming door het vermogen zich aan te passen aan een veranderlijke omgeving. Ze kunnen (1) sediment (zand en slib) invangen en daarmee verticaal groeien met zeespiegelstijging; (2) de bodem stabiliseren door de wortelstructuren van de vegetatie, waardoor de erodeerbaarheid van de bodem daalt; en (3) golven dempen door ruwheid van vegetatie en de bodem, waardoor de golfenergie voor het achterland verminderd wordt. Terwijl kwelders zich aan kunnen passen aan een veranderlijke omgeving, blijven meer traditionele maatregelen voor kustbescherming, als dijken en zeeweringen, statisch over tijd. Dus door het combineren van traditionele maatregelen en ecosystemen in Nature-Based Flood Defenses (NBFD), wordt kustbescherming duurzaam.

De mate van bescherming van een NBFD is afhankelijk van de omvang van het ecosysteem. Desondanks is de effectiviteit, voorspelbaarheid en betrouwbaarheid van een NBFD over de levensduur van deze infrastructuur (bijvoorbeeld 50 jaar) nog onbekend, aangezien lange-termijn kennis van ecosysteemdynamiek in tijd en ruimte ontbreekt. Ten gevolge hiervan wordt lokale implementatie van NBFD belemmerd. Om kwelders te gebruiken in NBFD moet de natuurlijke dynamiek en de variabele omvang van het systeem in kaart worden gebracht. Ondanks dat eerdere studies de drijvende processen achter laterale dynamiek hebben geïdentificeerd, is de laterale variabiliteit van de kwelderbreedte (kust-dwars) niet uitgebreid onderzocht en gekwantificeerd. Het is essentieel om voor een specifieke locatie te weten hoever een kwelder zeewaarts kan uitgroeien, voordat de kwelder zich weer terugtrekt. Echter, is weinig bekend over de amplitude van deze groeiende en terugtrekkende beweging. Vandaar dat dit proefschrift als onderzoeksdoel heeft: (1) het ontwikkelen van generieke kennis van de biofysische parameters die de laterale locatie van de kwelderrand bepalen, en (2) het toepassen van deze kennis, zodat de bijdrage van kwelders aan kustbescherming tegen overstromingen bepaald kan worden over tientallen jaren. Gebaseerd op dit onderzoeksdoel is de hoofdvraag van dit proefschrift: wat is de lange-termijn (50 jaar) variabiliteit van de locatie van de kwelderrand en wat is de gerelateerde variabiliteit van de golfdempende capaciteit van kwelders?

In hoofdstuk 2 wordt de variabiliteit van de breedte van de vooroever, bestaande uit een kale getijdeplaat en een begroeide kwelder, onderzocht. Een beschikbare dataset,

over een periode van 65 jaar, bestaande uit bathymetrische data grofweg beschikbaar iedere twee jaar, is gebruikt om 36 profielen te verkrijgen van zes vooroevers in de Westerschelde. De variabiliteit van de breedte van de getijdeplaat en kwelder is daarmee gekwantificeerd. Vervolgens is de golfdemping gesimuleerd middels het model Simulating WAves Nearshore (SWAN) gedurende dagelijkse omstandigheden met en zonder begroeiing en gedurende extreme omstandigheden (m.a.w. condities die statistisch gezien eens per 10.000 jaar voorkomt). De ruimtelijke variabiliteit van de breedte van de volledige vooroever en de breedte van de begroeide kwelder was groter dan de temporele variabiliteit. De temporele verandering van de breedte van de kwelder volgde de veranderingen van de volledige vooroever niet. Dit suggereert een veranderende vorm van de vooroever. Een bijdrage aan de golfdemping is geobserveerd voor alle vooroevers, zowel gedurende dagelijkse als extreme condities, waardoor de golfenergie op de landwaartse dijk lager is. Golfdemping door de kale getijdeplaat was minimaal en onafhankelijk van de breedte, terwijl een relatie is gevonden tussen de golfdemping en breedte van de begroeide kwelder: hoe langer de kwelder, des te groter de golfdemping.

Inzicht in de biofysische parameters die de locatie van de kwelderrand bepalen (m.a.w. de grens tussen de kale getijdeplaat en begroeide kwelder) is verkregen in hoofdstuk 3. Een unieke dataset is verzameld, bestaande uit dagelijkse bodemhoogte veranderingen (het integratief resultaat van de fysische forcering en sediment karakteristieken) op zes transecten gesitueerd op kwelders in het Noordzee gebied. Bovendien zijn verschillende biofysische parameters gemeten, zoals sediment karakteristieken, de inundatie periode en chlorofyl-a waarden. Seizoensmatige patronen zijn geobserveerd in de bodemhoogteveranderingen op de getijdeplaat, maar ontbraken op de kwelder. Deze verschillen kunnen mogelijk verklaard worden door de aanwezigheid van diatomeeën op de getijdeplaat (beschreven door chlorofyl-a) en continue aanwezigheid van vegetatie op de kwelder. Een afnemende golfhoogte is geobserveerd van de zeewaartse zijde van de getijdeplaat tot de landwaartse zijde van de kwelder. Een directe relatie tussen bodemhoogteverandering en golfhoogte is niet gevonden, mogelijk door de meer geleidelijke verandering van de golfhoogte over het profiel, terwijl de bodemhoogteverandering abrupt afneemt op de kwelderrand. Een combinatie van de verschillende parameters impliceert dat bodemhoogteverandering en inundatieperiode rondom de kwelderrand een indicatie geven van de ontwikkeling van de kwelderrand door het beïnvloeden van vegetatiegroei. De locatie van de kwelderrand wordt beperkt door twee interacterende factoren: inundatieperiode en bodemhoogteverandering. Vestigende vegetatie kan hogere inundatiestress weerstaan als de bodem meer stabiel is, zodat vegetatiegroei niet teveel verstoord wordt. Andersom, om een meer dynamische bodem te weerstaan die vegetatiegroei verstoord, is een lagere inundatiestress benodigd, zodat planten voldoende snel groeien om te herstellen van de stress door de dynamische

bodem. Deze resultaten suggereren dat bodemhoogteverandering belangrijk is in het bepalen van de laterale locatie van de kwelderrand.

In hoofdstuk 4 is de dynamische omvang van kwelders onderzocht door een state-of-the-art biogeomorfologisch model. De invloed van de magnitude van homogene forcering en sedimentbeschikbaarheid op kwelderontwikkeling is gesimuleerd over tientallen jaren. Kwelderontwikkeling is gesimuleerd door het online gekoppeld modelleren van hydrodynamica (getij en golven), morfodynamica en vegetatiegroei. Hiervoor is gebruik gemaakt van het numerieke Delft3D – Flexible Mesh model, gekoppeld aan een vegetatiegroei-module in Python. Kwelderontwikkeling onder invloed van milde golfcondities (significante golfhoogte van 0,00m, 0,05m, 0,10m en 0,15m), karakteriserend voor de lage-energie omgeving in estuaria, is berekend over een periode van 50 jaar. De sedimentbeschikbaarheid is gevarieerd (10mg/L, 25mg/L en 50mg/L) voor simulaties met gemiddelde golfhoogtes geobserveerd in het veld (0.10m). De gesimuleerde temporele variabiliteit van de kwelderrand, enkel beïnvloed door de magnitude van golfcondities, kwam goed overeen met de variabiliteit geobserveerd in het veld. In het model breidde de kwelder zich zeewaarts uit gedurende lage golfforcering (0,00m en 0,05m) en trok de kwelder zich landwaarts terug gedurende hogere golfforcering (0,10m en 0,15m). Desondanks kon een omschakeling van een terugtrekkende naar een uitbreidende kwelder plaatsvinden, door het verhogen van de sedimentbeschikbaarheid. Deze resultaten impliceren een grote gevoeligheid van de laterale beweging van de kwelderrand ten aanzien van kleine veranderingen in het golfklimaat en sedimentbeschikbaarheid, die het zelfs mogelijk maken om een terugtrekkende kwelder naar een uitbreidende kwelder te transformeren.

De invloed van meer extreme golven op de ontwikkeling van kunstmatige kwelders is onderzocht in hoofdstuk 5. De effecten van korte-termijn hoge golven (uren tot dagen) op de lange-termijn ontwikkeling van kwelders (jaren tot decennia), en de gevoeligheid van dit op de snelheid waarmee planten hun eigen omgeving stabiliseren in verschillende ontwikkelingsstadia (m.a.w. pionier kwelder, gevestigde kwelder en volwassen kwelder), is verkend. Het numerieke online gekoppelde Delft3D – Flexible Mesh model gebruikt in hoofdstuk 4 is uitgebreid in hoofdstuk 5. De toenemende sterkte van vegetatie en de kwelderbodem over de tijd dat vegetatie aanwezig is, is toegevoegd in het model. De veerkracht van een ontwikkelende kunstmatige kwelder is onderzocht door het opleggen van korte-termijn extreme golven (significante golfhoogte van 1.0m, 2.0m en 3.0m) op kwelders die zich hebben ontwikkeld over een periode van 2 tot 20 jaar. Een duidelijke kwelderrand is geobserveerd na 5 jaar ontwikkeling, en de vegetatie en bodem was vrijwel volledig ontwikkeld na 10 jaar. De laterale kwelderbreedte en vegetatiebedekking na een ontwikkeling van 5 jaar werden sterk beïnvloed door de hoge golven. Niettemin, na een ontwikkeling van 10 jaar en meer was de invloed van hoge golven op de

kwelderontwikkeling klein. Dat geeft een bijna volledig afgenomen gevoeligheid weer voor hoge golven. Hoewel de golfdempende capaciteit van de kwelder relatief groot was na enkel 2 jaar kwelderontwikkeling, belemmerde de golven de vegetatiegroei en daarmee de kwelder ontwikkeling sterk gedurende de eerste 5 jaar. Dus aanvullende beschermende maatregelen zijn (tijdelijk) nodig om een kunstmatige kwelder in staat te stellen de initiële 5 jaar ontwikkeling door te komen. Zodra de kwelder is gevestigd na 5 tot 10 jaar is de vegetatie in staat om hoge golven te weerstaan, zonder aanvullende maatregelen. Echter, maatregelen om de stabiliteit van de kwelder en het ecosysteem intact te houden na 15 jaar ontwikkeling (volwassen kwelder), zoals kwelderverjonging, zijn wellicht nodig.

Over het algemeen kan geconcludeerd worden dat: op grote schaal wordt de omvang van de kwelder beïnvloed door geografische grenzen die de kwelder omsluiten, zoals zeewaartse geulen en landwaartse dijken. Op een kleinere ruimtelijke schaal wordt de locatie van de kwelderrand beperkt door twee interacterende factoren: inundatieperiode en bodemhoogteverandering. Bovendien is de zeewaartse groei en landwaartse terugtrekking van de kwelderrand gedreven door de magnitude van de lange-termijn dagelijkse milde golfcondities (decennia) en sedimentbeschikbaarheid. Periodes met relatief lage golven en/of hoge sedimentbeschikbaarheid stellen de kwelder in staat om lateraal te groeien, terwijl periodes met hoge golven en/of lage sedimentbeschikbaarheid resulteren in een terugtrekkende kwelder. Op een tijdschaal van dagen beïnvloeden korte-termijn hoge golfcondities de vestiging van kweldervegetatie, dit resulteert in een toename van de bodemhoogte waar vegetatie zich kan vestigen. Ten slotte is de bijdrage van kwelders aan kustbescherming onderzocht in dit proefschrift. Zowel kunstmatige kwelders als bestaande kwelders dragen bij aan golfdemping gedurende verschillende hydrodynamische condities. Hoe groter de omvang van de kwelder (kust-dwars) en hoe dichter de vegetatie, hoe groter de bijdrage aan golfdemping is. Echter, kleine veranderingen van hydrodynamische en morfodynamische parameters kunnen resulteren in een verandering van de omvang van de kwelder, en hebben daarmee direct invloed op de golfdempende capaciteit.

Contents

1 Introduction

1.1 | Intertidal ecosystems

Land use in the coastal zone is a delicate trade-off between economic stakes and ecological values, providing welfare to the population. The interface between land and sea is often occupied by ecosystems like mangroves and salt marshes (Giri et al., 2011; Mcowen et al., 2017). Both are coastal wetland ecosystems, located in the intertidal zone, where vegetation thrives (Fig. 1.1). The intertidal zone is the coastal area inundated during high tide, and exposed at low tide. Mangroves and salt marshes appear in sheltered areas in estuaries with rather low hydrodynamic energy, at the interface of fresh riverine and saline coastal waters.

Intertidal ecosystems like salt marshes are amongst the most valuable ecosystems worldwide (Costanza et al., 1998; De Groot et al., 2012), providing a multitude of ecosystem services, among which contributing to coastal safety. Despite the extensive range of valuable functions, the global areal extent of these ecosystems is decreasing globally with 1-2% per year (Duarte et al., 2008).

Meanwhile the current population density in low-lying coastal areas, where intertidal ecosystems thrive, is more than five times higher than the global mean (Neumann et al., 2015). 70% of the world's megacities (more than 1.6 million inhabitants) is located in the coastal zone now (Duarte et al., 2008). Moreover, the population in low-lying coastal areas is still growing (Small and Nicholls, 2003), potentially degrading intertidal ecosystems and decreasing the accommodation space for coastal protection. However, for people to live in low-lying coastal areas, coastal protection is a prerequisite, especially now sea level rise and extreme storm events due to climate change increase flood risks (Donnelly et al., 2004; Knutson et al., 2010; Lin et al., 2012; IPCC, 2014).

Intertidal ecosystems can contribute to coastal protection by having the ability to adapt to a changing environment (Kirwan and Megonigal, 2013). Due to this adaptive ability these ecosystems can contribute to wave attenuation under a large range of environmental settings. Conventional infrastructure on the other hand remains fixed over time (Borsje et al., 2011; Temmerman et al., 2013). The wave attenuating capacity of salt marshes depends on the size and characteristics of the landscape (Vuik et al., 2016). To use salt marshes for coastal protection, the long-term variability of the intertidal zone must be known. However, studies describing the long-term variability of the the extent (i.e. size) of salt marshes are not available. So the predictability and reliability of salt marshes to contribute to coastal protection over a decadal timescale remains rather unknown (Temmerman et al., 2013; Bouma et al., 2014). **Hence, the focus of this thesis is unravelling the decadal variability of the salt marsh width and the processes defining the location of the salt marsh edge.**

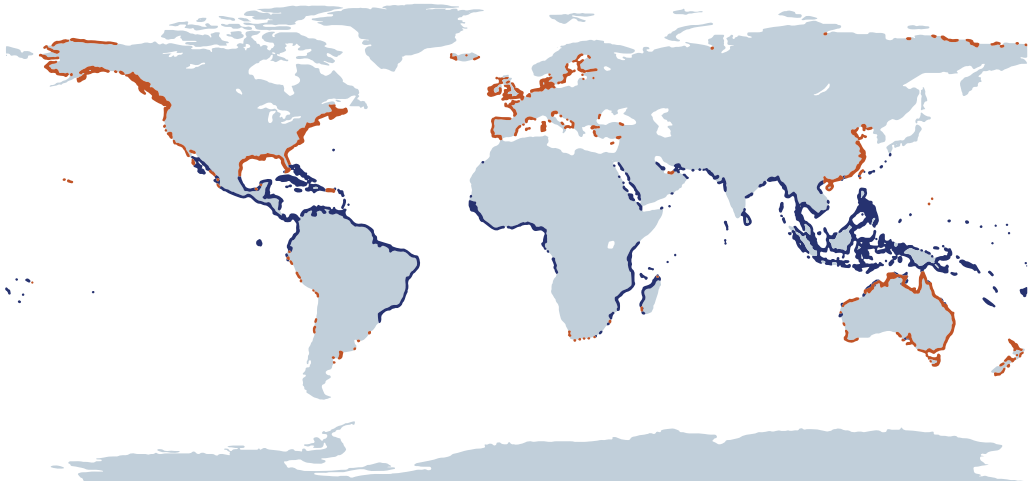

Figure 1.1 | Global distribution of salt marshes (orange) (Mcowen et al., 2017) and mangroves (blue) (Giri et al., 2011).

1.2 | Nature Based Flood Defenses

Flood protection strategies using the ability of ecosystems to contribute to flood safety can be listed under Nature Based Flood Defenses (NBFD). NBFD are part of the innovative Building with Nature (BwN) approach, in which the natural system with its ecosystem services is central (de Vriend et al., 2015). Ecosystems are able to dissipate hydrodynamic energy (e.g. Vuik et al., 2016) and can grow with sea level rise (e.g. Kirwan and Megonigal, 2013) making them resilient to climate change, whereas conventional infrastructure is static and does not adapt to a changing environment (Borsje et al., 2011; Table 1.1, adapted after Temmerman et al., 2013). Despite successful implementation of conventional structures in flood protection, there are ecological drawbacks. The presence of conventional structures decrease the extent of tidal habitats due to a lack of landward accommodation space (Doody, 2004, 2013), and often hamper a smooth transition from marine to terrestrial environments. These drawbacks can be minimized by using the BwN approach, which eventually might lead to enhanced ecosystem functioning (Day et al., 2000; Borsje et al., 2011).

Salt marshes have the ability to: (1) trap sediment, enabling the bed level to increase and consequently keep up with sea level rise to a certain extent (Kirwan and Megonigal, 2013; Kirwan et al., 2016); (2) stabilize the bed of the vegetated area by the roots of the established vegetation (Ford et al., 2016), thereby decreasing the erodibility of the intertidal area (Kirwan et al., 2010; Silliman et al., 2012); (3) dissipate wave energy due to bed and vegetation roughness and thereby decreasing the wave energy at the landward

area. The longer and more densely vegetated the foreshore (i.e. intertidal area in front of a dike), the higher the wave attenuating capacity (Fig. 1.2) (e.g. Vuik et al., 2016);

The performance of infrastructure for water and flood protection is sensitive to climate change. In general, current infrastructure is based on a singular optimal adaptive strategy, focussing on a single function. The use of intertidal ecosystems in this infrastructure increases the flexibility and is therefore suitable for adaptive coastal management (Cheong et al., 2013). Moreover, combining intertidal ecosystems and floodplains with conventional measures such as seawalls and dikes might increase the cost-effectiveness (Turner et al., 2007; Broekx et al., 2011). Adopting a managed and/or adaptive strategy by building in flexibility is a prerequisite to deal with climate change (Gersonius et al., 2013). Therefore, adaptive strategies should be adopted in institutional arrangements and vice versa design and construction of these measures must fit in the institutional arrangements (Table 1.1; Governance) (Turner et al., 2007; Janssen et al., 2014; Whelchel et al., 2018).

Although the distinct functionality of salt marshes for coastal safety is extensively proven (Table 1.1; Safety) (e.g. Vuik et al., 2016) and their resilience towards climate change seems larger than conventional solutions, these systems are only used in a range of (pilot)projects (e.g. Vuik et al., 2019; Zhu et al., 2019). Pilot projects are scattered around the world, remain rather small and a large part of these projects are for research purposes only, while the application of conventional solutions is mainstream (Maris et al., 2007; Mazik et al., 2007; Broekx et al., 2011; Temmerman et al., 2013; Baptist et al., 2019a; Baptist et al., 2019b; Rahman et al., 2019). Currently, simplifying assumptions of homogeneity of marsh characteristics are commonly used in many studies assessing the contribution of salt marshes to coastal protection, for example temporal static vegetation (Anderson and Smith, 2014), a fixed boundary between flat and marsh (e.g. Yang et al., 2012), a marsh that does not change during an extreme event (e.g. Vuik et al., 2016). However, when introducing foreshores in coastal defense schemes, coastal managers and planners should recognize that systems with both tidal flats and salt marshes are neither homogeneous, nor static (Reed et al., 2018). Although knowledge on ecological properties of the salt marsh and their dependency on the physical environment is growing (Table 1.1; Ecology), the predictability and reliability of the value of the total salt marsh landscape for coastal protection over a period of decades remains rather unknown (Temmerman et al., 2013; Bouma et al., 2014). **Hence, this thesis will contribute to designing NBFD with salt marshes by quantifying the decadal variability of the salt marsh.**

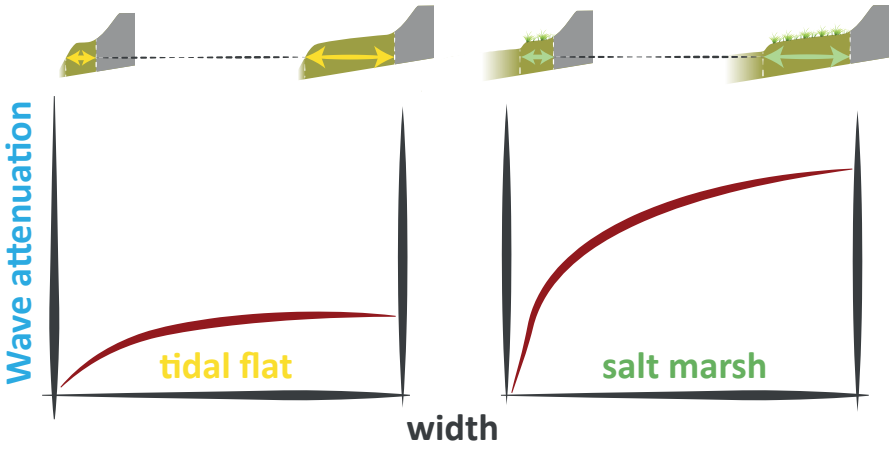

Figure 1.2 | Impression of wave attenuating capacity of foreshores consisting of either a bare tidal flat or a vegetated salt marsh. Approximation of the wave attenuation of the foreshore is based on Vuik et al. (2016).

Table 1.1 | Comparison of characteristics of conventional flood defenses and nature based flood defenses with salt marshes. Characteristics are related to governance, safety, ecology or biogeomorphology, with the latter being the focus of this thesis. The references explain the statements for the nature based flood defenses with salt marshes.

	Characteristics	Conventional flood defenses	Example references conventional flood defenses	Nature based flood defenses with salt marshes	Example references nature based flood defenses
Governance	Development phase	Mainstream	(Kabat et al., 2009)	Pilot	(Borsje et al., 2011)
	Recreation potential	Rather small, due to impact in landscape of structure	-	Rather large, due to conservation or construction of natural landscape	(Turner et al., 2007; Broekx et al., 2011)
	Institutional arrangements	Implemented	(Vrijling, 2001)	Not yet fully implemented	(Janssen et al., 2014; Whelchel et al., 2018) (general eco-engineering; dunes)
	Design and construction	Full range of calculation methods available, lot of experience with construction	(Bakker and Vrijling, 1980; Vrijling, 2001; EurOtop, 2016)	Results from pilot projects and full-scale projects available	(Mazik et al., 2007; Broekx et al., 2011; Baptist et al., 2019a; Baptist et al., 2019b)

	Characteristics	Conventional flood defenses	Example references conventional flood defenses	Nature based flood defenses with salt marshes	Example references nature based flood defenses
Safety	Stable under extreme wave conditions	Yes	(Smith et al., 1995)	Yes, proven to a certain extent	(Möller et al., 2014)
	Attenuation of hydrodynamic energy	Yes	(Smith et al., 1995)	Yes, depending on salt marsh width	(Barbier et al., 2010; Vuik et al., 2016) (Zhang et al., 2012)
	Life-cycle costs	High, due to maintenance and adaptation to climate change	(Smits et al., 2006; Broekx et al., 2011; Cheong et al., 2013; Vuik et al., 2019)	Low, if the environment allows (site specific)	(Broekx et al., 2011; Cheong et al., 2013; Vuik et al., 2019)
Ecology	Transition between land and sea	Hard, degradation of existing ecosystem	(Smits et al., 2006; Temmerman et al., 2013)	Soft, conserving and enhancing ecosystem development	(Irmler et al., 2002; Van Eerden et al., 2005; Friess et al., 2012)
	Water quality	Might decrease when water bodies become enclosed	(Temmerman et al., 2013; van Wesenbeeck et al., 2014)	Increases due to salt marsh system	(Nelson and Zavaleta, 2012)
	Carbon sequestration	No	-	Yes	(Chmura et al., 2003; Duarte et al., 2008)
	Food provision	No	-	Yes, space for habitat	(Dahdouh-Guebas et al., 2000; Walters et al., 2008) (mangroves)
	Biomechanical properties of vegetation enhancing wave attenuation.	Only little by dikes with a grass cover	(Seijffert and Philipse, 1991; Scheres and Schüttrumpf, 2019)	Yes, e.g. size, stiffness, breakability.	(Vuik et al., 2018a; Zhu et al., 2019)

	Function or variable	Conventional flood defenses	Example references conventional flood defenses	Nature based flood defenses with salt marshes	Example references nature based flood defenses
Biogeomorphology	Stabilizing the intertidal bed	Only very locally at the structure	(Smith et al., 1995)	Yes, with root systems, decreasing the erodibility	(Kirwan et al., 2010; Ford et al., 2016)
	Sustainability	Low, regular maintenance is needed	(Smits et al., 2006)	High, self-maintaining if the environment allows	(Borsje et al., 2011; Temmerman et al., 2013)
	Accommodation space	Small	-	Rather large due to natural dynamics	(Temmerman et al., 2013; Vuik et al., 2016)
	Elevation increase	No	-	Yes, when sufficient sediment is available SLR and subsidence can be counteracted with natural dynamics	(Kirwan et al., 2010; Fagherazzi et al., 2012; Kirwan and Megonigal, 2013; Kirwan et al., 2016)
	Decadal wave attenuating capacity	Yes	(Smith et al., 1995)	Unknown, depends on variability of the characteristics of the landscape.	(Balke et al., 2011)
	Decadal resilience of developing flood defense to extreme storms	Yes, resilient after construction	(Smith et al., 1995)	Unknown, depends on the development of aboveground and belowground biomass.	(Brooks et al., 2020)

1.3 | Dynamics of the intertidal area

The bare tidal flat and vegetated salt marsh, together the foreshore, is located in the intertidal area (Fig. 1.3). The dynamics of both areas are closely related, and there is a need for understanding the connection between those neighbouring ecosystems (Bouma et al., 2016).

1.3.1 | Bare tidal flats

Bare tidal areas, fronting salt marshes (Fig. 1.3; Fig 1.4; left panel), are shaped by tides and waves. Their development depends on external sediment supply on yearly timescales,

tidal range on a daily timescale, wave action on a daily timescale, but also extreme waves during events (Bearman et al., 2010) and biology on a seasonal timescale (Widdows and Brinsley, 2002; Andersen et al., 2005). Relatively small tidal ranges, large wave heights and decreased sediment supply result in smaller tidal flats, whereas larger tidal ranges, smaller wave heights and extensive sediment supply results in large tidal flats (Kirby, 2000; Friedrichs, 2011), giving accommodation space for salt marshes to develop.

Moreover, biological effects contribute to the development of the tidal flat on a seasonal timescale. Bio-aggregation and bio-adhesion enhance deposition by shoreward transporting sediment from sub-tidal channels to neighboring tidal flats or increasing the settling velocity, thereby stabilizing the tidal flat (Andersen et al., 2005; Friedrichs et al., 2008). On the contrary bioturbation increases the erodibility, thereby destabilizing the tidal flat (Widdows and Brinsley, 2002; Widdows et al., 2004).

1.3.2 | Salt marshes

Salt marshes, i.e. saltwater marshlands or saline marshes are found in the temperate and arctic climate zone (Adam, 2002; Mcowen et al., 2017). Once the deposition of fine sediment at a tidal flat leads to an appropriate elevation, salt tolerant plants are able to establish, increasing the contribution of vegetation to the formation of the landscape (Fig. 1.3). At the same time, a higher bed elevation means less influence of physical forcing. The highest elevation salt marsh vegetation can grow is confined by Highest Astronomical Tide (HAT), whereas the seaward extent is limited by Mean High Water Neap (MHWN) (Fig. 1.3) (Adam, 2002). Nevertheless, it is suggested that the exact seaward location is more delicate and defined by the local tidal range and inundation frequency (Balke et al., 2016).

The unique salt marsh habitat provides a range of ecosystem services: a habitat and nursery ground for flora and fauna (Irmler et al., 2002; Van Eerden et al., 2005), filtering water e.g. from nitrogen (Nelson and Zavaleta, 2012), consumption and aquaculture (Dahdouh-Guebas et al., 2000; Walters et al., 2008) and carbon sequestration (Chmura et al., 2003; Duarte et al., 2013). Moreover, they contribute to coastal safety by stabilizing the bed by the root systems of the vegetation (Ford et al., 2016), accumulating and trapping sediment and thereby increasing the bed level (Kirwan et al., 2010; Fagherazzi et al., 2012; Willemsen et al., 2016), attenuating storm surges (Zhang et al., 2012), and attenuating waves by roughness of the bed and vegetation (Barbier et al., 2008; Möller et al., 2014; Vuik et al., 2016).

Although the extent and more specifically the width of the salt marsh is directly related to its ecosystem services, the global extent (140×10^6 ha) is decreasing with 1-2% per year,

which is larger than the global yearly loss of tropical forests (Duarte et al., 2008). 25% to 50% of the historical global salt marsh coverage is already lost (Duarte et al., 2008; Crooks et al., 2011). Loss of intertidal ecosystems is driven by e.g. urban development, conversion to aquaculture, overexploitation, decreased sediment supply, reduced landward accommodation space, subsidence and climate induced changes (e.g. Adam, 2002; Alongi, 2002; Lotze et al., 2006; Duke et al., 2007).

Vegetation appearing at salt marshes is herbaceous and low woody vascular halophytic (Adam, 2002) (Fig. 1.4). Vegetation species can only grow in these environments, if they are salt tolerant (i.e. halophytic) (Allen and Pye, 1992). In Europe, part of the temperate zone, the upper marsh is dominated by *Juncus maritimus*, while there is a widespread occurrence of *Atriplex portulacoides* (Adam, 2002). In the North Sea area the pioneer species cord grass (*Spartina spp.*) and glasswort (*Salicornia spp.*) are frequently occurring (e.g. Van der Wal et al., 2008; Rupprecht et al., 2015). Two distinct geomorphological elements can be observed in these marshes (Allen, 2000): (1) a vegetated platform being regularly flooded during high tide, and (2) networks of tidal channels, starting at the tidal flat, flowing into the salt marsh and diminishing in the interior of the marsh.

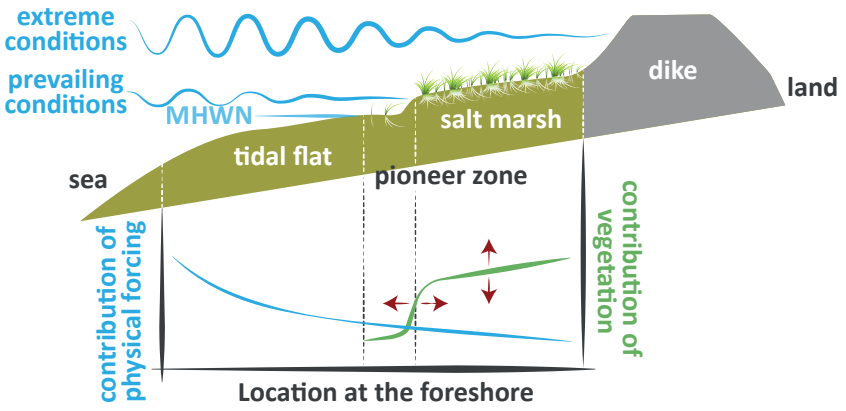

Figure 1.3 | Impression of the foreshore profile (consisting of the tidal flat and salt marsh) with a dike at the landward side (not to scale). Prevailing conditions are focussed on the salt marsh edge, while the foreshore is fully inundated during extreme conditions. Mean high water neap (MHWN), marks the seaward salt marsh edge. From the seaward to the landward side of the marsh it is hypothesized that the contribution of physical forcing to the development of the foreshore decreases, whereas the contribution of the vegetation increases.

Figure 1.4 | The tidal flat and salt marsh with common cord grass (Spartina anglica) at Hellegat at the southern shores of the Westerschelde estuary in the southwest of the Netherlands, where a small cliff of tens of centimeters can be observed between the vegetated marsh and bare flat (left); and the constructed pioneer salt marsh with glasswort (*Salicornia spp*) at Marconi near Delfzijl in the Ems-Dollard Estuary in the northeast of the Netherlands. Pictures by P. Willemsen

1.3.3 | Biogeomorphological interaction at the tidal flat and salt marsh

Feedbacks between ecology, morphology and hydrodynamics can be observed at the tidal flat and salt marsh, being part of the biogeomorphological interactions shaping the landscape. Darwin (1892) already hypothesized that invertebrates were able to affect landscape dynamics by bioturbation. Although the concept of abiotic-biotic coevolution was encapsulated in a large range of studies in the 20th century, a biogeomorphological perspective , coupling living organisms with earth surface processes and landforms, was not explicitly integrated (Corenblit et al., 2008). Ecological and geomorphic concepts converged by the end of the 20th century to a biogeomorphological perspective , for example by biogeomorphic (Viles, 1988) and ecogeomorphic (Thoms and Parsons, 2002) approaches.

Ecology and geomorphology together compose the term biogeomorphology. Ecology is the study of relationships between biota and their environment, whereas geomorphology is the study of landforms and their formation. Factors that define the environment can be abiotic (physical and chemical), biotic (other organisms) and anthropogenic (human). Abiotic geomorphological processes may affect biota, whereas biota may affect geomorphological processes. So the discipline biogeomorphology is the study of interaction between geomorphological processes and biota (Baptist, 2005a).

The general biogeomorphological loop in the intertidal area can be described as follows (Fig. 1.5): hydrodynamics, consisting of tidal flows and waves, drive sediment transport, resulting in bed level change that shape the topography of intertidal areas

(Baptist, 2005b). Finally, the bed topography affects the hydrodynamics. Secondary processes, generally having a smaller influence, describe the influence of the intertidal bed topography on sediment transport (i.e. due to bed forms), sediment transport on hydrodynamics (i.e. suspended sediment affecting turbulence) and the hydrodynamics on the bed topography. When present, vegetation plays a significant role in this loop, it affects the hydrodynamics by presenting additional roughness in the water column, thereby exerting drag force on the flow (e.g. Maza et al., 2015). Moreover, vegetation affects the bed topography by decreasing hydrodynamic energy, thereby trapping sediment (Friess et al., 2012). However, hydrodynamics also affect vegetation, by decreasing the rate of plant growth with increasing inundation frequency and period (e.g. Balke et al., 2016). Moreover, large changes in bed topography might lead to loss of vegetation (e.g. Bouma et al., 2016) (Fig. 1.5).

The biogeomorphological loop is affected by processes on different timescales. Periodic changes as well as instantaneous disturbances affect the processes and feedback between processes. Temporal inequalities in hydrodynamics, e.g. tides, extreme events and storm seasons, affect sediment transport and vegetation development (Allen, 2000). Moreover, seasonality drives the suspended sediment concentration (e.g. van Maren et al., 2015), thereby affecting the rate of accretion. External factors such as storminess, relative sea level rise and a changing tidal amplitude influence different processes in the loop as well (Allen, 2000).

Biogeomorphological interaction on the vegetated salt marsh can also be described by the feedback loop (Fig. 1.5). A two-way biophysical coupling describes the feedback between biota, and hydrodynamics and morphodynamics (Murray et al., 2008). Brushes, reeds and grasses decrease the tidal flows and wave orbital velocities (e.g. Nepf, 1999; Rupprecht et al., 2017), thereby enhancing sediment deposition (Murray et al., 2008). The elevation of the marsh platform grows with sediment deposition, depending on the suspended sediment concentrations, increasing the relative height of the salt marsh in the tidal frame. With that, hydrodynamic energy decreases (e.g. Vuik et al., 2016), increasing the bed stability and the inundation period becomes shorter (Bouma et al., 2016). Hence, enabling vegetation growth, resulting in increasing vegetation densities, but also enabling other types of vegetation to grow (Morris et al., 2002). So the density of the vegetation drives the vertical growth of the salt marsh platform; vice versa, the relative elevation of the salt marsh platform in the tidal frame drives the vegetation density and type of vegetation that appears (Murray et al., 2008), completing the biogeomorphological feedback loop, driven by hydrodynamic energy.

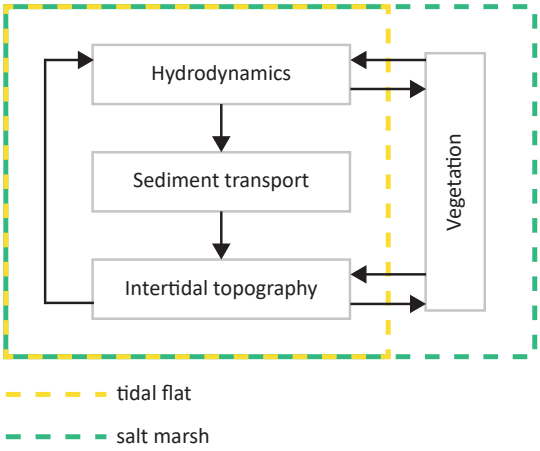

Figure 1.5 | The biogeomorphological feedback loop explaining feedback (arrows) between hydrodynamics, morphodynamics (sediment transport and intertidal topography) and vegetation. Primary processes are highlighted with arrows. Biogeomorphological processes at the salt marsh comprise the full biogeomorphological feedback loop (green dashed box), whereas vegetation is not included in the feedback loop describing processes at the tidal flat (yellow dashed box). The figure is modified after Tsujimoto (1999) and Borsje (2012).

The salt marsh edge defines the transition zone between the bare tidal flat and the vegetated salt marsh, with a discontinuity by having a relative stable marsh platform adjacent to a dynamic tidal flat, as a result of vegetation presence (Fig. 1.3; Fig 1.4; left panel). Whereas a clear distinction can be made in the processes occurring either on the bare tidal flat and vegetated salt marsh (Fig. 1.5), the geographical location of the marsh edge and thereby the bare flat and the vegetated marsh, is temporally variable. The marsh edge is able to grow seaward and extend landwards (e.g. Van der Wal et al., 2008; Singh Chauhan, 2009), thereby changing the cross-shore width of the vegetated salt marsh.

Lateral dynamics of the salt marsh edge have been observed (Harmsworth and Long, 1986; Van der Wal et al., 2008) and are related to changes in sea level (Allen, 2000), differences in wind and waves (Reed, 2001; van der Wal and Pye, 2004; Callaghan et al., 2010), channel deepening and migration (Pringle 1995; Pye, 1995; Cox et al., 2003) and intertidal sedimentation (van der Wal et al., 2002).

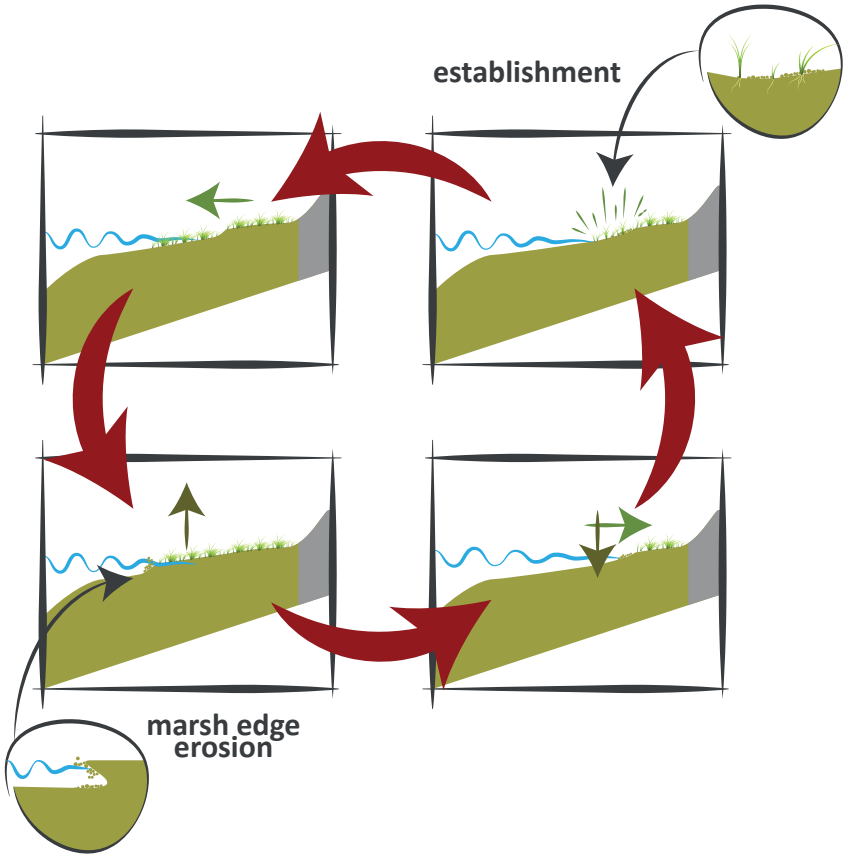

Figure 1.6 | Visualization of the processes underlying the seaward growth and landward retreat of the salt marsh. Vegetation establishment (top right), leads to seaward extension of the marsh (top left). Increasing physical stresses lead to the formation of a cliff (top left) and eventually to cliff erosion (bottom left), resulting in the landward retreat of the salt marsh (bottom right). These processes occur over multiple decades. Not to spatial scale.

Whether the salt marsh edge grows seaward or retreats landward depends on two key processes: lateral marsh erosion initiating the retreat and the start of lateral growth by seedling establishment (Bouma et al., 2016) and clonal growth from established plants (Silinski et al., 2016). Vegetation growth at the salt marsh edge depends on seedling establishment, driven by the absence of both short-term and long-term disturbances (Fig. 1.6). Whether seedling establishment is possible depends on the inundation frequency and period (Balke et al., 2016) and bed level change, possibly leading to uprooting and/or burial of seedlings (Hu et al., 2015b). So decreasing inundation stresses and stress due to bed level change enhances seedling establishment (Fig. 1.6; top right). Once the seedlings have established and stresses remain rather low, the marsh can extend seaward. Due to

accumulation of sediment at the seaward edge, physical stresses increase, and the marsh develops towards a critical state. Once this state is reached, physical disturbances lead to the formation of a cliff (Fig. 1.6; top left), which eventually starts eroding (Fig. 1.6; bottom left). Once cliff erosion is initiated the marsh retreats landward (Van de Koppel et al., 2005). Erosion of the marsh edge is a continuous process depending on the exposure to the prevailing daily wave conditions (Fagherazzi et al., 2013; Fagherazzi, 2014; Wang et al., 2017) (Fig. 1.6; bottom right). Key factors driving the marsh edge retreat rate are wave exposure and the presence of pioneer vegetation seaward from the marsh edge (Wang et al., 2017). Hence, small rates of marsh edge retreat inherently mean smaller waves and increasing presence of pioneer vegetation, which tends towards initiation of lateral marsh growth, again starting with seedling establishment (Fig. 1.6; top right). Whether successive phases of retreat or expansion are initiated, depends on the hydrodynamic forcing. Changing hydrodynamic forcing over periods of decades might even result in an only expanding or only retreating salt marsh.

1.4 | Research gap

The complex dynamics involving both the tidal flat and salt marsh emphasize the need of studying them together to assess their contribution to wave attenuation (Reed et al., 2018). Current studies indicate that short-term sediment dynamics determine the long-term development of the marsh, thereby highlighting the importance of understanding the connectivity between both ecosystems (Bouma et al., 2016). However, sufficient long-term studies describing the ecosystem dynamics are not available, so the effectiveness of NBFD over the design period of flood defenses (e.g. 50 years) and both the predictability and reliability of their coastal defense function remains rather unknown (Temmerman et al., 2013; Bouma et al., 2014).

Although it is challenging to predict the specific character of tidal flat-wetland systems decades in the future (Reed et al., 2018), knowledge on the natural biotic and abiotic environment is required for implementation of NBFD (de Vriend et al., 2015). To upscale pilot-projects, the monitoring of biophysical interactions should be extended from short-term (months to years) to long-term (decades) (Borsje et al., 2011). The local implementation should be extended to regional use of nature based flood defenses. A mechanistic understanding of ecosystem dynamics both in space and time enables the path to large-scale application (Bouma et al., 2014), but is currently missing.

Specifically, for applying salt marshes in nature based flood defenses, the natural dynamics of the system should be mapped, understood and quantified. Although previous studies identified the processes driving the expansion and retreat of the salt

marsh, the lateral variability of the marsh width did not receive much attention so far in scientific literature and is not yet quantified. It is key to know for a particular location how far a marsh can laterally grow seaward before the maximum extent is reached and/or it will start retreating landward (Bouma et al., 2016). However, little is known about the extent over which the salt marsh can expand and retreat (Van der Wal et al., 2008). **Assessing the connectivity of tidal flats and salt marshes is key to identify and quantify ecosystem dynamics (Bouma et al., 2016), and to obtain a mechanistic understanding and quantification of the lateral variability of the marsh edge.**

1.5 | Research objective

A systematic assessment of the dynamics of a combined system of bare tidal flats and vegetated salt marshes, together determining the variability of the salt marsh edge, is required at a decadal timescale. The assessment should include salt marshes in multiple estuaries, thereby enabling development of generic knowledge.

Hence, this study aims: **(1) to provide a generic understanding of the fundamental biophysical parameters determining the lateral location of the salt marsh edge in natural existing salt marsh and (2) to apply this knowledge to determine the contribution of foreshores to coastal protection over a decadal timescale.**

1.6 | Research questions, approach and outline

Based on the research objective, the key question of this thesis is: **What is the long-term (50 year) variability of the location of the salt marsh edge and what is the corresponding variability of the wave attenuating capacity of salt marshes?**

1.6.1 | Research questions and approach

Four research questions are identified to assess the variability of the salt marsh edge over a decadal timescale (Fig. 1.7):

RESEARCH QUESTION 1, presented in Chapter 2: **What is the variability of foreshores, consisting of tidal flats and adjacent salt marshes, in an estuary over a decadal timescale; and to what extent can foreshores safely act as additional defense measure?**
The long-term (50+ years) variability of the foreshore width is quantified using field observations from the bed elevation that has been developed over the same period. Subsequently the wave attenuating capacity of both the tidal flat and salt marsh is

determined using a numerical model. The wave attenuating capacity of the foreshore is assessed over a period of decades with a temporal resolution of years, for transects representing multiple salt marshes in a single estuary (Chapter 2).

RESEARCH QUESTION 2, presented in Chapter 3: **What physical factors confine the location of the marsh edge on a daily to annual timescale?**

To obtain a better understanding of the physical factors constraining the location of the marsh edge, and with that the cross-shore salt marsh width affecting the wave attenuating capacity, field observations are conducted at the transition of the tidal flat and salt marsh. Measurements of biophysical parameters such as: bed level change, inundation time, wave height and microphytobenthos are conducted to determine the location of the salt marsh edge in this parameter space. Measurements are conducted for a period exceeding a single year with a temporal resolution of minutes to days. Measurements are obtained at six transects located in three different estuaries around the North Sea (Chapter 3).

RESEARCH QUESTION 3, presented in Chapter 4: **How does the biophysical development and extent of salt marshes depend on the magnitude of homogeneous hydrodynamic forcing and sediment availability?**

The dynamic extent of the salt marsh is assessed by numerically modelling bed level change and vegetation growth under influence of a variety of homogeneous mild wave conditions representing daily weather conditions and differences in sediment availability. A 2-dimensional numerical model (depth-averaged) is further developed to systematically assess the salt marsh development under influence of the magnitude of homogeneous wave forcing and sediment availability. The landscape development and location of the salt marsh edge are simulated over a period of 50 years with a temporal resolution of seconds to hours for an alongshore foreshore area of 1 kilometer (Chapter 4).

RESEARCH QUESTION 4, presented in Chapter 5: **What is the influence of short-term wave forcing (hours to days) on long-term salt marsh development (years to decades), and the sensitivity of this for the rate by which plants stabilize their own environment in different stages of development (i.e. pioneer marsh, established marsh and mature marsh)?**

The development and vulnerability of a developing artificial salt marsh is assessed by extending the numerical model used to answer the previous research question (3). The model is further developed to assess the strength and stability of establishing salt marshes forced with mild wave conditions on the long-term (years to decades), and forced with large wave conditions on the short-term (hours to days). To combine short-term and long-term development, the temporal developing strength of the vegetation and marsh substrate, by which the salt marsh is stabilized is included. The landscape development is

simulated and assessed for a period of decades with a temporal resolution of seconds to hours for an alongshore foreshore area of 1 kilometer (Chapter 5).

1.6.2 | Outline of the thesis

The research questions introduced in the current chapter (Chapter 1. Introduction), are discussed in Chapters 2, 3, 4 and 5 (Fig. 1.7). Chapters 2 and 3 focus on observations and identifying parameters driving the salt marsh edge and wave attenuating capacity of the foreshore. Chapters 4 and 5 assess the influence of the magnitude of biophysical parameters on the dynamics of the salt marsh edge, using a numerical model. Finally, the obtained knowledge is put in perspective in the discussion (Chapter 6), and the main conclusions and recommendations for future research are presented (Chapter 7 and Chapter 8).

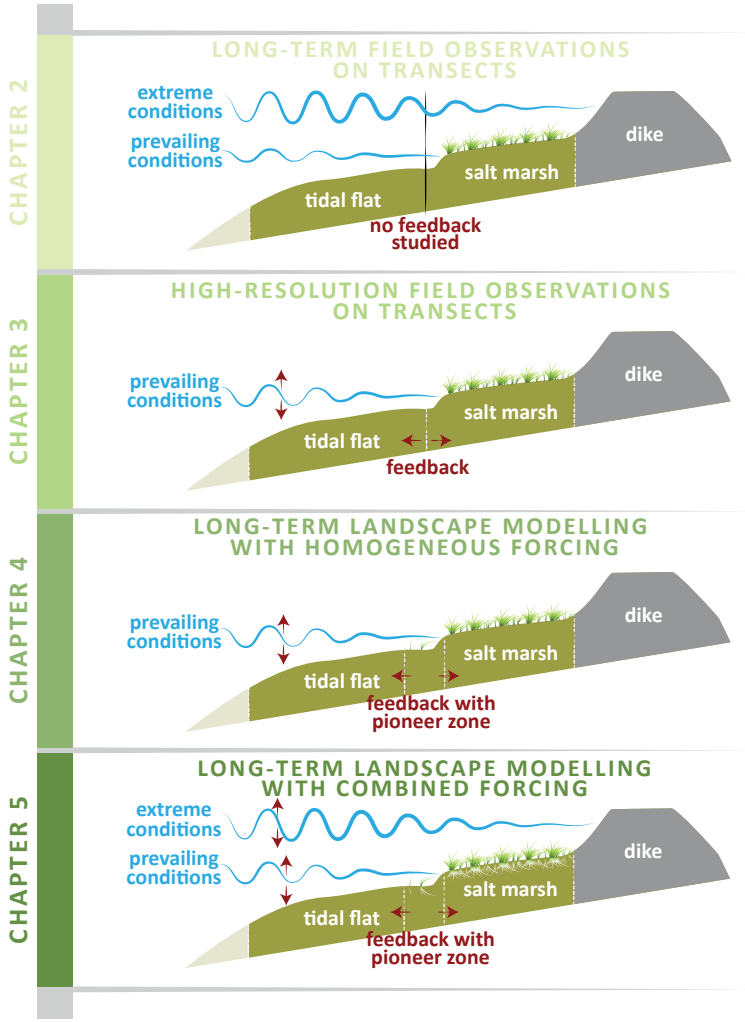

Figure 1.7 | Research approach and outline of the thesis.

2

Field-based decadal wave attenuating capacity of combined tidal flats and salt marshes

Published as: Willemsen, P. W. J. M., Borsje, B. W., Vuik, V., Bouma, T. J., & Hulscher, S. J. M. H. (2020). Field-based decadal wave attenuating capacity of combined tidal flats and salt marshes. *Coastal Engineering*, *156*, 103628.

Abstract

Foreshores consisting of both bare tidal flats and vegetated salt marshes are found worldwide and they are well studied for their wave attenuating capacity. However, most studies only focus on the small scale: just some isolated locations in space and only up to several years in time. In order to stimulate the implementation of foreshores serving as reliable coastal defense on a large scale, we need to quantify the decadal wave attenuating capacity of the foreshore on the scale of an estuary. To study this, a unique bathymetrical dataset is analyzed, covering the geometry of the Westerschelde estuary (The Netherlands) over a time-span of 65 years. From this dataset, six study sites were extracted (both sheltered sites and exposed sites to the prevailing wind direction) and divided into transects. This resulted in 36 transects covering the entire foreshore (composed of the bare tidal flat and the vegetated salt marsh). The wave attenuation of all transects under daily conditions (with and without vegetation) and design conditions (i.e. events statistically occurring once every 10,000 years) was modelled.

Overall, the spatial variability of the geometry of a single foreshore was observed to be much larger than the temporal variability. Temporal changes in salt marsh width did not follow the variability of the entire foreshore. Both under daily and design conditions, vegetation contributes to decreasing wave energy and decreases the variability of incoming wave energy, thereby decreasing the wave load on the dike. The southern foreshores, sheltered from the prevailing wind direction, were more efficient in wave attenuation than the exposed northern foreshores. A linear relation between marsh width and wave attenuation over a period of 65 years was observed at all marshes. The present study provides insights needed to calculate the length of a salt marsh to obtain a desired minimum wave attenuating capacity.

2.1 | Introduction

Estuaries are complex landscapes shaped by bio-physical interactions and anthropogenic influences. They are located at the interface of fresh riverine and saline coastal waters, providing a range of ecosystem services such as habitat provision, food production, space for recreation and accessibility over water (e.g. Barbier et al., 2010). However, living near estuaries also comes with flood risks from riverine and coastal sources. Nevertheless, the population density in these areas is high and still growing (Small and Nicholls, 2003; Syvitski et al., 2009). Moreover, extreme storm events and sea level rise increase flood risks in the coastal zone, as an insurmountable consequence of climate change (Donnelly et al., 2004; Knutson et al., 2010; Lin et al., 2012; IPCC, 2014). As a result, estuaries become increasingly vulnerable to flooding and communities inhabiting these areas are in need of improved flood protection.

The population and economic value of the estuaries hinterland are generally protected by conventional coastal engineering solutions, such as groins, revetments, breakwaters and sea walls. Those conventional measures are increasingly challenged by regional and global changes, including climate change-induced Sea Level Rise (SLR), increased storm intensity and land subsidence (Syvitski et al., 2009). These conventional solutions are static and do not adapt to a changing climate (Borsje et al., 2011; Temmerman et al., 2013).

Foreshores, consisting of a bare tidal flat and vegetated salt marsh, can serve as add-on to conventional coastal defenses (Kirwan et al., 2010; Gedan et al., 2011; Möller et al., 2014). Firstly, salt marshes occur widely in tempered climate zones (Mcowen et al., 2017), so they can be applied globally. Secondly, foreshores can dissipate wave energy due to the bottom profile and vegetation (e.g. Vuik et al., 2016), consequently being suitable to attenuate wave energy in front of a dike. Thirdly, marshes are sustainable and in that they can cope, to a certain extent, with SLR (Kirwan and Megonigal, 2013; Kirwan et al., 2016). By dissipating hydrodynamic energy, sediment is trapped in the marsh, enabling vertical growth of the bed (Bouma et al., 2007; Van Wesenbeeck et al., 2008).

Thus, salt marshes have high potential for a contribution to coastal protection, despite the uncertainty as a consequence of using vegetation and thereby introducing intrinsic biological factors (Bouma et al., 2014). Moreover, salt marshes and tidal flats might be cost-effective locally and more flexible and thereby suitable for adaptive coastal management compared to conventional coastal engineering solutions (Turner et al., 2007; Broekx et al., 2011; Cheong et al., 2013), which is a prerequisite for dealing with flood risks due to climate change (Gersonius et al., 2013).

So far, the significant wave attenuating capacity of foreshores within the timescale of events (e.g. extreme storm events) is proven for specific aspects in wave flumes (e.g. Coops et al., 1996), and give mechanical understanding of vegetation stiffness (Bouma et al., 2005), standing biomass, (Bouma et al., 2010), extreme storms (Möller et al., 2014) and wave-current interaction (Maza et al., 2015). Field studies give insights in wave attenuation with realistic conditions on a larger scale (Möller, 2006; Yang et al., 2012; Vuik et al., 2016). These studies prove the significant wave attenuating capacity for a specific setting of a foreshore for a specific moment in time: a snapshot. Within the timescale of seasons, field measurements at transects perpendicular to the marsh edge between salt marsh and tidal flat suggest a relative stable salt marsh with a more variable seaward situated tidal flat (Andersen et al., 2006; Vuik et al., 2018a; Willemsen et al., 2018). Moreover, at this seasonal timescale, measurements over a stretch of salt marsh (50m width), suggest a continuous contribution of the marsh to wave attenuation (Vuik et al., 2018a).

Although all these studies actually measure the wave attenuation, they still focus on the relative small scale, i.e. some isolated locations in space and at most up to several years in time, and do not capture extreme conditions over long-term salt marsh settings. Moreover, to our knowledge superimposing extreme conditions over long-term foreshore settings measured in the field, to give unique long-term insights, has not been done before. The long-term persistence of wave-attenuating ecosystems has been identified as a key-bottle neck hampering application of intertidal habitats for coastal protection (Bouma et al. 2014). Moreover, wave attenuation is known to be highly location-specific, depending on bio-physical settings such as foreshore width and the geometry of both the vegetated salt marsh and bare tidal flat (Vuik et al., 2016). Hence, the key question addressed in this paper is: what is the variability of foreshores, consisting of salt marshes and adjacent tidal flats, in an estuary over a decadal time-scale; and to what extent can foreshores safely act as additional defense measure? We will quantify the long-term (50+ years) variability of the wave attenuating capacity of foreshores in a full estuary, by combined long-term large-scale bathymetrical field data and numerical model analysis for calculating wave attenuation.

The structure of this chapter is as follows. In section 2.2 the study area is introduced, followed by a description of the long-term bathymetrical data. Consecutively the numerical model analysis for calculating wave attenuation is described, including vegetation representation and the scenarios that were assessed. Section 2.3 presents the variability of the bathymetry of the foreshore, followed by the contribution of the foreshore to wave attenuation under extreme scenarios and under daily scenarios, that have not been measured before. In section 2.4 the main findings of this paper are discussed. We end by drawing some conclusions in section 2.5.

2.2 | Bathymetrical field data analysis and wave modelling

2.2.1 | Long-term foreshore elevation

Historical elevation data of foreshores, from the subtidal up to the higher elevated parts, which are only submerged during extreme high water, is scarce. In general, bathymetrical data representing the subtidal area has sufficient coverage. However, the data coverage for the higher elevated vegetated salt marsh is often lacking. In addition, long-term (50+ year) datasets with consecutively collected elevation data is even more scarce. Nevertheless, such datasets are available for the entire Westerschelde estuary in the Netherlands. In the Westerschelde estuary, multiple foreshores are present (Fig. 2.1), which can be differentiated by the prevailing wind direction being southwest. This results in a dichotomy of wind exposure, with foreshores at the northern shores being exposed and foreshores at the southern shores being sheltered from the prevailing wind direction (Callaghan et al., 2010). The long-term wave attenuating capacity of six foreshores, three at the exposed and three at the sheltered shores in the Westerschelde (Fig. 2.1), was analyzed. Elevation data for those nearshore areas were captured in extensive bathymetrical datasets, called 'Vaklodingen'. The data was collected since 1925-1935 by the Ministry of Infrastructure and the Environment (former Ministry of Transport Public Works and Water Management). After post-processing, the data was stored in grids with a cell size of 20m x 20m (De Kruif, 2001; Wiegman et al., 2005). The vertical accuracy of the Vaklodingen data was 0.54m in the 1950s increasing to 0.11m since 2001 (Marijs and Parée, 2004).

We constructed two-dimensional transects, to enable assessment of the wave attenuating capacity (cf. Horstman et al., 2014). Bathymetrical data from the Vaklodingen was interpolated over the transects. The direction of the transects was parallel to the wave direction under design conditions, obtained from a database with the results of 2D wave simulations, carried out in the context of dike safety assessments in the Netherlands (Gautier and Groeneweg, 2012; Groeneweg and Van Nieuwkoop, 2015). Transects that interfered with the land boundary, due to the position of the study site in the curvature of the dike, were excluded (i.e. the average design wave direction for a foreshore was just landward directed due to the shape of the foreshore). The alongshore spacing between transects (i.e. number of transects over a certain alongshore foreshore length) was selected in a way to capture the alongshore variability of the geometry and wave attenuation. This spacing was based on a transect refinement study (section 2.2.2.3). For determining the foreshore width, mean high water spring (MHWS) was used to represent the landward boundary. The seaward boundary of the foreshore was

represented by mean low water spring (MLWS). Both water levels were assumed to be static over time, although an increase of the tidal amplitude over time has been observed in the Westerschelde (Taal et al., 2015), possibly changing the boundaries of the transects as a consequence. However, the hydrodynamic input parameters also change with a changing tidal amplitude, as it is assumed resulting in only minor changes to the wave attenuating capacity. Missing data causing incomplete transects at the intertidal or higher parts were interpolated over time per transect (cf. Vuik et al., 2019). In case the first year to be analyzed from a certain transect was incomplete, the known position of the dike toe was used for spatial interpolation, after which temporal interpolation was applied.

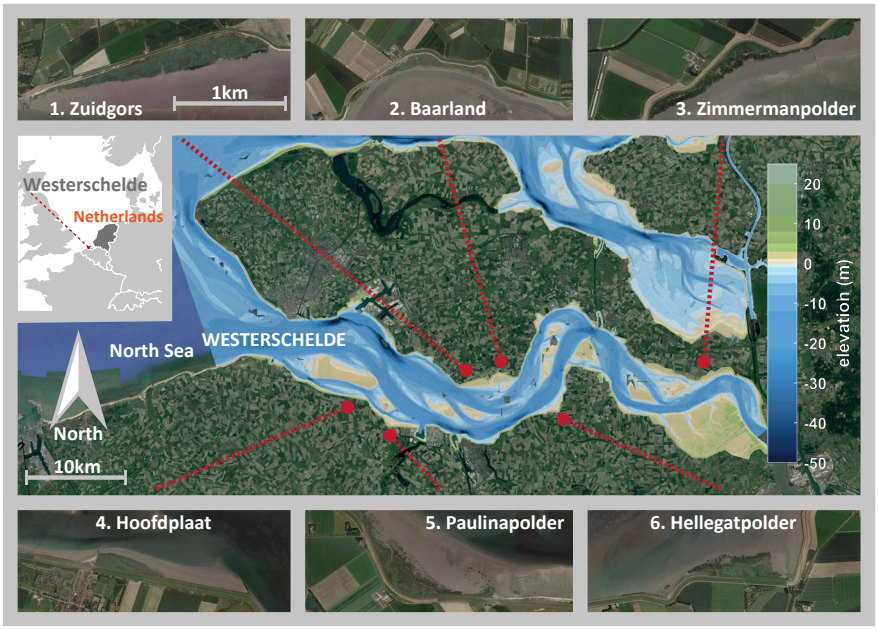

Figure 2.1 | Six analyzed foreshores (top and bottom panels) in the Westerschelde, indicated with red dots (center), located in the Southwestern part of the Netherlands (see inlay in center panel). Bathymetrical data of 2014 is presented in the center panel (elevation in meter with respect to mean sea level).

2.2.2 | Modelling wave attenuation

Wave attenuation over the foreshore was computed using the spectral wave model SWAN (Simulating WAves nearshore; Booij et al., 1999; Ris et al., 1999). In this model, the vegetation module for wave attenuation was developed by Méndez and Losada (2004) and implemented in SWAN by Suzuki et al. (2012). The model was calibrated, validated and applied previously on two foreshores in the southwestern delta of the Netherlands:

3. Zimmermanpolder (Bath) at the exposed northern shore and 6. Hellegatpolder at the sheltered southern shore (Fig. 2.1), where energy dissipation (i.e. wave heights) by foreshores under storm conditions was accurately simulated using the SWAN model (Vuik et al., 2016). In the current study the wave attenuating capacity of foreshores under different conditions was assessed. Daily occurring environmental settings (with and without vegetation) and environmental settings based on design conditions (event with a statistical recurrence time of 1/10,000 year) were used (Fig. 2.2). Under design conditions, it was assumed that vegetation present at the marsh was bent over or broken and lying flat at the bed (Vuik et al., 2018a; Vuik et al., 2018b).

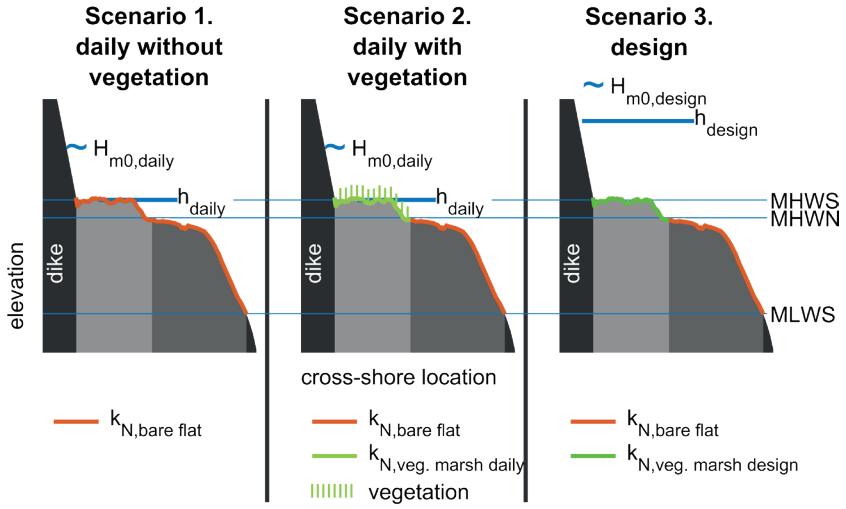

Figure 2.2 | Schematic overview of the foreshore, consisting of a bare tidal flat (dark grey), vegetated salt marsh (light grey) and dike (black) for obtaining wave attenuation under different scenarios. Hydrodynamic parameters used are: mean high water spring (MHWS), mean high water neap (MHWN), mean low water spring (MLWS), water level (h), significant wave height (Hmo) and the Nikuradse roughness length (kN). Scenarios assessed were: (1) daily without explicitly accounting for vegetation by using a single Nikuradse roughness length $k_{N,bare\ flat}$, (2) daily with explicitly accounting for vegetation by using a different Nikuradse roughness length for the bare foreshore ($k_{N,\ bare\ flat}$) and the bed of the vegetated foreshore under the vegetation ($k_{N,\ veg.\ marsh\ daily)}$ and explicitly taking into account vegetation structures, (3) design conditions by using a different Nikuradse roughness length for the bare foreshore ($k_{N,\ bare\ flat}$) and for the vegetated foreshore ($k_{N,\ veg.\ marsh\ design}$) by taking into account stem breakage and hydrodynamic parameters under design conditions.

2.2.2.1 | *Vegetation characteristics and bottom roughness*

The marsh edge position was determined by using a tidal benchmark, since the marsh edge position was not recorded for the full period of data. In literature, the seaward marsh edge has often been approximated by using a tidal benchmark (McKee and Patrick, 1988;

Bakker et al., 2002; D'Alpaos et al., 2007; Balke et al., 2016). The tidal benchmark mean high water neap (MHWN) has been used previously to define the marsh edge (Doody, 2007), and this benchmark was used to study salt marsh dynamics in the Westerschelde as well (Van der Wal et al., 2008). Therefore, the tidal benchmark MHWN from Van der Wal et al. (2008) was adopted in the present study to define the salt marsh edge (table 2.1).

Vegetation characteristics at the marsh edge were obtained by Vuik et al. (2016), for the brackish salt marsh Zimmermanpolder (3; called Bath in Vuik et al. (2016)) and more salty salt marsh Hellegatpolder (6). The brackish species *Scirpus* maritimus was found at Zimmermanpolder (3), while the salty species *Spartina anglica* was found at Hellegatpolder (6). More mixed vegetation was present at the higher marsh, but was not taken into account, because a major part of the waves is attenuated at the marsh edge, especially under daily conditions. Collected vegetation characteristics have been averaged to obtain general values for the mean vegetation height (h_{veg}), stem density ($N_{v,o}$), stem thickness ($b_{v,o}$) and these values were used as input for SWAN (table 2.2). The general characteristics derived from both salt marshes were assumed to be representative for the whole Westerschelde.

Under daily conditions, the long-term contribution of vegetation to the wave attenuating capacity of foreshores was assessed by explicitly including and excluding vegetation in wave modelling. The scenario including vegetation was assumed to be representative for summer conditions with maximum biomass, while the scenario excluding vegetation was assumed to be representative for winter conditions, with minimum vegetation biomass. Daily conditions without vegetation in scenario 1 (Fig. 2.2; panel 1) were represented with a constant Nikuradse roughness length scale ($k_{N,bare\ flat}$) of 0.001m for the entire profile (Vuik et al., 2019), for only assessing the contribution of the morphology. The Nikuradse values used, were derived from Manning roughness coefficients presented in Wamsley et al. (2010), by using the conversion equation in Bretschneider et al. (1986). Vegetation was explicitly included in the model in scenario 2 (Fig. 2.2; panel 2). Daily conditions with vegetation were represented with a Nikuradse roughness length scale of 0.001m at the bare tidal flat ($k_{N,bare\ flat}$) and 0.02m at the vegetated foreshore ($k_{N,veg.\ marsh\ daily}$) representing the bed under the vegetation (Vuik et al., 2016; table 2.2). Under design conditions, scenario 3, (Fig. 2.2; panel 3) the roughness at the marsh due to broken vegetation was represented by a Nikuradse roughness length scale $k_{N,veg.\ marsh\ design}$ of 0.05m (Wamsley et al., 2010), whereas the roughness at the bare tidal flat in front of the marsh ($k_{N,bare\ flat}$) was represented again with the value of 0.001m (Vuik et al., 2019). So following Vuik et al. (2019), vegetation in scenario 3 was not included in SWAN using the vegetation module, but using an adapted Nikuradse roughness length.

2.2.2.2 | *Hydrodynamic boundary conditions*

Hydrodynamic boundary conditions for approximating the daily wave attenuating capacity (Fig. 2.2; panel 1 & 2) representing the water level were derived from tidal characteristics. Mean High Water Spring (MHWS) , being the highest common occurring water level at which large parts of the salt marsh contribute to wave attenuation, was derived from Van der Wal et al. (2008). Daily wave characteristics used, were $H_{mo,daily}$ = 0.2m and $T_{m-1,o,daily}$ = 3s (Callaghan et al., 2010; Hu et al., 2015a; Hu et al., 2015b) (table 2.2; Fig. 2.2). Energy gain due to wind was not accounted for in the calibrated SWAN model (Vuik et al., 2016), since wind input was assumed to be insignificant over small foreshore lengths.

The hydrodynamic boundary conditions under design conditions (table 2.1; Fig. 2.2; panel 3) were obtained from the WTI (legal assessment instrument; in Dutch: 'wettelijk toetsingsinstrumentarium') (Gautier and Groeneweg, 2012; Groeneweg and Van Nieuwkoop, 2015) representing an event statistically occurring once every 10,000 year. This safety level has been used previously to assess the safety of the Dutch dikes. Both water levels and wave characteristics are available along every 250m of coastline. Water levels, wave period and wave height at the eastern and western side of each study site were averaged, thereby avoiding hydrodynamic parameters that were influenced by the topography of the study site (e.g. by refraction and shoaling) (Fig. 2.3; top panel). The design wave direction was selected at the center of the salt marsh (table 2.1). Herein is the wave direction the result of the wind direction and rotation due to refraction.

Bulk drag coefficients C_D were derived in Vuik et al. (2016) by calibrating the SWAN model for optimal reproduction of measured wave attenuation by vegetation. However, these calibrated values were meant to describe wave attenuation during storms, for which flexibility of vegetation plays an important role. This resulted in values significantly below 1.0. The current study explicitly includes vegetation structures for wave attenuation under daily conditions (Fig. 2.2; panel 2), with small waves and low water depth. In these circumstances, bending of the plants will be limited, and we assumed the drag force will resemble that of rigid cylinders, for which a value of approximately 1.0 is appropriate (Suzuki and Arikawa, 2010). Therefore, C_D = 1.0 was taken into account in all SWAN simulations for daily conditions explicitly including vegetation (scenario 2).

2.2.2.3 | *Transect refinement*

To assess the wave attenuating capacity of a foreshore, the landscape was represented using transects parallel to the design wave direction (Fig. 2.3; center panel). The spacing between the transects (i.e. the alongshore distance between two transects) was selected in a way that the spatial variability of the foreshores (i.e. variability along the dike within

a single salt marsh) was fully captured. The geometry of the foreshore for a specific transect and associated wave attenuating capacity was calculated for transects with a different alongshore spacing, i.e. the distance between transects was measured over the landward stretch of the dike to be able to relate the results to dike safety. An initial spacing of 1000m was selected, because the alongshore length of the foreshores just exceeded 1000m at some foreshores. A transect spacing of 1000m does not include the minimum and maximum transect width of the foreshore, and as a consequence neither the full variability in wave attenuation. The same holds for a transect spacing of 500m. The full variability of the foreshore was captured by a transect spacing of 250m, a smaller spacing of e.g. 125m did not add more detail. So a transect spacing of 250m was selected to capture the maximum variability with the largest spacing (i.e. least amount of transects) for computational efficiency (Fig. 2.3; bottom panels).

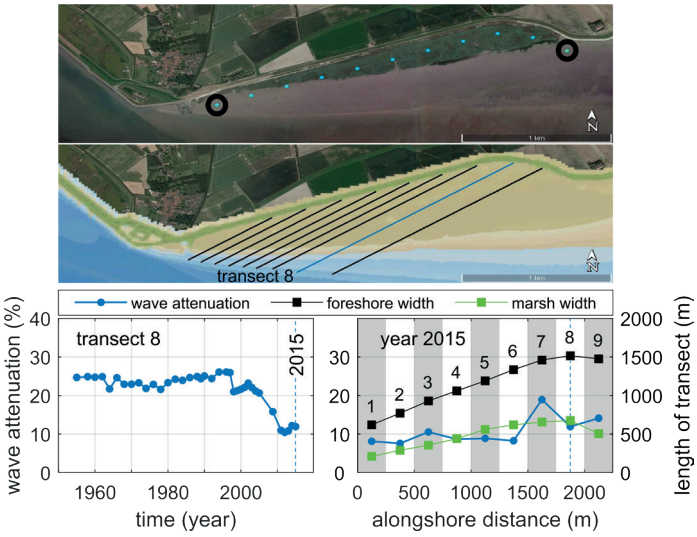

Figure 2.3 | The method for assessing wave attenuation at the foreshore Zuidgors for a single transect and a single year. The top panel shows locations (blue dots) where significant wave heights under design conditions were provided (Gautier and Groeneweg, 2012; Groeneweg and Van Nieuwkoop, 2015). Hydrodynamic characteristics (water level, wave height, wave direction) at both alongshore boundaries of the foreshores were averaged to obtain boundary conditions for the wave model (black circles; top panel). The bed elevation was derived from the Vaklodingen dataset (background colors in center panel indicate the bathymetry of 2014). Transects parallel to the design wave direction with an alongshore spacing of 250m, measured at the dike, are indicated with black lines (center panel). The blue line (center panel) highlights transect 8, for which the temporal variation of wave attenuation is shown (bottom left panel). The vertical dashed blue line (bottom left panel) highlights the last year assessed (2015). The wave attenuating capacity in the last year 2015 for all nine transects at the marsh is highlighted with the blue line (left vertical axis; bottom right panel). The black line indicates the width of the assessed foreshore, whereas the green line indicates the width of the vegetated salt marsh (both on the right vertical axis).

Table 2.1 | Characteristics of the analyzed foreshores and input values for wave modelling.

	Local water level boundaries			Vaklodingen		Local design conditions			
Study site	MLWS (m)	MHWN/ marsh edge (m)	MHWS/ Daily water level (m)	Period of data availability (year - year)	Number of years included (-)	Design water level (m)	Design wave height (m)	Design wave period (s)	Design wave direction (º)
	h_{MLWS}	h_{MHWN}	h_{daily}	-	-	h_{norm}	$H_{mo,design}$	$T_{m-1,o,design}$	dir
1 Zuidgors	-2.31	1.85	2.63	1955-2015	37	6.04	1.655	4.725	233
2 Baarland	-2.28	1.83	2.62	1955-2015	37	6.13	1.72	4.35	238
3 Zimmerman-polder	-2.46	2.14	3.04	1951-2015	51	6.71	1.82	4.15	212
4 Hoofdplaat	-2.06	1.59	2.34	1950-2015	42	5.78	2.36	4.55	323
5 Paulina	-2.16	1.73	2.54	1955-2015	41	5.89	2.15	4.7	344
6 Hellegatpolder	-2.25	1.81	2.61	1955-2015	52	6.32	2.56	4.95	301

Table 2.2 | General input parameters for wave modelling.

Parameter	Symbol	Value	Unit	Source
Daily wave height	$H_{mo,daily}$	0.2	m	Callaghan et al., (2010); Hu et al. (2015a)
Daily wave period	$T_{m-1,o,daily}$	3	s	Hu et al. (2015b)
Mean vegetation height	h_{veg}	0.24	m	Vuik et al. (2016)
Vegetation stem density	$N_{v,o}$	865	$1/m^2$	Vuik et al. (2016)
Vegetation stem thickness	$B_{v,o}$	5.1	mm	Vuik et al. (2016)
Nikuradse roughness length scale for bare tidal flats	$k_{N,bare\ flat}$	0.001	m	Vuik et al. (2019)
Nikuradse roughness length scale for salt marsh under design conditions	$k_{N,veg.marsh\ design}$	0.05	m	Vuik et al. (2019); Wamsley et al. (2010)
Nikuradse roughness length scale for salt marsh under daily conditions	$k_{N,veg.\ marsh\ daily}$	0.02	m	Vuik et al. (2016)
Bulk drag coefficient	C_D	1.0	-	Suzuki and Arikawa (2010)
Transect spacing	S_{pacT}	250	m	Transect refinement (section 2.2.2.3)

2.3 | Results

2.3.1 | Long-term foreshore geometry

2.3.1.1 | *Temporal variability*

The foreshore geometry was assessed by analyzing historical bed level data. The cross-shore width of both the vegetated salt marsh and complete foreshore (between MLWS and MHWS) were found to be variable over space and time. The width of the vegetated part did not follow the total width of the foreshore per definition. At a representative transect at Paulinapolder, the width of the total foreshore increased by a 100 meters over 60 years. Nevertheless the width of the salt marsh was highly variably with a minimum width of 80m and a maximum width of 310m in the first decades (Fig. 2.4; location PAU). Moreover, at Zimmermanpolder the total foreshore width in the first decade was decreasing (from 1530m to 1140m), while the width of the vegetated part was increasing with tens of meters (Fig. 2.4; location ZIM). Zooming in on the single foreshores, the average width (averaged over all transects of the foreshore) of the bare tidal flat was always larger than the average width of the adjacent vegetated salt marsh, i.e. on average the part of the foreshore covered by vegetation does never exceed 50% (Fig. 2.5). The part of the foreshore covered by vegetation was relatively high at Zuidgors and Paulinapolder, exceeding 32%, while below 20% at the other foreshores. In general the mean width of the salt marsh remained stable (except during the last decade at Baarland), whereas the mean width of the total foreshore showed a more dynamic behavior (Fig. 2.5). At Zuidgors, Baarland, Zimmermanpolder and Hellegatpolder changes of hundreds of meters occurred within a period of 5 years only. The latter is supported by strong changes of the total foreshore width observed at a single representative transect in periods of a few years only, e.g. in the first decades of the analysis at Zimmermanpolder (ZIM) and Hellegatpolder (HEL) and the last decade at Baarland (BAA) (Fig. 2.4).

The change of the width of the vegetated salt marsh over a period of a single year remained small, with a change of maximum tens of meters in the range of the 10^{th} and 90^{th} percentile (Appendix 2.A). Both positive and negative outliers of hundreds of meters were observed over a single year (Fig. 2.6; Appendix 2.A). The marsh width change increased with increasing length of observation periods, i.e. the longer the observation period, the larger the difference between maximum and minimum width of the salt marsh width, indicating a continuous change over the entire period. However, when observing the change over the longest periods (marsh width change over more than 30 years), the change in width decreased. Moreover, the range between minimum and maximum change was largest over the periods between 11

and 20 and 21 and 30 years, with differences between the minimum and maximum of 100 to 200 meters at e.g. Hoofdplaat (smallest) and almost a kilometer at Baarland (largest). While the range became constant or even decreased over the long-term, the median of the change showed different behavior per entire foreshore. A continuous increase was observed at Baarland (0m to 60m), Zimmermanpolder (5m to 130m), and Hoofdplaat (0m to 33m), while a decreasing marsh width was observed at Paulinapolder (0m to -115m) and Hellegatpolder (0m to -55m). At Zuidgors (between -5m and 25m) the median change was observed to vary around zero (Appendix 2.A). It was striking that in general, the largest increase in marsh width change (between 10th and 90th percentile) occurred in periods between 1 and 10 years and 11 and 20 years (Fig. 2.6). This observation in combination with a flattening range between the maximum and minimum marsh width change over the long-term might indicate an increasing stability over a longer period.

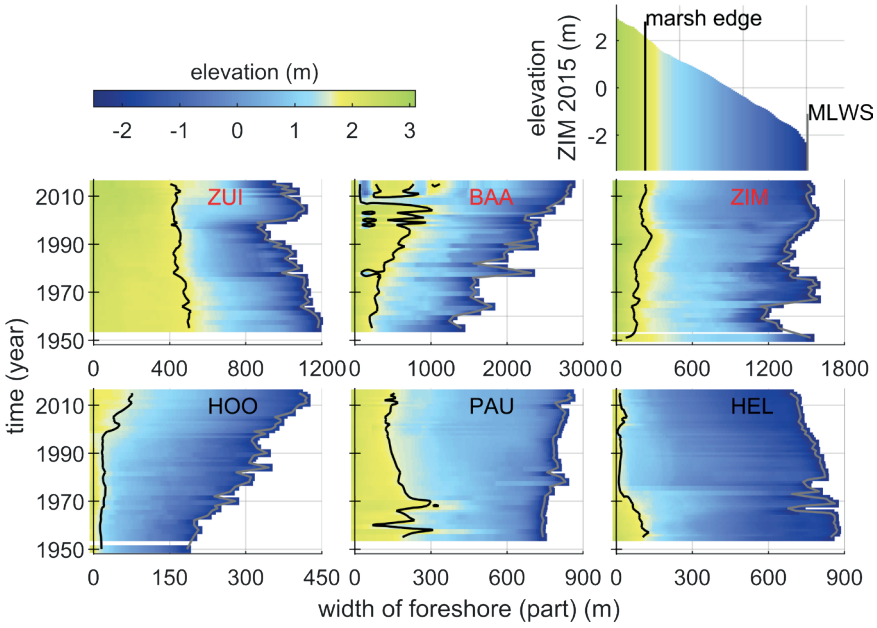

Figure 2.4 | Change in width of foreshore (horizontal axis) in time (vertical axis) for the 6 foreshores studied. The color indicates the elevation with respect to mean sea level, whereas the black line indicates the marsh edge and the gray line mean low water spring (MLWS). Per foreshore, a representative transect is chosen and followed in time, as shown for Zimmerman in 2015 (top right). Abbreviations indicate locations as indicated in Fig. 2.1; red letters highlight exposed sites, while black letters highlight sheltered sites from the prevailing wind direction.

2.3.1.2 | *Spatial variability*

At Zuidgors, the average width of the salt marsh (483m; see Appendix 2.A, table 2.9, for the average width of the vegetated salt marsh and bare tidal flat of all foreshores) was observed to be much smaller than the width of the tidal flat (1116m) (Fig. 2.5). However, the width of the vegetated salt marsh in a single year was highly variable, showing differences of up to 600m over an alongshore salt marsh stretch of 2000m (Fig. 2.5). The most western part of the foreshore at Zuidgors showed less variability in foreshore width compared to the eastern part, probably due to the geographical features surrounding the foreshore. One of the main features is the presence of a channel in front of the foreshore (Fig. 2.1; Fig. 2.3; top panels). The vegetated foreshore part at the eastern side of the center has more landward accommodation space, due to the shape of the dike. Due to the contribution of those boundaries, the spatial variability remained stable (Fig. 2.4; Fig. 2.5). Geographical features like dikes and jetties, did also drive the spatial variability within a single year at the other locations. At Baarland, Zimmermanpolder and Paulinapolder, the salt marsh width was smaller at the alongshore edges of marsh, while being larger at the central part of the marsh due to the recessed dike, similar to Zuidgors. At Hoofdplaat and Hellegat polder jetties and an outflow channel affected the spatial variability of the salt marsh. At Baarland the spatial variability of both the total foreshore and the salt marsh remained small, with some peaks up to a 1000m for the foreshore and hundreds of meters at the salt marsh. The little variability might be caused by a small channel appearing close to the salt marsh edge (Fig. 2.1). At Zimmermanpolder the spatial variability of the salt marsh was approximately 200m, whereas the spatial variability of the total foreshore reached 1200m. The spatial variability of the foreshores at the sheltered shores remained constant (Fig. 2.5), being 300m to 500m for both the total foreshore and salt marsh at Hellegatpolder and Paulinapolder, while both the average width and variability increased at Hoofdplaat (Fig. 2.5).

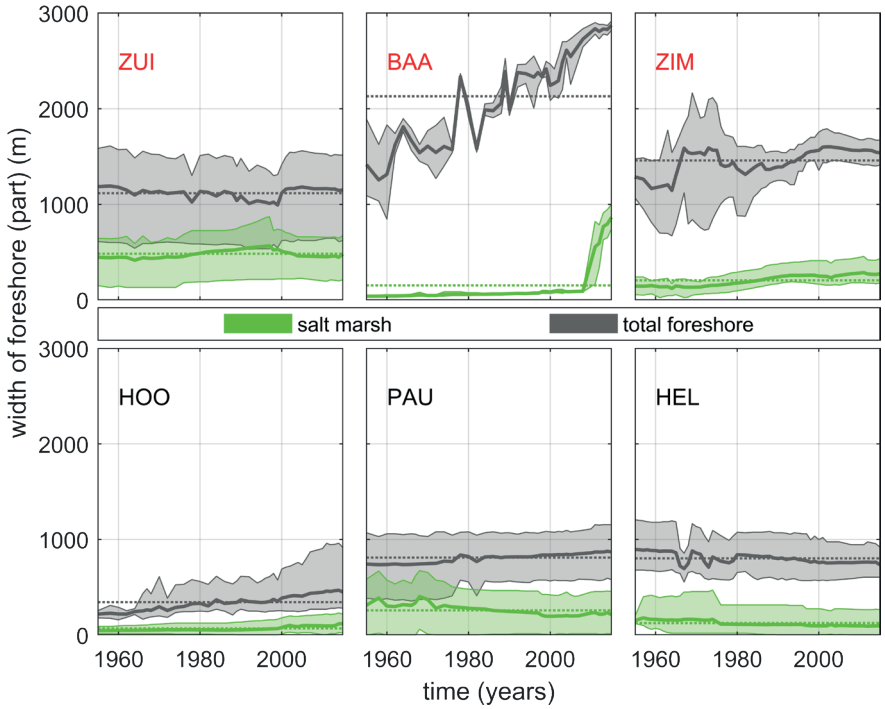

Figure 2.5 | Change in width of the foreshore (vertical axis) over time (horizontal axis) in which distinction is made in salt marsh width (green area) and total foreshore width (gray area) The shading indicates the minimum and maximum width (spatial variability of a single salt marsh), the thick line in the center of the shading indicates the spatial mean width and the dotted line indicates the overall mean width. Abbreviations indicate locations as indicated in Fig. 2.1; red letters highlight exposed sites, while black letters highlight sheltered sites from the prevailing wind direction.

2.3.1.3 | *Spatial versus temporal variability*

The width of transects between MLWS and MHWS of a single foreshore was highly variable, e.g. at Zuidgors ranging between 600m and 1500m (Fig. 2.3). However, the spatial variability remained constant over time, i.e. the range of the width of all transects of a single foreshore remained stable(Fig. 2.5). The spatial variability of the salt marsh at Zuidgors slightly decreased with tens of meters only, this was observed more distinct at the sheltered site Hellegat with approximately 200m, whereas an increasing spatial variability was observed at Hoofdplaat both for the total foreshore and salt marsh. The average total foreshore width increased with 250m, while the variability increased from less than 100m to 600m. Those changes might have been the result of accretion between the jetties and/or changes in the seaward navigation channel. Large differences of spatial variability over time was observed at Zimmermanpolder, in the first decades.

Nevertheless, the variability of the foreshore in a single year decreased from a maximum of 1200m to 260m, while the width of the salt marsh remained constant over time (Fig. 2.5). Most striking was the temporal variability at Baarland, where the total foreshore width increased from approximately 1400m to 2800m and the salt marsh width increased from 40m to 860m, while the spatial variability was small.

In general, the average width of foreshore parts of a single foreshore was larger in space than in time, i.e. the width of the foreshore (parts) remained constant over time while more variation was observed over a single foreshore in a single year (Fig. 2.5). However there were exceptions, the temporal variation at Baarland was larger than the spatial variation, probably due to a small channel in front of the foreshore undershooting MLWS, only appearing in a part of the assessed period. The, in general larger, spatial variability indicated that the alongshore variability of the geometry caused by geographical boundaries (e.g. dikes and channels), was larger than the variability of a single transect influenced by hydrodynamics, morphodynamics and vegetation growth. The latter implies that a large part of the variability of the foreshore geometry captured in a single observation, represents the variability of the width of the foreshore (parts) over the long-term (60 -70 years).

2.3.1.4 | *Exposed shores versus sheltered shores*

The average width of foreshores, parallel to the design wind direction, in the Westerschelde ranged between 344m and 2130m (Fig. 2.5), with an average vegetated part ranging between 7% and 42% of the total foreshore width. The average width of the foreshores at the northern shores (1583m), exposed to the prevailing wind direction, of the Westerschelde was larger than at the southern shores (652m), sheltered from the prevailing wind direction. Therefore the foreshores at the sheltered shores consisted of a steeper gradient, since the width was measured between two vertical positions fixed in time (MHWS and MLWS). The average salt marsh width at the exposed shores was 280m, whereas 151m at the sheltered shores. This is a vegetated part of 18% and 23% respectively. In general the smaller sheltered foreshores showed a smaller marsh width change over the assessed period. However, it appeared that the marsh at the sheltered foreshores were retreating (PAU and HEL) or slightly increasing (HOO). The marshes at the exposed foreshores were relative stable (ZUI) or even expanding (BAA and ZIM), in spite of their location exposed to the prevailing wind direction (Fig. 2.6).

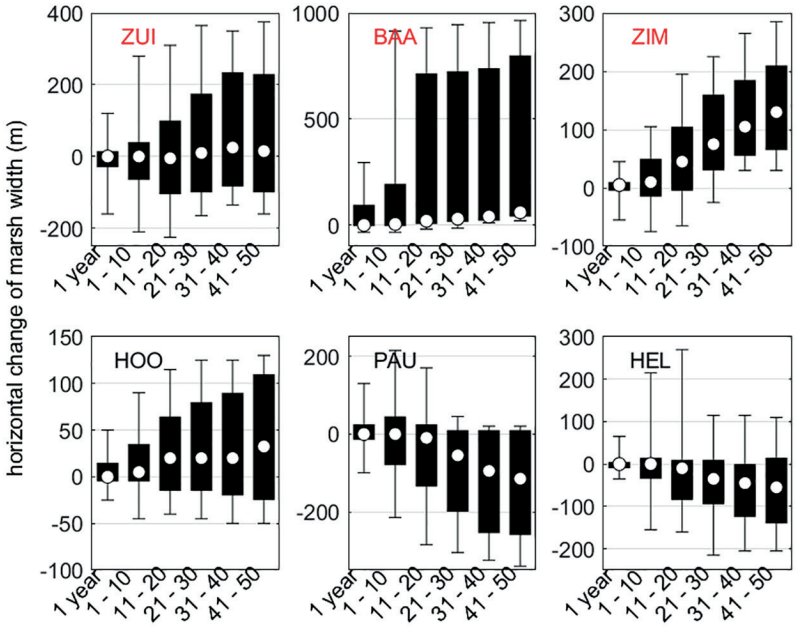

Figure 2.6 | Marsh width change (vertical axis) over a period of a single year, periods between 1 and 10, 11 and 20, 21 and 30, 31 and 40 and 50 years (horizontal axis). The white marker indicates the median, the 10th and 90th percentile are highlighted by the black bar, while the whiskers at the top and bottom of the black bar indicate the maximum and minimum change over a specific period. Abbreviations indicate locations as indicated in Fig. 2.1; red letters highlight exposed sites, while black letters highlight sheltered sites from the prevailing wind direction.

2.3.2 | Long-term wave attenuating capacity

The wave attenuation was calculated for three different scenarios, (1) attenuation under daily conditions over the transects, (2) attenuation under daily conditions over the transects, explicitly accounting for vegetation, (3) attenuation under design conditions over the transects, accounting for broken vegetation (Fig. 2.2). The wave attenuating capacity of a single transect was defined as the smallest value found for the wave attenuation for the assessed period, to indicate the natural capacity of the foreshore, without additional management. Those values for all transects of a single foreshore, result in a characteristic range of the wave attenuating capacity of a single foreshore. The transect with the smallest wave attenuation marks the lower limit of the range.

2.3.2.1 | *Daily conditions*

The range of wave attenuation under daily conditions (scenario 1) was large, between 10% and 100% at the exposed shores and 0% and 100% at the sheltered shores. The large wave attenuation was almost entirely the result of attenuation at the salt marsh. Inclusion of vegetation (scenario 2), representing summer conditions, leads to higher wave attenuation and a lower variability, especially at the foreshores located at the exposed shores. The attenuation ranged between 60% and 100%, with only a single lower peak at Zuidgors and Baarland of approximately 30% to 40%. Under both scenarios for daily conditions, the waves were almost always fully attenuated by the foreshore, probably due to depth-induced wave breaking. Nevertheless, this was at least partly accomplished by the presence of vegetation, stabilizing the profile. The comparison of the wave attenuation for both scenarios under daily conditions indicates that vegetation increased the wave attenuating capacity of the foreshore and decreased the variability of wave attenuating capacity of the foreshore, thereby decreasing the wave load at the dike.

2.3.2.2 | *Design conditions*

Under design conditions, a significant contribution to the wave attenuation was observed for all transects (Fig. 2.7). The largest contribution to wave attenuation under design conditions was observed at foreshores with a wide vegetated part. For foreshores with a relatively small vegetated part, the bare tidal flat was a large contributor to wave attenuation (up to 18%) (Fig. 2.8). In general, a constant baseline attenuation of 2% to 18% was the result of wave attenuation by the tidal flat. Whereas attenuation as a result of the salt marsh was more variable, more or less following the width of the salt marsh. At most foreshores, the spatial variability of the wave attenuation in a single year (spatially; e.g. 5% to 20% at Zuidgors), exceeded the temporal variability of a single transect over the entire measurement period. However, this cannot be adopted as a general rule, e.g. at Baarland the temporal variability was larger than the spatial variability. Moreover, in some years the spatial variability of the wave attenuating capacity could have been neglected, while the temporal variability of a single transect over the assessed period was 20% (comparing a vertical spatial and horizontal temporal cross-section in Fig. 2.7).

A general relation between width of the foreshore and wave attenuation under design conditions was not found. However, when distinguishing the wave attenuation by the vegetated salt marsh and bare tidal flat, a unique relation per foreshore was observed. The wave attenuation of the salt marsh was found to be a function of the width of the salt marsh (Fig. 2.8). The longer the salt marsh, the larger the wave attenuation under design conditions, given a maximum observed marsh length of approximately 1000m.

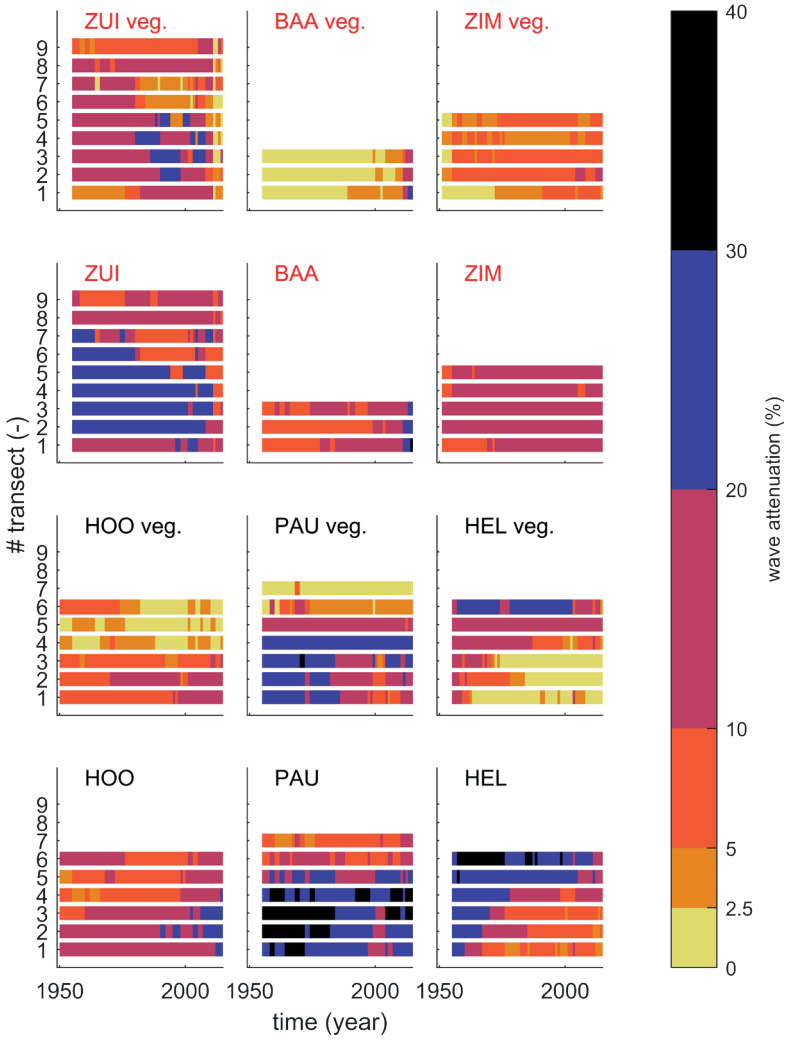

Figure 2.7 | Wave attenuation (i.e. % of incoming wave; indicated by colors) under design conditions (i.e. extreme event statistically occurring once every 10000 years) for both the vegetated part of the foreshore (panels with "veg." behind location name) and the total foreshore. The time is indicated at the horizontal axis, whereas the different transects are presented at the vertical axis. Abbreviations indicate locations as indicated in Fig. 2.1; red letters highlight exposed sites, while black letters highlight sheltered sites from the prevailing wind direction.

A fit of the relation showed a rather strong approximation (R^2: ZUI is 0.61; BAA is 0.99; ZIM is 0.87; HOO is 0.76; PAU is 0.86; HEL is 0.86), with the smallest R^2 at Zuidgors, also indicated by the 95%-confidence interval (Fig. 2.8; coefficients for the linear model y = ax + b are presented in Appendix 2.B, where y is the wave attenuation, x is the vegetated

marsh width and a and b are the linear coefficients). A clear distinction was observed between the foreshores at the exposed and sheltered shores of the Westerschelde. The wave height, water level ratio under extreme conditions was also larger at the sheltered shores, due to slightly lower water levels and larger waves, which might possibly affect the effectiveness of the wave attenuation. The wave attenuation at the sheltered foreshores was larger per meter of salt marsh, despite the shorter width of both the total foreshore and salt marsh. So the effectiveness of wave attenuation under design conditions, per meter marsh width, was observed to be larger for the foreshores with a smaller width.

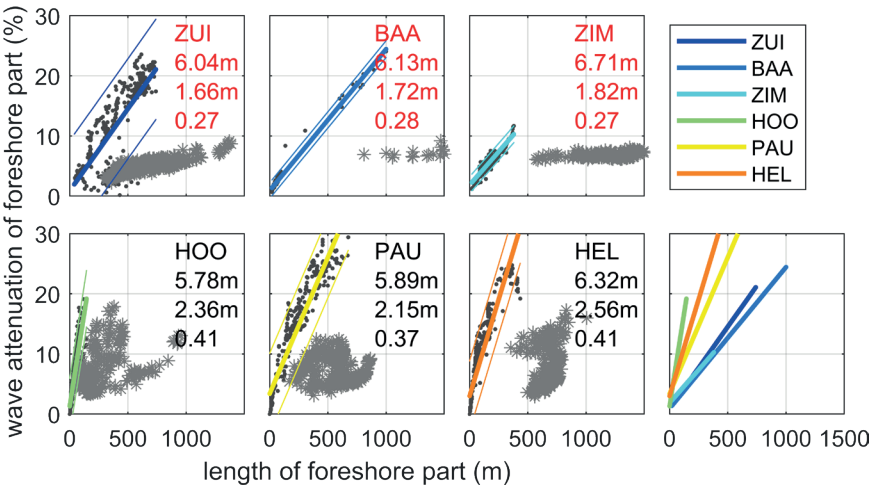

Figure 2.8 | Contribution of both foreshore parts to wave attenuation under design conditions (i.e. extreme event statistically occurring once every 10000 years) for all transects and years. The width of the bare (grey asterisk) and vegetated foreshore (black dot) are indicated at the horizontal axis, their contribution to the wave attenuation under design conditions is plotted at the vertical axis. The colored thick line per panel, indicates the fit of the relation between vegetated foreshore width and wave attenuation and the colored thin lines indicate the 95% confidence interval. Abbreviations indicate locations as indicated in Fig. 2.1; red letters highlight exposed sites, while black letters highlight sheltered sites from the prevailing wind direction. The three numbers in each panel characterize the foreshore, from top to bottom: the extreme water level, extreme wave height and the wave height / water level ratio respectively. All relations are summarized in the bottom right panel.

2.4 | Discussion

The decadal persistence of wave-attenuating ecosystems was identified as key-bottle neck hampering application of intertidal foreshores for coastal protection (Bouma et al., 2014). In this study, the decadal wave attenuating capacity of foreshores under daily and extreme conditions was studied estuarine-wide. The key-findings were: (1) foreshores always contribute to wave attenuation both under daily and design conditions; (2) under daily conditions, vegetation contributes to decreasing wave energy and decreases the variability of incoming wave energy; (3) under design conditions, foreshores located at shores sheltered from the prevailing wind direction were more efficient in wave attenuation than foreshores located at exposed shores, which might be related to the geometry of the foreshore. Moreover, the bare tidal flat caused a baseline wave attenuation, while the additional contribution of the vegetated salt marsh appeared to be related to marsh width: the larger the marsh width, the larger the wave attenuation.

2.4.1 | Contribution of foreshores to coastal safety

The protective value of (vegetated) foreshores by wave attenuation has been proven in recent years, even under extreme conditions (Barbier et al., 2008; Gedan et al., 2011; Shepard et al., 2011; Möller et al., 2014). However, the protective value depends on the bio-geomorphological settings of the foreshore (Vuik et al., 2018b), which vary over time (Bouma et al., 2014). Based on long-term field data and modelling, this study emphasizes the presence of an added value for coastal safety under all bio-geomorphological settings present in an entire estuary (e.g. 6 foreshores, a total of 36 transects, over 65 years). Whereas previous studies calculate the wave attenuating capacity for a single setting, multiple settings not using long-term field measurements and/or the short-term (e.g. Bouma et al., 2010; Yang et al., 2012; Möller et al., 2014; Vuik et al., 2016), this study quantifies the range of wave attenuating capacity under different scenarios for salt marsh settings measured in the field over the long-term. Moreover a minimum wave attenuating capacity was observed from 6% to 12% at the exposed northern shores and 3% to 27% at the sheltered southern shores under design conditions (table 2.3; Fig. 2.8). Even wave attenuation under daily conditions always benefits from the presence of vegetation by increasing the wave attenuating capacity and narrowing the bandwidth of incoming waves, decreasing the wave load at the dike continuously over 65 years (Fig. 2.9).

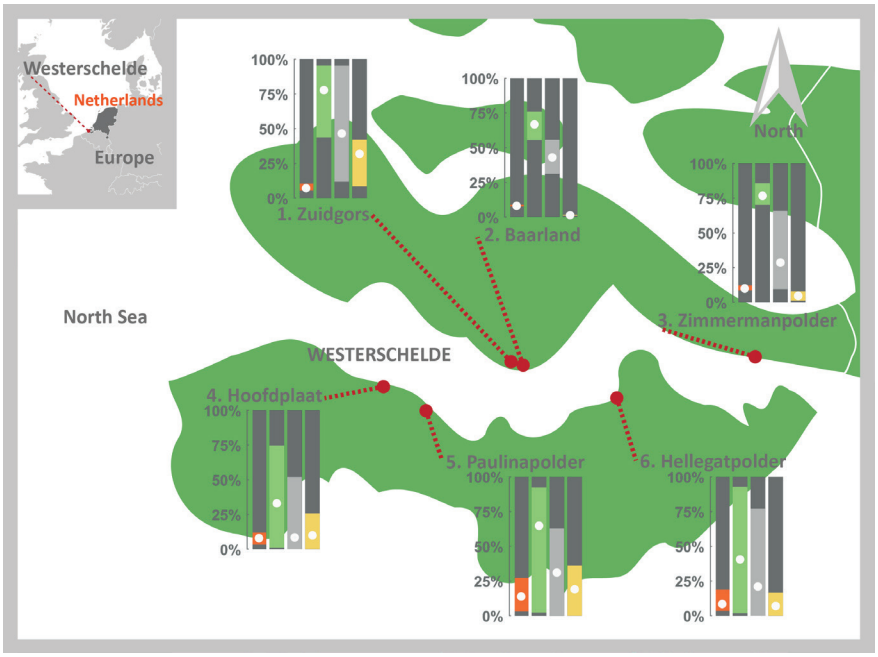

Figure 2.9 | Summary of the range of wave attenuation averaged per foreshore and the range of width of the vegetated salt marsh. Spatial mean (white dot) and variability (minimum and maximum indicated by the bar) of the wave attenuating capacity under design conditions (orange), daily conditions with explicitly accounting for vegetation (green) and daily conditions without vegetation (grey) and the related coverage of vegetation relative to the total length of the foreshore (yellow).

Only the existence of the vegetated foreshores over a period of 60 to 70 years, already proves the resilience of those ecosystems to external (anthropogenic) influences. Moreover, the width of the foreshore (parts) specifically assessed in this study remained quite similar over time (Fig. 2.5). The resulting wave attenuation varied over space (transects) and time (development over the assessed period), but delivers a continuous contribution to the wave attenuation (Fig. 2.9). Nevertheless, the development of foreshores might be less stable in other estuaries, e.g. rapidly expanding near the mouth of the Yangtze river, China (Yang et al., 2001; Zhang et al., 2004), or retreating foreshores affecting the contribution to wave attenuation. Results of the current study delivers prove and builds upon previous studies emphasizing the instantaneous contribution of foreshores to coastal protection (Turner et al., 2007; Kirwan et al., 2010; Gedan et al., 2011). Insights in short to medium-term (days to several years) vegetation establishment and growth, defining the marsh edge and partly the wave attenuating capacity, have been obtained (Bouma et al., 2016; Willemsen et al., 2018; Poppema et al., 2019). However long-term limits (design period) of vegetation growth defining the local range of the width of

the vegetated foreshore need to be studied, to exploit the relation between the width of the vegetated foreshore and wave attenuation (Fig. 2.8). This might result eventually in parameter values contributing to stable practical implementation of foreshores as add-on in coastal protection schemes and managing the foreshore to supply, maintain and possibly increase the minimum wave attenuating capacity.

2.4.2 | The location of the marsh edge

This study highlights the importance of the boundary between the bare tidal flat and vegetated salt marsh, since both foreshore parts have a different role in attenuating waves under design conditions. The tidal flat causes a baseline wave attenuation, while unique linear relations were found between the marsh width and the wave attenuation. In this study, the location of the seaward marsh edge was based on tidal characteristics. However, the marsh edge is determined by multiple bio-physical processes: it has been hypothesized that the location of the marsh edge is driven by both bed level change and inundation period (Balke et al., 2016; Bouma et al., 2016). This might lead to a marsh edge, slightly off MHWN. Moreover, it is assumed that the marsh edge instantly replies to a changing morphology, which is not possible due to a time lag between bio-physical feedback mechanisms (Poppema et al., 2019). However, field measurements on vegetation presence were not available for all the years. So a general tidal characteristic was assumed, similar to previous studies (McKee and Patrick, 1988; Bakker et al., 2002; D'Alpaos et al., 2007; Doody, 2007; Van der Wal et al., 2008). It is expected that this does not or only slightly affect the wave attenuating capacity, since the marsh edge expands or retreats only meters to tens of meters over a period of a single to a few years (Van der Wal et al., 2008). So it might be expected that the relation between vegetation width and wave attenuation becomes even more pronounced when using a more precise location of the marsh edge.

By comparing wave attenuation between scenario 1 (excluding vegetation) and scenario 2 (explicitly accounting for vegetation), the increasing contribution of vegetation presence was assessed. A clear bandwidth of the wave attenuating capacity was observed with and without vegetation (Fig. 2.9). Increasing presence of vegetation resulted in an increased maximum wave attenuating capacity at all assessed foreshores. Moreover, at the northern shores the minimum wave attenuating capacity increased as well, thereby decreasing the uncertainty of the wave attenuating capacity due to the presence of vegetation. The latter, probably due to the absence of the very short (vegetated) foreshore parts at the northern shores. The wave attenuating capacity of the short foreshores occurring at the southern shores, might be less dominated by presence of vegetation.

2.4.3 | Wave attenuating capacity of a foreshore profile

The contribution of the foreshore to water safety is determined by the foreshore bathymetry and (state of the) vegetation (Vuik et al., 2018b). However, both bathymetry and vegetation cover are changing over time and space, due to naturally occurring bio-physical dynamics (Bouma et al., 2014). Bed level change and inundation time determine the cross-shore location of the marsh edge (Bouma et al., 2014; Balke et al., 2016), which can change several hundreds of meters over the assessed period of 60 to 70 years, but only tens of meters over a period of multiple years. The long-term change has been observed to change the wave attenuation of a single foreshore transect.

The cross-shore location of the marsh edge is known to show cyclic alternations between landward retreat and seaward expansion (Allen, 2000; Singh Chauhan, 2009). Consequently, implying that the minimum and maximum wave attenuating capacity might be found by knowing the extremes of the cyclic behavior. However, cyclic alternations have not been observed in this study. Moreover, all foreshores have location-specific parameters in addition to the width of the vegetated foreshore affecting the wave attenuating capacity. Yet, the width of the salt marsh determines the major part of the wave attenuating capacity and takes into account local settings when zooming in on a single foreshore by the steepness of the relation (Fig. 2.8).

Differences in wave attenuation of foreshore transects were observed between foreshores located at the exposed northern and sheltered southern shores (table 2.3; Fig. 2.8). The wave attenuating capacity was larger at the exposed shores (table 2.3), although the effectivity (i.e. wave attenuation per meter foreshore) was larger at the sheltered shores (Fig. 2.8). This might be explained by the shape of the foreshore profile, which is shorter and consequently steeper at the southern shores. Moreover, geographic features as (maintained) channels and landward dikes are hard boundaries affecting the shape of the profile. The wave height/water depth - relation under design conditions is larger at the southern shores, locally resulting in a larger impact of the bottom on the wave attenuation, as studied by Maza et al. (2015). Contrasting with the study of Maza et al. (2015), currents were not included, although they might affect wave attenuation over a vegetated area. However, due to the geographical boundaries (e.g. dikes, jetties) in the Westerschelde estuary surrounding the studied foreshores, it was assumed that currents have a minor influence. However, to our knowledge, experiments including currents with extremes close to parameter values in the current study (water levels up to 6.71m at the boundary and 4.47m at the marsh edge and wave heights up to 2.56m) are not available. Nevertheless, to better understand the long-term wave attenuating capacity of foreshores under extreme conditions it is recommended to study the influence of currents on long-term wave attenuating under extreme conditions at different field sites.

The foreshore is shaped due to exposure to wind direction, with the southern shores more sheltered to the dominant wind direction (Callaghan et al., 2010), although foreshores at the southern shores are exposed to high waves more often (i.e. largest average wave heights) and are exposed to the longest fetches (Van der Wal et al., 2008). So, the steep and short foreshores at the southern shores sheltered from the prevailing wind direction are exposed to the on average largest waves and longest fetches, shaping these foreshores. Regardless the vegetated part of those foreshores are highly effective in attenuating waves, more effective than the northern foreshores exposed to the dominant wind direction with smaller wave heights, wave height / water depth - relation and fetch. This implies the existence of a feedback mechanism between hydrodynamics, foreshore shape and wave attenuation. To better understand the feedback between hydrodynamics (currents and waves), long-term morphology, ecology and wave attenuation on the spatial scale of a landscape, a process-based 2-dimensional (depth-averaged) or 3 dimensional model can provide insights in the dynamics of the foreshore as a whole. Moreover the long-term wave attenuating capacity of the foreshore under a range of hydrodynamic conditions can be studied.

2.4.4 | Implications for global application of nature based flood defenses

Nature based flood defenses (NBFD) are gaining ground globally (Cheong et al., 2013; Temmerman et al., 2013). Although the area of vegetated foreshores declines (e.g. Valiela et al., 2001), the worldwide occurrence of both mangroves and salt marshes is large (Giri et al., 2011; Mcowen et al., 2017). A stable vegetated foreshore contributes to coastal safety under design conditions. By combining an already existing foreshore with a landward dike, or encourage the growth of a vegetated foreshore in front of an already existing dike, existing infrastructure can be more efficiently utilized for coastal protection. By combining previous literature and the knowledge gained in the current study a contribution can be made to the design and maintenance of hybrid coastal defense structures, which is a next step in implementing NBFD. This hybrid coastal protection infrastructure can benefit from the knowledge gained in this study. The protective value of the already present foreshore or the needed width of the vegetated foreshore under extreme conditions can be estimated, and with that the increase of the dike height that might be prevented. The natural variability of the marsh width over a specific period (Fig. 2.6), indicates the long-term stability and instantaneous (1 year) changes. When using foreshores as coastal defense, the effect of too large long-term variability on wave attenuation might be counteracted by maintenance. By using the relation of the range of wave attenuation under different scenarios and the foreshore width, quantified in the current study, one might estimate the added value of maintaining a certain foreshore width. However, accommodation space, which should

not be accounted for in the minimum wave attenuating capacity of the foreshore, is needed for instantaneous changes driven by e.g. extreme weather events. Maintaining vegetated foreshores to use their wave attenuating capacity, sustains the ecosystem services provided as well. Moreover, by stimulating the growth and expansion of existing, realigned and new vegetated foreshores, ecosystem services such as habitat provision, food production, space for recreation and accessibility over water (e.g. Barbier et al., 2010) might expand as well. Although the precise relation between vegetated foreshore width and wave attenuation under extreme conditions is location-specific, this study already gives insights in the bandwidth of this linear relation and thereby an estimate of the value for coastal protection.

2.5 | Conclusions

Bathymetrical data was analyzed to assess the variability of the geometry of foreshores. This data was combined with bio-physical parameters to calculate the wave attenuation at six study sites in the Westerschelde, the Netherlands, over a period of 60 to 70 years, which is longer than the design period of hard coastal protection structures. Six foreshores were analyzed, three at the northern shores exposed to the prevailing wind direction and three at the southern shores sheltered from the prevailing wind direction of the estuary. A clear distinction was applied to separate the bare tidal flat and vegetated salt marsh, allowing to explicitly study the contribution of the vegetated foreshore (i.e. the salt marsh). The foreshores were assessed to unravel the key question of this study: what are the dynamics of foreshores in an estuary over a decadal time-scale and to what extent can foreshores safely act as additional defense measures?

The total foreshore width at the exposed shores appeared to be longer than at the sheltered shores, resulting in steeper profiles at the sheltered shores. In general, the mean value and the temporal variability of the foreshore width and marsh width remained relatively constant over time. Although the foreshore width remained relatively constant, the width of the salt marsh did not follow the dynamics of the total width of the foreshore at the individual transects. In general, the temporal variability of the salt marsh width increased in the first decades, but flattens subsequently, indicating a constant variability of the width over the long-term. The spatial variability of the foreshore geometry was observed to be larger than the temporal variability, implying that a large part of the variability captured in a single observation in time, might represent the variability of the width of the foreshore (parts) over the long-term (60-70 years).

The vegetation present at the foreshore decreased the variability of the wave attenuation under daily conditions, thereby increasing the reliability of the contribution of the

foreshore to coastal safety. A continuous contribution to the coastal safety was found under design conditions, decreasing the wave load at the landward dike. A clear distinction was observed between the foreshores at the exposed northern and sheltered southern shores of the Westerschelde. The wave attenuation at the sheltered shores was larger per meter of salt marsh, despite the shorter width of both the total foreshore and salt marsh. So the long-term effectiveness of wave attenuation under design conditions (i.e. wave attenuation per meter of vegetated salt marsh) was observed to be larger for the foreshores with a smaller width and steeper profile. Nevertheless, the total wave height attenuated over the full salt marsh was larger at the marshes with a larger width at the exposed northern shores. In general, the tidal flat caused a baseline wave attenuation under all circumstances, while a linear relation was found between the wave attenuation and the width of the salt marsh, given a maximum observed marsh length of approximately 10000m. The longer the vegetated salt marsh, the larger the wave attenuation. The relations found, valid for an entire foreshore, can contribute to designing hybrid structures for coastal defense.

Acknowledgements

This work is part of the research program BE SAFE, which is financed by the Netherlands Organization for Scientific Research (NWO) (grant 850.13.010). Additional financial support has been provided by Deltares, Boskalis, Van Oord, Rijkswaterstaat, World Wildlife Fund, and HZ University of Applied Science. Bas W. Borsje was supported by the Netherlands Organization for Scientific Research (NWO-STW-VENI; 4363). Data and scripts in support of this manuscript are available at https://doi.org/10.4121/uuid:4c25347f-f71e-466b-be3c-1fe8f8d8784c.

Appendix 2A

Table 2.3 | Marsh width change over a period of a single year, periods between 1 and 10, 11 and 20, 21 and 30, 31 and 40 and 50 years, for Zuidgors.

Zuidgors (ZUI)	Median (m)	Minimum (m)	Maximum (m)	10th percentile (m)	90th percentile (m)
1 year	0	-160	120	-30	15
1 – 10 years	0	-210	280	-65	40
11 – 20 years	-5	-225	310	-105	100
21 – 30 years	10	-165	365	-100	175
31 – 40 years	25	-135	350	-84	235
41 – 50 years	15	-160	375	-100	230

Table 2.4 | Marsh width change over a period of a single year, periods between 1 and 10, 11 and 20, 21 and 30, 31 and 40 and 50 years, for Baarland.

Baarland (BAA)	Median (m)	Minimum (m)	Maximum (m)	10th percentile (m)	90th percentile (m)
1 year	0	-35	295	-5	95
1 – 10 years	5	-35	915	-5	194
11 – 20 years	50	-20	930	5	715
21 – 30 years	30	-15	945	15	725
31 – 40 years	40	10	955	20	740
41 – 50 years	60	20	965	40	800

Table 2.5 | Marsh width change over a period of a single year, periods between 1 and 10, 11 and 20, 21 and 30, 31 and 40 and 50 years, for Zimmermanpolder.

Zimmermanpolder (ZIM)	Median (m)	Minimum (m)	Maximum (m)	10th percentile (m)	90th percentile (m)
1 year	5	-55	45	-5	10
1 – 10 years	10	-75	105	-15	50
11 – 20 years	45	-65	195	-5	105
21 – 30 years	75	-25	225	30	160
31 – 40 years	105	30	265	55	185
41 – 50 years	130	30	285	65	210

Table 2.6 | Marsh width change over a period of a single year, periods between 1 and 10, 11 and 20, 21 and 30, 31 and 40 and 50 years, for Hoofdplaat.

Hoofdplaat (HOO)	Median (m)	Minimum (m)	Maximum (m)	10th percentile (m)	90th percentile (m)
1 year	0	-25	50	-5	15
1 – 10 years	5	-45	90	-5	35
11 – 20 years	20	-40	115	-15	65
21 – 30 years	20	-45	125	-15	80
31 – 40 years	20	-50	125	-20	90
41 – 50 years	33	-50	130	-25	110

Table 2.7 | Marsh width change over a period of a single year, periods between 1 and 10, 11 and 20, 21 and 30, 31 and 40 and 50 years, for Paulinapolder.

Paulinapolder (PAU)	Median (m)	Minimum (m)	Maximum (m)	10th percentile (m)	90th percentile (m)
1 year	0	-100	130	-15	25
1 – 10 years	0	-215	215	-80	45
11 – 20 years	-10	-285	170	-135	25
21 – 30 years	-55	-305	45	-200	10
31 – 40 years	-95	-325	20	-255	10
41 – 50 years	-115	-340	20	-260	10

Table 2.8 | Marsh width change over a period of a single year, periods between 1 and 10, 11 and 20, 21 and 30, 31 and 40 and 50 years, for Hellegatpolder.

Hellegatpolder (HEL)	Median (m)	Minimum (m)	Maximum (m)	10th percentile (m)	90th percentile (m)
1 year	0	-35	65	-10	5
1 – 10 years	0	-155	215	-35	15
11 – 20 years	-10	-160	270	-85	10
21 – 30 years	-35	-215	115	-95	10
31 – 40 years	-45	-205	115	-125	0
41 – 50 years	-55	-205	110	-140	15

Table 2.9 | Average width (m) of the marsh and bare tidal flat over the assessed period and all transects per foreshore.

Location	Average width marsh (m)	Average width bare tidal flat (m)
Zuidgors (ZUI)	483	634
Baarland (BAA	152	1977
Zimmermanpolder (ZIM)	205	1253
Hoofdplaat (HOO)	69	275
Paulinapolder (PAU)	258	552
Hellegatpolder (HEL)	125	677

Appendix 2B

Table 2.10 | Coefficients for determining relation between the vegetated marsh width and wave attenuation. The relation can be determined using y = ax + b, where a and b are linear coefficients, y is the wave attenuation and x is the width of the marsh.

Location	Coefficient a	Coefficient b
Zuidgors (ZUI)	0.0273	0.8726
Baarland (BAA	0.0235	0.9051
Zimmermanpolder (ZIM)	0.0222	1.8731
Hoofdplaat (HOO)	0.1232	1.3113
Paulinapolder (PAU)	0.0453	3.3875
Hellegatpolder (HEL)	0.0643	3.0042

3

Quantifying bed level dynamics at the transition of tidal flat and salt marsh: can we understand the lateral location of the marsh edge?

Published as: Willemsen, P. W. J. M., Borsje, B. W., Hulscher, S. J. M. H., Van der Wal, D., Zhu, Z., Oteman, B., Evans, B., Möller, I., Bouma, T. J. (2018). Quantifying Bed Level Change at the Transition of Tidal Flat and Salt Marsh: Can We Understand the Lateral Location of the Marsh Edge? *Journal of Geophysical Research: Earth Surface, 123*(10), 2509-2524.

Abstract

Bed level dynamics at the interface of the salt marsh and tidal flat have been highlighted as a key factor connecting the long-term biogeomorphological development of the marsh to large-scale physical forcing. Hence, we aim to obtain insight into the factors confining the location of the marsh edge (i.e., boundary between tidal flat and salt marsh). A unique data set was collected, containing measurements of daily bed level changes (i.e., integrative result of physical forcing and sediment properties) at six intertidal transects in the North Sea area. Moreover, various biophysical parameters were measured, such as sediment characteristics, waves, inundation time, and chlorophyll-*a* levels. The data show that both bed level change and waves decreased from the lower intertidal flat toward the marsh edge and further diminished inside the marsh. However, no direct general relation was found between local waves and bed level change. Bed level change inside the marsh was always small, regardless of local wave energy. By combining the data sets, we demonstrate that the location of the lower marsh edge is restricted by two interacting factors: inundation time and bed level change. For vegetation establishment to withstand longer inundation stress, which slows down plant growth, more stable bed levels are required so that plants are not heavily disturbed. Conversely, to withstand more dynamic bed levels that disturbs plant growth, lower inundation stress is needed, so that plants grow fast enough to recover from the stress. The results suggest that bed level change, in addition to inundation stress, is important in determining the position of the marsh edge.

3.1 | Introduction

Tidal flats and salt marshes are widespread co-evolving ecosystems in the coastal region (Fagherazzi et al., 2006; Mcowen et al., 2017). They provide multiple ecosystem services like carbon sequestration (Chmura et al., 2003; Duarte et al., 2013), filtering water (Nelson and Zavaleta, 2012), providing a habitat and nursery ground (Irmler et al., 2002; Van Eerden et al., 2005), and improving coastal safety by stabilizing the bed and attenuating waves (Temmerman et al., 2013; Vuik et al., 2016). Especially the contribution of salt marshes to coastal defense by attenuating waves even under extreme conditions has been increasingly recognized and assessed in recent years (Barbier et al., 2008; Gedan et al., 2011; Shepard et al., 2011; Moller et al., 2014). This protective value benefits from salt marshes being able to counteract both sea level rise (SLR) and land subsidence by sediment accretion (Kirwan et al., 2016). However, it has been noted that large-scale application of salt marshes for coastal defense requires in-depth understanding of their long-term lateral dynamics and persistence (Bouma et al., 2014).

Lateral dynamics determine the cross-shore location of the marsh edge and thereby the width of a salt marsh. In many locations, the marsh edge shifts up to several meters per year and is known to show cyclic alternations between erosion and expansion on a decadal or longer timescale (Allen, 2000; Van der Wal et al., 2008; Singh Chauhan, 2009). The switch between these two phases is determined by two key processes: initiation of marsh erosion (i.e., start of retreat) and seedling establishment (i.e., start of expansion) (Bouma et al., 2016). Whereas the rate of marsh erosion is determined by frequent flooding and wave events (Fagherazzi, 2014; Wang et al., 2017), the onset of erosion may originate from a discontinuity by having a stable marsh-bed level platform next to a dynamic tidal flat, where the bed level can vary greatly over time (Bouma et al., 2016). The process of seedling establishment at the tidal flat is mainly affected by the physical parameters: relative elevation in the tidal frame, determining the inundation frequency and period, possibly drowning seedlings (Balke et al., 2016), and bed level dynamics, possibly uprooting and/or burying seedlings (Hu et al., 2015b). This raises the question if the location of the marsh edge may be determined by the bed level dynamics and inundation period at the tidal flat fronting the marsh edge.

Bed level dynamics is an interesting parameter in that it integrates a suite of physical and biological processes on the tidal flat and salt marsh: wave and/or tidal forcing exerting bed shear stresses (Friedrichs, 2011; Green and Coco, 2014; Hunt et al., 2015; Hu et al., 2017), grain size properties determining the critical erosion threshold (Grabowski et al., 2011; Deegan et al., 2012), bioturbation and bio-aggregation (seasonally) modifying the critical erosion threshold of the bed (Andersen et al., 2005; Murray et al., 2008; Corenblit et al., 2011), and external sediment supply controlling sedimentation rates

(Mariotti and Fagherazzi, 2010; Hu et al., 2015c; Willemsen et al., 2016). By affecting both cliff initiation and seedling establishment, short-term bed level dynamics (i.e., seasonal and shorter changes in sediment elevation) at the tidal flat in front of a marsh has been indicated as the driving mechanism that connects long-term cyclic behavior of the marsh to large-scale physical forcing (Bouma et al., 2016). However, to date, only very few measurements of the short-term bed level dynamics exist nearby the tidal flat - salt marsh transition. Previous studies have mainly focused on the occurrence of seasonality in sedimentation and erosion (e.g. Herman et al., 2001), and in hydrodynamic forcing (Callaghan et al., 2010). Hence we aim to quantify the bed level dynamics at the marsh edge across a number of contrasting locations.

Whereas long-term bed level dynamics, i.e. accretion and erosion of the top tens of centimeters of the bed, have been studied extensively using a suite of methods with a temporal resolution of weeks to months (e.g., erosion pins (Stokes et al., 2010), a steel reference plate (Andersen et al., 2006) and accretion poles (O'Brien et al., 2000)), methods for monitoring daily-bed level changes, such as the PEEP system (Lawler, 2008) remain scarcely applied due to high costs (for review see Hu et al., 2015a). The Surface Elevation Dynamic (SED) sensor was developed and tested as affordable way to collect long-term measurements of daily bed level dynamics (Hu et al., 2015a). Hu et al. (2015a) showed the principle, accuracy and application of these sensors for understanding the morphodynamics of tidal flats.

To obtain a better understanding of the factors confining the location of the marsh edge, and if bed level dynamics and inundation period may be important in this, we (1) deployed SED-sensors at the transition between salt marsh and tidal flat for a range of contrasting locations, and (2) coupled these SED-measurements to a range of biophysical parameters such as sediment characteristics, wind waves, inundation time and chlorophyll-*a* levels of the sediment (indicating diatoms).

3.2 | Materials and Methods

3.2.1 | Study sites

The study sites are situated around the North Sea, with sites in the Westerschelde, Wadden Sea and Thames estuary (Fig. 3.1) and comprise measurements from different field studies. The four main study sites are located in the Westerschelde. The Westerschelde estuary (51°20'N; 4°E; Fig. 3.3.1), is located in the south-western delta of the Netherlands (Fig. 3.1). The Westerschelde is a mesotidal to macrotidal estuary and is tide-dominated, having a semi-diurnal tide (Baeyens et al., 1997). Salinity at the mouth of the Westerschelde (near Vlissingen) is around 25 psu and around 10 psu at the Dutch-Belgian border, increasing during summer and decreasing during winter (Damme et al., 2005). The prevailing wind direction in the Westerschelde estuary is south-west, measured by the KNMI (Royal Netherlands Meteorological Institute) at Hansweert (Fig. 3.1). The sites at the northern shore are exposed and the sites at the southern shore are more sheltered from the prevailing wind (Callaghan et al., 2010). Four sites in the Westerschelde were studied, two at the northern shore of the estuary at approximately 20 km and 50 km from the mouth and two at the southern shore at approximately 15 and 27 km from the mouth (Fig. 3.1; Table 3.1). The two most western located study sites were saline during the most recent measurements (approximately 20-25 psu), while the eastern study sites were mostly brackish (approximately 15-20 psu) (Damme et al., 2005). The field sites in the Westerschelde were 1. Zuidgors (E), 2. Zimmermanpolder (E), 3. Paulina (S) and 4. Hellegat (S), with "E" indicating exposed and "S" indicating sheltered from the prevailing wind (Fig. 3.1). The spring tidal range increases from approximately 4.4m at the most western study site to 5.5m at the most eastern study site (Van der Wal et al., 2008). Pioneer species occurring at the different study sites were mainly perennial common cord grass (*Spartina anglica*) and the annual glasswort (*Salicornia spp*.). Common saltmarsh grass (*Puccinellia maritima*), annual seablite (*Suaeda maritima*), and sea aster (*Aster tripolium*) vegetation occurs higher in the marsh. The most eastern marsh (upstream), 2. Zimmermanpolder (E), has a more brackish environment. Seaside bulrush (*Bolboschoenus maritimus*) and common reed (*Phragmatis australis*), occurs apart from Spartina (Van der Wal et al., 2008).

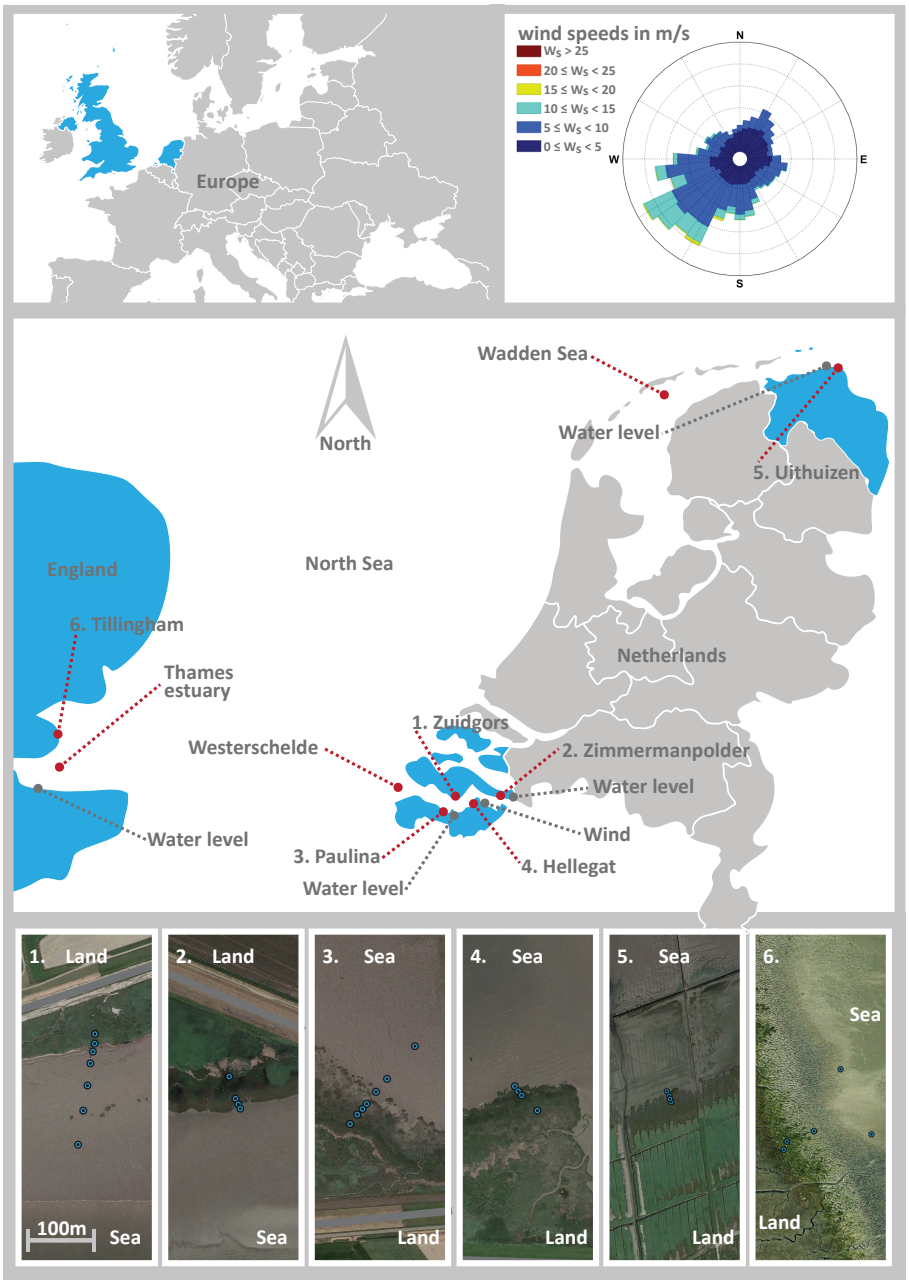
Europe
wind speeds in m/s
$W_S > 25$
$20 \le W_S < 25$
$15 \le W_S < 20$
$10 \le W_S < 15$
$5 \le W_S < 10$
$0 \le W_S < 5$
N
E
S
W
North
Wadden Sea
Water level
5. Uithuizen
England
North Sea
6. Tillingham
Thames estuary
Netherlands
1. Zuidgors
Westerschelde
2. Zimmermanpolder
Water level
Wind
3. Paulina
4. Hellegat
Water level
Water level
1. Land
Sea
100m
2. Land
Sea
3. Sea
Land
4. Sea
Land
5. Sea
Land
6.
Sea
Land

Figure 3.1 | Overview of the study sites in the Westerschelde and Wadden Sea in the Netherlands, and the Thames Estuary in England, Europe (top panels). Wind speeds (top right panel) were measured in 2015 and 2016 at Hansweert (grey dot indicated by wind, at the mid panel), by the KNMI (Royal Netherlands Meteorological Institute). Two sites in the Westerschelde were located at the most wind exposed northern shore sites (1. Zuidgors (E) and 2. Zimmermanpolder (E)) and two sites at the more sheltered southern shore (3. Paulina (S) and 4. Hellegat (S)). The 5th and 6th site were located in the Wadden Sea (5 .Uithuizen) and Thames estuary (6. Tillingham), respectively. The measurement points at all sites were allocated at the interface of the tidal flat and salt marsh (bottom panels), approximately perpendicular to the water line. Seven measurement points were located at the most Western sites (1. Zuidgors (E) and 3. Paulina (S)) and four measurement points at the most Eastern sites (2. Zimmermanpolder (E) and 4. Hellegat (S)) in the Westerschelde. At 5. Uithuizen (Wadden Sea) four measurement points were used for collecting data, while at 6. Tillingham (Thames estuary) five measurement points were used for collecting data. Additional water level data (grey dots indicated with water level), representing the tidal changes, were obtained from Rijkswaterstaat (Dutch department of waterways and public works), at Terneuzen (western site) and Bath (eastern site) in the Westerschelde and Uithuizerwad in the Wadden Sea. Water level data for Tillingham in the Thames estuary was obtained from the British Oceanographic Data Centre (BODC), at Sheerness. (source aerial imagery: google earth)

Table 3.1 | Locations of the study sites and periods in which bed level data was collected.

Study site	Location	Start data collection	End data collection	Locations relative to marsh edge (negative is landward) [m]
1 Zuidgors (E)	51°23'21.95"N, 3°50'7.51"E; Westerschelde	October 2015	October 2016	-20; -5; 5; 25; 60; 100; 155
2 Zimmerman-polder (E)	51°24'8.05"N, 4°10'32.15"E; Westerschelde	February 2015	June 2016	-50; -15; -5; 5
3 Paulina (S)	51°20'59.73"N, 3°43'3.37"E; Westerschelde	February 2015	June 2016	-42.5; -25.5; -17.5; -2.5; 22.5; 47.5; 127.5
4 Hellegat (S)	51°21'59.33"N, 3°56'44.67"E; Westerschelde	December 2014	Augustus 2016	-50; -15; -5; 5
5 Uithuizen	53°27'24.57"N, 6°39'32.07"E; Wadden Sea	March 2015	March 2016	-15; -10; -5; 2.5
6 Tillingham	51°41'40.37"N, 0°56'32.80"E; Thames Estuary	July 2015	July 2016	-5; 7.5; 52.5; 125; 130

To generalize physical mechanisms driving the marsh edge, the bed level dynamics of the Wadden Sea (5. Uithuizen) and Thames estuary (6. Tillingham) were studied accordingly. The Wadden sea is a mesotidal to macrotidal estuary (Dieckmann et al., 1987), with a tidal range of about 4.0m near the study site. Vegetation species occurring at study site 5. Uithuizen, were the pioneer plants: common glasswort (*Salicornia europaea*), common salt marsh grass (*Puccinellia maritima*), common cordgrass (Spartina anglica) and the

more mature plant species landwards: couch grass (*Elymus athericus*), sea aster (Aster tripolium) and seepweed (*Suaeda maritima*). The Thames estuary is a macrotidal estuary, with a tidal range of about 4.8m near the study site (Reed, 1988). Vegetation species occurring at study site 6. Tillingham were the pioneer species common saltmarsh-grass (*Puccinellia maritima*), common cordgrass (*Spartina*) and common glasswort (*Salicornia*) and the higher marsh species sea purslane (Atriplex portulacoides), sea aster (*Aster Tripolium*) and couch grass (*Elymus athericus*) (Rupprecht et al., 2015).

3.2.2 | Field data collection and laboratory analysis: bed level dynamics, sediment characteristics waves, inundation time and diatoms

Bed level dynamics were collected at all six study sites using the recently developed SED-sensors (Hu et al., 2015a; Hu et al., 2017). The data was collected over a period of two years (Table 3.1). The stand-alone SED-sensor was developed to continuously obtain high resolution temporal bed level data. The measuring section of the SED-sensor consists of 200 adjacent light sensitive cells (i.e. phototransistors) of 2 mm, resulting in a measurement domain of 400mm. When installing the SED-sensor in the field, half of the measuring section was below the bed level and the other half was above the bed level. The instrument was installed firmly in the sediment, since the total length below the bed level was approximately 70 cm. Bed level measurements were taken every 30 minutes. The SED-sensor was used before to obtain bed level dynamics at a tidal flat (Hu et al., 2015a). Both at location 1. Zuidgors (E) and 3. Paulina (S), seven SED-sensors were installed (Fig. 3.1): at 1. Zuidgors (E) five instruments were allocated at the tidal flat and two at the salt marsh and at 3. Paulina (S) three instruments were allocated at the tidal flat and four at the salt marsh (Table 3.1). At location 2. Zimmermanpolder (E) and 4. Hellegat (S) four sensors were installed (Fig. 3.1): three at the salt marsh and one at the tidal flat (Table 3.1). The SED-sensors were installed at transects lined approximately perpendicular to the water line. At location 5. Uithuizen, four instruments were installed: one at the tidal flat and three at the salt marsh, while at location 6. Tillingham five instruments were installed: four at the tidal flat and 1 at the salt marsh (Table 3.1; Fig. 3.1). The initial elevation of the transects was measured using an RTK-GPS device with a precision in the order of 1cm.

Erosion pins were used to record bi-monthly changes of the local surface level. The erosion pin is a very thin metal rod (i.e., to prevent scouring) with a height marker on top, and a ring around the pin. The pin was pushed into the sediment, till the marker was at a fixed height above the sediment, with a metal ring placed around the pin on top of the soil surface. Every two months (bi-monthly), bed level dynamics were measured. The distance from the marker to the soil surface and the ring buried into the sediment were

measured. After each measurement, the erosion pins were re-installed at least 10 cm from their original position for preventing disturbances from the earlier measurements. Three pins were deployed per SED-sensor location.

Sediment samples were collected from the upper 3cm of the surface with a cut-off syringe at all measurement locations (near the SED sensors) of the study sites in the Westerschelde. The sediment samples were freeze-dried in the laboratory, and average grain size diameter (D50) of the sediment was determined using a Malvern laser particle sizer.

Wave measurements were conducted at field sites 2. Zimmermanpolder (E) and 4. Hellegat (S). At both marshes, a wave gauge (Ocean Sensor Systems, Inc., USA) was located near every SED-sensor, eight wave gauges in total. The pressure sensor of the wave gauges was installed approximately 0.10m above the bed. Pressure was measured by the wave gauges with a frequency of 5 Hz over a period of 7 min, every 15 min. The local atmospheric pressure, hydrostatic pressure and the dynamic wave pressure, included in the measured signal were separated during post-processing (Vuik et al., 2016). The dynamic wave pressure was used for determining the significant wave height (Hm0), derived from the wave spectrum. A continuous pressure signal was not present at all study sites, so for determining the inundation time, data were used from Rijkswaterstaat (Dutch department of waterways and public works), for consistency at all five Dutch study sites. The data were obtained at Terneuzen, Bath and Uithuizerwad (Fig. 3.1; indicated by water level). Processed data at the measurement locations were available every 10 minutes. Water level data for Tillingham (England) were used from the British Oceanographic Data Centre (BODC). The data were obtained at the South side of the Thames estuary, at Sheerness, data were available every 15 minutes.

The bed of intertidal areas can be stabilized by diatoms (Austen et al., 1999; Andersen et al., 2005). An indicator for the biomass of this microphytobenthos and the bio-stabilization is the chlorophyll-*a* level of the sediment (Staats et al., 2001). The chlorophyll-*a* level of the sediment was measured bimonthly from November 2015 until July 2016 at 1. Zuidgors (E). Chlorophyll-*a* samples were collected of the upper 1cm of the sediment, using a small cut-off syringe. Samples were taken at the SED-sensors. Around each sensor, six replicate samples were taken and merged into one sample. After storage at -80 deg C for at least 1 day, they were freeze-dried (at -20 deg C) in a dark room for 72 hours and then brought to the -80 deg C freezer again for storage prior to further analysis in the laboratory. The samples were homogenized and photosynthetic pigments of a subsample were extracted using a cell homogenizer after addition of 10 ml acetone (90%) and glass beads. The extract was centrifuged and absorption was measured with a spectrophotometer.

3.2.3 | Field data analysis

The bed level dynamics at the different measurement locations were obtained by converting the raw data from the SED sensors (Appendix 3.A), setting the first obtained measurement equal to zero and referring all other bed level measurements to this first point. The maximum positive and negative dynamics per measurement location were selected for determining the amplitude of the bed level dynamics over the entire measurement period. The amplitude of the bed level dynamics per measurement location was seasonally obtained, for spring (March-May), summer (June-August), fall (September-November), winter (December-February). The maximum positive and negative bed level dynamics were selected, because this is an important parameter for seedling establishment in the proper season (i.e. once a threshold for erosion or sedimentation is exceeded seedlings will not be able to establish (Bouma et al., 2016)).

Bed level measurements by SED-sensors were validated using erosion pin measurements at 1. Zuidgors (E). The latter is the conventional technique for measuring bed level dynamics in coastal and fluvial areas and is widely applied (e.g. Sirvent et al., 1997; Arens et al., 2004). The three measurement pins per SED sensor were averaged and the standard deviation was determined. The bed level dynamics measured with the SED-sensors were compared with bed level dynamics measured with erosion pins.

The maximum significant wave height (H_{mo}) was determined per tidal inundation, using the wave gauges at 2. Zimmermanpolder (E) and Hellegat (S). The maximum significant wave height was only determined for tidal inundations after which bed level dynamics were measured. For each selected tidal inundation the maximum significant wave height was obtained and all obtained values were averaged per season per measurement location. Water level data obtained from Rijkswaterstaat measurement locations (Fig. 3.1) were compared with the bed level height of all measurement locations, since wave gauges were only located at two study sites. The periods of inundation were initiated once the water level exceeded the bed level at the measurement location and stopped when the water level was below the bed level again. Tidal inundations, after which bed level dynamics were obtained, were taken into account only. The inundation period was averaged per season as well as per measurement location.

Finally chlorophyll-*a* variations at 1. Zuidgors (E) were calculated by subtracting the consecutive measured chlorophyll-*a* levels of the sediment.

3.3 | Results

3.3.1 | Quantifying daily bed level dynamics across seasons at salt marsh – tidal flat interface

The bed level dynamics near the vegetation edge, both at the marsh and tidal flat, were observed with SED sensors at all study sites. The observations at four study sites in the Westerschelde, the Netherlands revealed that the largest bed level dynamics occurred at the most seaward measurement locations (Fig. 3.2; bottom panels) and that the bed level dynamics decreased towards the vegetated marsh (Fig. 3.2; top panels). Measurements obtained by the SED-sensor were comparable with the measurements obtained by the erosion pins (Fig. 3.2; red bars), having a correlation (R2) of 0.74, without a systematic deviation. The standard deviation over the three erosion pin measurements, per measurement location, was highest at the most seaward measurement locations during the spring and summer season (Fig. 3.2). The much higher temporal resolution of the SED-sensors allowed exact timing when changes occur, and calculating the variability in bed level, in-between pin readings (e.g. as standard deviation).

The largest positive bed level change (sedimentation) was observed in the spring and summer season (March – May; Fig. 3.3) and was most pronounced at the tidal flat of the wind-exposed northern shores, i.e. 1. Zuidgors (E) and 2. Zimmermanpolder (S) (Fig. 3.3A and 3.3B resp.).The spring sedimentation reversed during the summer (June - August), followed by maximum negative bed level change (erosion) during fall (September – November) and winter (December – February; Fig. 3.3). A relative stable bed level was observed at the locations landward from the marsh edge at 1. Zuidgors (E), while more dynamic behavior was observed at the gradually changing profile at 2. Zimmermanpolder (E) (Fig. 3.3A and 3.3B). The pattern of seasonal variation was less pronounced at the sheltered sites (Fig. 3.3C and 3.3D resp.). However, In general a clear distinction was observed between bed level dynamics at the tidal flat (relative large) and salt marsh (relative small).

The largest amplitude of the bed level dynamics over the entire measurement period (derived from the seasonal amplitude) at 1. Zuidgors (E) and 3. Paulina (S) revealed that dynamics were larger close to the seaward edge, and decreased towards the marsh edge (Fig. 3.4). In general, the bed level dynamics landward from the marsh edge remained below the bed level dynamics seaward from the marsh edge. Only the bed level dynamics very nearby the marsh edge, just inside the pioneer, and just landward of the marsh edge (i.e., within a range of 10 meter), did not show a consistent trend at the wind exposed sites (Fig. 3.4; sites 1 and 2). In general, present results clearly show that bed level dynamics decrease (i.e., sediment stability increases) in the presence of vegetation.

When comparing exposed versus sheltered sites, most pronounced bed level dynamics were observed at the exposed northern shores.

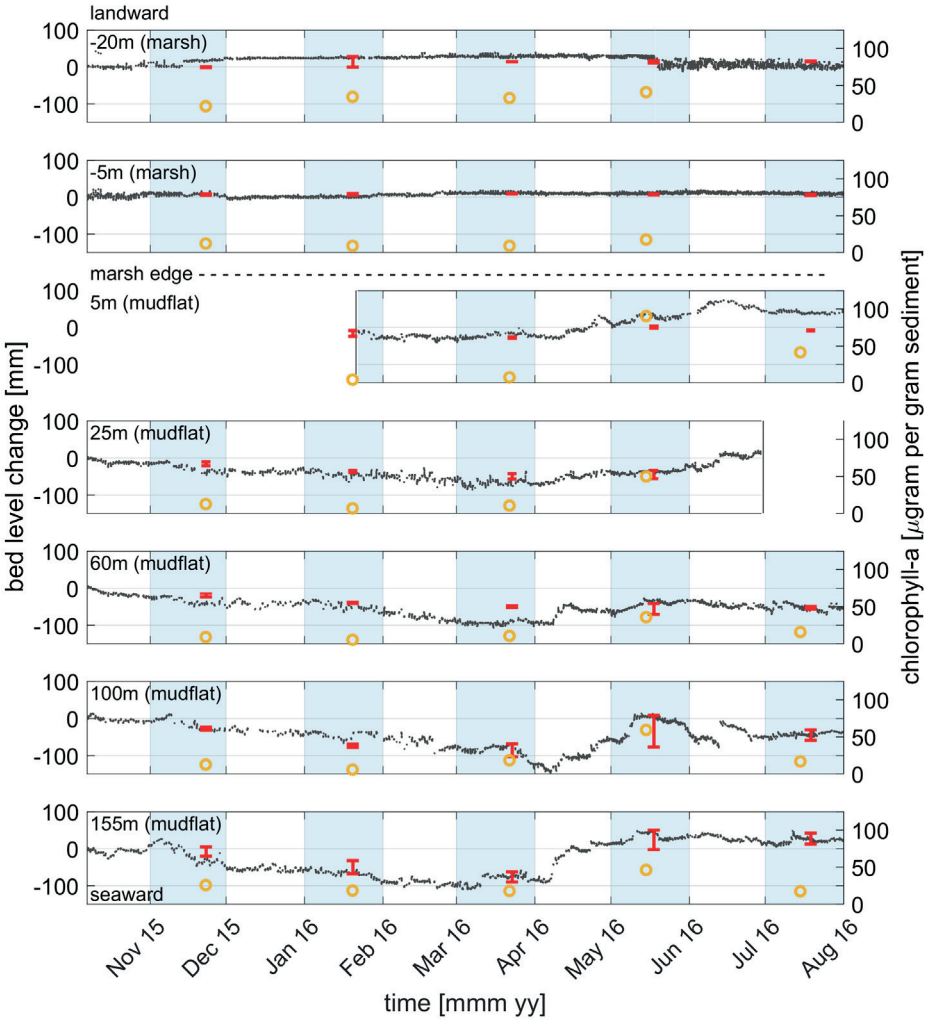

Figure 3.2 | Comparison of obtained bed levels (left y-axis) using SED sensors (grey dots) and erosion pins (red bars) with standard deviation, obtained at 1. Zuidgors (E). Chlorophyll-*a* levels (yellow markers; right y-axis) were obtained at the same measurement locations. The top panel indicates the most landward position at the transect and the bottom panel the most seaward position. Values at the top left of each panel describe the distance to the marsh edge. The obtained bed level dynamics with SED sensors were relative to the first SED sensor measurement.

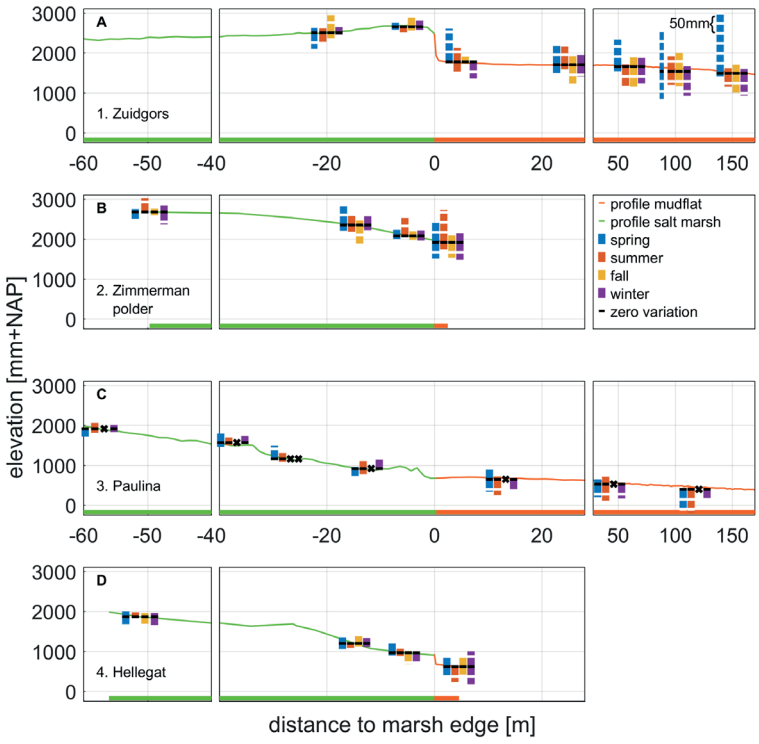

Figure 3.3 | Minimum and maximum bed level dynamics per season for (from top to bottom) 1. Zuidgors (E), 2. Zimmermanpolder (E), 3. Paulina (S) and 4. Hellegat (S). The initial bed level profile can be observed by the green (salt marsh) and orange (mudflat) line. The bed level dynamics per season, per measurement location are showed by four bars, with zero bed level dynamics at the initial bed level profile (black line), maximum sedimentation (bar above the profile) and maximum erosion (bar below the profile), a single part of the bar (in between two white lines) is equal to 25mm change. Missing data for a specific season is indicated with a cross.

3.3.2.1 | *Sediment characteristics*

Out of the four study sites in the Westerschelde, the average grain size diameter (Fig. 3.5) was smallest at the most western locations (1. Zuidgors (E) and 3. Paulina (S)), closest to the mouth of the estuary and largest more inland (2. Zimmermanpolder (E) and 4. Hellegat (S)). There was no general trend over the tidal flat and salt marsh. It was observed that the average grain size was smallest at the most landward location in the salt marsh for the most inland locations (2. Zimmermanpolder (E) and 4. Hellegat (S)).

The observed average grain sizes at 1. Zuidgors (E) and 3. Paulina (S) were all in the same range (20 - 50µm), no specific differences between the tidal flat and salt marsh were observed (Fig. 3.5). The observed average grain size does not show similar patterns as the patterns observed for bed level dynamics (Fig. 3.4).

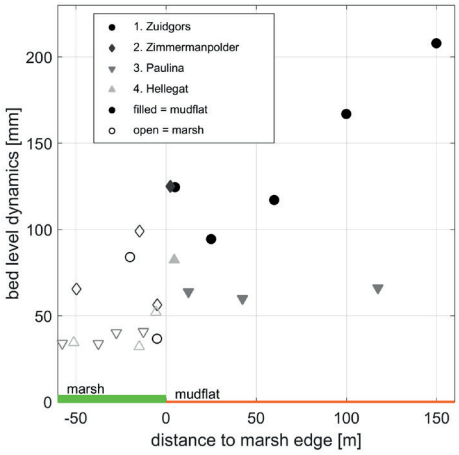

Figure 3.4 | Bed level dynamics (seasonal maximum obtained bed level change minus seasonal minimum obtained bed level change) per measurement location (indicated by different markers). Bed level dynamics at the marsh are indicated with open markers, while bed level dynamics at the mudflat are indicated with filled markers.

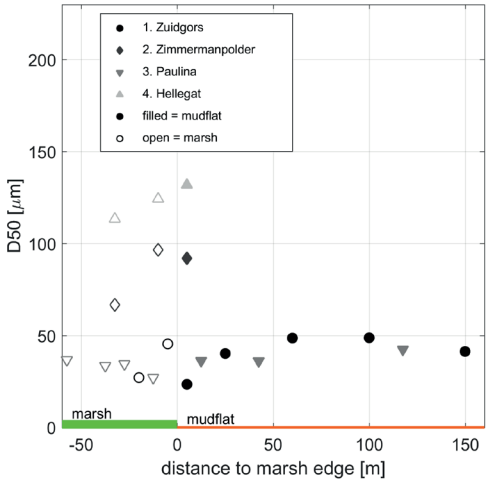

Figure 3.5 | Grain size (D50) measured at the cross-shore transects of the four study sites in the Westerschelde (indicated by different markers). The grain size at the marsh is indicated with open markers, while the grain size at the mudflat is indicated with filled markers.

3.3.2.2 | *Can waves explain bed level dynamics?*

Measurements of waves at study sites 2. Zimmermanpolder (E) and 4. Hellegat (S), showed that the maximum significant wave height observed per tide, averaged over all obtained tides, at 4. Hellegat (S) exceeded the values found at 2. Zimmermanpolder (E) (Fig. 3.6). At both sites waves were highest seaward from the marsh edge and decreased when passing the marsh edge. Waves attenuated further when propagating over the marsh. This pattern was observed for all seasons (Fig. 3.6). At 2. Zimmermanpolder (E) the maximum significant wave height was highest in winter and lowest in summer, while at 4. Hellegat (S) there was a less distinctive pattern. The highest waves, observed at the tidal flat seaward from the marsh edge at both sites, were related with the largest bed level change (Fig. 3.3; Fig. 3.6). However in the marsh, the waves attenuated further, while the bed level dynamics did not show a similar pattern.

For all measurement locations at study site 4. Hellegat (S), the bed level dynamics were smallest in the summer season (Fig. 3.3), divergent from the observed wave height (Fig. 3.6). Finally at 4. Hellegat (S), bed level dynamics in the marsh were quite similar in spring, fall and winter, while being lower in the summer (Fig. 3.3). This pattern was not found in the waves observed at the marsh (Fig. 3.6). At 2. Zimmermanpolder (E), the pattern of bed level dynamics was less distinctive (Fig. 3.3), while a clear seasonal pattern was identified for the observed waves (Fig. 3.6). At 2. Zimmermanpolder (E), bed level dynamics in fall were smallest instead of summer (Fig. 3.3). While at 4. Hellegat (S) it was observed that bed level dynamics in summer were smallest and larger in the other seasons (Fig. 3.3), with a less distinctive seasonal pattern observed for the wave height (Fig. 3.6).

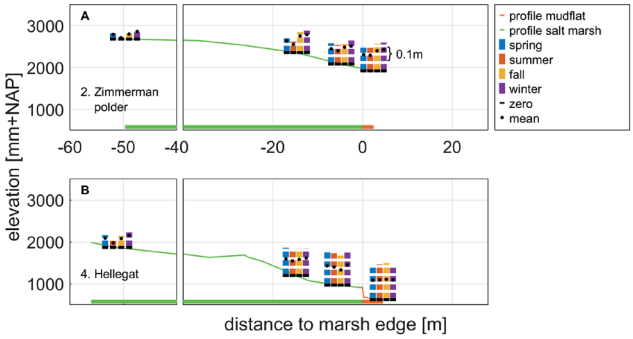

Figure 3.6 | Observed wave heights per season for study site 2. Zimmermanpolder (E) and 4. Hellegat (S). The bed level profile is indicated by the green (salt marsh) and orange (mudflat) line. The observed wave heights per season, per measurement location is showed by four bars, with no wave height at the bed level profile (black line), and the average wave height per season indicated by a black dot, a single part of the bar (in between two white lines) is equal to 0.05m.

3.3.2.3 | *Can inundation time explain short-term bed level dynamics?*

The tidally averaged inundation time over the entire measurement period showed a relation with the maximum averaged bed level change (Fig. 3.7). In general the bed level dynamics decreased with a decreasing tidal inundation. However different relationships between bed level dynamics and inundation time were observed at the different transects (Fig. 3.7). Relative large bed level dynamics with small inundation times appeared at the northern shores (locations 1 and 2), while relative small bed level dynamics combined with larger inundation times were observed at the southern shores of the Westerschelde (locations 3 and 4). All study sites at the marsh were higher elevated, with short inundation times. The tidal flat, located at a lower elevation, had longer inundation times. The interface from tidal flat to marsh was characterized by a cliff at 1. Zuidgors (E) and 4. Hellegat (S), while a smoother transition appeared at 2. Zimmermanpolder (E) and 3. Paulina (S) (Fig. 3.3).

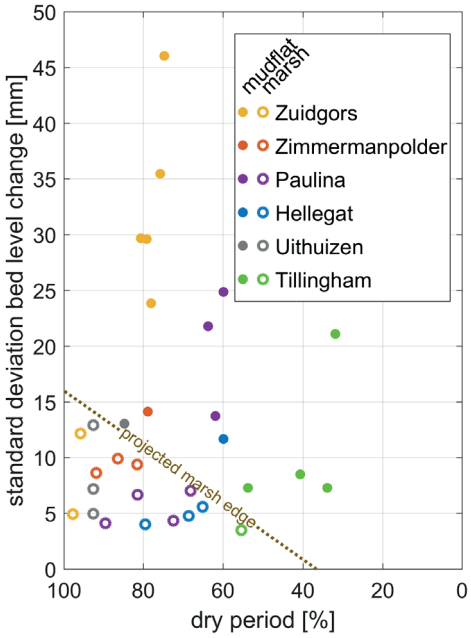

Figure 3.7 | Relation between maximum averaged bed level change and average inundation time per measurement transect, being the basis for the location of the marsh edge. The measurement locations at the tidal flat (top part) are indicated by a filled marker, while the measurement points at the marsh (bottom left part) are indicated by an open marker.

A distinct pattern was revealed when taking into account all six study sites (Fig. 3.7). A point cloud representing all measurement locations at the salt marsh and a point cloud representing all measurement locations at the tidal flat, could be dissected by a sharp border. This line indicates that the location of the lower marsh edge is restricted by two interacting factors: to withstand longer inundation requires more stable bed levels at the marsh edge and vice versa; withstanding more dynamic sediment requires less inundation at the marsh edge (Fig. 3.7). Thus as hypothesized in previous studies, inundation time (or dry period) and bed level dynamics are important parameters for vegetation growth and occurrence.

3.3.2.4 | *Can chlorophyll-a explain short-term bed level dynamics?*

Chlorophyll-*a* levels, obtained at 1. Zuidgors (E), increased in Spring (Fig. 3.2; yellow markers). At the tidal flat a clear correlation was observed between the chlorophyll-*a* levels of the sediment – which is a proxy for the presence of microphytobenthos – and bed level reply, i.e. bed level dynamics (R2 is 0.56). Chlorophyll-*a* levels of the sediment at the tidal flat were in the same order as chlorophyll-*a* of the sediment at the salt marsh (Fig. 3.2). However, at the marsh, the bed level dynamics were almost always equal to zero, implying a smaller influence of chlorophyll-*a* of the sediment to bed level dynamics and/or a stabilizing influence of the vegetation cover.

In the period November - January at the tidal flat, both a decreasing chlorophyll-*a* level of the sediment and decreasing bed level was observed (Fig. 3.2). In the period January – March, the chlorophyll-*a* levels of the sediment slightly increased, however erosion of the bed was observed. An opposite relation was observed in the period May – July, both chlorophyll-*a* levels and bed levels increased (Fig. 3.2).

3.4 | Discussion

To obtain a better understanding of the factors confining the location of the marsh edge and reveal the role of short-term bed level dynamics in this, bed level dynamics and multiple bio-physical parameters were obtained at a range of contrasting sites at the transition between the salt marsh and mudflat. Combining all measurements across sites showed that the location of the lower marsh edge can be indicated by two interacting factors: inundation time and bed level dynamics. Building on existing knowledge (e.g. Hinde, 1954; McKee and Patrick, 1988; Suchrow and Jensen, 2010; Bouma et al., 2016), present results emphasize that in addition to inundation period, bed level dynamics is an important process in determining the position of the marsh edge.

3.4.1 | Field data collection and processing

Field data was collected at six study sites in the North Sea area. Processed bed level data previously obtained by the SED-sensor at the mudflat at 1. Zuidgors (E), were validated using Sedimentation Erosion Bars (SEBs), confirming the accuracy of measurements obtained by SED-sensors (Hu et al., 2015a). The SED and erosion pin measurements obtained at the 1. Zuidgors (E) salt marsh confirm the applicability of the SED-sensor in intertidal vegetated areas. The SED-sensor measurements at the mudflat, obtained in this study, also showed a good correlation with the erosion pin measurements ($R2 = 0.74$). The developed method (Appendix 3.A) for converting raw data to bed level data was not capable to detect a bed level for all obtained measurements, e.g. the last (part of September and October) measurements conducted at 1. Zuidgors (E), did not result in sufficient bed level heights after conversion. However, the obtained bed level dynamics were comparable with studies wherein similar measurements were conducted (e.g. Lawler, 2005; Hu et al., 2017).

3.4.2 | Towards understanding spatial and temporal patterns in short-term bed level dynamics

In this study we showed that bed level dynamics increased from the marsh edge towards the seaward side of the mudflat. This confirms the findings of earlier studies having spatial data on short-term bed level dynamics (e.g. Hu et al., 2015c; Bouma et al., 2016). It furthermore agrees with long-term studies (multiple years) that also showed increasing bed level dynamics over the mudflat towards the sea (e.g. O'Brien et al., 2000; Andersen et al., 2006; Hu et al., 2017). The previously mentioned studies were extended by the present study with measurements at the transition from tidal flat to marsh, resulting in observations both at the vegetated marsh and bare flat. The seasonal bed level dynamics were obtained over multiple contrasting sites, capturing short-term variability per season by longer-term (year) measurements. Seasonality was earlier observed in the long-term studies, with in general positive bed level change (sedimentation) in spring and summer and negative bed level change (erosion) in fall and winter. This was also observed in the current study at the wind-exposed locations at the northern shores in the Westerschelde, but not at the sheltered southern shores in the Westerschelde.

The largest bed level dynamics were observed at the locations at the northern shores of the Westerschelde (Fig. 3.3), which are both located perpendicular to the prevailing southwestern winds (Wang et al., 2017) and hence indicated as wind-exposed by Callaghan et al. (2010). Location 4. Hellegat (S) was not indicated as exposed, as it is sheltered to the southwestern winds, however the maximum fetch length at 4. Hellegat (S) occurring with western winds was larger than the maximum fetch length at the other

locations in the Westerschelde (Van der Wal et al., 2008). The differences in fetch also affected the maximum significant wave height (Fig. 3.6), being higher at 4. Hellegat (sheltered) than at 2. Zimmermanpolder (exposed). The orientation of the study sites in the Westerschelde towards the prevailing wind and the observed hydrodynamics only partly explained the bed level dynamics.

The large accretion at the tidal flats in the Westerschelde, as observed in the spring season, was probably caused by increasing chlorophyll-*a* levels, which is in agreement with earlier observations (Austen et al., 1999; Andersen et al., 2005). In contrast to this dominant ecological parameter at the mudflat in spring, it seemed that the ongoing erosive trend in fall and winter (Fig. 3.2) occurred due to the absence of a stabilizing ecological parameter, allowing the increasing influence of wind imposed waves. This is supported by earlier observations, were wind imposed waves became more dominant in the winter (Callaghan et al., 2010). The temporal alternating importance of different biological and physical parameters for bed level dynamics show the complexity of the system wherein the bed level dynamics were influenced by bio-physical processes.

In contrast to the highly variable bed levels at the mudflat, the bed levels remained much more constant at the marshes (Fig. 3.3). Experimental results by Spencer et al. (2016) also showed highly stable bed levels at a marsh during hydrodynamic high energy conditions. Location 2. Zimmermanpolder (E) seemed like an exception here, having a more dynamic bed level at the marsh. Perhaps this might be explained by the fact that *Bolboschoenus maritimus* (*Scirpus maritimus*) was the dominant pioneer vegetation type, whereas *Spartina anglica* was the dominant pioneer species at all other locations in the Westerschelde. With Spartina having a higher biomass and higher stem density compared to *Scirpus*, apparently the sediment stabilizing ability of *Spartina* is also larger. In addition to the more variable bed levels at the marsh of 2. Zimmermanpolder (E), the maximum significant wave heights (H_{mo}) at the marsh were more variable both spatial and temporal over the different seasons, than at 4. Hellegat (S). Finally the average grain size of the sediment was much coarser at the eastern locations in the Westerschelde (Fig. 3.5), indicating possibly a less cohesive sediment, more vulnerable to erosion. So the deviant bed level dynamics at the marsh of 2. Zimmermanpolder (E) could be possibly explained by a different vegetation species, more variable wave heights and a coarser sediment.

3.4.3 | The location of the marsh edge

The marsh edge is able to extend seaward and retreat landward (Allen, 2000; Cox et al., 2003; Van der Wal et al., 2008), affecting the width of the marsh. A smaller marsh width decreases the capacity of wave attenuation (e.g. Vuik et al., 2016), making in-depth understanding of the dynamics driving marsh width key to being able to use marshes

for coastal defense (Bouma et al., 2014). At 1. Zuidgors (E), marsh edge erosion is taking place for decades, and a clear cliff has formed, while at 2. Zimmermanpolder (E) the *Scirpus* vegetation does not have a marsh cliff, likely because the now retreating *Scirpus* at the marsh edge was relatively recently (1990s) established. At the southern shores of the Westerschelde a cliff was observed at 4. Hellegat (S), while not being observed at 3. Paulina (S), probably due to the expanding marsh edge here (Van der Wal et al., 2008).

The daily bed level dynamics, driven by the combination of a number of ecological and physical processes (e.g. Mariotti and Fagherazzi, 2010; Corenblit et al., 2011; Friedrichs, 2011; Deegan et al., 2012; Green and Coco, 2014), have been shown to determine the elevation in the tidal prism where seedlings of salt marsh pioneer species can establish (Bouma et al., 2016). Moreover, bed level dynamics at the tidal flat adjacent to a stable marsh platform have also been identified as the process driving cliff initiation (Bouma et al., 2016). Present results agree and extend beyond Bouma et al. (2016), by showing that across multiple sites, the location of the marsh edge appears to depends on the combined effect of daily bed level dynamics and inundation period. In case of a high daily bed level dynamics the marsh edge will occur at relative high elevations with little inundation stress. In contrast, at locations with little bed level dynamics, the marsh edge tolerates longer inundation and will occur at relative low elevations (Fig. 3.7).

The daily bed level dynamics at the tidal flat may be expected to depend on wave formation, which depends on the tidal-flat elevation relative to mean sea level (Mariotti and Fagherazzi (2010). The effect of waves observed at the different measurement sites in the present study, mainly showed a relation with the bed level dynamics at the tidal flat if present, where waves were substantially higher than in the marsh. Changes in the tidal prism, affecting inundation period and possible bed level dynamics via wave formation, resulted in the past in changes from a seaward extending marsh edge to a landward retreating marsh edge (Cox et al., 2003). When distinguishing ship and wind waves, in the Westerschelde no evidence was found to relate the marsh edge growth or retreat to ship waves (Cox et al., 2003).

Present results imply that the bed level dynamics and inundation period near the marsh edge can be seen as an indicator for the development of the marsh edge. It also emphasizes the importance of well-considered anthropogenic interventions in estuaries in the context of salt marsh change and flood protection, since anthropogenic interventions can affect bed level dynamics and the inundation period (Allen, 2000; Cox et al., 2003). Moreover increasing storm intensity (e.g. Knutson et al., 2010) and sea level rise (Donnelly et al., 2004) in the face of climate change, may possibly also affect bed level dynamics and inundation times at the tidal flat and near the salt marsh edge. This may lead to a shifting marsh edge and thus changes in marsh width.

3.5 | Conclusions

Bed level dynamics, obtained with the SED sensors, at four study sites in the Westerschelde, the Netherlands, decreased from the tidal flat towards the marsh edge. The largest positive bed level change (sedimentation) occurred in spring and the largest negative bed level change (erosion), was observed in winter. The bed level dynamics in spring were related to the presence of diatoms (indicated by chlorophyll-*a* levels) at the tidal flat. However a generic relation between bed level dynamics and differences in hydrodynamics over the seasons was not found. The smallest bed level dynamics were found in the salt marshes, indicating the potential for including the stable marsh in coastal defense schemes. The potential was also supported by the decreasing wave heights over the marsh towards the landward dike, without a similar trend for the bed level dynamics. Present results from three different tidal basins (six study sites) suggest that the location of the marsh edge is determined by interactive effects of bed level dynamics and inundation time. When bed level dynamics are high, the marsh is observed to occur at higher elevations with shorter inundation stress. And vice versa, when bed level dynamics are low, the marsh is observed to occur at lower elevations with longer inundation stress. If the present finding is extrapolated, it has major implications for the management of coastal zones (i.e. controlling specific physical processes) if we want to maximize marsh width for flood safety.

Acknowledgments

This work is part of the research programme BE SAFE, which is financed by the Netherlands Organisation for Scientific Research (NWO) (grant number 850.13.010), and part of the EU FP7 project FAST (Foreshore Assessment using Space Technology) (grant number 607131). Additional financial support has been provided by Deltares, Boskalis, Van Oord, Rijkswaterstaat, World Wildlife Fund and HZ University of Applied Science. Bas W. Borsje was supported by the Netherlands Organization for Scientific Research (NWO-STW-VENI; 4363). We acknowledge V. Vuik for providing the wave data, J. de Mey for preliminary work on processing raw data obtained with the SED sensor, and the NIOZ for analyzing the samples in the laboratory and for providing technical assistance. Finally, we acknowledge the useful comments provided the reviewers. Data and scripts in support of this manuscript are available at https://doi.org/10.4121/uuid:c0be318c-9858-4a05-a546-782e29b4abef.

Appendix 3
A field data processing of SED sensors

The SED-sensor collects measurements of the bed level by running a current through the light-sensitive cells, which is transformed into a voltage over a resistor (Hu et al., 2015a). In general the voltage output for underground light-sensitive cells is zero, a transition zone to a higher voltage output is showed by the light-sensitive cells around the bed level. The light-sensitive cells above the bed show a higher voltage output (Fig. 3.8). Consequently, the raw data of the array of light-sensitive cells typically shows a tilted S-shaped curve. The exact shape of the curve may be influenced by factors affecting the light intensity surrounding the SED-sensor, like time of day, cloudiness, water level variations, vegetation biomass and dirt/algae on the sensor. The influence of biological and physical processes on the voltage profile for the different measurement intensities was extensively tested. Experiments were conducted to determine the applicability of the SED-sensor surrounded by dense vegetation as well as the applicability with algae and dirt at the transparent cover.

To be able to work well under different light intensity, the SED-sensor contains resistors with three different resistances: high, medium and low. All sensitivities were used to translate measurements obtained under different light intensities into bed level dynamics. The different sensitivities maximize the period measurements can be conducted. The method developed to analyze the raw data from the SED-sensor uses the high sensitivity with low light availability (e.g. dusk and dawn). This further elaborates on the method developed by Hu et al. (2015a), wherein only one sensitivity was used and a threshold in the voltage profile was used for determining the bed level.

Another factor that may influence the level where the sediment-air transition is detected is when scouring holes occur around the SED-sensor. Scouring holes may occur when conducting measurements using equipment mounted in the bottom of intertidal area. Scouring holes around SED-sensors were only observed around some SED-sensors at the mudflat, having a depth of maximum 5 cm. The typically tilted S-curved signal was influenced by the scouring hole, showing two transition zones when a scouring hole appears.

An autonomous script was developed to process the raw data of the measurements, meaning no contextual data representing measurements of e.g. water levels or day- and nighttime were added. The voltage data obtained by the SED-sensor ranges between 0-3.3V and is scaled to store as 12-bit integers ranging between 0 and 4095. To process the data, the following steps were taken. Before obtaining the bed level, the raw data was preprocessed. The noise was reduced in three steps (Fig. 3.8; panels 2 and 3):

1 To create a consistent profile of all light sensors, the value of the belowground sensors was set to zero, by determining the vertical highest located light sensor with output zero and forcing all output vertically below this sensor to be zero.
2 The voltage curves were standardized for comparing the different sensitivities within a single time step.
3 The data was filtered per curve using a third-order one-dimensional median filter, to decrease the remaining general noise appearing due to discrepancies between the light-sensitive sensors in the SED-sensor.

After preprocessing the raw data, bed levels were obtained by approximating the preprocessed signal with a single (Eq. 3.1) or double (Eq. 3.2) arctan function. For a single arctan approximation the bed level was found at parameter b (Eq. 3.1; Fig. 3.8) and for a double arctan approximation the bed level was found at the minimum of parameter b and d (Eq. 3.2; Fig. 3.8). Whether a single or double arctan function was used, depends on the coefficient of determination for measured versus approximated data (R^2). The coefficient of determination was calculated using the sum of squares of residuals (SS_{resid}) and the total sum of squares (SS_{total}; Eq. 3). SS_{resid} is the sum of the squared differences of the measured and predicted value, while SS_{total} is the sum of the squared differences of the measured and the average value. In general a curve with a single transition zone was approximated best by a single arctan function and a curve with a double transition zone was approximated best by a double arctan function (Fig. 3.8; panels 4 and 5).

$$a * \arctan(x - b) + e \qquad \text{Equation 3.1}$$

$$a * \arctan(x - b) + c * \arctan(x - d) + e \qquad \text{Equation 3.2}$$

$$R^2 = 1 - \frac{SS_{resid}}{SS_{total}} \qquad \text{Equation 3.3}$$

To reduce the uncertainty of the bed level measurements per time step, multiple adjacent measurements were used to obtain window averaged (window of 6 hours) bed levels. In order to average the data, isolated measurements per time step (one or two measurements surrounded by time steps without a measurement) were removed.

Possible outliers occurred due to the different vertical locations of the transition zone when comparing voltage curves from the different sensitivities during a single measurement. Differences in voltage curves for the low, mid and high sensitivity measurement during increasing or decreasing light intensities were probably the cause. However, in this study the small amount of outliers observed were almost all dampened by window averaging the processed data.

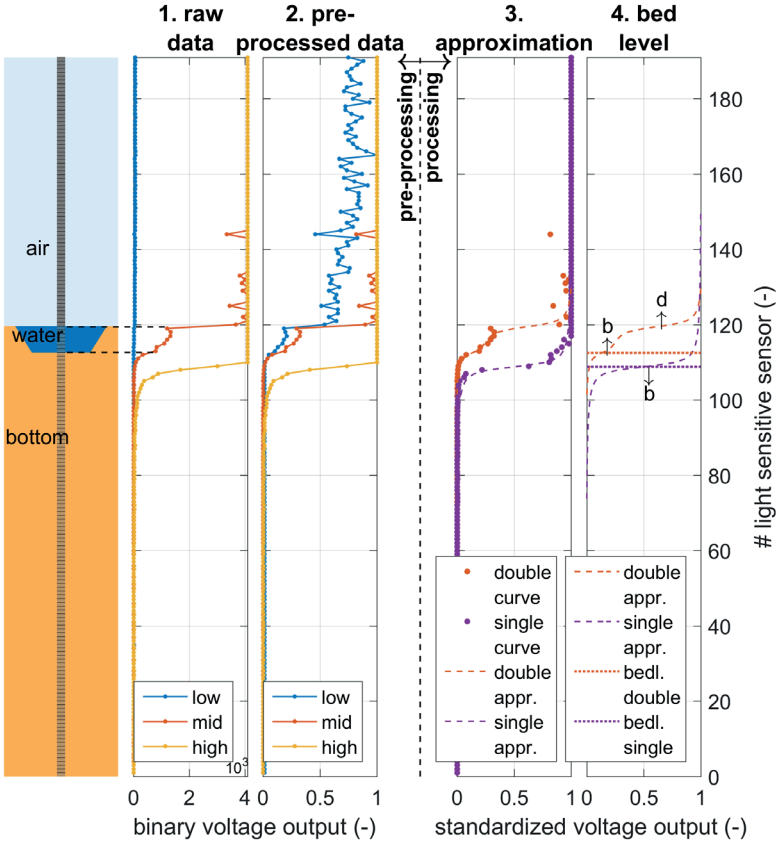

Figure 3.8 | The different steps of pre-processing and processing the data. A schematic sensor located in a scouring hole (panel 1), from a measurement at 1. Zuidgors (E). The raw data of the different sensitivities, low (blue), mid (red) and high (blue) is showed in panel 2. The raw data is pre-processed and standardized in panel 3. The mid sensitivity is used to approximate using a double arctan function (red; panel 4), also pre-processed data is added that is approximated with a single arctan curve (purple; panel 4). The bed levels for both curves were obtained using the single and double arctan approximations and were found at parameter b for a single arctan approximation and at the minimum value of parameter b and d for a double arctan approximation (panel 5).

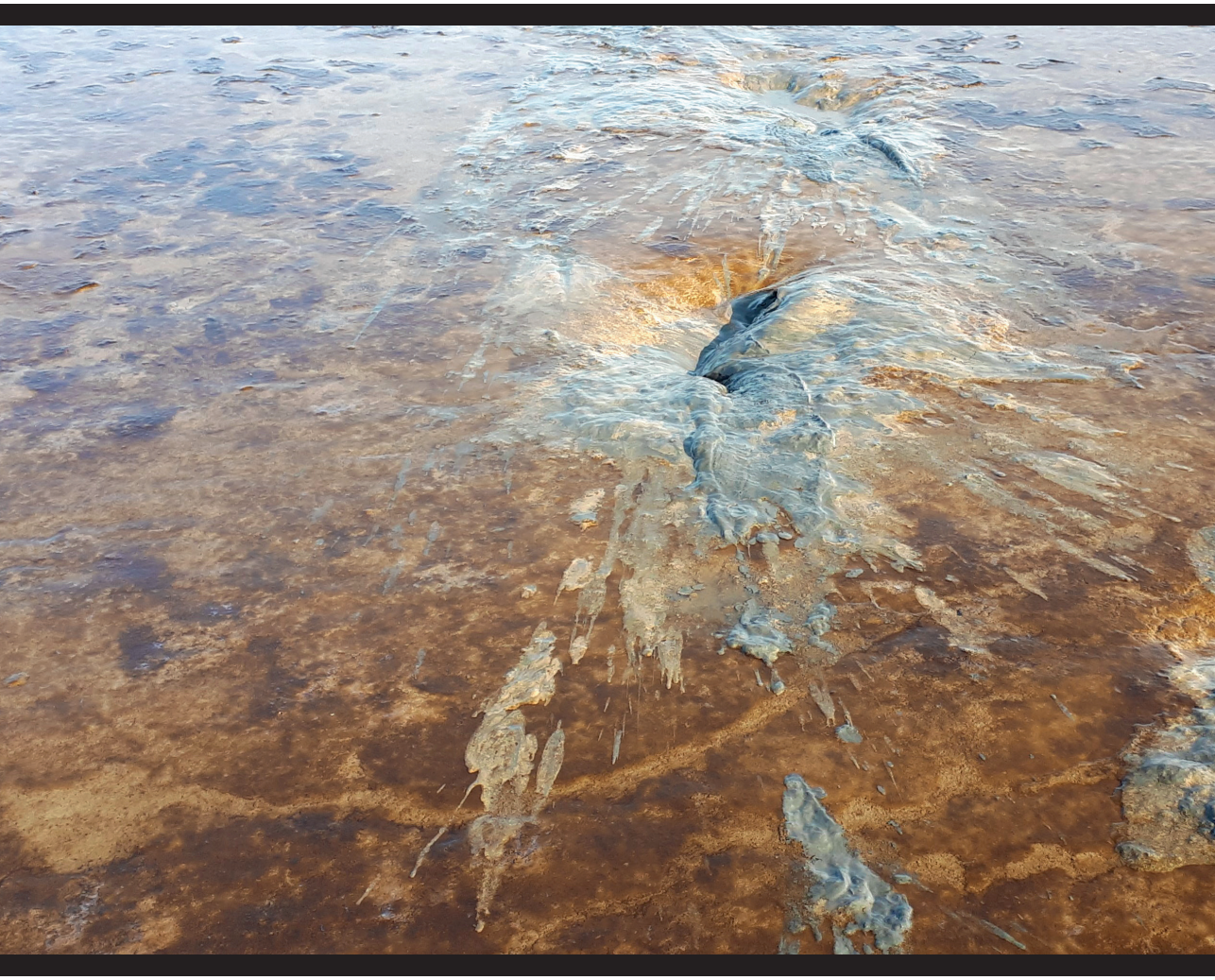

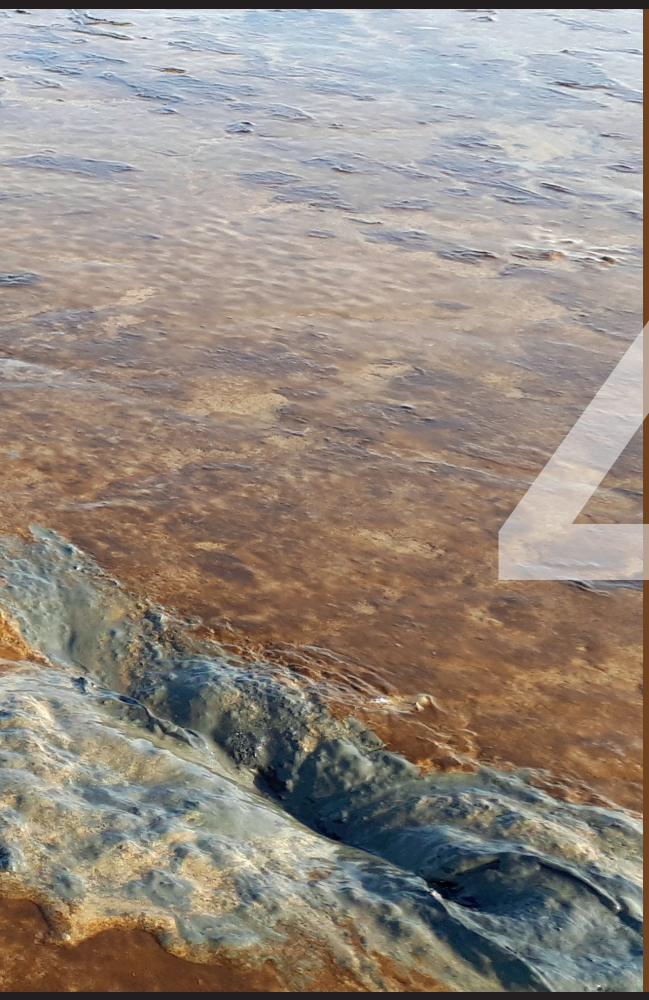

4

Modelling decadal salt marsh development: variability of the salt marsh extent under influence of waves and sediment availability

Submitted as: Willemsen, P. W. J. M., Smits, B.P., Borsje, B. W., Herman, P. M. J., Dijkstra, J. T., Bouma, T. J., & Hulscher, S. J. M. H. (submitted). Modelling decadal salt marsh development: variability of the salt marsh extent under influence of waves and sediment availability.

Abstract

Salt marshes can contribute to coastal protection, but the magnitude of the protection depends on the width of the marsh. The cross-shore width of the marsh is to a large extent determined by the delicate balance between seaward growth and landward retreat as a result of sedimentation and erosion processes. The influence of the magnitude of daily occurring mild weather conditions and sediment availability on the decadal development and variability of salt marsh width has not been systematically assessed. This paper investigates how the magnitude of homogeneous hydrodynamic forcing, combined with sediment availability, affects the biophysical development, and more specifically retreat and expansion of salt marshes. The dynamic extent of the salt marsh is assessed by modelling online-coupled hydrodynamics (tides and waves), morphodynamics and vegetation growth using the numerical Delft3D – Flexible Mesh model, coupled with a vegetation growth module in Python. Salt marsh development under mild nearshore wave conditions (significant wave height Hs of 0.00m, 0.05m, 0.10m and 0.15m), typical for rather low-energy environments in estuaries, combined with suspended sediment concentrations of 10mg/L, 25mg/L and 50mg/L (for H_s = 0.10m), is computed over a 50-year period.

Simulated patterns occurring around the salt marsh edge agreed well with field observations. The simulated temporal variability of the salt marsh edge, affected by the magnitude of wave conditions and sediment availability only, corresponds to the variability observed in the field. In the model, the salt marsh extended seaward at low wave forcing (H_s = 0.00m and H_s = 0.05m), and retreated landwards at higher wave forcing (H_s = 0.10m and H_s = 0.15m). Nevertheless, the salt marsh forced with higher waves was able to switch from a retreating extent towards an expanding extent, with increasing sediment availability. The magnitude of the wave forcing was responsible for the general elevation of the salt marsh profile, whereas the suspended sediment concentration was responsible for the steepness of the profile. Cliff formation was observed when the wave height exceeded a threshold of 0.10m. Vegetation was unable to establish seaward from the cliff for wave heights over 0.15m. Insight in the development of salt marshes under daily occurring mild wave conditions and sediment availability opens opportunities for assessing the long-term contribution of these systems to Nature-Based Flood Defenses.

4.1 | Introduction

Salt marshes are able to stabilize the coast by attenuating hydrodynamic energy and can increase the bed level by trapping sediment (Bouma et al., 2005; Kirwan and Megonigal, 2013; Kirwan et al., 2016). In the last decades, the stabilizing character of salt marshes and their wave attenuating capacity has led to an increasing interest in incorporating them in coastal protection (King and Lester, 1995; Borsje et al., 2011; Gedan et al., 2011; Shepard et al., 2011; Temmerman et al., 2013; Vuik et al., 2019). A recent historic analysis reveals that marshes have significantly contributed to flood safety in the past, with marsh width being a key parameter for their flood defense value (Zhu et al., 2020b). Salt marshes can very well withstand the short-term stress of storm conditions and keep their wave attenuation capacity during storms, as has been demonstrated in large-scale flume experiments (Möller et al., 2014), in the field (Kirwan and Megonigal, 2013; Kirwan et al., 2016; Vuik et al., 2016) and in combined field and model studies (Willemsen et al., 2020).

Climate change is expected to modify the environmental conditions along the coast, primarily through increased Sea Level Rise (SLR), and also through the prevalence of storms, which are predicted to be more severe and more frequent in the future (Leckebusch and Ulbrich, 2004; Emanuel, 2005; Kolker et al., 2009; Knutson et al., 2010). Compared to conventional coastal protection, salt marshes have better abilities to cope with climate change effects by adapting to changing environmental conditions (Borsje et al., 2011).

The interaction between the vegetation, hydrodynamics and sediment dynamics plays a key role in all of these adaptations (Bouma et al., 2016; Willemsen et al., 2018). Plants need minimum growth rates to withstand the different stressors of the physically demanding saltmarsh habitat (Balke et al., 2013). A trade-off exists between different forms of stress. As an example, for vegetation to establish at low locations with long inundation stress, bed levels need to be very stable. Conversely, establishment of vegetation on dynamic beds will only be possible at lower inundation stress and thus higher elevation relative to mean sea level (Bouma et al., 2016; Willemsen et al., 2018). Lateral dynamics of the marsh edge are driven by two phases, lateral retreat and expansion, that show cyclic alternations over time in many locations (Allen, 2000; Van de Koppel et al., 2005; Van der Wal et al., 2008; Singh Chauhan, 2009). Lateral retreat is initiated by cliff formation, which occurs if a marsh expands to far out on the tidal flat (Bouma et al., 2016). The retreat rate is driven by flooding frequency and continuously occurring normal weather conditions, causing marsh edges that are exposed to prevailing wind direction to retreat faster (Fagherazzi, 2014; Wang et al., 2017). Expansion is initiated by seedling establishment (Bouma et al., 2016) and subsequent growth of clonal shoots (Silinski et al., 2016).

The feedback mechanisms are fundamental for the vertical and lateral growth and retreat of the salt marsh. Provided sufficient sediment is available to be trapped by the vegetation, salt marshes grow with sea level rise (e.g. Kirwan et al., 2010; Kirwan et al., 2016; Best et al., 2018). During storm events sediment supply towards the salt marsh increases, due to resuspension of sediment from the tidal flat and increased water levels over the marsh. This enhances vertical growth of salt marshes during storms (Kolker et al., 2009; Schuerch et al., 2013). This positive effect of wind-driven waves on vertical accretion during extreme events contrasts with the lateral erosion at the marsh edge, caused by relatively small waves during continuous mild weather conditions (Callaghan et al., 2010; Tonelli et al., 2010; Fagherazzi, 2014). Taking all these effects into account, the lateral development of a salt marsh, i.e. seaward extension or landward retreat, depends on (1) the relative elevation to mean sea level (Temmerman et al., 2004; Mariotti and Fagherazzi, 2010), (2) the sediment supply (Mariotti and Fagherazzi, 2010; Ladd et al., 2019), (3) the wave climate (Fagherazzi, 2014), and obviously (4) the moment in the tidal phase (i.e. spring-neap) at which storms occur, which affects bed shear stresses due to waves. For the use of salt marshes in a hybrid coastal flood defense, a quantitative understanding of the dynamics of the cross-shore marsh width on decadal timescales is essential (Bouma et al., 2016).

The vertical growth of salt marshes, as influenced by sediment supply, wave climate and sea level rise, is well-studied (e.g. Temmerman et al., 2004; Schuerch et al., 2013). Also the retreat of the marsh edge over a rather short timescale (years) has been analyzed with coupled field observations and modelling studies (e.g. Tonelli et al., 2010; Bendoni et al., 2016). However, no systematic assessment has been made of the effect of homogeneous, but different levels of relatively mild wave conditions on the long-term expansion and retreat of an established marsh. Moreover, the long-term biological development around the salt marsh edge affected by sediment availability and homogenous waves is not yet described in detail. To assess both the seaward growth and landward retreat of the salt marsh edge in a single model, a detailed long-term process-based description of interaction between hydrodynamics, morphodynamics and vegetation development is a prerequisite.

In this paper we aim to understand the retreat and expansion of the salt marsh due to homogeneous hydrodynamic forcing and sediment availability. We will assess the dynamic lateral extent of the salt marsh by modelling bed level change and vegetation growth over a period of 50 years in a two dimensional (depth-averaged) model, focused on the salt marsh edge. The biophysical settings of the model are based on field observations of existing salt marshes in the Netherlands.

4.2 | Methods

We developed a coupled model representing the feedbacks between hydrodynamics, morphodynamics and vegetation dynamics. The interaction between tides, waves, sediment transport, bed level change and vegetation development describes the decadal development of a salt marsh. Using this set-up, the role of homogeneous mild wave conditions, derived from daily weather conditions, and sediment availability derived from the locally occurring range, are systematically assessed.

4.2.1 | Physical settings of the salt marsh

Parameter settings and salt marsh characteristics were derived from salt marshes in the Westerschelde estuary (southwestern part of the Netherlands (Fig. 4.4.1)). The spring tidal range at the center of the Westerschelde (Zuidgors salt marsh; 51° 23' N, 3° 50' E) is 4.93 m, with MHWN (mean high water neap) at 1.85m+MSL (mean sea level) and MHWS (mean high water spring) at 2.63m+MSL (Van der Wal et al., 2008; Willemsen et al., 2020). The salinity is approximately 20-25 psu (Damme et al., 2005). The northern shores are more exposed to the most frequently prevailing winds from the southwest than the sheltered southern shores (Callaghan et al., 2010). Vegetation species in the pioneer zone (lower marsh) are mostly the perennial common cord grass (*Spartina anglica*) and the annual glasswort (*Salicornia spp*.). Higher up in the marsh dominant species are common saltmarsh grass (*Puccinellia maritima*), annual seablite (*Suaeda maritima*), and sea aster (*Aster tripolium*) (Van der Wal et al., 2008).

Detailed bathymetric data in the intertidal zone of the Westerschelde are extensively available (De Kruif, 2001; Marijs and Parée, 2004; Wiegman et al., 2005). The initial bathymetry from the model was derived from decadal field observations of elevation data in a marsh on the northern shore (Zuidgors) and one on the southern shore (Paulinapolder) (Willemsen et al., 2020). The salt marshes contrast in wind exposure and development of the salt marsh edge. Zuidgors at the northern shores is exposed to the prevailing wind direction and the marsh edge is retreating, whereas Paulinapolder is sheltered from the prevailing wind direction and the marsh edge is expanding. Both salt marshes are located in a landward inflection of the dike, relatively sheltered from longshore currents (Fig. 4.1). The dataset from Willemsen et al. (2020) was used to compare field observations of the decadal dynamics of the salt marsh edge over the past 60 years (1955 - 2015) with model results (section 4.3.3.3).

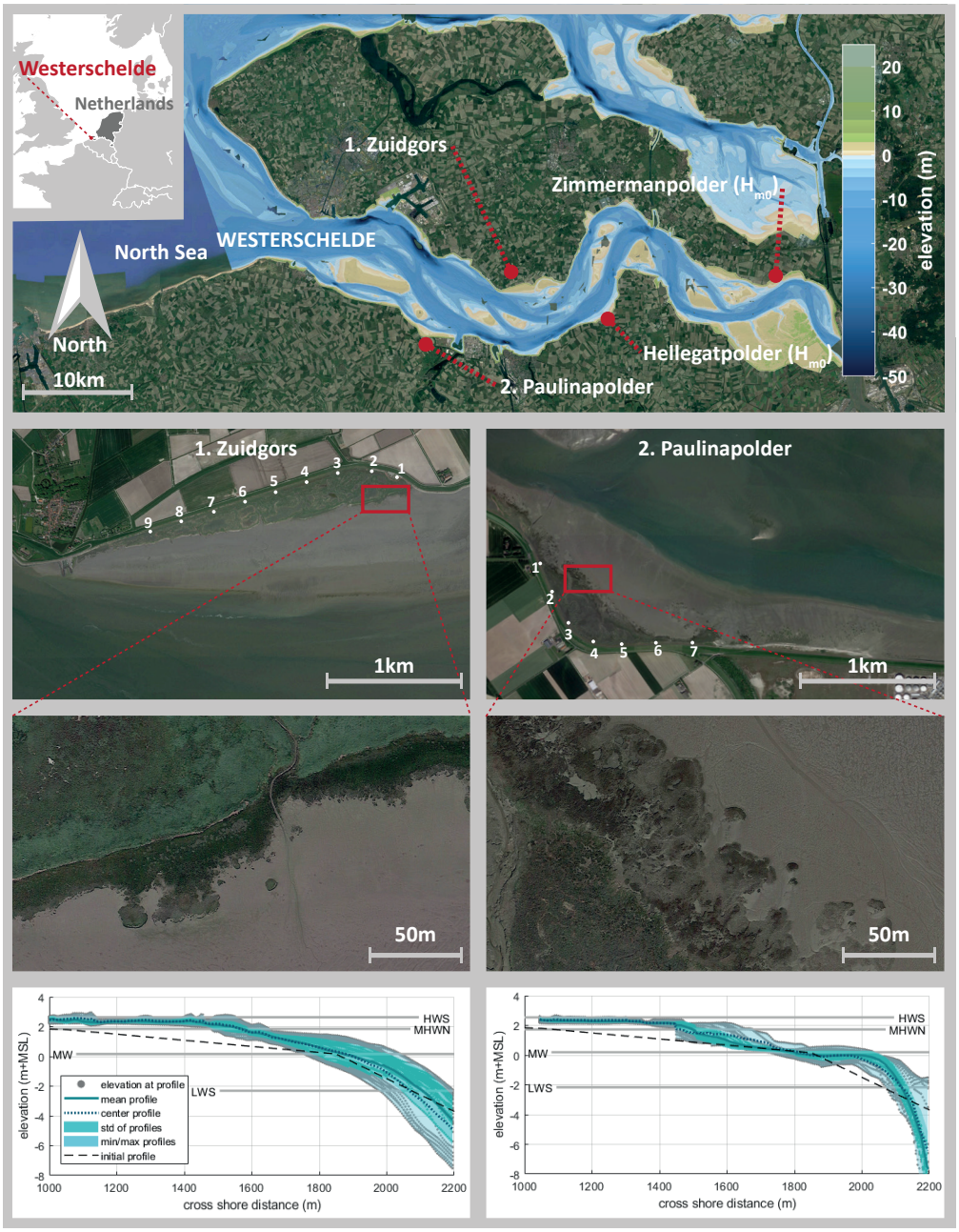
Westerschelde
Netherlands
North Sea
WESTERSCHELDE
1. Zuidgors
Zimmermanpolder (H m0)
Hellegatpolder (H m0)
2. Paulinapolder
North
10km
20
10
0
-10
-20
-30
-40
-50
elevation (m)
1. Zuidgors
1km
2. Paulinapolder
1km
50m
50m
HWS
MHWN
MW
LWS
elevation at profile
mean profile
center profile
std of profiles
min/max profiles
initial profile
elevation (m+MSL)
cross shore distance (m)

Figure 4.1. The Westerschelde estuary in the Netherlands (top panel), whereupon model settings are based. The overlay shows the bathymetry from 2015 (De Kruif, 2001; Marijs and Parée, 2004; Wiegman et al., 2005). Two salt marshes located in the center of the estuary, i.e. Zuidgors at the northern shores exposed to the prevailing wind direction (left panels) and Paulinapolder sheltered from the prevailing wind direction (right panels) were used to determine parameter settings for the model. An aerial picture highlights the salt marsh and fronting tidal flat (second row of panels), with a zoom on the vegetation edge to indicate features and characteristics at the marsh edge, e.g. creeks and vegetation patches (third row of panels). The white dots (second row of panels) highlight the starting points of the transects used to derive the variability of the salt marsh edge from field measurements over a 40 year period (Willemsen et al., 2020). The numbers refer to the profile numbers used in Figure 4.7. Profiles of both study sites measured in the period 1955-2015 in the center of the marshes and tidal characteristics were used to determine the initial profile in the model (bottom row of panels). This data was collected by the Ministry of Infrastructure and the Environment (former Ministry of Transport Public Works and Water Management) (De Kruif, 2001; Wiegman et al., 2005). Source aerial imagery: Google Earth.

4.2.2 | Biogeomorphological model description

4.2.2.1 | *Hydrodynamic and morphodynamic model*

The Delft3D Flexible Mesh (Delft3D - FM) model was used in the current study to simulate hydrodynamics, sediment dynamics and morphological processes. This model and its predecessor Delft3D are widely used in coastal, estuarine and riverine systems (e.g. Ruessink and Roelvink, 2000; Lesser et al., 2004; Kernkamp et al., 2011; Achete et al., 2016). The unsteady shallow water equations in the flow module D-Flow FM (Flexible Mesh) are solved two dimensionally (depth-averaged, 2DH), which shows similar results for hydrodynamics and deposition rates as three-dimensional (3d) models (Horstman et al., 2015).

D-Waves was used to simulate waves (Deltares, 2019c). D-Waves is based on the third generation SWAN (Simulating WAves Nearshore) spectral wave model (Booij et al., 1999; Ris et al., 1999). SWAN can be used to simulate the evolution of random, short-crested wind-generated waves in coastal regions. The model computes wave propagation, wave generation by wind, non-linear wave-wave interaction and dissipation.

Transport of cohesive sediment was calculated using D-Morphology (Deltares, 2019b) by solving the advection-diffusion equation for suspended sediment, whilst sedimentation and erosion are calculated with the Partheniades-Krone equations (Partheniades, 1965).

Shear stresses exerted by vegetation on the flow were taken into account by using the trachytopes model in D-Flow FM (Deltares, 2019a). The flow resistance is parameterized by means of a bed roughness determined by plant dimensions following Baptist (2005b).

Wave attenuation by vegetation is resolved by the Méndez-Losada equation (Méndez and Losada, 2004; Suzuki et al., 2012).

4.2.2.2 | *Dynamic vegetation growth model*

Vegetation establishment and growth for *Spartina anglica* was calculated by the population dynamics balance equation in (Eq. 4.1) (Temmerman et al., 2007; Schwarz et al., 2014). The change of the total stem density over time was calculated as a result of vegetation establishment (est; Eq. 4.2), lateral expansion of plants through diffusion to neighboring cells (diff; Eq. 4.3), clonal growth of plants up to the maximum carrying capacity by using a logistic function (growth; Eq. 4.4), plant mortality caused by shear stress due to flow and waves (flowwave; Eq. 4.5) and plant mortality due to inundation stress (inund; Eq. 4.6) .

$$\frac{\partial n_b}{\partial t} = \left(\frac{\partial n_b}{\partial t}\right)_{est} + \left(\frac{\partial n_b}{\partial t}\right)_{diff} + \left(\frac{\partial n_b}{\partial t}\right)_{growth} - \left(\frac{\partial n_b}{\partial t}\right)_{flowwave} - \left(\frac{\partial n_b}{\partial t}\right)_{inund} \quad \text{Equation 4.1}$$

$$\left(\frac{\partial n_b}{\partial t}\right)_{est} = r_{01}\,(P_{est}) * n_{b,o} \quad \text{Equation 4.2}$$

$$\left(\frac{\partial n_b}{\partial t}\right)_{diff} = D\left(\frac{\partial^2 n_b}{\partial x^2} + \frac{\partial^2 n_b}{\partial y^2}\right) \quad \text{Equation 4.3}$$

$$\left(\frac{\partial n_b}{\partial t}\right)_{growth} = r * \left(1 - \frac{n_b}{K}\right) n_b \quad \text{Equation 4.4}$$

$$\left(\frac{\partial n_b}{\partial t}\right)_{flowwave} = -n_b * C_{tau} * (\tau - \tau_{cr,p}),\ when\ \tau > \tau_{cr,p} \quad \text{Equation 4.5}$$

$$\left(\frac{\partial n_b}{\partial t}\right)_{inund} = -n_b * C_{inund} * (H - H_{cr,p}),\ when\ H > H_{cr,p} \quad \text{Equation 4.6}$$

Where $\frac{\partial n_b}{\partial t}$ represents the change of the stem density per cell over time in days [stems m^{-2} d^{-1}]. r_{01} (P_{est}) is a function generating at random either a 0 (with probability 1 - P_{est}) or a 1 (with probability P_{est}). The random numbers were generated independently per time step and per cell in the model domain. $n_{b,o}$ is the initial stem density [m^{-2}], D is the plant diffusion coefficient [m^2 d^{-1}], x and y are the horizontal spatial coordinates [m], r is the intrinsic growth rate of the stem density [d^{-1}], K is the maximum carrying capacity of

the stem density (i.e. maximum number of stems that can be present) [m^{-2}], C_{tau} is the plant mortality coefficient due to bed shear stress [d^{-1} ($N\ m^{-2}$)$^{-1}$], τ is the bed shear stress exerted by flow and waves [$N\ m^{-2}$], $\tau_{cr,p}$ is the critical bed shear stress for plant mortality [N m-2], C_{inund} is the plant mortality coefficient due to inundation stress [$d^{-1}\ m^{-1}$], H is the inundation height [m], and $H_{cr,p}$ is the critical inundation height at high tide [m].

4.2.2.3 | *Biogeomorphological coupling*

The vegetation growth module was set up in Python. This module was coupled to the hydrodynamic (both flow and wave) and the morphological Delft3D - FM model through BMI (Basic Model Interface) (Peckham et al., 2013). BMI exchanges memory location pointers between the Delft3D-FM and Python models. Consequently, model parameters and (state) variables are exchanged through memory, thus avoiding any file writing and reading when switching between the codes. The flow model simulates tidal flow with a computational time step of maximum 30 s; this timestep decreases if the maximum Courant number of 0.7 is exceeded (Deltares, 2019a). The wave model was set up to simulate wave propagation every 3600s.

Morphological change was calculated every computational timestep ('online'). However, the morphological change was multiplied with an acceleration factor ('MorFac'; Roelvink, 2006) of 100 every single timestep. The computation of a subsequent hydrodynamic timestep uses the morphological change multiplied by the acceleration factor, ensuring that the hydrodynamic computations are carried out using the correct bathymetry. Applying this factor means that 3.6 days of hydrodynamic calculations represents the morphological change of approximately a single year, i.e. 180 hydrodynamic days represent 50 years. A full spring-neap cycle of approximately 14 days represents the morphological change of 3.9 years. The acceleration factor used in this study was equal to the acceleration factor used in Best et al. (2018), whereas earlier studies of salt marsh development used an acceleration factor of approximately 700 (Temmerman et al., 2007). The vegetation development was calculated once every 100 morphodynamic days (i.e. once every single hydrodynamic day); the change in vegetation over a time step of nominally one day, corresponds to vegetation change over 100 days in the morphological timescale. The physical variables driving vegetation development (e.g. inundation height and bed shear stress), were cumulatively stored every hydrodynamic computational timestep (of maximum 30 s), for calculating vegetation dynamics every hydrodynamic day. Vegetation dynamics was modelled as a year-averaged process and does not vary seasonally, even though several vegetation time steps occur in a single morphological year.

The full model was controlled in Python. First, the vegetation establishment was calculated over the model grid. Next, the flow, wave and morphodynamic model were

executed over the vegetation timestep, which is a hydrodynamic day (equal to 100 days of morphodynamics and vegetation development). After a day, hydrodynamic results over the vegetation time step were used to inform the vegetation growth and decay. In addition, new vegetation establishment was calculated. The results of the vegetation model, i.e. new vegetation presence and density (plant dimensions were considered constant), were used to set a new vegetation roughness field in Delft3D-FM. Then a new loop of hydrodynamic and morphodynamic calculations started (Fig. 4.2).

4.2.3 | Model setup

4.2.3.1 | *Model domain*

The model domain of the depth-averaged flow model represented an area with a cross-shore width of 2500m and an alongshore length of 1000m (Fig. 4.3). The cell size applied over the full domain is 5m, both in x- and y-direction. The domain of the wave model was larger in the alongshore direction (i.e. 2000m) to prevent boundary effects. The cell size over the outer wave domain was 15m, both in x- and y- direction. A grid with a smaller cell size was nested in the larger wave model, the alongshore length of the inner grid is 1100m with a cell size of 5m both in x- and y-direction.

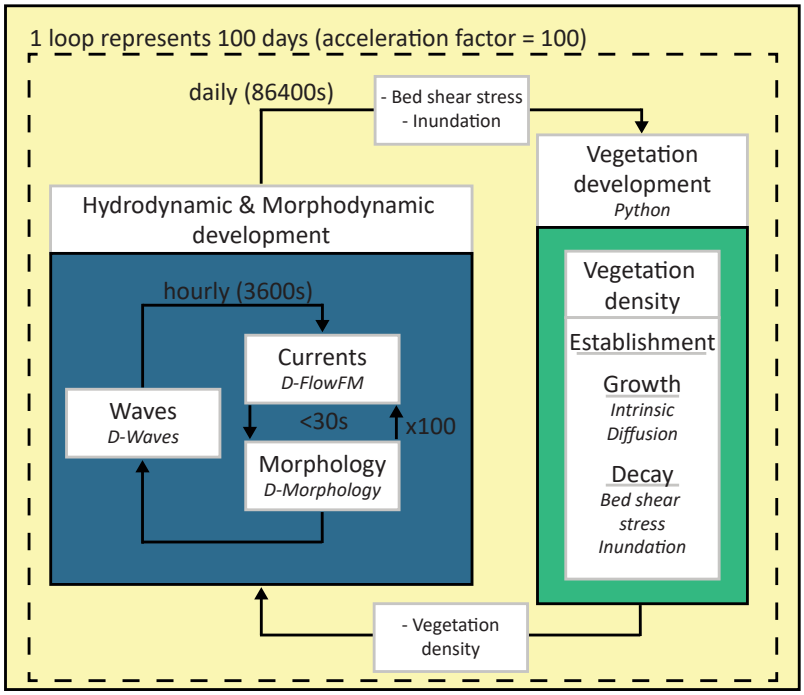

Figure 4.2 | Flowchart of modelling approach and online coupling of interactive computation of hydrodynamic, morphodynamic and vegetation development using the Basic Model Interface (BMI). BMI is used for initializing and orchestrating the full model. D-Flow FM and D-Morphology compute currents and morphological change at least every 30s. Once every hour (3600s) bed shear stresses due to waves are computed using D-Waves. Computed bed shear stresses are combined with results from D-Flow FM for a full hour. Vegetation density is computed once every day (86400s), using bed shear stresses and inundation calculated in the hydrodynamic and morphodynamic model. The updated vegetation density per grid cell is used as input for the hydrodynamic and morphodynamic model for the subsequent time steps. To reduce the computational time to approximately five days for a 50 year run, an acceleration factor of 100 is applied on morphological change.

4.2.3.2 | *Topography*

A typical initial profile was derived from the dataset presented in Willemsen et al. (2020). The direction of the profiles was aligned to the wind direction during an extreme event statistically occurring once every 10,000 years (Willemsen et al., 2020) (Fig. 4.1), to be able to compare the simulated dynamics of the salt marsh edge with field observations. Relative to MSL, the initial bed level height at the most seaward location of the domain is -7 m, well below MLWS (mean low water spring) of -2.31m (Zuidgors)

and -2.16m (Paulina). The bed level increased to the local mean sea level (0.16m at Zuidgors; 0.19m at Paulinapolder) over a distance of approximately 650m. Subsequently the bed level reached MHWN, which is 1.85m at Zuidgors and 1.73m at Paulina, over a distance of 800m (Fig. 4.1; bottom panels). This part of the profile was explicitly chosen to be linear, to prevent imposing a convex-up or concave-up profile affecting vegetation establishment and growth at the tidal flat and potential marsh area and thereby already tending towards an expanding or retreating salt marsh. MHWN has been used previously as fixed elevation threshold for vegetation growth in the Westerschelde (Doody, 2007; Van der Wal et al., 2008). Finally, the topography increased to MHWS (mean high water spring; 2.63m at Zuidgors; 2.54m at Paulina) over the last 1050m of the domain. The initial topography was uniform in alongshore direction. Random perturbations in the range of -1cm - +1cm were added on to the initial bed elevation of each grid cell for initiation of pattern development (c.f. Best et al., 2018).

4.2.3.3 | *Boundary conditions and model parameters*

The model contained a single open boundary at the southern end of the model extent (Fig. 4.3). The other three boundaries were closed. The water levels at the open boundary were constructed using the semidiurnal M2 and S2 tidal constituents, resulting in a repeated spring-neap tidal cycle. The range of the tidal signal was 4.93m with a mean tide level of 0.16m (Van der Wal et al., 2008). MLWS and MHWS were -2.32m and 2.64m respectively and MLWN and MHWN were -1.52m and 1.85m respectively. Wave forcing was applied to the model by continuously imposing a mild wave height and wave period at the open southern boundary. The wave height at the boundary was based on measurements of the wave height seaward of the vegetation edge at a marsh at the northern and southern shores of the Westerschelde (Hellegatpolder and Zimmermanpolder resp.; Fig. 4.1). The average wave height (H_{mo}) measured over approximately a year at both locations was approximately 0.11m with a standard deviation of 0.07m to 0.08m (Willemsen et al., 2018). The continuous wave heights used in the model scenarios, were situated around this average. Wave heights in the model were specified as the significant wave height (H_s), which is similar, though not equal, to the wave height (H_{mo}). Suspended sediment concentrations (SSC) measured in the stream channel of the Westerschelde generally ranged between approximately 10mg/L and 75mg/L (10^{th} and 90^{th} percentile) (Van Damme et al., 1999; Temmerman et al., 2004). In the current model the vertically averaged suspended sediment concentration was varied between 10mg/L and 50mg/L at the open boundary.

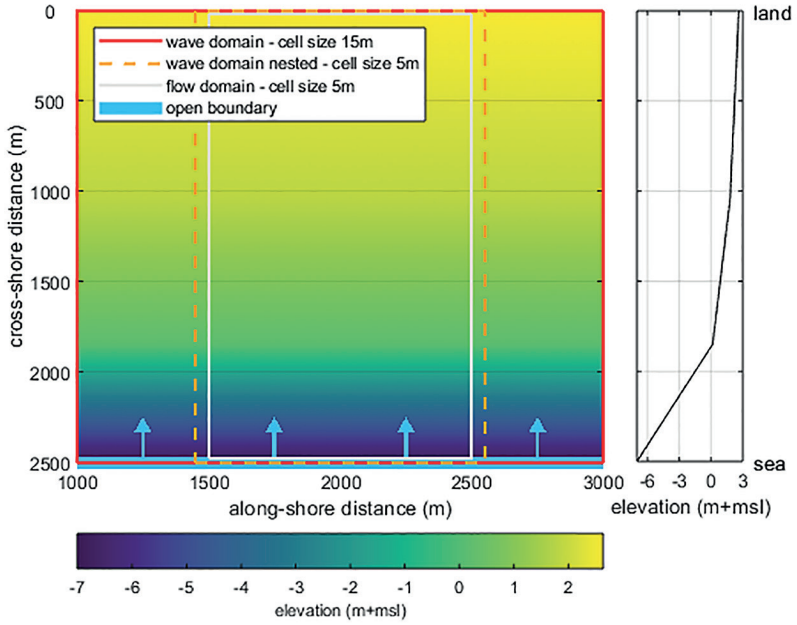

Figure 4.3 | The flow model domain extending over 1000m in alongshore direction and 2500m in cross-shore direction for the flow model (grey box). The flow model has a computational cell size of 5m. The wave domain is larger, extending over 2000m in alongshore direction. The cell size of the outer wave domain (red box) is 15m, whereas a nested inner domain (orange dashed box) with a cell size of 5m is used. An open boundary is imposed at the south side of the domain (left panel; blue line and arrows). Colors indicate the bed level elevation, for which the initial profile (right panel) started at -7m, increased to mean sea level, further increased to mean high water neap and is completed at mean high water spring.

4.2.3.4 | *Hydrodynamic model parameters*

A uniform Manning bed roughness of 0.023 s m-1/3 was used, which is slightly higher than the value for open waters (Wamsley et al., 2010), because of the location in the intertidal (Table 4.1). Manning values were comparable with values used in previous studies on salt marshes in general and salt marshes in the Westerschelde (e.g. Best et al., 2018). The horizontal eddy viscosity and eddy diffusivity should be typically in the range of 1 to 10 m^2 s for grid cell dimensions of tens of meters or less and were both set to 10 m^2 s, which is the default value (Deltares, 2015).

4.2.3.5 | *Morphodynamic model parameters*

A uniform fine cohesive sediment was applied in the model, generally appearing at tidal flats and salt marshes in the Westerschelde (Willemsen et al., 2018). Default values were used for the reference density for hindered settling calculations, specific density of the material and dry bed density of the sediment with voids, respectively 1600kg m^{-3}, 2650kg m^{-3} and 500kg m^{-3} (Table 4.1). The settling velocity for the cohesive sediment was set to 0.5mm s^{-1}, which is approximately the settling velocity of the average grain size diameter found around the salt marsh edge in the Westerschelde (Willemsen et al., 2018). A value of 0.5N m^{-2} was applied for the critical bed shear stress for erosion, whereas the critical bed shear stress for deposition was set to 1000N m^{-2} enabling sedimentation unrestricted by bed shear stresses. The erosion parameter was set to 5 * 10^{-5}kg m^{-2} s^{-1} (Best et al., 2018; Deltares, 2019b). To decrease the computational time an acceleration factor of 100 was applied (Fig. 4.2).

Table 4.1 | Hydrodynamic and sediment parameter settings used in the model study.

Parameter	Symbol	Value	Unit	Source
Uniform friction coefficient	n	0.023	s $m^{-1/3}$	Wamsley et al. (2010); Deltares (2019a)
Eddy viscosity	v	10	m2 s^{-1}	Deltares (2015)
Eddy diffusivity	D	10	m2 s^{-1}	Deltares (2015)
Reference density	$\rho_{s,o}$	1600	kg m^3	Best et al. (2018); Deltares (2019b)
Specific density	ρ_s	2650	kg m^3	Best et al. (2018); Deltares (2019b)
Dry bed density	$\rho_{s,dry}$	500	kg m^3	Best et al. (2018); Deltares (2019b)
Settling velocity cohesive sediment	ω_s	0.5	mm s^{-1}	Willemsen et al. (2018)
Critical bed shear stress for erosion	$\tau_{cr,e}$	0.5	N m^{-2}	Best et al. (2018); Deltares (2019b)
Critical bed shear stress for deposition	$\tau_{cr,d}$	1000	N m^{-2}	Best et al. (2018); Deltares (2019b)
Erosion parameter	M	5 * 10^{-5}	kg m^{-2} s^{-1}	Best et al. (2018); Deltares (2019b)
Acceleration factor	AF	100	-	-

4.2.3.6 | *Vegetation growth*

Vegetation growth was simulated by changing the stem density according to the population dynamics model. In this study the salt marsh species *Spartina anglica* (cordgrass) was simulated. The drag coefficient (C_D) of vegetation depends on hydrodynamic conditions and the vegetation species. The drag coefficient under storm conditions for *Spartina anglica* was previously calibrated to be 0.5 (Vuik et al., 2016). Under small wave heights it can be assumed that the stems are rigid, for which a C_D coefficient of 1.0 is commonly used (Suzuki and Arikawa, 2010). In the current study a value of 0.7, in between the previous values, was used, to take into account various conditions and vegetation of different ages. Average values were assumed for the stem height (0.5 m) and stem thickness (4.3 mm) (Temmerman et al., 2007), whereas the vegetation density was variable, driven by the population dynamics model. The establishment chance (P_{est}), was equal to 1% (Eq. 4.2) ; vegetation establishes at 1% of the area, representative for a slow colonizer like *Spartina anglica* (Schwarz et al., 2018). The intrinsic growth rate of the vegetation (r) was equal to 1 per vegetation time step, which is in this study equal to a single hydrodynamic day and 100 morphodynamic days due to the use of an acceleration factor. The maximum stem density (K) was 1200 stems m-2 (van Hulzen et al., 2007) (Eq. 4.4).

First the vegetation establishment, $\left(\frac{\partial n_b}{\partial t}\right)_{est}$ was calculated (Eq. 4.2). The subsequent growth and decay (Eq. 4.3,4. 4, 4.5, 4.6) in the next vegetation timestep was solved using an ordinary differential equation solver, iterating towards the solution (c.f. Soetaert et al., 2010).

Table 4.2 | Vegetation growth parameters used in the model study. The vegetation time steps are defined in hydrodynamic days, equal to 100 morphodynamic days.

Parameter	Symbol	Value	Unit	Source
Chance of vegetation establishment	P_{est}	0.01		Schwarz et al. (2018)
Initial vegetation density of established vegetation	$n_{b,o}$	200	m^{-2} day^{-1}	van Hulzen et al. (2007)
Intrinsic growth rate of vegetation	r	1	Day^{-1}	van Hulzen et al. (2007)
Maximum carrying capacity of stem density	K	1200	Stems m^{-2}	Temmerman et al. (2005)
Vegetation diffusion coefficient	D	0.2	m^2 day^{-1}	van Hulzen et al. (2007)
Vegetation mortality coefficient due to bed shear stress	C_{tau}	30	Day^{-1} (N m-2)$^{-1}$	van Hulzen et al. (2007)
Critical bed shear stress for vegetation mortality	$\tau_{cr,p}$	0.26	N m^{-2}	van Hulzen et al. (2007)
Vegetation mortality coefficient due to inundation stress	C_{inund}	3000	Day^{-1} m^{-1}	van Hulzen et al. (2007)
Critical inundation height for vegetation mortality	$H_{cr,p}$	1.1	m	van Hulzen et al. (2007)
Uniform vegetation diameter	B_{veg}	0.0043	m	Temmerman et al. (2005)
Uniform vegetation height	h_{veg}	0.5	m	Temmerman et al. (2005)

4.2.4 | Model scenarios

Four scenarios were simulated with different homogeneous significant wave heights (H_s). Marshes only affected by tidal flow are simulated with a significant wave height (H_s) of 0.00m, whereas the influence of both waves and tidal flow were assessed for waves with a height (H_s) of 0.05m, 0.10m and 0.15m (Table 4.3). The wave period (Tm_{01}) at the boundary was based on a constant wave steepness of 0.01. A suspended sediment concentration of 10 mg/L was imposed at the boundary for all four scenarios. The suspended sediment concentration was varied for the scenario with a significant wave height of 0.10 m, since this wave height is closest to values occurring in the field (Callaghan et al., 2010; Willemsen et al., 2018). The suspended sediment concentrations imposed at the boundary were 10 mg/L, 25 mg/L and 50 mg/L (Table 4.3). The scenario runs covered a period of 50 years. The computational time of a single run was limited to approximately five days (2 cores @ 3.50 GHz; 32 GB memory).

Table 4.3 | Scenarios with a varying wave height and suspended sediment concentration.

Scenario	Wave height, Hs (m)	Suspended sediment concentration, SSC (mg/L)
1	0.00	10
2	0.05	10
3	0.10	10
4	0.10	25
5	0.10	50
6	0.15	10

4.3 | Results

4.3.1 | Salt marsh development and marsh-edge patterns after 50 years under homogeneous wave conditions

After 50 years of development in the model, the salt marsh edge revealed distinct features typically occurring at salt marshes in the field (Fig. 4.1; Fig. 4.4). The form and presence of those features depended on the incoming wave forcing at the seaward boundary. A homogeneous wave forcing of 0.00m (Hs) resulted in the formation of creeks landward from the vegetation edge (Fig. 4.4; first row of panels). The creeks extended landward with multiple branches over a cross-shore width of 200m. The large creeks showed an alongshore spacing of approximately 100m. Moreover, vegetation patches with a diameter ranging from approximately 5m (the size of a single computational cell) to 50m were found seaward from the salt marsh edge (Fig. 4.4; first row of panels).

A sawtooth pattern was observed after salt marsh development of 50 years with a homogeneous wave forcing of 0.05m (H_s; Fig. 4.4; second row of panels), approximately at the same cross-shore location as the marsh edge developed without waves. Four to five coves formed over an alongshore distance of 1000m. An area with vegetation patches formed seaward from the marsh edge. Nevertheless, the cross-shore width of the area with patches was smaller than the area with patches resulting from the run without waves.

The development of the salt marsh edge under a homogeneous wave forcing of 0.10m (H_s; Fig. 4.4; third row of panels) showed similarities with the development of the marsh edge under a significant wave height of 0.05m (i.e. Fig. 4.4; second row of panels). A sawtooth pattern developed with vegetation patches appearing seaward from the marsh edge. However, the alongshore variability of both the patterns and the patches was larger. Moreover, a gradient of vegetation density formed in the alongshore direction (Fig. 4.4; third row of panels).

The marsh edge showed no pattern at all in the model scenario with the largest wave forcing (H_s = 0.15m; Fig. 4.4; fourth row of panels). The straight marsh edge was formed as no new vegetation could establish in front of the existing marsh edge due to the larger waves, as visible from the abrupt transition from 1200 to 0 stems m^{-2} at the edge.

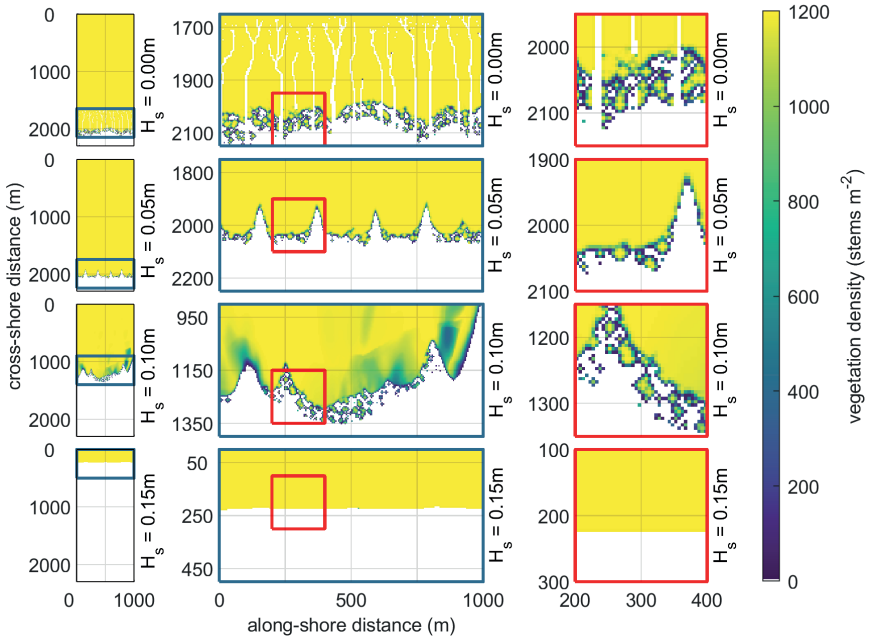

Figure 4.4 | The vegetation density at the salt marsh in year 50, with continuous wave forcing. The model was forced with a significant wave height of 0.00m, 0.05m, 0.10m and 0.15m (from top to bottom). The full model domain is visualized in the left panels with the blue box indicating a zoom window around the vegetation edge. The zoom of the vegetation edge is highlighted in the second column of panels. A zoom (red box) indicating the different features at the salt marsh edge is highlighted in the right panels. Note that the cross-shore location of the marsh edge after 50 years is different, depending on the wave forcing (see left panels and y-axis of the second and third row of panels).

4.3.2 | Cross-shore profile characteristics and variability at the marsh edge

The development of the cross-shore profile was highly affected by the wave forcing (Fig. 4.5). The alongshore averaged profile after 50 years of salt marsh development remained rather similar to the initial profile with low wave forcing (H_s = 0.00m and H_s = 0.05m). With increasing wave forcing at the boundary (H_s = 0.10m and H_s = 0.15m), a cliff formed at the landward side of the domain, approximately 200m from the landward boundary.

Homogeneous waves of Hs = 0.10m, resulted in a cliff with a height of approximately 1.00m, whereas homogeneous wave forcing of 0.15m resulted in a cliff with a height of 4.00m (Fig. 4.5). The extreme magnitude of the latter cliff, which is not observed in the field, is probably a result of the homogeneity of the wave forcing, which is more diverse in reality. Where the wave height determines the general height of the profile, the suspended sediment concentration determines the steepness of the profile (Fig. 4.5). The alongshore variability of the profile after 50 years of salt marsh development decreased with increasing wave heights (Fig. 4.5; standard deviation). Smaller wave heights allowed patterns with large alongshore variability to develop (e.g. creek formation inside and outside the vegetated area and development of vegetation patches; Fig. 4.4; Fig 4.6), resulting in larger alongshore variability of the bed elevation (Fig. 4.7).

Over time, the development of the vegetated salt marsh after initial establishment largely depended on the wave forcing. Without waves and with small waves (Hs = 0.00m and H_s = 0.05m), the salt marsh extended seaward, while the salt marsh retreated landward with larger homogeneous wave forcing (H_s = 0.10m and H_s = 0.15m; Fig. 4.6). However, with larger suspended sediment concentrations, the marsh was able to switch from an retreating towards an extending marsh (H_s = 0.10m; Fig. 4.6). The final location of the salt marsh edge was quickly reached for the lower wave heights (H_s = 0.00m and H_s = 0.05m), a slight seaward extension of tens of meters only was observed over the last four decades (Fig. 4.6). Nevertheless, differences were observed in the development of vegetated salt marshes with larger wave heights (H_s = 0.10m and H_s = 0.15m): the occurrence of a cliff in the bathymetry largely affected vegetation growth. Vegetation was still able to establish in front of the cliff with H_s = 0.10m over a cross-shore width of over 1000m, although the variability of the vegetation density in this area was rather high due to the wave forcing (200 – 1200 stems m^{-2}). However, vegetation was not able to establish in front of the cliff with the largest homogeneous wave height (H_s = 0.15m; Fig. 4.6), resulting in an abrupt transition from a vegetation density of 1200 to a density of 0 stems m^{-2}. The latter resulted in a rather small decadal variability of the cross-shore location of the marsh edge (Fig. 4.7). This deviates from the increasing variability of the location of the marsh edge with increasing wave heights between wave heights (H_s) of 0.00m and 0.10m.

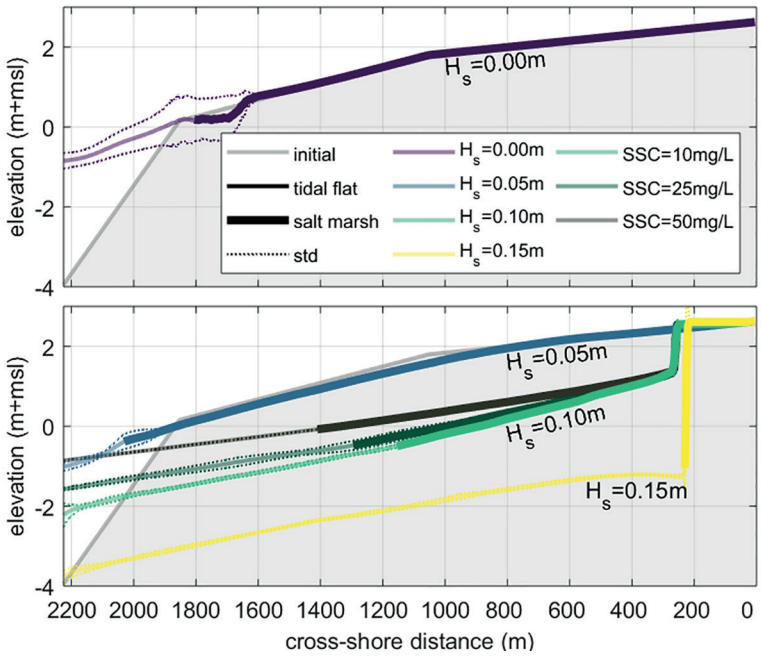

Figure 4.5 | Final alongshore averaged profiles after 50 year salt marsh development under different wave forcing and sediment availability (colored profiles in both panels). The top panel highlights the results for the development without waves, whereas the bottom panel indicates the results for development with waves (H_s = 0.05m, H_s = 0.10m, H_s = 0.15m) and with a suspended sediment concentration at the boundary of 10mg/L, 25mg/L and 50mg/L for the scenario with a wave height of 0.10m. The profile of the vegetated salt marsh is presented with a thick line, whereas the profile of the bare tidal flat is indicated with a smaller line in both subplots. The standard deviation of the alongshore averaged profile is highlighted with the dotted line. The initial profile is presented in the background (gray).

Patterns incising in the bed and vegetation were observed to be largest with the smallest wave heights (Fig. 4.4; Fig. 4.6). Creeks developed in model runs without waves and reached a cross-shore width of up to 500m. Multiple branches originating from a single creek were observed. Landward development of the creeks developed by incising in the vegetation and resulted in meandering branches, whereas the straighter parts developed inside the area with establishing vegetation patches. Vegetation was not able to establish in front of existing creeks, due to larger inundation times and rather high bed shear stresses (Fig. 4.4; Fig. 4.6). Periodic incisions were observed in the results of the runs with larger wave heights (H_s = 0.05m and H_s = 0.10m). A sawtooth pattern with two to four coves was observed at the salt marsh edge. Creeks were not able to form, probably due to enhanced suspended sediment concentrations induced by the wave

forcing, resulting in an alongshore smoothed bottom. The latter was also observed in the alongshore standard deviation of the profile (Fig. 4.5). The occurrence of patterns decreased with increasing wave heights. No patterns were observed in the results of the run with H_s = 0.15m, due to the formation of a cliff, preventing vegetation to establish in the lower elevated parts of the profile.

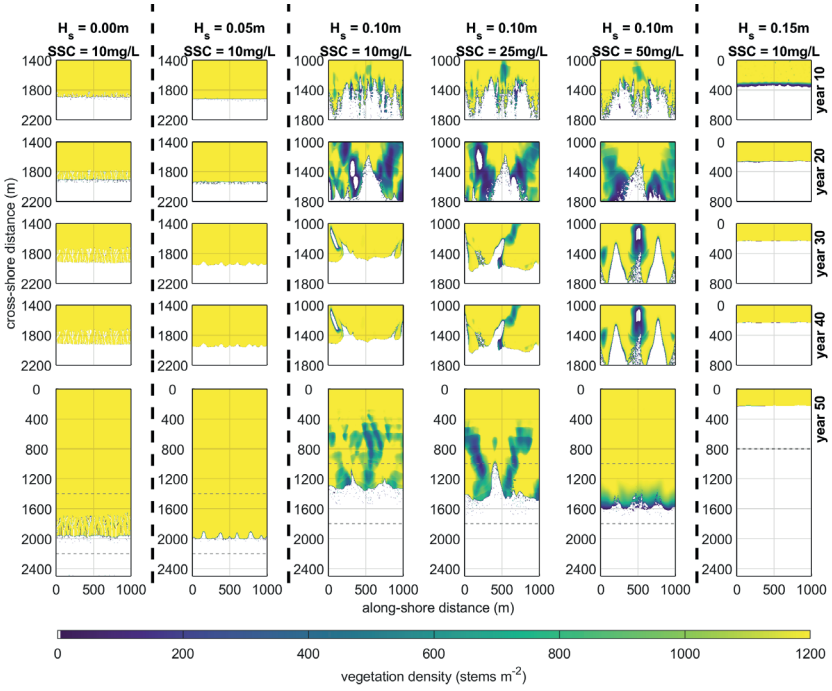

Figure 4.6 | The development of the vegetation density (colormap) at the salt marsh around the edge per 10 year (columns of panels from top to bottom). The resulting vegetation density after 50 years is presented for the full domain (bottom row of panels). The area around the vegetation edge that is presented in the first four rows of panels is indicated in the full domain (bottom row of panels) with a dashed box. The model was forced with a significant wave height of 0.00m, 0.05m, 0.10m and 0.15m and a suspended sediment concentration of 10 mg/L, 25 mg/L and 50 mg/L (rows of panels from left to right).

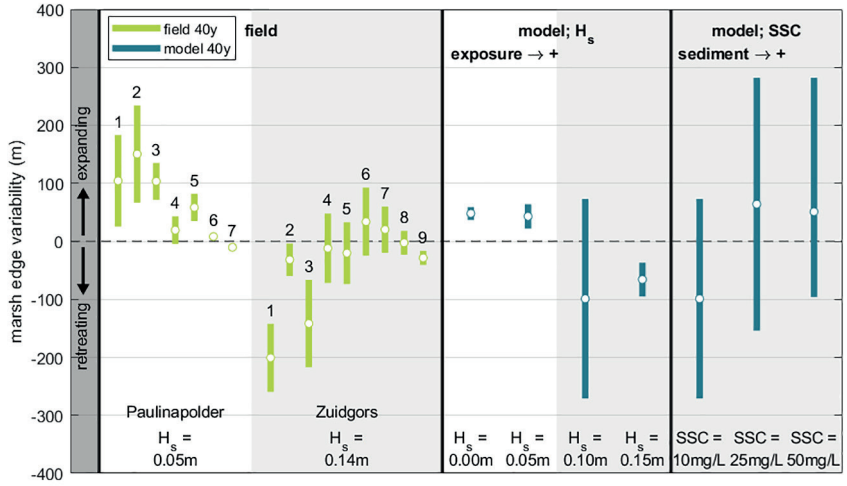

Figure 4.7 | Variability of the marsh edge, i.e. mean location of the marsh edge (white marker) and standard deviation (bar). The variability was derived from field data (left part of the figure) over a period of 40 years (1975-2015) and from the model over a period of 40 years (right part of the figure). The numbers above the bars representing field data correspond to the transects shown in figure 4.2. The results both from the field and model are sorted with an increasing wave exposure (left and center part; from left to right); the model results with a default suspended sediment concentration of 10 mg/L, and increasing sediment availability (right part; from left to right). The study sites Paulinapolder and Zuidgors were used for comparison (Fig. 4.1). The marsh edge retreats if the variability is negative (decreasing marsh width), whereas the marsh edge expands if the variability is positive (increasing marsh width).

4.3.3 | Comparing modelled marsh edge characteristics to field observations

To validate the model predictions, the variability of the marsh edge was quantified using field data from the salt marshes Zuidgors and Paulinapolder in the Westerschelde estuary (Fig. 4.1. Generally, over a 40 year period (1975 – 2015), the marsh edge at Zuidgors (exposed to the prevailing wind direction) retreated, whereas the marsh edge at Paulinapolder (sheltered from the prevailing wind direction) expanded (Fig. 4.7). This can be explained by the hydrodynamic energy occurring in both systems. Generally high hydrodynamic energy results in increasing bed level dynamics, a lower bed elevation and longer inundation periods; an environment in which vegetation is not able to establish. On the contrary, low hydrodynamic energy leads to less bed level dynamics and inundation periods remain rather small, giving vegetation the opportunity to establish (Bouma et al., 2016; Willemsen et al., 2018). The mean wave height observed seaward

from the marsh edge at the tidal flat, specifically during calm conditions was 0.14m at Zuidgors (standard deviation of 0.06m), versus 0.05m at Paulinapolder (standard deviation of 0.03m) (Callaghan et al., 2010).

An expanding marsh edge was observed (Fig. 4.7) for the model scenarios both without wave forcing (Hs = 0.00m) and with rather small continuous wave forcing (H_s = 0.05m). The modelled marsh edge expanded seaward over 50 meters on average over a period of 40 years, which corresponds to the average variability of the marsh edge at Paulinapolder (Fig. 4.7). Moreover, the modelled average of the marsh edge variability, relative to the initial location of the modelled period, corresponds with observations at Paulinapolder.

A retreating marsh edge was observed at the model runs with larger continuous wave forcing (H_s = 0.10m and H_s = 0.15m), although with increasing sediment availability the marsh was also able to expand. This is generally supported by the field observations at the Zuidgors marsh, were transects both were expanding and retreating at a single marsh. The simulated marsh edge retreated landward with 120 meters on average over a period of 40 years (H_s = 0.10m and H_s = 0.15m), but was also able to extend over a length of approximately 60m with larger suspended sediment concentrations, corresponding to the average variability of the marsh edge at the exposed marsh Zuidgors (Fig. 4.7). Pioneer vegetation was not able to establish seaward from the existing marsh in the model run with H_s = 0.15m (Fig. 4.7). However, vegetation patches were observed in the model runs with smaller wave forcing (H_s = 0.00m, 0.05m and 0.10m). Vegetation patches appearing after 50 years of model development were similar in size (5m – 50m) as the patches observed in the field (Fig. 4.1; third row of panels). The amount of pioneer vegetation growing in patches generally decreases with larger wave heights in the model, which is observed in the field as well.

4.3.4 | Biophysical response of marshes to waves: marsh width, height and vegetation patterns at the marsh edge

The salt marsh responded differently to different homogeneous wave forcing. Different responses were observed for increasing wave height, with a homogeneous suspended sediment concentration of 10 mg/L: (1) the cross-shore marsh width and marsh platform height was largest in the absence of waves (Fig. 4.8; panel 1, 2, 3); (2) the marsh width and height remained rather similar, whereas the alongshore variability decreased with small waves (H_s = 0.05m). Alongshore periodic vegetation patterns appeared at the marsh edge (Fig. 4.6; second row of panels); (3) Both the marsh width and height decreased with medium waves, since vegetation was not able to establish at a lower elevation (H_s = 0.10m), and the alongshore variability of both largely increased (Fig. 4.8; panel 1, 2, 3). The cross-shore variability of vegetation density was observed (Fig. 4.6; third row

of panels); and (4) the marsh width and height further decreased with large waves (Hs = 0.15m). Moreover, the variability of the marsh width and height decreased to almost zero (Fig. 4.8; panel 1, 3), at the same time a lack of variability in vegetation density was observed (Fig. 4.6; fourth row of panels), since vegetation was almost not able to establish at lower heights (Fig. 4.8; panel 2).

The modelled cross-shore width of the salt marsh was affected by wave height (Hs). The mean width was approximately 2000m for low wave heights (H_s = 0.00m and Hs = 0.05m). Once the wave height increased to H_s = 0.10m and larger, initiation of cliff formation was observed (Fig. 4.5) and the width of the salt marsh decreased to 1300m (H_s = 0.10m) and 220m (H_s = 0.15m). The salt marsh width was affected by cliff formation, with the appearance of cliffs depending on the wave forcing (Fig. 4.8; panel 1). The decreasing salt marsh width, was probably driven by a decreasing elevation of the full profile, and the vegetation being unable to grow at lower elevations with increasing wave heights (Fig. 4.8; panel 2).

The mean height of the vegetated salt marsh platform changed with the incoming wave height as well (Fig. 4.8; panel 2). The height of the platform decreased with increasing wave heights. Although cliff formation was initiated when the wave height exceeded 0.10m, a clear threshold affecting the height of the salt marsh platform was not observed for wave heights between H_s = 0.00m and H_s = 0.10m. The average height of the salt marsh platform decreased from 1.55m+MSL to 1.49m+MSL to 1.18m+MSL. Once the wave height increased (H_s = 0.15m), the platform height suddenly increased (2.60m+MSL).

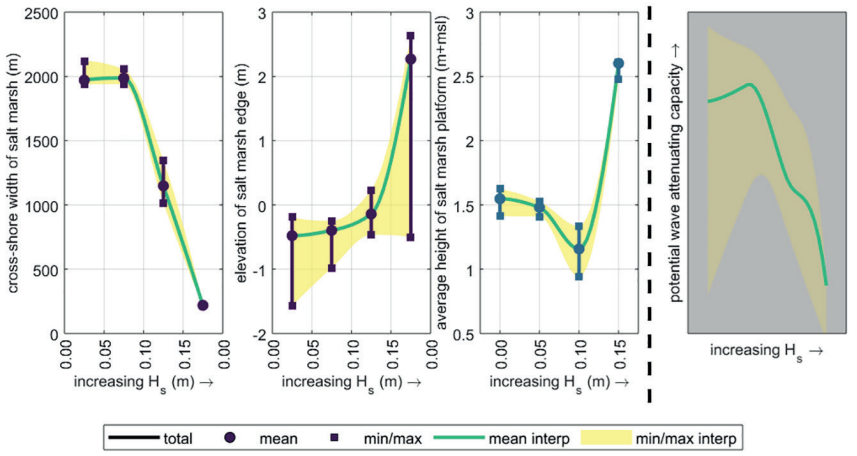

Figure 4.8 | Cross-shore width of the vegetated salt marsh (panel 1), the height of the salt marsh edge (panel 2) and the height of the salt marsh platform (panel 3) for a suspended sediment concentration of 10 mg/L, both averaged first over the alongshore direction of the salt marsh and second averaged over the last ten years of the model run. The total length and height of the salt marsh is highlighted with a single line. The mean values are indicated by the circular marker, while the minimum and maximum values are indicated by the square marker. The green line highlights the mean, interpolated over salt marsh development forced with different wave heights (H_s), whereas the interpolated minimum and maximum are indicated with a yellow area. Since the wave forcing drives the development of the cross-shore width, the location of the salt marsh edge and the platform height of the salt marsh; and all these parameters are related to the wave attenuating capacity, the wave attenuating capacity is indirectly associated to the forcing. A qualitative impression of the potential wave attenuating capacity is outlined in panel 4 and discussed in section 4.4.2.

4.4 | Discussion

To enable implementation of marshes in hybrid flood defenses, it is essential to understand the long-term marsh width dynamics (Bouma et al., 2014; Bouma et al., 2016; Willemsen et al., 2020). The current study showed that the salt marsh is able to grow seaward at low wave forcing (H_s = 0.00m and H_s = 0.05m), and retreats landwards at higher wave forcing (H_s = 0.10m and H_s = 0.15m). Nevertheless, the salt marsh forced with higher waves was able to switch from a retreating extent towards an expanding extent, with increasing sediment availability. However, with increasing waves, the cross-shore profile did not only decrease, the elevation of the lower marsh edge increased as well, resulting in an enhanced retreat of the salt marsh edge.

4.4.1 | Biogeomorphological modelling of the salt marsh width

Previous model studies have assessed processes driving salt marsh development, e.g. on a 2-dimensional (depth-averaged) and 3-dimensional landscape scale (Temmerman et al., 2007; Best et al., 2018). Similar model studies highlight salt marsh development on a timescale of centuries, and aim to assess salt marsh development and/or loss due to sea level rise and changes in sediment availability (Kirwan and Murray, 2007; Kirwan et al., 2010; D'Alpaos and Marani, 2016; Mariotti and Canestrelli, 2017). The latter study highlights that retreat of the salt marsh edge is likely to dominate marsh loss on a timescale of centuries, instead of platform drowning. Simplified models indicate that the salt marsh edge retreats due to wave-induced erosion (Mariotti and Fagherazzi, 2010; Tambroni and Seminara, 2012; Mariotti and Fagherazzi, 2013), thereby enabling marsh loss. Nevertheless, wind waves are not always included in models describing salt marsh development (Temmerman et al., 2005; Temmerman et al., 2007; Belliard et al., 2015). The current study builds upon and extends the previous studies, by explicitly quantifying lateral salt marsh retreat and expansion affected by homogeneous mild wave conditions. By stepwise increasing the wave height, the variability of retreat and expansion of the salt marsh edge can be specifically related to schematic wave climates. Moreover, the sediment availability was changed for waves with a height of 0.10m, to assess whether an increasing sediment availability enables a switch from a retreating to a seaward expanding salt marsh edge.

Salt marsh width is variable over time and the salt marsh edge retreats landward and/or expands seaward with several meters a year (Allen, 2000; Cox et al., 2003; Francalanci et al., 2013; Wang et al., 2017). More specific in the Westerschelde estuary, a general landward retreat of the salt marsh edge is observed at Zuidgors and Zimmermanpolder at the northern shores from 1982 till 2004, whereas a general expanding trend of the salt marsh edge is observed at Paulinapolder and other salt marshes at the southern shores over the same period of 22 years (Van der Wal et al., 2008). These differences between sites may be related to their relative wind exposure. The salt marshes at the northern shores (e.g., Zuidgors) of the Westerschelde estuary are classified as exposed to the prevailing south-westerly winds, whereas the salt marshes at the southern shores (e.g., Paulina) are more sheltered (Callaghan et al., 2010). Even though the daily variability of the wave heights was not considered in this study (i.e., we used a homogeneous wave height to clearly distinguish processes affecting the salt marsh width), the modelled variability of the marsh edge position corresponds well with field observations (Fig. 4.7).

Despite the similarity of the modelled and measured marsh width variability, the range of marsh width (difference between minimum and maximum) for a medium wave height (H_s = 0.10m) and the height of the cliff for a large wave height (H_s = 0.15m), do deviate

from field observations. A more variable wave forcing would probably lead to a smaller range of marsh width variability for model runs with medium waves and less extreme cliff heights for model runs with large waves. Short events with larger waves, which are not included in the model runs, may result in more disturbances, thereby decreasing the amount and duration of calm periods wherein vegetation can establish (Hu et al., 2015b). Moreover, during large wave events, hydrodynamic exposure and bed level change will increase, thereby increasing vegetation mortality (Temmerman et al., 2007) and landward retreat of the marsh edge (Bouma et al., 2016; Willemsen et al., 2018). Vice versa, during periods with rather small waves in a variable wave climate, establishment of vegetation is not disturbed and therefore enhanced (Bouma et al., 2016), resulting in a seaward expanding salt marsh.

In this model exploration, other processes have also been simplified. For example, critical bed shear stresses for erosion were kept constant, even though we know that the longer vegetation is present in a certain area, the stronger the bed becomes (Wang et al., 2017). Moreover, the default suspended sediment concentration imposed at the boundary was in the lower part of the range occurring in the Westerschelde estuary. In general, the salt marsh width and height of the platform is smaller with low suspended sediment concentrations and increases with increasing suspended sediment concentrations (Temmerman et al., 2004; Mariotti and Fagherazzi, 2010). The current study shows, with feedback between hydrodynamics, morphodynamics and vegetation growth, increasing sediment concentrations resulted in a higher marsh platform due to more sedimentation (c.f. Temmerman et al., 2004; Mariotti and Fagherazzi, 2010), thereby decreasing the exposure to waves. This will enhance vegetation growth, enabling the marsh to maintain its position for a longer period. Vice versa, a lower suspended sediment concentration might result in less sedimentation, increasing the exposure to waves and inundation, eventually leading to a smaller marsh (c.f. predictions of Zhu et al., 2020b).

The computational domains for the flow and wave model used in this study prevent boundary effects from occurring, as can be seen in the results (e.g. Fig. 4.6). Morphology and vegetation dynamics are similar at the outsides (east and west) and center of the flow domain. The resolution of the grid (grid cell size) is sufficiently high to prevent influence of the resolution on the hydrodynamics (Bomers et al., 2019b). However, the grid cell size might hamper smaller scale dynamics, like small-scale creek development, although this was not the focus of the current study. The present study focuses on the effect of a constant wave height only. A logical next extension would be to investigate how this interacts with a variable bed strength by a spatio-temporal dynamic critical bed shear stress.

4.4.2 | Implications for Nature-Based Flood Defenses

An important ecosystem service of salt marshes is their wave attenuating capacity, which increases the coastal safety locally (Temmerman et al., 2013). The reduction of the significant wave height (i.e. wave attenuating capacity) of a vegetated foreshore can be explained by the width of the vegetated foreshore and the reduced water depth over such accreted vegetated foreshores (e.g. Möller and Spencer, 2002; Vuik et al., 2016; Willemsen et al., 2020). The current model results indicate the development of wider vegetated foreshores at places with less wave forcing and increasing sediment availability. Moreover, model result highlight a decreasing height of the marsh platform, with larger wave forcing, until the cliff exceeds a certain height, and vegetation is not able to grow seaward from the cliff. When combining the relations of the imposed wave exposure and modelled marsh dimensions, a general non-linear trend can be observed: the development of salt marshes under larger homogeneous wave heights might lead to a smaller potential wave attenuating capacity (Fig. 4.8; qualitative impression in panel 4). Still, the wave attenuating capacity related to a simulated average wave height of 0.10m, which typically occurs at salt marshes in the Westerschelde, is relatively large (Fig. 4.8; Willemsen et al., 2018).

This study emphasizes once more that the widest salt marshes occur at the lowest-energy environments, sheltered from incoming high waves. However, the salt marsh extends with an increasing sediment availability, although the effectivity of increasing the suspended sediment availability seems not infinite. Salt marsh expansion over a period of 40 year is almost similar for a sediment availability of 25 mg/L and 50 mg/L. Nevertheless, an increasing sediment availability can change a retreating marsh towards and expanding marsh, by decreasing the steepness of the profile (Fig. 4.5; Fig. 4.7). The cross-shore width of the salt marsh decreases with increasing homogeneous wave heights. In the low-energy environments where salt marshes thrive, they can contribute to the wave attenuation of extreme storm events, provided that their cross-shore width is sufficient large (Vuik et al., 2016). Ironically, even though wide saltmarshes are very effective in wave attenuation, they generally occur only where waves are small. However, the area of application might largely increase by enhancing marsh growth with engineering measures and using salt marshes as part of a Nature-Based Flood Defense (e.g. Vuik et al., 2019).

Artificial structures like brushwood dams can assist in enhancing vegetation establishment and growth. Lower wave heights enable salt marsh vegetation to establish (Poppema et al., 2019), by decreasing bed level dynamics (Bouma et al., 2016; Cao et al., 2018) and seedling mortality (Cao et al., 2019). This is also observed in this study, lower wave heights enable vegetation to establish at a lower elevation (Fig. 4.8; panel 2).

Additionally, a decreasing inundation period and frequency leads to better opportunities for vegetation to grow (Balke et al., 2016). Moreover, suspended sediment can easily settle because of the presence of the structures, thereby increasing the bottom level (Siemes et al., 2020). Combined with the results from the current study, using artificial structures will lead to a larger marsh width, due to the absence of small continuous waves. Specifically during storms with a water level set up, the salt marsh stimulated with artificial structures will be flooded. The, enhanced, larger salt marsh width will contribute more to the wave attenuation (Willemsen et al., 2020).

There is a paradox both in the model result predicting continuous retreat of the salt marsh edge, and in observations confirming such retreat over decadal timescales. If the conditions would not have been better for salt marsh development in the past, resulting in an expanding marsh, there would not be a retreating saltmarsh at all. Some elements in the landscape should, at least during certain periods of time, permit the salt marsh to develop before it enters into a phase of retreat. Tidal flats in front of salt marshes are candidate landscape elements for that. Tidal flats can effectively dissipate wave energy under daily conditions (Callaghan et al., 2010). Seaward expansion of tidal flats can be a consequence of spatial shifts in tidal channels, or of changes in sediment availability. Increasing the accommodation space for intertidal systems or stimulating growth of tidal flats with engineering measures, might enhance seaward expansion of salt marshes (Callaghan et al., 2010; Bouma et al., 2016). Stimulating sedimentation at tidal flats with e.g. sediment disposals and nourishments can result in a switch from an erosive phase to an accreting phase (de Vet et al., 2020), which is shown for salt marshes in the current study. This is also confirmed by the long-term analyses by Ladd et all (2020) who showed that marsh width over the last 150 years in 25 estuaries and embayments spread over the UK, critically depended on suspended sediment concentrations. An accreting tidal flat might lead to a decreasing daily wave height at the marsh. Lower wave heights at the marsh edge result in expanding salt marshes, following the results of the current study, but also experimental studies on marsh establishment (Hu et al., 2015b; Cao et al., 2019; Zhu et al., 2020a). An increasing salt marsh width leads to a larger wave attenuating capacity (Vuik et al., 2016; Willemsen et al., 2020), hence enabling the use of saltmarshes in Nature-Based Flood Defenses once more.

4.5 | Conclusions

A biogeomorphological model was presented to assess the dynamic cross-shore salt marsh width. Salt marsh development was modelled over a period of 50 years forced with homogeneous wave heights and differences in sediment availability. The salt marsh development was assessed to answer the key question addressed in this paper: How

does the biophysical development and extent of salt marshes depend on the magnitude of homogeneous hydrodynamic forcing and sediment availability?

The long-term retreat or advancement of saltmarshes in the field corresponded with the model results. Under average mild weather conditions, represented by homogeneous rather small significant wave heights (Hs of 0.00m, 0.05m, 0.10m and 0.15m), the salt marsh width was intrinsically vulnerable to erosion. Key responses of the salt marsh development observed in this study were that with increasing wave height there was/were (1) increasing possibilities for cliff formation, (2) a decreasing platform height, increasing the vegetation mortality, (3) a decrease of periodic alongshore patterns, and (4) a large cross-shore variability in vegetation density with a medium wave height (Hs = 0.10m), which decreased to an absence of cross-shore variability in vegetation density with the largest wave height of 0.15m. Moreover, with increasing sediment availability, (5) the slope of the profile decreased, and (6) the marsh was able to switch from retreat to expansion although the elevation of the profile was generally determined by the homogeneous wave forcing.

The relative importance of the development of salt marshes under homogeneous continuous wave heights and sediment availability highlights the possibilities for long-term contribution of these systems to Nature-Based Flood Defenses. However, this study also indicates that small changes in the magnitude of hydrodynamic energy and sediment availability, result in rather large variability in marsh width, enabling even to transform from a retreating marsh to expansion. So while conventional gray coastal infrastructure can be applied generically, salt marshes in Nature-Based Flood Defenses are more location specific due to spatially variable conditions. These model studies could inspire management measures and artificial structures for enhancing the development of tidal flat – salt marsh systems.

Acknowledgements

This work is part of the research program BE SAFE, which is financed by the Netherlands Organization for Scientific Research (NWO) (grant 850.13.010). Additional financial support has been provided by Deltares, Boskalis, Van Oord, Rijkswaterstaat, World Wildlife Fund, and HZ University of Applied Science. Bas W. Borsje was supported by the Netherlands Organization for Scientific Research (NWO-STW-VENI; 4363). We would like to thank A. Mourits for his contribution to the technical development of the model. We would also like to thank J. van der Werf for his review.

5

Modelling the influence of short-term high waves on the long-term stability of artificial salt marshes

Abstract

Nature based flood defenses, combining grey and green coastal protection infrastructure, can contribute largely to coastal protection. However, when constructing such a system, the salt marsh needs time to establish and develop towards its full strength. Hence, this study aims to systematically assess the influence of short-term wave forcing (hours to days) on long-term salt marsh development (years to decades), and the sensitivity of this for the rate by which plants stabilize their own environment in different stages of development (i.e. pioneer marsh, established marsh and mature marsh). The biogeomorphological development of the artificial salt marsh is simulated using the numerical Delft3D Flexible Mesh model including vegetation dynamics and is extended with a spatio-temporal variable bed substrate strength. The resilience of the developing artificial marsh is assessed by imposing short-term high waves (significant wave height of 1.0m, 2.0m and 3.0m) on artificial marshes developed for a period of 2 to 20 years.

A clear marsh edge was observed after a development period of 5 years and the vegetation and bed substrate was almost fully developed after 10 years of development. The cross-shore marsh width and vegetation cover largely changed over the first 5 years of development under influence of high waves. Especially the largest waves resulted in a decreasing marsh width and vegetation cover. Nevertheless, after a development period of 10 years or more, the salt marsh edge remained rather stable, indicating an almost completely decreased vulnerability to short-term high waves. Still, the stability and wave attenuating capacity slightly decreased after the salt marsh developed for 10 to 15 years, probably due to an increasing discontinuity between tidal flat and salt marsh. This indicates a development period in which the stability is optimal, which is approximately 5 to 15 years in this study.

Although the wave attenuating capacity was relatively large after 2 years of development already, the waves hampered the vegetation growth and thereby the development of the salt marsh approximately over the first 5 year. So additional protective measures are (temporarily) needed to enable the artificial marsh to establish for over the initial 5 to 10 years of development. Moreover, measures to keep the marsh stability and ecosystem services intact after 15 years, such as marsh rejuvenation, might be necessary.

5.1 | Introduction

Current coastal protection is challenged by climate change, altering hydrodynamic conditions in the coastal area. Increased Sea Level Rise (SLR) is expected and storms are predicted to be more severe and frequent in the near future (Leckebusch and Ulbrich, 2004; Emanuel, 2005; Kolker et al., 2009; Knutson et al., 2010). Generally, coastal areas are protected by conventional engineered structures such as dikes and sea walls (Borsje et al., 2011), often referred to as grey infrastructure. However, the resilience of coastal protection will increase by combining the static grey infrastructure with more dynamic green nature based infrastructure, such as salt marshes (Cheong et al., 2013; Spalding et al., 2014; Vuik et al., 2016; Reed et al., 2018; Zhu et al., 2020b). Salt marshes have the ability to adapt to changing environmental conditions driven by climate change; they can grow with SLR by trapping sediment, provided sufficient availability of sediment (e.g. Kirwan et al., 2010; Kirwan et al., 2016; Best et al., 2018; Schuerch et al., 2018). Moreover, established marshes with mature vegetation are able to withstand storm-conditions and attenuate waves (Kirwan and Megonigal, 2013; Möller et al., 2014; Kirwan et al., 2016; Vuik et al., 2016; Willemsen et al., 2020; Zhu et al., 2020b).

Whereas conventional coastal protection is mainstream, Nature Based Flood Defenses (NBFD), consisting of a combination of grey conventional infrastructure and a green salt marshes, are to date still mainly used in pilot projects. Stimulating salt marsh growth as part of flood defense, to decrease the pressure on the dike either by wave attenuation or water storage, is applied in several projects in the North Sea area: (1) the Mud Motor is designed to bring harbor sediments to nearby tidal flats and salt marshes to increase the bed elevation (Baptist et al., 2019b); (2) the bed elevation of salt marshes was mimicked by a sand-nourishment in the Marconi project. Mud was mixed through the top layer and brushwood dams were constructed to create the optimal conditions for salt marsh vegetation to grow (Baptist et al., 2019a); (3) in the Belgian Scheldt estuary reclaimed land was converted to floodplains by landward displacement of dikes and building sluices through dikes to have a limited inundation time, allowing marsh development while remaining water storage capacity for high river discharges (Maris et al., 2007; Broekx et al., 2011; Temmerman et al., 2013); (4) Various managed realignment projects were carried out across the UK, to create space for marsh formation. For example in the Humber estuary, an existing seawall, protecting former agricultural land was breached at two locations to enhance coastal protection and restore habitat (Mazik et al., 2007).

The pilot projects aim at stimulating establishment of pioneer vegetation mechanistically either by decreasing hydrodynamic energy to reduce bed-level dynamics and shifting from net erosion to net accretion (Balke et al., 2016; Cao et al., 2018) or by reducing the inundation frequency and duration e.g. by increasing the bed level elevation (Balke et

al., 2016). This should eventually lead to a mature marsh from which the bed remains stable also after establishment and can resist wave-drive erosion due to high waves and even storm conditions (Knutson et al., 1982; Yang et al., 2012; Spencer et al., 2015; Spencer et al., 2016; Vuik et al., 2016). However, the resistance of the marsh substrate at the marsh front, i.e. directly seaward of and within the pioneer zone, to instantaneous hydrodynamic forcing is unknown (Brooks et al., 2020), despite being of key importance in controlling both vegetation establishment and the overall marsh width (Bouma et al., 2016; Willemsen et al., 2018). Moreover, although we know that plant(root) growth enhances the stability (i.e., decrease the erodibility) of the salt marsh substrate (Le Hir et al., 2007; Kirwan et al., 2010; Turner, 2011; Silliman et al., 2012; Ford et al., 2016), it remains unknown after which period the marsh substrate is sufficiently stable to resist specific wave conditions and how this stability develops over time. Vegetation establishment in the pioneer zone requires first an inundation free period, followed by windows were large disturbance (i.e., large changes in bed level due to high bed shear stresses) are absent (Hu et al., 2015b; Poppema et al., 2019). The likelihood of salt-marsh seedling survival is reduced if wave energy increases (Cao et al., 2019), and if morphological changes are abrupt due to instantaneous hydrodynamic storm events (Cao et al., 2018). Eventually this results in a salt marsh edge, with its location depending on the balance between inundation stress and wave-induced bed level dynamics (Balke et al., 2016; Bouma et al., 2016; Willemsen et al., 2018). So for a pioneer marsh to develop towards an established stable marsh that is able to withstand high waves, hydrodynamic disturbances should be relatively small during the initial establishment period. At this moment, it is however not fully clear how small those hydrodynamic disturbances from waves should be and for how long such calm period should last. Moreover, it is unknown whether the stability remains or changes after establishment is successful and a mature marsh develops.

To enable large-scale implementation of Nature Based Flood Defenses (NBFD), consisting of a combination of grey conventional infrastructure and a green salt marshes, requires that we are able to model the long-term dynamics of marsh width under hydrodynamic realistic conditions (Bouma et al. 2014). In these models it is key to include *i)* vegetations establishment, *ii)* the effect of established vegetation on sediment stability and *iii)* extreme hydrodynamic conditions that include storm events that affect vegetation establishment and subsequent survival. Previous model studies have assessed the decadal development of salt marshes including feedback between hydrodynamics, morphodynamics and vegetation growth on a 2-dimensional (depth-averaged) and 3-dimensional landscape scale (Temmerman et al., 2007; Best et al., 2018; Willemsen et al., submitted). However, these models are simplified by using homogeneous tides and/or continuous homogeneous (mild) waves as forcing. Moreover, the studies are simplified by assuming a spatial and temporal uniform bed strength within the vegetation by using spatio-temporal homogeneous values for the critical bed shear stress and erodibility,

similar to studies highlighting marsh development over a period of several hundred years (Mariotti and Fagherazzi, 2010; Mariotti and Canestrelli, 2017). To improve the prediction of the overall marsh width, and to enable the construction of artificial salt marshes as NBFD, it is needed to include in models *both* the spatio-temporal dynamic strength of the salt marsh substrate, *and* the sensitivity of establishing marsh vegetation to high waves.

In this modelling study, we aim to systematically assess the influence of short-term wave forcing (hours to days) on long-term salt marsh development (years to decades), and the sensitivity of this for the rate by which plants stabilize their own environment in different stages of development (i.e. pioneer marsh, established marsh and mature marsh). We thereby specifically aim to provide insight in how to construct salt marshes at places where they are needed as NBFD. We therefor model the biophysical development of salt marshes under combined long-term mild hydrodynamic conditions and short-term high waves. For this, the numerical Delft3D Flexible Mesh (Delft3D – FM) model, including vegetation dynamics (Willemsen et al., submitted), is extended with a variable strength of the marsh substrate. The resilience of an establishing marsh is systematically assessed by imposing a range of schematic extreme storm conditions at artificial salt marshes in different stages of development.

5.2 | Methods

5.2.1 | Physical settings of the artificial salt marsh

To systematically assess the influence of high waves on artificially created salt marshes within NBFD, the bathymetry of the bare area was based on the bathymetry of two existing salt marshes with a dike at the landward side. This way, we ascertain that there is a range of elevations where marsh plants can establish, and limitations will be imposed by wave climate in relation to sediment stability.

The two salt marshes used are located in the Westerschelde estuary (southwestern part of the Netherlands (Fig. 5.1). The spring tidal range near both marshes (51° 23' N, 3° 50' E), is 4.93m, with MHWN (mean high water neap) at 1.85m+MSL (mean sea level) and MHWS (mean high water spring) at 2.63m+MSL (Van der Wal et al., 2008; Willemsen et al., 2020). Vegetation species occurring in the pioneer zone are mostly the perennial common cordgrass (*Spartina anglica*) and the annual glasswort (*Salicornia spp.*). More landward in the higher marsh, the observed dominant species are common saltmarsh grass (*Puccinellia maritima*), annual seablite (*Suaeda maritima*), and sea aster (*Aster tripolium*) (Van der Wal et al., 2008).

Detailed bathymetrical data (20m x 20m gridded) from the salt marshes Zuidgors and Paulinapolder (Fig. 5.1) are used to construct an initial bathymetry for the model used in this study (c.f. Willemsen et al., submitted). Both salt marshes are located in a landward inflection of the dike, sheltered from longshore currents. Since vegetation at Zuidgors and Paulinapolder is already present for decades, it is assumed that this profile is suitable for salt marsh establishment. So the elevation of the vegetated part is also suitable for constructing an artificial salt marsh.

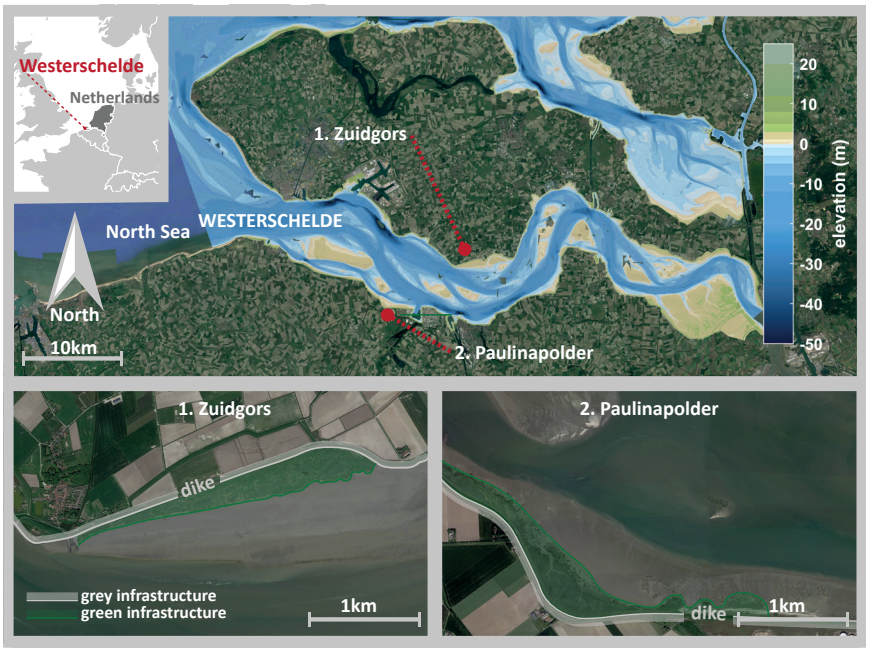

Figure 5.1 | Two salt marshes, Zuidgors and Paulinapolder, located at the center of the Westerschelde estuary in the Netherlands (top panel). Both salt marshes (green infrastructure) are fronting a dike (grey infrastructure) (bottom panels).

5.2.2 | Biogeomorphological model description

5.2.2.1 | *Hydrodynamic and morphodynamic model*

This study applied the Delft3D Flexible Mesh (Delft3D – FM) model to simulate hydrodynamics, sediment dynamics and morphological processes. Delft3D - FM is the successor of Delft3D. Both models are widely used to model fluvial and marine systems (e.g. Ruessink and Roelvink, 2000; Kernkamp et al., 2011; Achete et al., 2016; Bomers et al., 2019b). The unsteady shallow water equations in the flow module D-Flow FM (Flexible

Mesh) are solved two dimensionally (depth-averaged, 2DH), which shows similar results as three-dimensional (3D) models (Horstman et al., 2015).

Waves are simulated using D-Waves (Deltares, 2019c), which is based on the third generation SWAN (Simulating WAves Nearshore) spectral wave model (Booij et al., 1999; Ris et al., 1999). This model is suitable for simulating the evolution of random, short-crested wind-generated waves near and in coastal areas. The model computes wave propagation, wave generation by wind, non-linear wave-wave interaction and dissipation.

Cohesive sediment transport is calculated using D-Morphology (Deltares, 2019b) by solving the advection-diffusion equation for suspended sediment, whilst sedimentation and erosion of cohesive sediments are calculated with the Partheniades-Krone equations (Partheniades, 1965).

Feedback from vegetation in salt marshes on the hydrodynamics are included both for flow and waves. The flow resistance imposed by the presence of vegetation is parameterized by a bed roughness calculated from the plant dimensions following Baptist (2005b). To mitigate excessive bed shear stresses, an additional term representing the flow resistance of the vegetation is included in the momentum equation too (Deltares, 2019a). The D-Waves model includes wave attenuation due to the presence of vegetation by using the Méndez-Losada equation (Méndez and Losada, 2004; Suzuki et al., 2012).

5.2.2.2 | *Dynamic vegetation growth model*

The vegetation growth model simulates temporal vegetation establishment and growth for every computational grid cell. The model is developed from the population dynamics balance equation (Eq. 5.1), previously used to simulate yearly to decadal vegetation growth with rather homogeneous hydrodynamic forcing (e.g. Temmerman et al., 2007; Schwarz et al., 2014). The stem density of the vegetation species *Spartina anglica* is simulated using multiple processes for vegetation development: vegetation establishment (est; Eq. 5.2), lateral expansion of plants through diffusion to neighboring cells (diff; Eq. 5.3), clonal growth of plants up to the maximum carrying capacity by using a logistic function (growth; Eq. 5.4), plant mortality caused by shear stress due to flow and waves (flowwave; Eq. 5.5) and plant mortality due to inundation stress (inund; Eq. 5.6) .

$$\frac{\partial n_b}{\partial t} = \left(\frac{\partial n_b}{\partial t}\right)_{est} + \left(\frac{\partial n_b}{\partial t}\right)_{diff} + \left(\frac{\partial n_b}{\partial t}\right)_{growth} - \left(\frac{\partial n_b}{\partial t}\right)_{flowwave} - \left(\frac{\partial n_b}{\partial t}\right)_{inund} \qquad \text{Equation 5.1}$$

$$\left(\frac{\partial n_b}{\partial t}\right)_{est} = r_{01}(P_{est}) * n_{b,0} \qquad \text{Equation 5.2}$$

$$\left(\frac{\partial n_b}{\partial t}\right)_{diff} = D\left(\frac{\partial^2 n_b}{\partial x^2} + \frac{\partial^2 n_b}{\partial y^2}\right) \quad \text{Equation 5.3}$$

$$\left(\frac{\partial n_b}{\partial t}\right)_{growth} = r * \left(1 - \frac{n_b}{K}\right) n_b \quad \text{Equation 5.4}$$

$$\left(\frac{\partial n_b}{\partial t}\right)_{flowwave} = -n_b * C_{tau} * (\tau - \tau_{cr,p}), \text{ when } \tau > \tau_{cr,p} \quad \text{Equation 5.5}$$

$$\left(\frac{\partial n_b}{\partial t}\right)_{inund} = -n_b * C_{inund} * (H - H_{cr,p}), \text{ when } H > H_{cr,p} \quad \text{Equation 5.6}$$

Where $\frac{\partial n_b}{\partial t}$ represents the change of the stem density per cell over time [stems m^{-2} d^{-1}]. r_{o1} (P_{est}) is a function generating at random either a 0 (with probability 1 - P_{est}) or a 1 (with probability P_{est}). Random numbers are generated independently per time step and grid cell, for the full model domain. $n_{b,o}$ is the initial stem density [m^{-2}], D is the plant diffusion coefficient [m^2 day^{-1}], x and y are the horizontal distances between cells [m], r is the intrinsic growth rate of the stem density [d^{-1}], K is the maximum carrying capacity of the stem density [m^{-2}], C_{tau} is the plant mortality coefficient due to bed shear stress [d^{-1} (N m^{-2})$^{-1}$], τ is the bed shear stress exerted by flow and waves [N m^{-2}], $\tau_{cr,p}$ is the critical bed shear stress for plant mortality [N m^{-2}], C_{inund} is the plant mortality coefficient due to inundation stress [d^{-1} m^{-1}], H is the inundation height [m], and $H_{cr,p}$ is the critical inundation height at high tide [m].

To account for the increasing belowground strength with the time vegetation is present, the population dynamics balance equation was expanded by applying a variable critical bed shear stress for plant mortality (Eq. 5.7). This equation extends the term accounting for plant mortality due to bed shear stresses (Eq. 5.5). The variable critical bed shear stress increases logistically over time when vegetation is present. It was assumed that the increase in additional bottom strength due to vegetation presence is equal to growing vegetation which is generally described by a logistic function (Nelder, 1961; Van de Koppel et al., 2005).

$$\frac{\partial \tau_{cr,p}}{\partial t} = r_{tcrp} * \left(1 - \frac{\tau_{cr,p}}{K_{tcrp}}\right) * \tau_{cr,p}, \text{ when } n_b > 0 \quad \text{Equation 5.7}$$

Where $\frac{\partial \tau_{cr,p}}{\partial t}$ represents the change of critical bed shear stress $\tau_{cr,p}$ over time [N m^{-2} d^{-1}]. r_{tcrp} is the growth rate [d^{-1}] and $K_{cr,p}$ is the maximum critical bed shear stress [N m^{-2}].

A similar formulation was applied to extend the morphodynamic model. A spatio-temporal varying critical bed shear was applied to account for the increasing strength with the time vegetation is present. This additional term, dynamically describing the critical bed shear stress for erosion, is described with a logistic function (Eq. 5.8).

$$\frac{\partial \tau_{cr,e}}{\partial t} = r_{tcre} * \left(1 - \frac{\tau_{cr,e}}{K_{tcre}}\right) * \tau_{cr,e}, \text{ when } n_b > 0 \qquad \text{Equation 5.8}$$

Where $\frac{\partial \tau_{cr,e}}{\partial t}$ represents the change of critical bed shear stress for bed erosion $\tau_{cr,e}$ over time [N m^{-2} d^{-1}]. r_tcre is the growth rate of the critical bed shear stress [d-1] and $K_{cr,p}$ is the maximum critical bed shear stress [N m^{-2}].

To account for a decreasing lateral expansion due to cliff formation at the salt marsh edge, the term describing lateral expansion (Eq. 5.3) was extended. Lateral expansion of vegetation was described by diffusion to all neighboring cells. However, lateral expansion of Spartina anglica is limited by elevation differences (Cao et al., In preparation). So the diffusion term (Eq. 5.3), was adapted to (Eq. 5.9):

$$\left(\frac{\partial n_b}{\partial t}\right)_{diff} = D\left(\frac{\partial^2 n_b}{\partial x^2}, \text{ when} \frac{\partial z}{\partial x} < dz_{crit} + \frac{\partial^2 n_b}{\partial y^2}, \text{ when} \frac{\partial z}{\partial y} < dz_{crit}\right) \qquad \text{Equation 5.9}$$

Where dz_{crit} is the critical bed level difference limiting lateral expansion [m].

5.2.2.3 | *Temporal resolution and biogeomorphological coupling*

Tidal flow and wave action is simulated with the hydrodynamic model. Tidal flow is simulated with a computational time step of maximum 30s (Table 5.1); if the maximum Courant number of 0.7 is exceeded, the timestep decreases (Deltares, 2019a). Wave action is calculated every 3600 seconds and subsequently combined with the timesteps of the flow model for the same 3600 seconds. The temporal resolution of the wave model is larger than the flow model to decrease computational time, but selected such that water level change due to the tide over a single wave timestep remains small. Morphological change is 'online' calculated every computational timestep of the flow model. The vegetation growth module is set-up in Python and online coupled to the hydrodynamic (both flow and wave) and morphological Delft3D – FM model (Willemsen et al., submitted). Model parameters and (state) variables are exchanged through memory by using BMI (Basic Model Interface) (Peckham et al., 2013). The full model is controlled in Python (Willemsen et al., submitted). Initially, vegetation establishment is calculated, followed by a hydrodynamic and morphodynamic model update over the vegetation timestep. Subsequently, hydrodynamic results are used to simulate the vegetation dynamics and development of the strength of the marsh substrate. Additionally, vegetation establishment in empty grid cells is calculated. Calculated vegetation dynamics (presence, density and strength of the marsh substrate) are used as input for the hydrodynamic and morphodynamic model (Fig. 5.2).

Long-term development of the salt marsh, forced with continuous mild wave conditions, is calculated using an acceleration factor ('MorFac'; Roelvink, 2006). The morphological change every timestep is multiplied with a factor 100, the resulting bathymetry is used for the computation of the subsequent hydrodynamic and morphodynamic timestep. By using an acceleration factor of 100, the morphological change of a single year is represented by approximately 3.6 days of hydrodynamics. Similar morphological acceleration factors were used in previous studies, e.g. factor 100 (Best et al., 2018; Willemsen et al., submitted) and factor 700 (Temmerman et al., 2007). Vegetation development is computed every 100 morphodynamic days (i.e. once every single hydrodynamic day); the change in vegetation over a time step of nominally one day, corresponds to vegetation change over 100 days in the morphological timescale. Although multiple vegetation time steps occur in a single morphological year, vegetation dynamics are modelled as a year-averaged process and do not vary seasonally.

After simulating the long-term (years) development of the salt marsh, the spatio-temporal critical bed shear stress for bed erosion is calculated (Eq. 5.8) and updated (Fig. 5.2). Subsequently, the short-term (days) development of the salt marsh under influence of high waves is simulated. Short-term simulations are executed without an acceleration factor, to prevent overestimation of the effect of high waves and thereby prevent overestimation of bed level change and vegetation mortality.

Table 5.1 | Computational timesteps of processes present in the biogeomorphological model

Process	Timestep	Acceleration factor (MorFac)	With acceleration factor (MorFac) representative for
Long-term runs (with MorFac)			
Flow	30 seconds	-	-
Wave	3600 seconds (1 hour)	-	-
Morphology	30 seconds	100	3000 seconds
Vegetation	86400 seconds (1 day)	-	100 days
Long-term runs (without MorFac)			
Flow	30 seconds	-	-
Wave	3600 seconds (1 hour)	-	-
Morphology	30 seconds	-	-
Vegetation	86400 seconds (1 day)	-	-

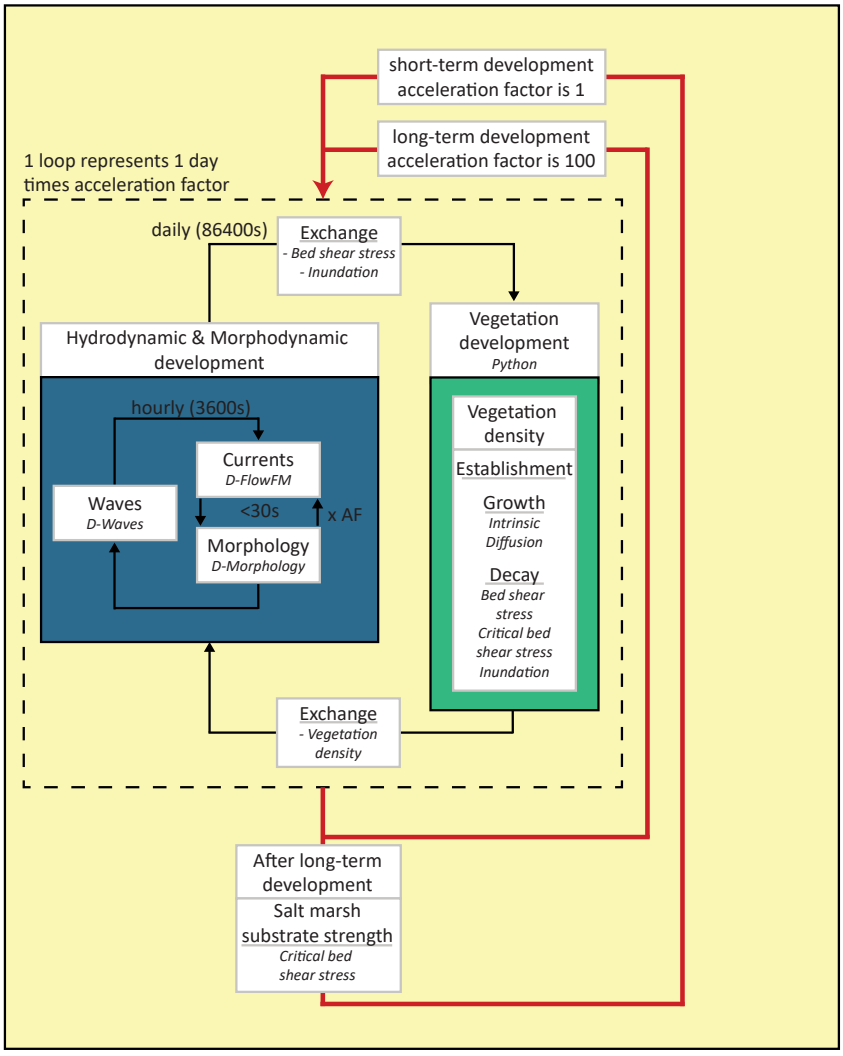

Figure 5.2 | Flowchart of modelling approach and online coupling of interactive computation of hydrodynamic, morphodynamic and vegetation development using the Basic Model Interface (BMI). BMI is used for initializing and orchestrating the full model. D-Flow FM and D-Morphology compute currents and morphological change at least every 30s. Once every hour (3600s) bed shear stresses due to waves are computed using D-Waves. Computed bed shear stresses are combined with results from D-Flow FM for a full hour. Vegetation density is computed once every day (86400s), using bed shear stresses and inundation calculated in the hydrodynamic and morphodynamic model. The updated vegetation density per grid is used as input for the hydrodynamic and morphodynamic model for the subsequent time steps. Long-term (years) development is calculated using an acceleration factor of 100. The substrate strength of the salt marsh is calculated after long-term development. This is used as input for the subsequent calculation of short-term (days). Adapted from Willemsen et al. (submitted)

5.2.3 | Model setup

5.2.3.1 | *Model domain and bathymetry*

The model domain of the depth-averaged model consists of a flow and wave model (Fig. 5.3). The flow domain extends over 1000m alongshore and 2500m cross-shore, with an applied cell size of 5m (both in x- and y-direction). The wave domain is larger in the alongshore direction (2000m), to prevent boundary effects. The cell size of the larger wave domain is 15m, whereas the cell size of the nested wave domain is 5m (both in x- and y-direction), to decrease computational time.

The initial profile is derived from salt marshes located in the Westerschelde (Fig. 5.1) existing for decades (c.f. Willemsen et al., 2020). The profile is initiated at -7m+MSL, well below MLWS (mean low water spring), which -2.31m+MSL at Zuidgors and -2.16+MSL at Paulinapolder. The bed level increases to local mean sea level over a distance of approximately 650m. Subsequently the bed level increases to MHWN, which has been used as threshold for vegetation establishment in the Westerschelde (Van der Wal et al., 2008), over a distance of 800m. Initially, a linear slope is used, to prevent imposing a convex-up or concave-up profile affecting vegetation establishment at the tidal flat and potential marsh area. The last 1050m of the cross-shore domain slopes towards MHWS (mean high water spring; 2.63m at Zuidgors; 2.54m at Paulina). The imposed bathymetry is uniform in alongshore direction. Random perturbations in the range of -1cm and +1cm are added to the initial bed elevation of each grid cell for initiation of pattern development (c.f. Best et al., 2018).

5.2.3.2 | *Boundary conditions and model parameters*

A single open boundary was imposed at the southern seaward end of the model domain (Fig. 5.3). A time series of water levels was imposed at the open boundary, consisting of local M2 and S2 tidal constituents. The range of the constructed spring-neap cycle was 4.93m, with a mean tide level of 0.16m (Van der Wal et al., 2008). Mild waves, with a wave height (H_s) between 0.00m and 0.15m were imposed at the open boundary. Using this wave forcing continuously, field observations of the cross-shore retreat and expansion of the marsh edge, can be approximated (Willemsen et al., submitted). The vertically averaged suspended sediment concentrations (SSC) were equal to 10 mg/L at the open boundary (Van Damme et al., 1999; Temmerman et al., 2004). The tidal signal, waves and suspended sediment concentrations were similar as previous model studies (Willemsen et al., submitted).

5.2.3.3 | *Hydrodynamic model parameters*

The roughness of the bed was represented with a uniform Manning bed roughness of 0.023s m-1/3, which is slightly higher than the value for open waters (Wamsley et al., 2010), because of the location in the intertidal zone (Table 5.2). These values are comparable with values used in previous studies considering salt marshes in the Westerschelde estuary (e.g. Best et al., 2018). The horizontal eddy viscosity and eddy diffusivity should be typically in the range of 1 to 10m2 s for grid cell dimensions of tens of meters or less and were both set to 10 m2 s, which is the default value (Deltares, 2015).

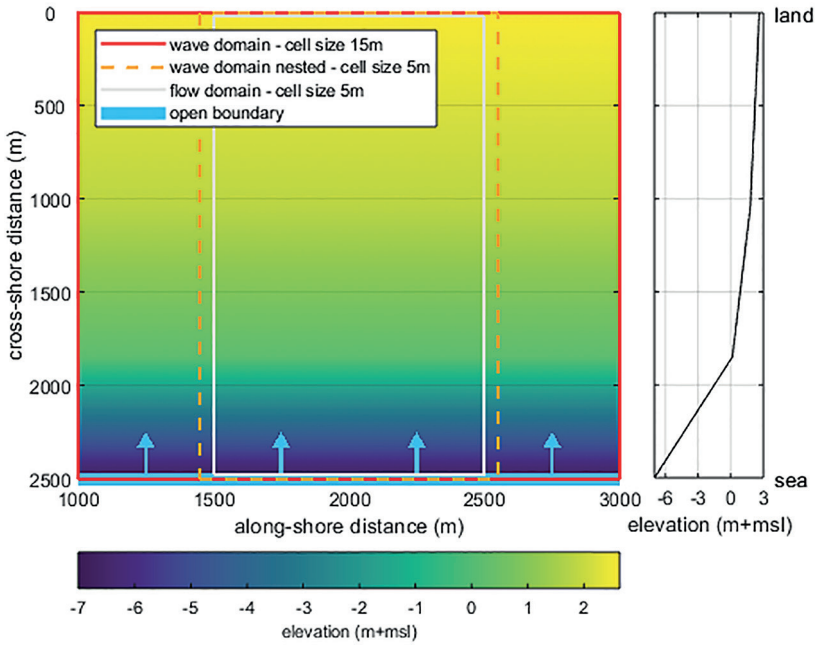

Figure 5.3 | The model domain consists of a flow domain (grey box; 1000m in alongshore direction; 2500m in cross-shore direction; grid cell size of 5m) and a larger wave domain (red box; 2000m in alongshore direction; 2500m in cross-shore direction; grid cell size of 15m) with a nested wave domain inside (orange dashed box; 1100m in alongshore direction; 2500m in cross-shore direction; grid cell size of 5m). An open boundary is imposed at the south side of the domain (left panel; blue line and arrows). Colors indicate the bed level elevation, for which the initial profile (right panel) started at -7m, increased to mean sea level, further increased to mean high water neap and is completed at mean high water spring.

5.2.3.4 | *Morphodynamic model parameters*

Cohesive sediments are generally appearing at tidal flats and salt marshes in the Westerschelde estuary, so a uniform fine cohesive sediment was applied (Willemsen et al., 2018). For the reference density, specific density and dry bed density of the sediment, default values were used, respectively 1600kg m^{-3}, 2650kg m^{-3} and 500kg m^{-3} (Table 5.2) (Deltares, 2019b). The settling velocity for the cohesive sediment was set to 0.5mm s-1, which is approximately the settling velocity of the average grain size diameter found around the salt marsh edge in the Westerschelde (Willemsen et al., 2018). The critical bed shear stress for deposition is set to 1000N m^{-2} enabling unrestricted sedimentation. The erosion parameter was set to 5 * 10^{-5}kg m^{-2} s^{-1} (Best et al., 2018; Deltares, 2019b).

For long-term development of the salt marsh under mild wave conditions, a uniform critical bed shear stress of 0.5N m^{-2} was applied (c.f. Willemsen et al., submitted). Since bed shear stresses increase largely under higher wave conditions, a better approximation of the strength of the bed substrate is important for a proper estimation of the dynamics at the marsh front (Brooks et al., 2020). So, after simulating the long-term development, a spatio-temporal varying critical bed shear stress for bed erosion was calculated, before simulating short-term development of the salt marsh under high waves. The spatio-temporal varying critical bed shear stress for bed erosion was calculated using logistic growth (Eq. 5.8). The maximum critical bed shear stress for bed erosion $K_{cr,e}$ [N m^{-2}] is measured in the field both at a natural and managed realignment site and is 3.0N m^{-2} (Watts et al., 2003). The growth rate of the critical bed shear stress for bed erosion $r_{cr,e}$ [N m^{-2} d^{-1}] was obtained using the same measurements. The critical bed shear stress of the managed realignment site was similar to and exceeding the critical bed shear stress of the natural marsh after a period of six year (Watts et al., 2003). So it was assumed that the critical bed shear stress is reached after six years, which is equal to a logistic growth rate of 0.046 N m-2 d-1 in the model (Table 5.2). To decrease the computational time an acceleration factor of 100 was applied (Fig. 5.2).

Table 5.2 | Hydrodynamic and sediment parameter settings used in the model study.

Parameter	Symbol	Value long-term	Value short-term	Unit	Source
Uniform friction coefficient	n	0.023	0.023	s $m^{-1/3}$	Wamsley et al. (2010); Deltares (2019a)
Eddy viscosity	v	10	10	m^2 s^{-1}	Deltares (2015)
Eddy diffusivity	D	10	10	m^2 s^{-1}	Deltares (2015)
Reference density	$\rho_{s,o}$	1600	1600	kg m^3	Best et al. (2018); Deltares (2019b)
Specific density	ρ_s	2650	2650	kg m^3	Best et al. (2018); Deltares (2019b)
Dry bed density	$\rho_{s,dry}$	500	500	kg m^3	Best et al. (2018); Deltares (2019b)
Settling velocity cohesive sediment	ω_s	0.5	0.5	mm s^{-1}	Willemsen et al. (2018)
Fixed critical bed shear stress for erosion	$\tau_{cr,e}$	0.5	Spatio-temporal variable between 0.5 and $K_{cr,e}$	N m^{-2}	Best et al. (2018); Deltares (2019b);
growth rate of the critical bed shear stress for bed erosion	$r_{cr,e}$	0.046	0.046/100	N m^{-2} d^{-1}	Watts et al. (2003)
maximum critical bed shear stress for bed erosion	$K_{cr,e}$	-	3.0	N m^{-2}	Watts et al. (2003)
Critical bed shear stress for deposition	$\tau_{cr,d}$	1000	1000	N m^{-2}	Best et al. (2018); Deltares (2019b)
Erosion parameter	M	$5 * 10^{-5}$	$5 * 10^{-5}$	kg m^{-2} s^{-1}	Best et al. (2018); Deltares (2019b)
Acceleration factor	AF	100	1	-	-

5.2.3.5 | *Vegetation growth*

The population dynamics model was extended to simulate vegetation growth, both under mild and high wave conditions. Establishment and growth of the pioneer salt marsh species Spartina anglica (cordgrass), commonly occurring in the Westerschelde estuary, was simulated. A value of 0.7 was used for the drag coefficient (C_D) (Suzuki and Arikawa, 2010; Vuik et al., 2016; Willemsen et al., submitted) (Table 5.3). Average values were assumed for the stem height (0.5m) and stem thickness (4.3mm) (Temmerman et al., 2007), whereas the vegetation density was variable, driven by the population dynamics model. The establishment chance (P_{est}), was equal to 1% (Eq. 5.2), representative for a slow colonizer like Spartina anglica (Schwarz et al., 2018). The intrinsic growth rate of the

vegetation (r) was equal to 1 per vegetation time step, which is in this study equal to a single hydrodynamic day and 100 morphodynamic days due to the use of a morphological acceleration factor. The maximum stem density (K) was 1200 stems m^{-2} (van Hulzen et al., 2007) (Eq. 5.4).

The spatio-temporal varying critical bed shear stress for vegetation mortality was calculated using logistic growth and depended on the presence of vegetation in a specific cell (Eq. 5.7). The maximum critical bed shear stress for vegetation mortality $K_{cr,p}$ [N m^{-2}] was calculated using flume experiments. Vegetation at established salt marshes with mature vegetation is able to resist significant wave heights of 0.91m, with a maximum orbital velocity of 0.936m s^{-1} (Möller et al., 2014). Using this experiment, the maximum occurring bed shear stress is calculated using Soulsby (1997), and is 6.6N m^{-2}. So a conservative estimation of the critical bed shear stress for vegetation mortality, $K_{cr,p}$, is 6.6N m^{-2}. Plant mortality is forced by inundation and critical bed stresses in the model. It is assumed that the critical bed shear stress for vegetation mortality increases with the presence of (Spartina) vegetation and the time the pioneer zone develops towards an established marsh. Critical bed shear stresses for erosion of a managed realignment site was similar to and exceeding the critical bed shear stress for erosion of the natural marsh after a period of six year (Watts et al., 2003). So it was assumed that the logistic growth rate of the critical bed shear stress for vegetation mortality was equal to the growth rate of the critical bed shear stress for erosion, which is 0.046 N m^{-2} d^{-1} in the model (Table 5.3)

Following Willemsen et al. (submitted), first the vegetation establishment, $\left(\frac{\partial n_b}{\partial t}\right)_{est}$ was calculated (Eq. 5.2). The extended formulations for growth and decay (Eq. 5.3, 4, 5, 6, 7, 9), in the next vegetation timestep, were solved using an ordinary differential equation solver in Python, iterating towards the solution (c.f. Soetaert et al., 2010).

Table 5.3 | vegetation growth parameters used in the model study.

Parameter	Symbol	Value long-term	Value short-term	Unit	Source
Chance of vegetation establishment	P_{est}	0.01	0.01	-	Schwarz et al. (2018)
Initial vegetation density of established vegetation	$n_{b,o}$	200	200/100	m^{-2} day^{-1}	van Hulzen et al. (2007)
Intrinsic growth rate of vegetation	r	1	1/100	day^{-1}	van Hulzen et al. (2007)
Maximum carrying capacity of stem density	K	1200	1200	Stems m^{-2}	Temmerman et al. (2005)
Vegetation diffusion coefficient	D	0.2	0.2/100	m^2 day^{-1}	van Hulzen et al. (2007)
Vegetation mortality coefficient due to bed shear stress	C_{tau}	30	30/100	day^{-1} $(N m^{-2})^{-1}$	van Hulzen et al. (2007)
Critical bed shear stress for vegetation mortality	$\tau_{cr,p}$	Spatio-temporal variable between 0.26 and $K_{cr,p}$	Spatio-temporal variable between 0.26 and $K_{cr,p}$	N m^{-2}	van Hulzen et al. (2007)
growth rate of the critical bed shear stress for vegetation mortality	$r_{cr,p}$	0.046	0.046/100	N m^{-2} d^{-1}	Watts et al. (2003)
maximum critical bed shear stress for vegetation mortality	$K_{cr,p}$	6.6	6.6	N m^{-2}	Möller et al. (2014)
Vegetation mortality coefficient due to inundation stress	C_{inund}	3000	3000/100	day^{-1} m^{-1}	van Hulzen et al. (2007)
Critical inundation height for vegetation mortality	$H_{cr,p}$	1.1	1.1	m	van Hulzen et al. (2007)
Uniform vegetation diameter	B_{veg}	0.0043	0.0043	m	Temmerman et al. (2005)
Uniform vegetation height	h_{veg}	0.5	0.5	m	Temmerman et al. (2005)

5.2.4 | Systematic assessment of the impact of high waves

The impact of high waves in artificially constructed marshes was assessed using different periods for vegetation growth and a range of wave heights. It was assumed that the bed elevation of an artificial salt marsh mimics the profile of a natural salt marsh for optimal vegetation growth. So first, a natural profile was developed, by simulating 50 years of development of tidal flat and salt marsh using an acceleration factor of 100. Second, the development of the artificial salt marsh was simulated using the suitable profile for vegetation to grow from the previous run. Full biogeomorphological development was simulated for 2, 5, 10, 15 and 20 years, using an acceleration factor of 100. Third, high waves of 1.0m, 2.0m and 3.0m were imposed at the boundary for a single day, without using an acceleration factor (Table 5.4). The recurrence time of these waves in the Westerschelde is minimum 10 to 100 years and maximum 10000+ years (Gautier and Groeneweg, 2012; Groeneweg and Van Nieuwkoop, 2015).

Computational time for the first two stages, where an acceleration factor of 100 was used, was approximately 1 day per 10 years of model simulation. The computational time for simulating high waves, without an acceleration factor, was approximately 0.25 days per single run, depending on the height of the wave. Model simulations were executed on a machine with 2 cores @ 3.50 GHz and 32 GB memory.

Table 5.4 | Model scenarios to assess the consequences of high waves on vegetation growth of a marsh in different phases (years) of establishment.

Model scenarios	Marsh development over equilibrium profile (year)	Significant wave height, at boundary (m)	Wave period at boundary (s)
2.1	2	1.00	3.5
2.2	2	2.00	5.0
2.3	2	3.00	5.5
5.1	5	1.00	3.5
5.2	5	2.00	5.0
5.3	5	3.00	5.5
10.1	10	1.00	3.5
10.2	10	2.00	5.0
10.3	10	3.00	5.5
15.1	15	1.00	3.5
15.2	15	2.00	5.0
15.3	15	3.00	5.5
20.1	20	1.00	3.5
20.2	20	2.00	5.0
20.3	20	3.00	5.5

5.3 | Results

5.3.1 | Initial development of the artificial salt marsh under mild wave conditions

After 50 years of model simulation, a bathymetry was developed suitable for vegetation growth. This profile was used as starting point for the artificial salt marsh to develop under mild waves (H_s in the range of 0.00m – 0.15m) over a period of 2, 5, 10, 15 and 20 years (Fig. 5.4; bottom panel). The longer the period for further biogeomorphological development of the profile, i.e. development of bed elevation and vegetation growth, the less space is available for vegetation to grow. Generally, the elevation of the bathymetry decreased over time and a rather large cliff of maximum 1.5m was observed (Fig. 5.4; bottom panel). However, after 15 years of biogeomorphological development, further bathymetrical changes remained small. Between 15 years and 20 years of biogeomorphological development, It was only observed that the transition between flat and marsh was more distinguished.

Vegetation presence after 2 year of development at the artificial profile was scattered, consequently a clear marsh edge was not observed (Fig 5.4; top panel; Fig. 5.5; first column of panels). After 5 years, vegetation density at the high marsh area, approximately 0m – 750m from the landward side, almost reaches the maximum density already. Moreover, the location of the marsh edge can be clearly distinguished at approximately 1225m from the landward side, although the marsh edge is still jagged (Fig 5.4; top panel; Fig. 5.5; second column of panels). After further development (10, 15 and 20 years), the vegetation density maximizes and the salt marsh edge was observed to be clearly present (Fig 5.4; top panel). A steep gradient of vegetation density was observed over tens of meters only, with no vegetation at the seaward side of the marsh edge and maximum vegetation density at the landward side. Although pioneer vegetation was observed at the seaward side of the marsh edge, the marsh edge slowly retreated landward. This suggests that the sediment trapping capacity of the pioneer zone was not able to keep up with the decreasing bed profile under influence of mild wave conditions (Fig. 5.5; third, fourth and fifth column of panels).

With the time vegetation is present, the strength of the marsh substrate increases, thereby increasing the critical bed shear stress both for bed erosion and vegetation mortality. After 2 year of marsh development, the critical bed shear stress only slightly increased, whereas after 5 year a clear increase can be observed due to the presence of vegetation (Fig. 5.4; middle panel). The critical bed shear stress for bed erosion increased from 0.5N m^{-2} to approximately 0.7N m^{-2} and the critical bed shear stress for vegetation mortality increased from 0.26N m^{-2} to a range between 1.0N m^{-2} and 3.0N m^{-2}. Moreover,

the variability (expressed in the standard deviation) of the critical bed shear stress was large, due to the patchy presence of the vegetation (Fig. 5.5; second column of panels). After 10 years the maximum critical bed shear stress was reached. It was observed that further development results in a decreasing variability, but an increasing discontinuity (i.e. steeper gradient) between the tidal flat and salt marsh (Fig. 5.4; middle panel).

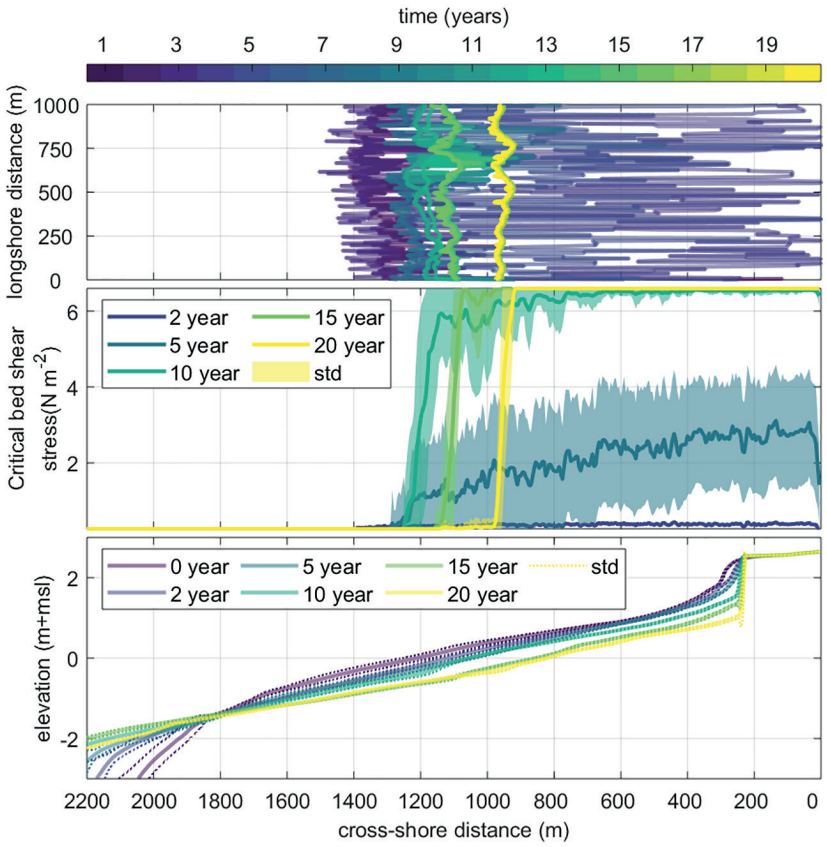

Figure 5.4 | 20-year development of the salt marsh edge (top panel). 2, 5, 10, 15 and 20 year development of the critical bed shear stress for vegetation mortality (longshore mean represented by the colored lines) and longshore standard deviation (colored fill) (middle panel). 0, 2, 5, 10, 15 and 20 year development of the bed elevation of the artificial salt marsh (bottom panel). The colored lines show the longshore mean, whereas the dotted lines indicate the standard deviation. Marsh development starts after 50 years development of the profile, to obtain optimal conditions for salt marsh vegetation to grow.

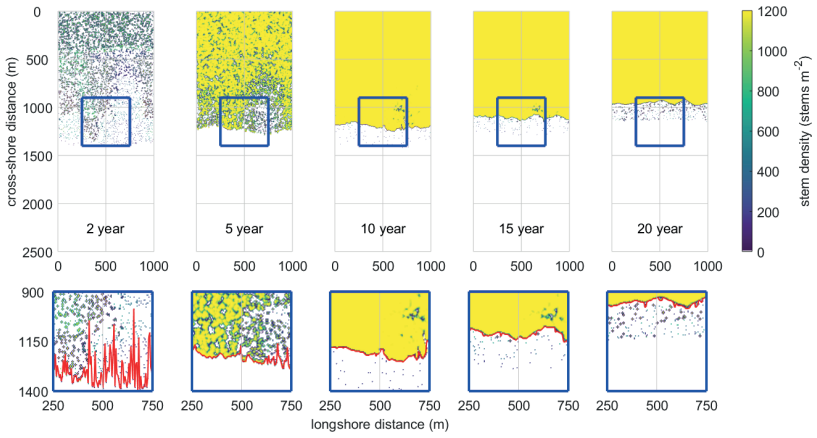

Figure 5.5 | Vegetation density after 2, 5, 10, 15 and 20 year of salt marsh development (from left to right). The blue box (top panels) indicate a zoom showed in the bottom row of panels. The location of the marsh edge is highlighted with a red line (bottom row of panels).

5.3.2 | High waves affecting artificial salt marsh establishment

The 2, 5, 10, 15 and 20 years developed artificial salt marshes under mild wave conditions, were subsequently forced with high waves of 1.0m, 2.0m and 3.0m, equal to a statistical recurrence of minimum 10 to 100 years and maximum 10000+ years in the Westerschelde (Gautier and Groeneweg, 2012; Groeneweg and Van Nieuwkoop, 2015). After the occurrence of these high waves the vegetation density and cover decreased (Fig. 5.6). Decreasing vegetation presence was observed in artificial marshes developed over a period of 2 and 5 years (Fig. 5.6; panels in first and second column). After high waves forced the marsh developed over a period of 10 years, vegetation retreat was more focused around the marsh edge (Fig. 5.6; panels in third column). Finally, after 15 and 20 years of salt marsh development, the density of a small vegetated area at the marsh edge decreased only. Additionally the density of the pioneer vegetation fronting the marsh edge decreased as well (Fig. 5.6; panels in third column).

Forcing with different wave heights leads to a differentiating decrease of vegetation density. A wave height of 1.0m resulted in a decrease of approximately 200 to 400 stems m^{-2}, whereas a wave height of both 2.0m and 3.0m resulted in a decrease of approximately 400 to 1000 stems m^{-2} (Fig. 5.6). A similar pattern was observed for the cross-shore width of the marsh and the area covered with vegetation (Fig. 5.7). The decrease of salt marsh width and vegetation cover was largest in the salt marsh that has

developed for 2 years, and slightly less in the 5-year developed marsh. The difference in wave height has largest effect in the 2-year developed artificial marsh. The marsh width decreased with approximately 14m, 44m and 50m for a wave height of 1.0m, 2.0m and 3.0m respectively. The cross-shore width of the artificial marsh only decreased with a maximum of 5m after the occurrence of high waves over a 5-year to 20-year developed marsh (Fig. 5.7; first panel). The area covered with vegetation (independent of density) decreased with approximately 7.5*10^4m2, 9.5*10^4m^2 and 10*10^4m^2, for a wave height of 1.0m, 2.0m and 3.0m respectively. The decrease was smaller for a 5-year developed marsh and remained stable at an artificial marsh that has developed for 10 or more years, with a value of maximum 1.2*10^4m^2 (Fig. 5.7; second panel).

The influence of waves with a wave height of 2.0m and 3.0m was rather similar, and only differed for a 2-year developed salt marsh. This inherently means that bed shear stresses and water level must be rather similar and suggest that higher incoming waves (Hs=3.0m), are attenuated more by the tidal flat in front of the marsh than lower waves. The decrease of the marsh width was low and stable already after more than 2 years of salt marsh development. This suggests that the growing strength of the salt marsh is effective after more than 2 year of development only. Although the location of the marsh edge was stable after more than 2 years of development, the vegetation in the salt marsh interior still decreased largely after the arrival of high waves at a 5-year developed artificial marsh. It was observed that the vegetation coverage of the full marsh became stable after more than 5 years of marsh development.

Interestingly, the artificial marsh seemed to be increasing vulnerable after 20 years of development. The decrease of marsh width and vegetation cover, after the artificial marsh was forced with high waves, became larger. It was observed that the marsh edge after 20 years of development was retreating (Fig. 5.5). So this might suggest that an already retreating marsh is more vulnerable to high waves. Consequently, the resilience of the artificial marsh was largest after approximately 10 to 15 years of development.

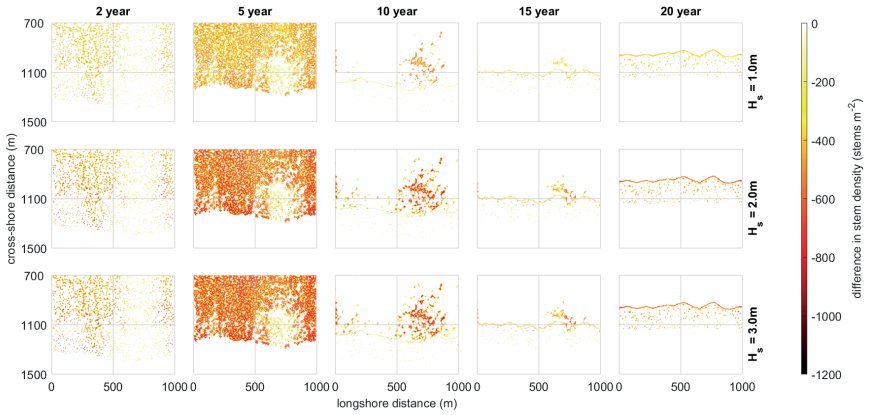

Figure 5.6 | Difference in vegetation density after the occurrence of high waves of 1.0m, 2.0m and 3.0m (from top to bottom) over an artificial salt marsh developed for 2, 5, 10, 15 and 20 years (from left to right).

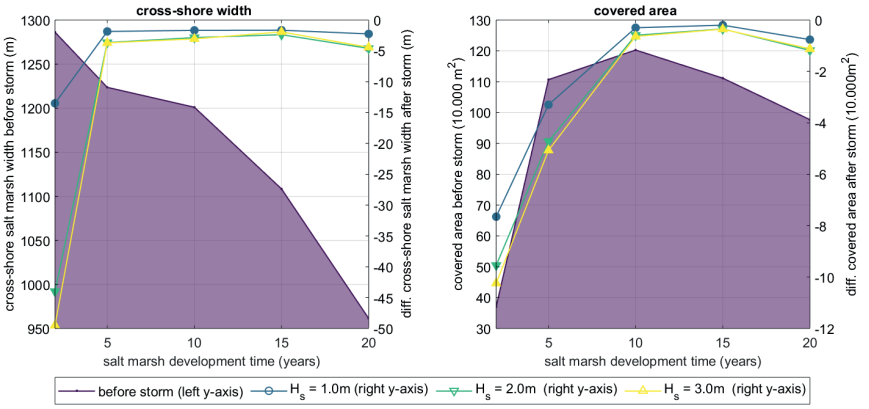

Figure 5.7 | Vegetation change after the occurrence of high waves, with the cross-shore salt marsh width and difference (left panel), vegetation cover and difference (center panel) and vegetation density in covered cells and difference (right panel).

5.3.3 | Wave attenuating capacity of artificial salt marshes

With the feedback of high waves on the development of the salt marsh, the feedback of the developing artificial marsh on the wave height was also observed. The incoming waves at the marsh edge were largest with spring tide and smaller during mean tide, most probably due the bottom friction exerted by the bare tidal flat already attenuating the waves before arriving at the marsh edge. The shape of the tidal flat, becoming less steep (Fig. 5.5), probably also results in larger incoming waves at the marsh edge after a longer development period of the artificial marsh (Fig. 5.8; top panels).

The wave attenuating capacity for waves of 1.0m was generally independent of the shape of the marsh and the development time. The wave attenuation was between 1% and 2% over the first 100m of salt marsh and increases to approximately 7% per 100m over a larger stretch of marsh during mean tide (Fig. 5.8; bottom panels). For larger waves with a wave height of 2.0m and 3.0m the wave attenuating capacity was between 2% and 4% per 100m during spring tide and slightly decreases with the time the marsh develops. This might be caused by the increasing vegetation density over time. During mean tide however, the wave attenuating capacity exceeds 10% per 100m, but generally decreases with the time the marsh develops in contrast to spring tide. This might be caused by the decreasing elevation of the salt marsh profile over time, resulting in a smaller influence of bottom and vegetation roughness (Fig. 5.8; bottom right panel).

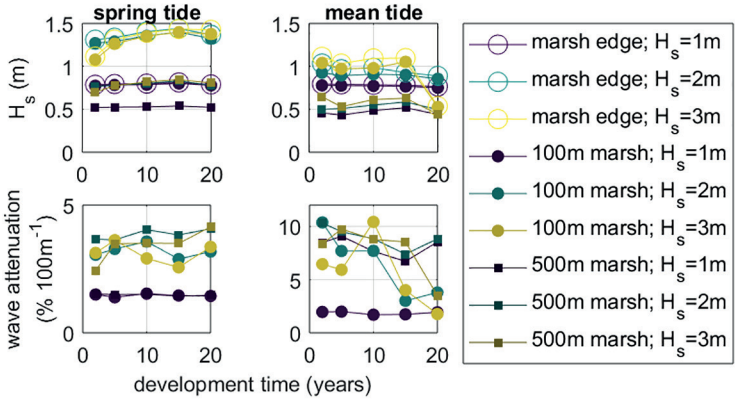

Figure 5.8 | Wave height (top panels) and wave attenuation (bottom panels) at the marsh edge, 100m and 500m in the marsh during spring tide (left panels) and a mean tide level (right panels).

5.4 | Discussion

Salt marshes are able to withstand large waves, caused by extreme storms (e.g. Möller et al., 2014; Zhu et al., 2020b). However, when constructing artificial salt marsh, vegetation should be able to establish without large disturbances. Hence, this study aimed to systematically assess the influence of high waves on the establishment of artificial marshes. The study shows that (1) the vegetation at the salt marsh is fully developed after a period of 10 years in the sense that a discontinuity between flat and marsh has emerged, (2) the vulnerability of the marsh edge and interior to high waves is already low after developing for 10 years, and (3) the wave attenuating capacity of the marsh is already present after a development of 2 years.

5.4.1 | Field observations and model simulations of establishing salt marshes

In established salt marshes, the vegetation contributes to an increasing strength of the substrate (Le Hir et al., 2007; Kirwan et al., 2010; Turner, 2011; Silliman et al., 2012; Ford et al., 2016). So the strength of the substrate below establishing vegetation, either in front of existing salt marshes or in artificial salt marshes, increases over time vegetation is present. However, measurements of the increasing strength, e.g. expressed as critical bed shear stress for erosion, lack (Brooks et al., 2020). Moreover, few studies are available that have measured the critical bed shear stress for erosion both in natural and artificial marshes (Watts et al., 2003). The current study used parameters from the available studies (Watts et al., 2003) and calculated parameter values using experimental studies (Möller et al., 2014). However, it is recommended to set-up field and lab experiments to measure the strength of the bed of the salt marsh front in seaward growing marshes and the strength of the bed in artificially and/or realigned salt marshes.

Although field measurements of marsh retreat under high wave conditions (equal to or larger than 1.0m, with a recurrence time exceeding 10 years) and strength of the substrate lack, continuous retreat of the marsh edge has been observed in the field. Field measurements at an established salt marsh existing for decades in the Westerschelde estuary indicate a relation between total hydrodynamic energy and retreat of the marsh edge (Wang et al., 2017; Van der Wal et al., In preparation). Over a period of 2.5 year, which is smaller than the recurrence time of the high waves assessed in the current study, the marsh edge retreat can exceed 1.5m in the Westerschelde in established marshes, although the wave height did not exceed 0.5m (Wang et al., 2017; Van der Wal et al., In preparation). However, marsh retreat can exceed 1.0m per year up till multiple meters a year (Day Jr et al., 1998; Reed, 2001; Van der Wal et al., 2008; Houser, 2010; Marani et al., 2011; McLoughlin et al., 2015; Bendoni et al., 2016). The simulated retreat of a 10-year (or more) developed marsh forced with a 1.0m wave in the current study was approximately 1.6m per storm. Although a wave with a wave height of 1.0m occurs statistically once every 10 to 100 year at that particular location (Gautier and Groeneweg, 2012; Groeneweg and Van Nieuwkoop, 2015), the simulated order of magnitude of retreat corresponds with field measurements.

The formulations for vegetation development in this thesis, have been used and compared with field observations previously for tides and tides and mild wave conditions (Temmerman et al., 2007; Willemsen et al., submitted). However, part of the formulations are based on actual bed shear stresses, which quickly increase with larger wave heights (Möller et al., 2014; Rupprecht et al., 2017). So extensions for the formulations, as proposed in the current study, are a prerequisite for including short-term large wave

conditions in biogeomorphological models to prevent an overestimation of marsh loss. Moreover, this highlights the importance of including the increasing strength of the substrate and biological traits, with the time biology is present, in biogeomorphological models including large wave conditions.

The methods developed in this study, enabled the exchange of parameters affected by biological dynamics between the hydrodynamic, morphodynamic and biological model (c.f. Willemsen et al., submitted). This created the possibility to combine simulations of long-term development under mild wave conditions and short-term development under large waves. Such a method can be applied to simulate landscape development in other systems were biophysical feedbacks are observed. For example in riverine areas (Murray et al., 2008; Oorschot et al., 2016; Williams et al., 2016), intertidal flats (Andersen, 2001; Andersen et al., 2005; Braat et al., 2019), offshore (Borsje et al., 2009; Damveld et al., 2020) and intertidal areas with mangroves (Horstman et al., 2015).

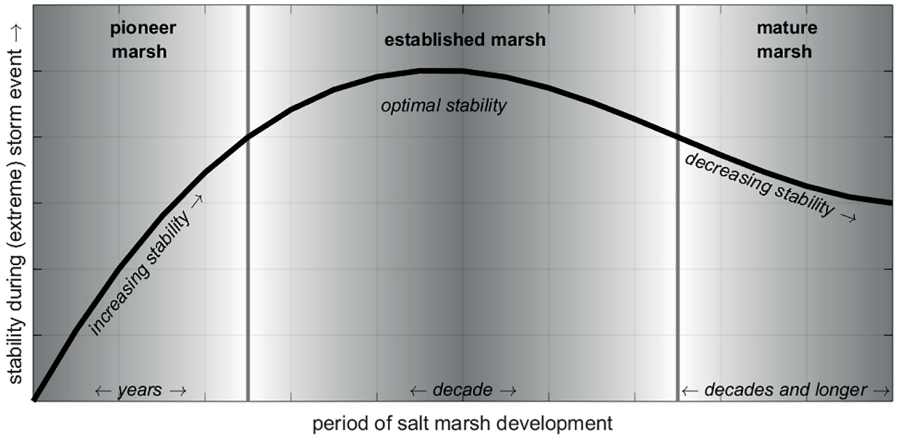

Figure 5.9 | Dynamic stability of the salt marsh over a 20 year development period.

5.4.2 | The development of artificial salt marshes for nature based flood defenses

Flume experiments have proven that established mature marshes are able to withstand and attenuate waves without the occurrence of significant erosion (Möller et al., 2014). The current model study extends this knowledge by assessing the resilience and stability of establishing artificial salt marshes. The study shows that artificial marshes are able to attenuate waves already after a 2-year development period, but their vulnerability to large waves remains until the marsh has developed for 5 to 10 years. The contribution to coastal protection after a 2-year development period and the little increase in wave

attenuation with increasing vegetation density (i.e. development time) during spring tide, corresponds with previous studies indicating a large contribution of the elevation of the salt marsh and a smaller additional contribution due to vegetation roughness (Vuik et al., 2018b). Nevertheless, a decreasing bed elevation, salt marsh width and vegetation cover after 10 to 15 years (Fig. 5.7), results in a decreasing wave attenuating capacity (Fig. 5.8). So, the stability of the salt marsh under (extreme) storm events and related wave attenuating capacity (1) increases during the first years of salt marsh development, (2) is optimal after approximately a decade of growth, and (3) slightly decreases when the marsh is mature (Fig. 5.9). The timescale of this mechanism depends on the local conditions, e.g. a wave climate with on average higher waves might lead to a smaller timescale, whereas a larger sediment availability might result in a longer timescale (Willemsen et al., submitted).

Although artificial marshes are almost directly able to attenuate waves, those waves hamper the vegetation growth and thereby the development of the salt marsh approximately over the first 5 year. So additional protective measures are necessary to enable the marsh to establish. Moreover, these measures can enhance sediment trapping (Siemes et al., 2020), thereby contributing to accretion of the establishing salt marsh. This might prevent the decreasing elevation of the profile over time with suspended sediment concentration in the lower range, which is observed in this study. The construction of brushwood or bamboo dams can contribute to vegetation establishment (e.g. Baptist et al., 2019a). These dams should be maintained for the years the arrival of large waves should be prevented. Moreover, biodegradable structures have a temporal function and can specifically contribute in the first years of development, when hydrodynamic and bed level dynamics should be tempered for vegetation to establish (Temmink et al., 2020). After the ecosystem has developed for more than a decade, salt marsh retreat might be initiated, with a decreasing resilience as consequence. Self-organization of the marsh can lead to a pioneer zone in front of the salt marsh edge, thereby rejuvenating the marsh naturally (Allen, 2000; Van der Wal et al., 2008; Singh Chauhan, 2009; Bouma et al., 2016), which increases the stability and resilience. Nevertheless, it might be necessary to apply artificial rejuvenation to keep the marsh stable, and thereby keep the ecosystem services such as wave attenuation intact (c.f. Baptist et al., 2004).

5.5 | Conclusions

A biogeomorphological model was extended to assess the influence of high waves on the development of artificial salt marshes. Long-term development was combined with short-term more extreme conditions and the strength of the salt marsh substrate was included. The artificial salt marsh, developing at an suitable bed elevation for 2, 5, 10, 15

and 20 years, was forced with a range of high wave conditions to answer the key question of this study: What is the influence of short-term wave forcing (hours to days) on long-term salt marsh development (years to decades), and the sensitivity of this for the rate by which plants stabilize their own environment in different stages of development (i.e. pioneer marsh, established marsh and mature marsh)?

After 5 years of development, a clear marsh edge appeared. The discontinuity between tidal flat and salt marsh was not only observed in the vegetation density, but also in the strength of the tidal flat and salt marsh substrate, represented by spatio-temporal varying critical bed shear stresses. The cross-shore marsh width and vegetation cover of the artificial marshes, developed for 2 to 5 years, largely changed after high waves arrived. Subsequently, after a development period of 10 year the salt marsh developed towards a more stable ecosystem. Still, the stability and wave attenuating capacity slightly decreased after the salt marsh developed for 10 to 15 years. Nevertheless, the wave attenuating capacity of the artificial salt marsh was already present after a development period of 2 years. This indicates a development period after which the stability is optimal, which is approximately 5 to 15 years in this study.

The construction of an artificial salt marsh almost directly results in a contribution to coastal protection. However, additional measures to protect the establishing artificial salt marsh from waves are necessary for approximately the first 5 years. The resilience of the artificial salt marsh after 5 to 10 years of development is sufficient to withstand large waves, without additional measures. However, measures to keep the marsh stability and ecosystem services intact after 15 years, such as marsh rejuvenation, might be necessary.

Acknowledgements

This work is part of the research program BE SAFE, which is financed by the Netherlands Organization for Scientific Research (NWO) (grant 850.13.010). Additional financial support has been provided by Deltares, Boskalis, Van Oord, Rijkswaterstaat, World Wildlife Fund, and HZ University of Applied Science. Bas W. Borsje was supported by the Netherlands Organization for Scientific Research (NWO-STW-VENI; 4363). We would like to thank A. Mourits, M. Nabi and E. de Goede for their contribution to the technical development of the model.

6

Discussion

The cross-shore width of the salt marsh is a clear indicator of the magnitude of ecosystem services of the salt marsh. The primary production of the salt marsh (e.g. Duarte et al., 2013), carbon storage (e.g. Duarte et al., 2005) and habitat extent (e.g. Irmler et al., 2002) increase with an increasing salt marsh width. Moreover, salt marshes are highlighted as sustainable contributors to coastal protection globally (King and Lester, 1995; Borsje et al., 2011; Gedan et al., 2011; Shepard et al., 2011; Temmerman et al., 2013; Vuik et al., 2019); to a certain extent, the larger the cross-shore salt marsh width, the larger the wave attenuating capacity of the marsh (Vuik et al., 2016). Hence, it is key to quantify the long-term salt marsh width and determine the biophysical processes driving the location of the salt marsh edge.

In this thesis the biogeomorphological development of salt marshes is quantified by: (1) assessing the decadal width of the bare tidal flat and vegetated salt marsh using bathymetrical data, (2) determining the dominant physical factors confining the location of the salt marsh edge by obtaining high-resolution field observations, (3) assessing the decadal development of an establishing salt marsh under influence of different homogeneous mild wave forcing, and (4) determining the over time increasing resilience of an establishing salt marsh affected by extreme storm conditions.

The discussion reflects on observations of the location of the salt marsh edge for determining the width of the salt marsh (section 6.1), considers state-of-the-art methods for modelling of biogeomorphological landscapes (section 6.2), reflects on methods for validating biogeomorphological models and field observations required for a holistic validation (section 6.3), and describes the use of intertidal ecosystems in Nature Based Flood Defenses (NBFD) in an era of climate change (section 6.4).

6.1 | Biophysical conditions driving the salt marsh edge and width

The location of the salt marsh edge is determined by the presence of vegetation. Biophysical conditions seaward from the marsh edge prevent vegetation from growing, whereas biophysical conditions at the landward location of the marsh edge are suitable for the presence of vegetation. Nevertheless, the local biophysical conditions can change (temporally) allowing vegetation to expand seaward from the marsh edge or resulting in vegetation mortality landward from the vegetation edge (Allen, 2000; Van der Wal et al., 2008; Singh Chauhan, 2009). New vegetation can colonize the tidal flat by establishment of individual seedlings (Hu et al., 2015b), and growth of clonal shoots (Silinski et al., 2016). Vegetation mortality can be initiated by cliff formation, a discontinuity occurring

if the salt marsh expands to far out on the tidal flat (Van de Koppel et al., 2005; Bouma et al., 2016). Whether vegetation growth or mortality occurs, leading to an expanding or retreating marsh edge, depends on spatio-temporal varying bio-physical conditions (e.g. Fagherazzi, 2014; Cao et al., 2019).

The results in this thesis indicate that the location of the marsh edge over a period of approximately one year is determined by the magnitude of both bed level change and inundation period (Chapter 3; Fig. 3.7). Once the inundation period at the salt marsh edge decreases, the magnitude of bed level change increases, which seems counter intuitive. After all, more exposure to inundation and an increasing number of inundations might indicate increasing hydrodynamic energy and increasing opportunities to capture extreme wave events. Hence, increasing bed level change with decreasing inundation period should be explained by parameters integrated in bed level change. Bed level change can be driven by waves (Friedrichs, 2011; Green and Coco, 2014; Hunt et al., 2015; Hu et al., 2017), grain size characteristics (Grabowski et al., 2011; Deegan et al., 2012), biological processes as bioturbation, bio-aggregation and the presence of a root zone modifying the critical erosion threshold of the bed (Andersen et al., 2005; Murray et al., 2008; Corenblit et al., 2011; Ford et al., 2016), consolidation of deposited sediments (Allen, 2000; Fagherazzi and Furbish, 2001; Chen et al., 2012) and external sediment supply controlling the rate of sedimentation and erosion (Mariotti and Fagherazzi, 2010; Hu et al., 2015c; Willemsen et al., 2016).

Larger magnitudes of bed level change were found to be related to smaller inundation periods at the marsh edge and vice versa (Chapter 3). In general, at marshes where the latter was observed, onshore winds occurred with a smaller frequency. These results suggest a relation between a higher frequency of onshore winds and smaller inundation periods, enhancing bed level change. Higher frequencies of onshore directed winds, inherently leads to more wave impact on the marsh edge. This is in line with Callaghan et al. (2010) and Wang et al. (2017) stating that wind exposure plays an important role in marsh edge development. Larger homogeneous waves continuously pounding at the marsh edge eventually result in a higher elevated marsh edge, since the marsh edge retreats towards its landward base (Chapter 4; Fig. 4.5 & Fig. 4.6) (Fagherazzi, 2014). Despite larger bed level change at the marshes with a higher frequency of onshore winds, the salt marsh edge does not necessarily retreat (table 6.1). Hence, the balance between dry period and bed level change does not explain the development of the marsh. Nevertheless, the marsh edge of both expanding and retreating marshes fits in the same balance of bed level change and inundation period, suggesting a geographical shift of dynamics with an expanding and retreating marsh (Fig. 6.1).

The balance of bed level change and inundation time driving the location of the marsh edge, was observed at marshes located in both macro- and mesotidal estuaries. This balance can be extrapolated to salt marshes worldwide, since macro- and mesotidal estuaries are found globally (Short, 1991). However, the observed salt marshes were all located in an area with a restricted fetch, because of the presence of other landmass, which decreases the applicability. Using the obtained balance, the location of the marsh edge can be estimated under changing environmental conditions such as: sea level rise (affecting inundation period), increasing storminess (affecting bed level change). An accurate estimate of the long-term location of the marsh edge under changing environmental conditions is a prerequisite for the associated ecosystem services.

Building on the results describing the balance between bed level change and inundation period, the location of the marsh edge in this parameter space does not necessarily determine the width of the marsh. For example, salt marshes with a higher elevated marsh edge at the northern shores of the Westerschelde (Chapter 3), can have a larger cross-shore width (Chapter 2). On the long-term, larger scale dynamics, outside the vegetated salt marsh, might play a role in thresholds of the salt marsh width. Obviously, dikes and urban areas at the landward side (Fig. 6.1) decrease accommodation space and might eventually enhance coastal squeeze (Doody, 2004, 2013; Torio and Chmura, 2013). At the seaward side of the salt marsh (Fig. 6.1), channel migration might affect marsh expansion or retreat (Van der Wal et al., 2008). In addition, an increasing frequency of high tides arriving at the marsh edge, due to dredging operations increases the risk of erosion (Cox et al., 2003), although a correlation between this frequency and marsh edge retreat was not found to be significant (Van der Wal et al., 2008). Moreover, once disturbances result in an insurmountable discontinuity between tidal flat and salt marsh, vegetation is not able to grow seaward from the marsh edge, resulting in a constantly retreating marsh (Fig. 6.1). This emphasizes the importance of quantifying the intrinsic processes of salt marsh expansion and retreat.

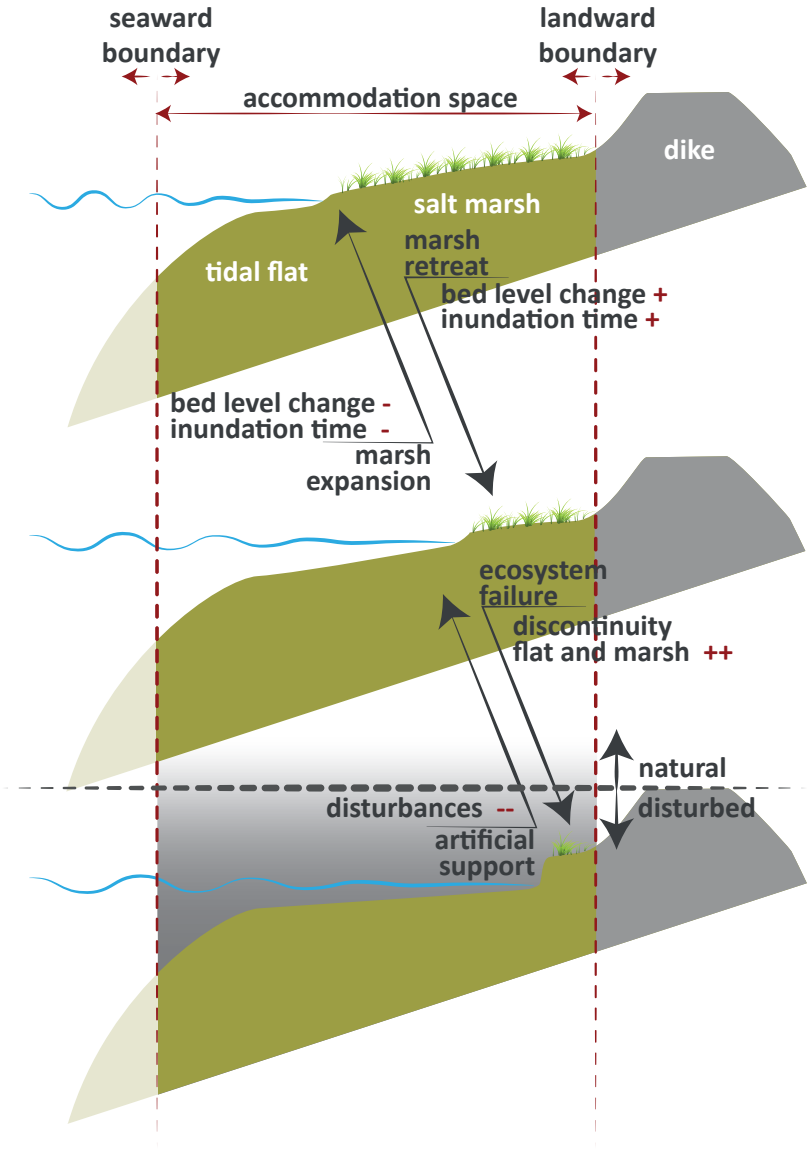

Figure 6.1 | Mechanisms describing salt marsh expansion and retreat. The accommodation space for the salt marsh is confined by the seaward and landward boundary. Phases of expansion and retreat are caused by either a small or a large magnitude of bed level change and inundation period in a natural system, i.e. large (+) bed level change and inundation time leads to a retreating salt marsh, whereas small (-) bed level change and inundation time leads to an expanding marsh. Once disturbances are too large (++) and exceed a certain threshold, the discontinuity between tidal flat and marsh increases such that vegetation cannot grow seaward from the marsh edge. If that is the case, salt marsh expansion can be enhanced with artificial measures, largely decreasing the disturbances (--), only.

Table 6.1 | Characteristics of biophysical parameters wind, waves and sediment at the salt marshes studied in this thesis. Collected wave heights are simplistically distributed over calm and stormy conditions, using an exceedance level of 30% applied on the wave height, similar to exceedance level Callaghan et al. (2010) used for distributing wave heights based on wind speed. Additional data is used from [a] (The Royal Netherlands Meteorological Institute (KNMI), 2020), [b] Callaghan et al. (2010), [c] Folmer et al. (2017), [d] Hu et al. (2020a), [e] Van der Wal et al. (2008), [f] Dijkema et al. (2009) and [g] van der Wal and Pye (2004).

	Salt marsh	Frequency of on-shore winds (%)	H_{mo} average calm (m)	H_{mo} average stormy (m)	D_{50} average [spatial variability] (µm)	Lateral marsh dynamics
rel. high frequency onshore winds	Zuidgors	54 [a]	0.14 [b]	0.23 [b]	39.2 [23.4 - 48.8]	Retreating [e]
	Zimmerman	53 [a]	0.07	0.19	85.0 [66.7 – 99.5]	Retreating [e]
	Uithuizen	43 [a]	0.02	0.22	87 [c]	Balance [f]
rel. low frequency onshore winds	Paulina	37 [a]	0.05 [b]	0.19 [b]	35.2 [27.0 – 42.4]	Expanding [e]
	Hellegat	40 [a]	0.08 0.08 [b]	0.20 0.18 [b]	123.2 [113.4 – 131.8]	Balance [e]
	Tillingham	-	-	-	22.0 [5.5 – 70.3] [d]	Retreating [g]

6.2 | Modelling dynamics of biogeomorphological landscapes

Simulating the interaction between hydrodynamics, morphodynamics and biological development has gained interest in the last decades. To understand the role of ecosystem engineers (such as salt marsh vegetation) in long-term landscape development, two-way coupled biogeomorphological models are necessary (Murray et al., 2008). Salt marsh development has been studied previously by idealized 1-dimensional models over decadal to centennial timescales (e.g. Mariotti and Fagherazzi, 2010; Mariotti and Fagherazzi, 2013; Mariotti and Carr, 2014), large-scale 2-dimensional (depth-averaged) and 3-dimensional basin scale models simulating infilling and emptying of a tidal basin (e.g. Kirwan and Murray, 2007; Mariotti and Canestrelli, 2017) and 2-dimensional (depth-averaged) and 3-dimensional landscape models on a single salt marsh scale (e.g. Temmerman et al., 2007; Schwarz et al., 2014; Best et al., 2018; Schwarz et al., 2018). Although all models simulate salt marsh development, the focus is generally on a specific aspect of the development, e.g. vertical marsh growth, channel development or salt marsh loss. A holistic process-based approach, assessing the conditions underlying vertical marsh expansion and retreat by movement of the marsh edge is missing, although this is characterized as an important process for marsh loss in several of these model studies (e.g. Mariotti and Canestrelli, 2017).

The model studies in this thesis build upon and extend on previous model studies by relating both expansion and retreat of the salt marsh edge to hydrodynamic forcing. This makes it possible to assess the extent of the salt marsh landscape and temporal variability of the landscape, thereby making it possible to quantify ecosystem services (Duarte et al., 2013). Quantification and eventually predicting landscape characteristics is a necessary step forward to implement salt marshes in e.g. Nature Based Flood Defenses (Temmerman et al., 2013; Bouma et al., 2016).

Model simulations were conducted using the state-of-the-art Delft3D – Flexible Mesh model for computing hydrodynamics (both flow and wave) and morphodynamics (Deltares, 2019a). A vegetation growth module was set up in Python and online coupled through BMI (Basic Model Interface) (Peckham et al., 2013). By using this model infrastructure a range of biophysical model parameters were exchanged via memory of the computational machine, avoiding any file reading and writing. The model infrastructure can be applied to other stand-alone modelling software, such as: MIKE 21 and MIKE 3 (Danish Hydraulic Institute, 2016) to extend previous models simulating estuarine environments with spatio-temporal fixed ecology (Freeman et al., 2015; Narayan et al., 2017), with spatio-temporal dynamic ecology; TELEMAC (e.g. Smolders et al., 2020), to extend models already including spatio-temporal dynamic vegetation (Schwarz et al., 2018), with other dynamic parameters for biogeomorphological development; and HEC-RAS (e.g. Bomers et al., 2019a), to take into account biogeomorphological dynamics in river floods. The development of this model infrastructure and ecological modules allows for a convenient introduction of more process-based biophysical development of the landscape, which is essential for understanding how ecosystem-engineers shape the landscape (Murray et al., 2008).

Although complex process-based models are necessary to understand the formation of landscapes, they require a lot of computational power (e.g. Willemsen et al., submitted). The model simulations and field measurements in this thesis indicate specific parameters affecting the location of the salt marsh edge, such as bed level change, inundation time and waves. Other important parameters are suspended sediment concentration and the impact of climate related parameters (e.g. droughts) (Hughes et al., 2012; Kirwan and Megonigal, 2013; Chapple and Dronova, 2017). An artificial neural network (ANN) can be trained (French et al., 1992; Raju et al., 2011; Bomers et al., 2019c), for example to estimate the salt marsh width by using long-term datasets of these parameters and aerial imagery to determine the salt marsh width, without using a complex process-based model. Previously, salt marshes have been characterized with such techniques (Morris et al., 2005). Machine learning techniques such as an ANN do not require the inclusion of all relevant underlying processes (French et al., 1992). Since these techniques are data-driven, the increasing availability of continuous measurement data and aerial imagery can increase the use. By using future scenarios of the parameters driving the location of

the marsh, the salt marsh width can be estimated relatively fast with an ANN, without including all complex processes.

In this thesis, vegetation growth was simulated using the population dynamics balance equation (Temmerman et al., 2007). The increase of vegetation density was based on the physical parameters bed shear stress and inundation time, whereas the vegetation density affected hydrodynamics (flow and wave) and morphodynamics (i.e. bed level change). To improve salt marsh development under (extreme) hydrodynamic forcing the increasing belowground strength of the salt marsh substrate was taken into account (Brooks et al., 2020), by applying a spatio-temporal varying critical bed shear stress. The simulation of ecological engineering species (Borsje et al., 2011) and physical-biological feedbacks (Murray et al., 2008) is not restricted to salt marshes. For example, biophysical feedbacks are observed in offshore sand wave dynamics (Damveld et al., 2020) and river development (Williams et al., 2016). The methods used to simulate development of biogeomorphological landscapes in the current study can be extended to assess the biogeomorphological development of other intertidal ecosystems, such as: stabilizing function of vegetation in mangroves and seagrass fields (Friess et al., 2012), stabilizing microphytobenthos and destabilizing macrofauna at tidal flats (Andersen, 2001; Andersen et al., 2005), vegetation growth affecting patterns in fluvial systems (Oorschot et al., 2016; Williams et al., 2016) and benthic species affecting sand wave development in marine systems (Damveld et al., 2020).

Temporal scales for simulating salt marsh dynamics in this thesis ranged from homogeneous decadal salt marsh development to development under daily extremes. Previous studies assessing the decadal development of the salt marsh edge, showed (cyclic) alternations between erosion and expansion (Allen, 2000; Singh Chauhan, 2009). This mechanism is supported by model results in this thesis, depending on homogeneous continuous wave forcing (Chapter 4), given that the cyclic alternations are a result of alternating forcing. However, the grid cell size in this thesis was 5m, whereas movement of the marsh edge might be in the order of tens of centimeters per year (Van der Wal et al., 2008; Wang et al., 2017). Increasing the grid resolution, would have resulted in a more precise simulation of the location of the marsh edge. Also the simulation of common patterns in salt marshes, such as creeks and vegetation patches, would benefit from an increasing grid resolution. However, computational time would largely increase. Moreover, a more process-based representation of mechanisms for marsh edge erosion (Francalanci et al., 2013; Bendoni et al., 2016), would have improved the results most probably. However, including those mechanisms would imply using both multiple bed and hydrodynamic layers in the vertical, again largely increasing the computational time. Nevertheless, validation of the simulated lateral movement of the marsh edge in this thesis showed good correspondence with field observations.

The marsh edge is also the location where hydrodynamic energy has the largest impact (Wang et al., 2017). Although mature established salt marsh landscapes are able to resist extreme wave conditions (Möller et al., 2014), the strength of the substrate at the marsh front where vegetation establishes needs quantification (Brooks et al., 2020). A first step in the schematic assessment of the increasing strength with the time a marsh develops was taken in this thesis (Chapter 5), by combined modelling of the decadal salt marsh dynamics of an establishing marsh and the impact of daily extreme conditions.

6.3 | Validation of models simulating biogeomorphological dynamics

By introducing biological processes in models simulating hydrodynamic processes and morphodynamic processes, the complexity of such models increases largely. Although holistic biogeomorphological perspectives appeared by the end of the 20th century only (Corenblit et al., 2008), already a large range of models were developed for solely simulating biogeomorphological development of salt marshes (Fagherazzi et al., 2012). Recent 2-dimensional and 3-dimensional process-based salt marsh models provide rather schematic simulations with a qualitative comparison with field sites (e.g. Kirwan and Murray, 2007; Mariotti and Canestrelli, 2017), use physical settings derived from literature and field sites (e.g. Best et al., 2018), and are validated by comparing vegetation and channel patterns (e.g. Temmerman et al., 2007; Schwarz et al., 2014; Schwarz et al., 2018).

Although Wiberg et al. (2020) states that general outcomes of morphodynamic models of marsh development should be qualitatively compared with behavior from a diverse set of marshes rather than quantitatively compared at one particular site, exactly the latter is necessary to locally quantify ecosystem services such as wave attenuating capacity and carbon storage. Moreover, both the intrinsic and extrinsic variability of the marsh extent needs to be determined (Bouma et al., 2014), since the contribution to coastal safety of a marsh decreases with a decreasing cross-shore marsh width (Chapter 2; Vuik et al., 2016). The validation of simulated biogeomorphological dynamics of salt marshes in this thesis (Chapter 4), does not comprise the full range of hydrodynamic, morphodynamic and biological processes, but does quantitatively compare the biological dynamics of the marsh edge with field data. Moreover, the simulated temporal variability of the marsh edge location was found to be comparable with field sites, implying that all relevant processes are taken into account.

To validate 2-dimensional and 3-dimensional landscape models simulating decadal salt marsh development, multiple spatial and temporal scales should be considered. The decadal timescale (i.e. a period of 50 to 100 years) is the largest temporal scale. Starting

data collection over such a long-term period is impossible when assessing dynamics, hence data on this period should be available from external sources. The simulated variability of this long-term period can be assessed by extensive bathymetrical datasets already available, such as: bathymetrical data in the Netherlands (De Kruif, 2001; Marijs and Parée, 2004; Wiegman et al., 2005), which is used in this thesis. By using (historical) aerial imagery, the vegetation cover of the entire salt marsh can be quantified and compared with temporal development of simulations (Van der Wal et al., 2008).

Recent developments as well as existing knowledge enable a range of possibilities for long-term monitoring in the field: periodic point measurements of sediment characteristics (e.g. Willemsen et al., 2016) and bed level change, periodic measurements of the bathymetry by using a LiDAR unmanned aerial vehicle (UAV) (e.g. Baptist et al., 2019b; Kogut and Weistock, 2019) or photogrammetry (e.g. Anderson et al., 2019), and biological coverage derived from aerial imagery collected by a UAV (e.g. Zhou et al., 2018) or assessing similar data in the Google Earth Engine (e.g. Campbell and Wang, 2020) fully covering the salt marsh. Moreover, periodic point data of bed level change (Baptist et al., 2019b), sediment characteristics (Willemsen et al., 2016) and measurements of the marsh substrate can be collected. Point data of hydrodynamics at the intertidal area, can be collected for periods of weeks (flow velocities) or periods of years (water level and waves) (e.g. Horstman et al., 2014; Vuik et al., 2016; Willemsen et al., 2016). More recently, several methods were developed for continuously measuring bed level change using stand-alone rather low-cost instruments based on light sensitive cells (Hu et al., 2015a; Chapter 3; Hu et al., 2020a), a laser (Hu et al., 2020b) and acoustic measurement equipment, which is currently tested at a constructed salt marsh (Baptist et al., 2019a). Continuously measuring bed level change is key to identify opportunities for pioneer vegetation to establish (Bouma et al., 2016; Poppema et al., 2019).

Although field measurements are widely used in hydrodynamic and morphodynamic validation of models, a generic framework for biogeomorphological validation of model does not exist. Apart from hydrodynamics and bed elevation, the morphological and biological development should be validated with (a selection of) the listed measurements. In this thesis the simulated salt marsh width and salt marsh edge variability is compared with field measurement, which is a first step in biogeomorphological validation, since both are driven by hydrodynamics, morphodynamics and vegetation development. Model performance is acceptable if these parameters are quantitatively comparable with field measurements over the simulated timescale. In addition, pattern size and spacing can be used for validation, as well as the time it takes for the patterns to develop. On a smaller spatial scale, simulated vegetation characteristics and their development can be quantitatively compared with measurements.

Although extensive field measurements might result in an overview of salt marsh dynamics, extremes are not often captured, since the return time generally exceeds the measurement period. Nevertheless, the dynamics of established mature marshes under extreme conditions were captured in the flume. These flume experiments revealed that established marshes are able to withstand extreme storms (Möller et al., 2014). Still, the strength of a marsh with establishing vegetation and the resistance of the marsh front is unknown (Brooks et al., 2020). So it is key to measure bed level change around the marsh edge under extreme conditions, in the field and/or flume, since these dynamics drive the long-term development of the marsh (Bouma et al., 2016).

6.4 | Applying intertidal ecosystems in Nature Based Flood Defenses

The salt marshes considered in this thesis are all located in the North Sea region, both in macro- and mesotidal regions. In these marshes, a broad range of vegetation species were observed. So the relation found between marsh width and wave attenuation is applicable to coastal salt marshes globally, although the magnitude of the marsh width/wave attenuation relation might be different at other locations. The quantitative relation between marsh width and wave attenuating capacity differs per salt marsh (Chapter 2; Fig. 2.8), depending on the bare tidal flat seaward from the salt marsh and small scale topography. The range of wave attenuation (reduction of significant wave height) over a stretch of marsh of 500m in the Westerschelde estuary ranges between approximately 10% and 35%. Moreover, salt marshes at foreshores with a steep profile can attenuate extreme waves with 10% over a distance of only 100m. This agrees with Vuik et al. (2016), assuming a rather large water depth at the bare tidal flat and salt marsh under extreme conditions. Model simulations in this thesis (Chapter 4, Fig. 4.8) highlight a strongly decreasing marsh width once cliff formation is initiated at the marsh edge (c.f. Van de Koppel et al., 2005). Moreover, the height of the marsh platform decreases, but eventually increases once the cliff is fully developed. Vuik et al. (2016) describes a decreasing wave attenuating capacity with a smaller marsh width and platform height. So the formation of a cliff can be seen as a first indicator of a decreasing contribution to coastal protection.

Whether the salt marsh expands seaward or retreats landward depends on bio-physical conditions (e.g. Fagherazzi, 2014; Cao et al., 2019), this is similar for tropical mangrove ecosystems (Fig. 6.1). Short-term dynamics determine the establishment of pioneer vegetation (Balke et al., 2011; Balke et al., 2013; Hu et al., 2015b), whereas long-term ecosystem-scale dynamics constrain the persistence of a certain ecosystem extent (Friess et al., 2012; Bouma et al., 2016). Since both salt marsh (Chapter 2) and mangrove

(e.g. Mazda et al., 1997; Horstman et al., 2014) ecosystems can largely contribute to coastal safety by wave attenuation, maintaining or even maximizing the extent of the ecosystem, without disturbing other ecosystems, is a prerequisite to secure a certain contribution to coastal safety. Disturbing surrounding ecosystems, but also the salt marsh itself, must be prevented to make sure ecosystem services of the intertidal zone remain (Gedan et al., 2009). Since the location of the ecosystem edge depends on inundation period (i.e. relative elevation in the tidal frame) and bed level change (integrating sediment characteristics, hydrodynamic energy, etc.) (e.g. Friess et al., 2012; Chapter 3), the magnitude of these parameters can be changed to enhance ecosystem expansion or stimulate vegetation establishment in constructed marshes.

Brushwood and bamboo dams can be constructed for decreasing hydrodynamic energy (e.g. de Vriend et al., 2015; Poppema et al., 2019), thereby creating a more stable bed. Also rigid constructions at the bed can be applied more seaward, either artificial using a rubble rock dam, or more naturally by using oyster or mussel reefs (e.g. Borsje et al., 2011). Another possibility is creating a double dike system, with which the tidal inundation can be controlled, and sediment is still able to accrete (e.g. Temmerman et al., 2013). Moreover, sedimentation can be enhanced by nourishments close to or at the location of the ecosystem (Baptist et al., 2019b; Siemes et al., 2020). Finally, the fastest option for creating an intertidal ecosystem is levelling the bed to the right elevation relative to the tide, whether or not combined with one of the previous measures (e.g. Baptist et al., 2019a) (Fig. 6.2).

To optimally use the ecosystem engineering capacity of salt marsh and mangrove vegetation, the temporal use of measures enhancing vegetation growth might be sufficient (e.g. biodegradable structures). If the windows of opportunity for vegetation establishment (Balke et al., 2011; Hu et al., 2015b) are created by additional measures, and the vegetation becomes mature (e.g. over a period of 10 years), the resilience might have increased such that additional measures are not necessary. Moreover, in urban areas where accommodation space is scarce (Temmerman et al., 2013), additional measures for enhancing vegetation growth should not be temporal applied, but continuously maintained, to decrease the variability of the ecosystem and maximize its services. Initial growth and maintenance should be supported by long-term field measurements with a sparse seasonal resolution, since changes are generally induced during the growth season (expansion) or periods with increasing hydrodynamic energy (retreat). Rather simple, but fast regression models (i.e. Wang et al., 2017) and field observations such as aerial imagery, combined in data assimilation methods (i.e. Rodell et al., 2004), can contribute to forecasting the state of the ecosystem and thereby its protective capacity. Moreover, these methods can be applied in data scarce areas, since satellite imagery is globally available.

Understanding the connectivity between ecosystems, e.g. the tidal flat and salt marsh or mangrove, is important (Bouma et al., 2016) for creating opportunities to stimulate an accreting marsh. For example, stimulating sediment accretion at tidal flats with sediment disposals and nourishments can result in a switch from an erosive to an accretive phase (Ladd et al., 2019; de Vet et al., 2020), which might eventually lead to an increasing salt marsh or mangrove extent. Not only large-scale methods can be applied, observations of subsequent patterns at newly establishing flats and marshes (Fig. 6.2) suggest a developing flat in the tidal frame, where drainage patterns evolve dewatering the bed and thereby increase the strength of the bed. Enhancing the emergence of patterns higher in the tidal frame with artificial measures, might result in seaward expansion of the marsh. A combination of the previous measures to stimulate the growth of the ecosystem and decrease the variability of the ecosystem extent, maximizes the wave attenuating capacity with as little as possible long-term uncertainties, thereby enabling large-scale application.

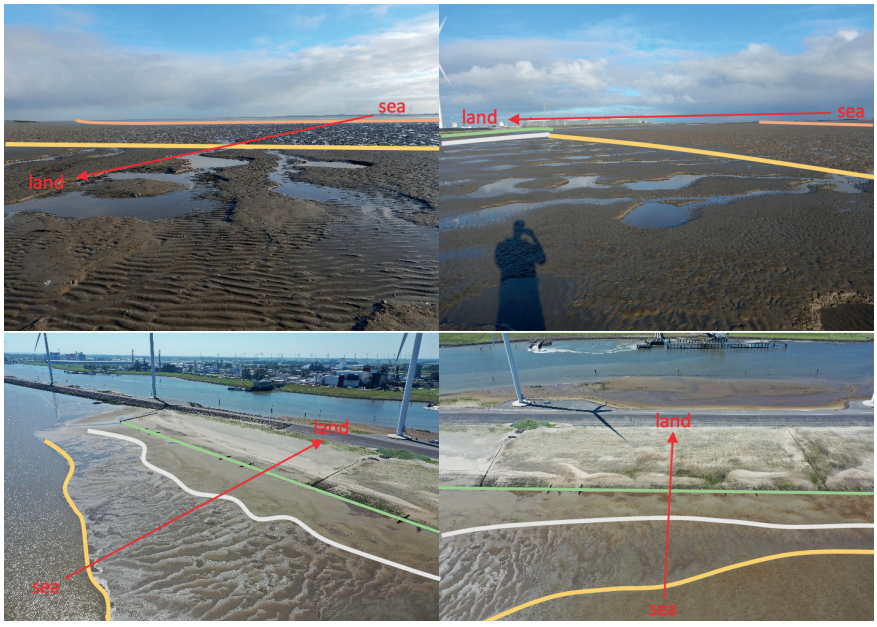

Figure 6.2 | Subsequent patterns observed at the Marconi salt marsh, constructed in 2017/2018. Subsequent bed patterns evolve from the sea towards the landward side (red arrow). Pictures top by Pim Willemsen, bottom by Ecoshape – Robert van der Veen.

7 Conclusions

The research presented in this thesis aimed at providing a generic understanding of the biophysical parameters driving the salt marsh width. The developed knowledge was used to quantify the variability of the salt marsh width and thereby the wave attenuating capacity of the salt marsh on a decadal timescale.

RESEARCH QUESTION 1: **What is the variability of foreshores, consisting of tidal flats and adjacent salt marshes, in an estuary over a decadal time-scale; and to what extent can foreshores safely act as additional defense measure?**

In Chapter 2, the variability of the foreshore width, consisting of a bare tidal flat and vegetated salt marsh was assessed. A dataset over a period of 65 years, including bathymetrical data approximately once every one or two years, was used to obtain 36 profiles covering six salt marshes in the Westerschelde estuary. The variability of the width of the tidal flat and salt marsh was quantified. Thereafter, the wave attenuation was simulated using the SWAN model under daily conditions with and without vegetation and under design conditions (i.e. events statistically occurring once every 10,000 years).

Generally, the spatial variability of the width of the flat and marsh was observed to be much larger than the temporal variability. Although the dynamics of a channel in front of the salt marsh and tidal flat might increase the temporal variability strongly. The temporal changes of the salt marsh width did not follow the changes of the width of the entire foreshore, suggesting a changing shape of the foreshore. The foreshores at the southern shores, sheltered from the prevailing wind direction were generally smaller, and were more efficient in attenuating waves (i.e. decrease of wave height per meter salt marsh width), whereas the foreshores at the northern shores, exposed to the prevailing wind direction were generally larger, and were less efficient in attenuating waves. The foreshores always contributed to wave attenuation, both under daily and design conditions, thereby decreasing the wave load at the landward dike. Wave attenuation at the bare tidal flat was small and rather independent of the width, whereas a relation was found between the wave attenuation and width at the vegetated salt marsh: the longer the salt marsh, the larger the wave attenuation.

RESEARCH QUESTION 2: **What physical factors confine the location of the marsh edge on a daily to annual timescale?**

Field observations of biophysical parameters close to the salt marsh edge were obtained in Chapter 3. A comprehensive dataset was composed, containing measurements of daily bed level changes and inundation time at transects located at six salt marshes in the North Sea area (Westerschelde estuary, Wadden Sea and Thames estuary). Moreover, a range of other biophysical parameters was measured, such as grain size characteristics,

waves and cholorphyll-a levels. Data was collected over a period of approximately a year at every salt marsh.

At all sites bed level change decreased from the lower tidal flat towards the marsh edge and the bed level remained rather stable in the salt marsh. Observations at the tidal flat suggested the presence of seasonal patterns, whereas these patterns were not observed in the marsh. Variations in bed level change at the tidal flat and salt marsh can be driven by the presence of vegetation and diatoms (approximated by chlorophyll-a levels). Measurements of the wave height showed a decreasing wave height from the seaward side of the tidal flat to the landward side of the salt marsh. A direct relation between bed level change and wave height was not found, possibly due to the more gradual decrease of wave height over the profile, whereas the bed level change abruptly decreases at the salt marsh edge. A combination of the different parameters implies that bed level change and inundation period near the marsh edge give an indication of the development of the marsh edge by controlling plant growth. If bed level change is high, the marsh is observed to occur at higher elevations with shorter inundation periods. Conversely, when bed level change is low, the marsh is observed to occur at locations were the inundation period is longer. Bed level change and inundation time chance only slightly going from tidal flat to salt marsh, implying a large sensitivity to bed level change and inundation time.

RESEARCH QUESTION 3: **How does the biophysical development and extent of salt marshes depend on the magnitude of homogeneous hydrodynamic forcing and sediment availability?**

In Chapter 4 the dynamics of the salt marsh edge were simulated on a landscape scale, 2-dimensional depth-averaged. The existing hydrodynamic and morphodynamic Delft3D – Flexible Mesh model was online coupled with a vegetation growth module in Python for the first time. Using this model setup, the influence of the magnitude of daily occurring mild weather conditions and sediment availability on the decadal development and variability of the salt marsh width was assessed. The model was continuously forced over a period of 50 years with a range of small homogeneous waves with a magnitude of 0.00m, 0.05m, 0.10m and 0.15m, representing daily weather conditions. The sediment availability was varied (10mg/L, 25mg/L and 50mg/L) for waves that were observed in the field on average (0.10m).

The simulated temporal variability of the marsh edge, only affected by the homogeneous magnitude of wave conditions, corresponds to the variability observed in the field. The marsh edge forced with small waves (0.00m and 0.05m) expanded over a 40-year period, whereas the marsh edge retreated when forced with larger waves (0.10m and 0.15m). Nevertheless, the salt marsh was able to switch from a retreating extent towards

an expanding extent, with increasing sediment availability. The magnitude of the wave forcing was responsible for the general elevation of the salt marsh profile, whereas the suspended sediment concentration was responsible for the steepness of the profile. Cliff formation was initiated with wave heights of 0.10m and larger. A fully developed cliff was observed with wave heights of 0.15m, resulting in vegetation unable to develop at the seaward side of the cliff. The results imply a large sensitivity of the lateral movement of the salt marsh edge to small changes in wave height and sediment availability, enabling even to transform from a retreating marsh to expansion. So while conventional gray coastal infrastructure can be applied generically, salt marshes in Nature-Based Flood Defenses are more location specific due to spatially variable conditions. This chapter shows that the right environmental conditions (e.g. wave height and sediment availability), which can be artificially achieved, can contribute to enhancing salt marsh growth.

RESEARCH QUESTION 4: **What is the influence of short-term wave forcing (hours to days) on long-term salt marsh development (years to decades), and the sensitivity of this for the rate by which plants stabilize their own environment in different stages of development (i.e. pioneer marsh, established marsh and mature marsh)?**

The sensitivity of the stability of artificial salt marshes to high waves was assessed in Chapter 5. The stability of the developing artificial marsh was simulated by imposing short-term high waves (significant wave height of 1.0m, 2.0m and 3.0m) on artificial marshes developed for a period of 2 to 20 years (long-term) under mild wave conditions. The numerical Delft3D – Flexible Mesh model with online vegetation coupling was extended to include the increasing strength of vegetation and salt marsh substrate with the time vegetation is present.

A clear marsh edge was observed after a development period of 5 years and the vegetation and bed substrate was almost fully developed after 10 years of development. The cross-shore marsh width and vegetation cover largely changed over the first 5 years of development under influence of high waves. Especially the largest waves resulted in a decreasing marsh width and vegetation cover. Nevertheless, after a development period of 10 years or more, the decreasing salt marsh extent remained small, indicating an almost completely decreased vulnerability to short-term high waves. Although the wave attenuating capacity was relatively large after 2 years of development already, the waves hampered the vegetation growth and thereby the development of the salt marsh approximately over the first 5 year. So additional protective measures are (temporarily) needed to enable the artificial marsh to establish for over the initial 5 years of development. Once the salt marsh is established after 5 to 10 years, it can withstand large waves , without additional measures. However, measures to keep the marsh stability and ecosystem services intact after 15 years (mature marsh), such as

marsh rejuvenation, might be necessary due to the increasing discontinuity between tidal flat and salt marsh.

KEY QUESTION: **What is the long-term (50 year) variability of the location of the salt marsh edge and what is the corresponding variability of the wave attenuating capacity of salt marshes?**

The four research questions all address a part of the key question. The temporal variability of the location of existing salt marshes fronting a dike or seawall is rather small at the assessed locations and stabilizes after multiple decades. Generally, the spatial variability of a salt marsh at a single point in time is larger, most probably due to geographical boundaries like dikes and channels and the biophysical dynamics caused by these boundaries. On a smaller scale, the location of the lower marsh edge is restricted by two interacting factors (Fig. 7.1): inundation time and bed level change. For vegetation establishment to withstand longer inundation stress, which slows down plant growth, more stable bed level are required so that plants are not disturbed. Vice versa, to withstand more dynamic bed levels that disturb plant growth, lower inundation stress is required, so that plants grow fast enough to recover from the stress. Moreover, the seaward growth and landward retreat of the marsh edge is driven by the magnitude of long-term (decades) daily mild wave conditions and sediment availability (Fig. 7.1). Periods of small waves enable the marsh to grow seaward and/or large sediment availability, whereas periods of larger waves and/or small sediment availability result in a retreating marsh edge.

The construction of artificial marshes is also hampered by high waves in the first years of development. High waves result in a retreating marsh (Fig. 7.1). So temporal additional measures are required to attenuate the waves before arriving at the establishing vegetation. Nevertheless, the wave attenuating function of the artificial marsh was enabled after a few years of development already. Both artificial marshes and existing salt marshes contribute to the wave attenuation and thereby coastal protection under a range of hydrodynamic conditions (Fig. 7.1). Generally, the larger the cross-shore width of the salt marsh and the denser the vegetation, the larger the stability and wave attenuation. However, small changes of hydrodynamic and morphodynamic parameters, result in a changing marsh width, thereby affecting the wave attenuating capacity.

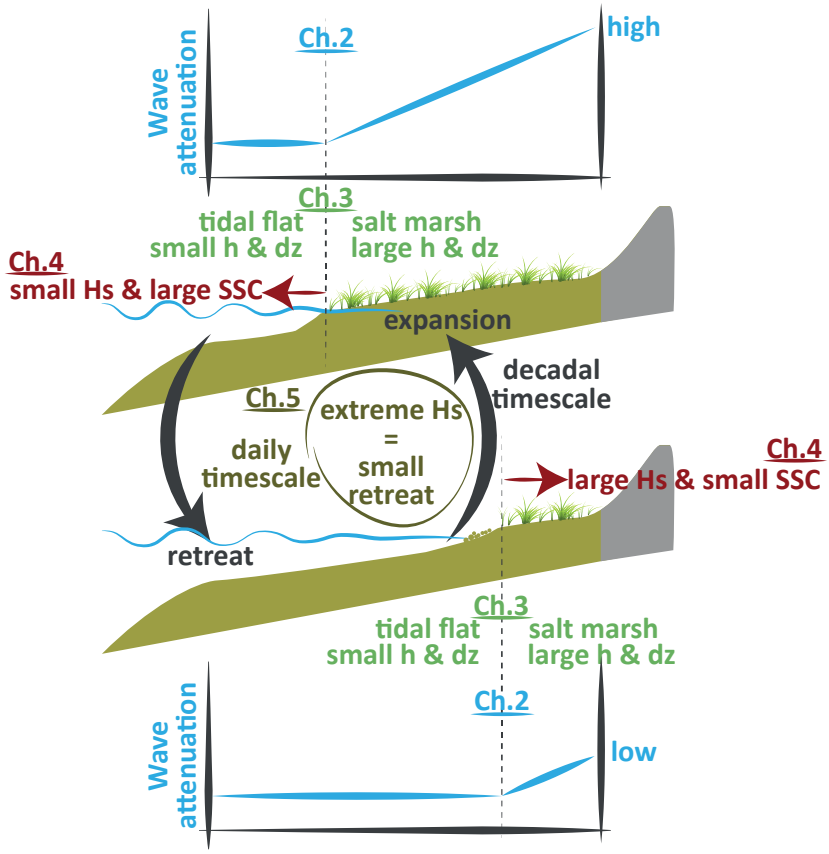

Figure 7.1 | Concluding summary of processes described in chapter 2 (blue), chapter 3 (green), chapter 4 (red) and chapter 5 (yellow).

8 Recommendations

Quantifying the extent and temporal variability of intertidal ecosystems is key to implement these ecosystems in coastal protection (Temmerman et al., 2013). In this thesis, the long-term biogeomorphological dynamics of an intertidal ecosystem are assessed. Parameters strongly affecting the width of the salt marsh are identified, whereby the wave attenuating capacity is quantified. This knowledge can be used to enhance salt marsh growth, to maximize ecosystem services. Based on these findings and the developed methods, a range of recommendations are suggested. The recommendations focus on (1) measuring biogeomorphological dynamics in the intertidal zone, (2) modelling biogeomorphological dynamics in the intertidal zone, (3) designing nature based flood defenses.

8.1 | Measuring biogeomorphological dynamics in the intertidal zone

R1 – Collecting a comprehensive dataset of field observations of salt marsh dynamics

To include salt marshes and other intertidal areas in coastal defense structures, their dynamics should be quantified (Temmerman et al., 2013; Bouma et al., 2014). For a holistic assessment of salt marsh dynamics, a combination of observational methods for hydrodynamics, morphodynamics and biological development should be applied. Those observations combined with existing (historical) data sources will result in an as complete as possible dataset to gain knowledge and validate computational models (R7). State-of-the-art measurement techniques enable high-resolution continuous point measurements and periodic measurements fully covering the salt marsh. Although in this thesis the decadal dynamics of the salt marsh width are indicated, the strength of the substrate, which can be assumed to grow with the presence of vegetation (Le Hir et al., 2007; Kirwan et al., 2010; Turner, 2011; Silliman et al., 2012; Ford et al., 2016), is not yet quantified. The developing strength of the substrate should be quantified to be able to determine the stability of the marsh during high wave events. It is recommended to assess the substrate strength at either an seaward expanding salt marsh or an artificially created marsh where vegetation growth is initiated. The potentially changing strength and composition of the substrate can be measured alongside measurements of hydrodynamics, morphodynamics and vegetation growth. Moreover, the measurement period should exceed the funding-driven appointments of a PhD student or Post-doc researcher, since phases of salt marsh growth and retreat have a decadal magnitude (Allen, 2000; Van der Wal et al., 2008; Singh Chauhan, 2009).

R2 – Assessing the resilience of establishing salt marshes to extreme storm events

It is known that established mature salt marshes are able to withstand the energy of rather large waves (Möller et al., 2014). However, comprehensive measurements of the resilience of establishing vegetation under extreme conditions are scarce. Despite the difficulty of obtaining such measurements, they contribute to knowledge of establishing salt marshes and stimulating salt marsh growth under extreme conditions. So it is recommended having a "storm chase team" ready for installing a set of instruments at a salt marsh where an extreme storm is expected. When remaining the instruments for a period of months to years in the field, an assessment of the recovery of the establishing salt marsh can be captured.

R3 – Assessing the resilience of establishing salt marshes under design conditions for coastal protection in the flume

Extreme storm events, for which coastal protection structures are designed, occur statistically once every thousands of years. Since it is very unlikely to capture these design conditions in the field, large-scale flume experiments should be set up to assess the resilience of establishing vegetation under these conditions. The growth period, needed to withstand an event of a specific magnitude, can be quantified by assessing the resilience of establishing salt marshes of different ages. Salt marsh vegetation with a different growth period can either be cultivated in the lab, or harvested from the field.

8.2 | Modelling biogeomorphological dynamics in the intertidal zone

R4 – Generalizing vegetation representation in process-based models

In this thesis the computational model Delft3D – Flexible Mesh has been used (Deltares, 2019a). The model in this thesis, online coupled with a vegetation growth module, represents growth of the reed *Spartina*. This vegetation species can be represented by a field of cylinders with different densities (e.g. Anderson and Smith, 2014). However, generally in models representing coupled vegetation growth, an approach that includes all vegetation characteristics (stem density, stem diameter and stem height) in multiple vertical layers can better represent brush like vegetation (e.g. Salicorna) and vegetation in general (e.g. mangroves; Horstman et al., 2015). This can be improved when extending

the model studies in this thesis. Moreover, the erodibility of the bed can be changed by changing the non-uniform critical bed shear stress. Applications for modelling environments with a spatio-temporal varying critical bed shear stress are extensive, since the erodibility of intertidal beds will change with the presence of roots (Le Hir et al., 2007; Kirwan et al., 2010; Turner, 2011; Silliman et al., 2012; Ford et al., 2016), biofilms by microphytobenthos like diatoms and bacteria (Tolhurst et al., 1999; Riethmüller et al., 2000; Stal, 2010) and macrofauna (Andersen, 2001; Andersen et al., 2005). Finally, when modelling the initial phases of salt marsh development it is recommended to take into account consolidation, for example because of the influence on channel formation (e.g. Fagherazzi and Furbish, 2001).

R5 – Process-based cliff dynamics

Marsh edge retreat can be initiated by different mechanisms (Francalanci et al., 2013; Bendoni et al., 2016). A retreating marsh leads to redistribution of sediment clumps, which might enhance establishment of pioneer vegetation seaward from the marsh edge. Including those processes in the biogeomorphological model used in this thesis, will result in a better representation of marsh edge dynamics. To include these dynamics, it is recommended to use multiple layers in the vertical dimension, since different processes play a role depending on the height.

R6 – Increasing efficiency of models

For understanding the mechanisms driving salt marsh development, process-based models are necessary. The computational time of these models can be decreased by using a multifidelity approach, where high-resolution model runs are used to train low-resolution models (Berends et al., 2019). This multifidelity approach can be used with the process-based models in the current study, assuming that the output of the low-fidelity model and detailed high-fidelity model are correlated. Moreover, once there is a general understanding of the parameters driving salt marsh development, including the width of the salt marsh, data-driven techniques can be used to predict the salt marsh width. For example regression models or artificial neural networks can be used (French et al., 1992; Morris et al., 2005; Raju et al., 2011). Moreover, the potential of using these techniques will increase, due to the increasing availability of continues measurements and aerial imagery.

R7 – Validation of biogeomorphological models

Recent biogeomorphological models are generally qualitatively validated with field observations, e.g. by comparing vegetation and channel patterns (e.g. Temmerman

et al., 2007; Schwarz et al., 2014; Best et al., 2018). In this thesis a first step in large-scale quantitatively comparing model simulations with field observations is made, by comparing the variability of the location of the salt marsh edge. Further developing the quantitative validation of biogeomorphological models is only possible by jointly setting up field studies and model studies, since the dynamics simulated should be specifically validated with field data. For example, pattern size and spacing can be used for validation, as well as the time it takes for the patterns to develop. On a smaller spatial scale, simulated vegetation characteristics and their development can be quantitatively compared with measurements. Moreover, hydrodynamics, sediment dynamics and biological development should be measured in the field (R1), such that a holistic validation can be applied using all three elements.

8.3 | Designing Nature Based Flood Defenses

R8 – Stimulating salt marsh growth in natural and artificial marshes

This thesis highlights the relation between salt marsh width and wave attenuating capacity (Chapter 2). However, temporal and spatial variability of the wave attenuating capacity is an inherent result of ecosystem dynamics. When applying salt marshes in Nature Based Flood Defenses, the minimum wave attenuating capacity of a marsh should be known and could be maximized by an increasing salt marsh width. Moreover, in estuaries with little accommodation space it might be convenient to decrease the variability of the ecosystem to secure a certain wave attenuating capacity. To do so, seaward growth of the salt marsh can be stimulated by (small-scale) structures like brushwood dams decreasing the hydrodynamic energy and thereby enhancing vegetation establishment. Traditionally, brushwood dams are shaped in large square sections (Bakker et al., 2002). However, vegetation establishment can also be stimulated by following natural patterns seaward from the marsh edge, e.g. by making a staggered grid of small dams resulting in vegetation patches and drainage channels. This establishing vegetation is able to withstand increasing disturbances with their age (Balke et al., 2011; Hu et al., 2015b). Hence, after the first stages (i.e. years) of vegetation growth are finished, those structures might become redundant. So it is recommended to conduct large-scale field experiments to (1) quantify the period additional structures are necessary, and (2) assess what temporal structures are most efficient and practical to implement.

R9 – Combining intertidal and shallow water ecosystems to maximize wave attenuation

Similar to salt marshes, tidal flats (Reed et al., 2018), mangroves (Horstman et al., 2014), oyster and mussel banks (Borsje et al., 2011), sea grass (Paul and Amos, 2011) and coral reefs (Costa et al., 2016) are able to attenuate waves. Methods used in this thesis can be used to assess the wave attenuating capacity of these other ecosystems as well. However, mostly a combination of these ecosystems are found in the near-coastal zone. So to assess the wave attenuating capacity in the near-coastal zone, it is recommended to consider all ecosystems appearing in this zone. Moreover, by stimulating the expansion of a single ecosystem to enhance the wave attenuating capacity, the extent of adjacent ecosystems might decrease and should be taken into account.

R10 – Assessing the global potential of wave attenuation and other ecosystem services by intertidal ecosystems

The biogeomorphological model in this thesis enables the possibility to quantify the extent of intertidal ecosystems under changing biophysical conditions, to improve their implementation in decision-making processes. Generally ecosystem services are related to the extent of the salt marsh. For example: the primary production of the salt marsh (e.g. Duarte et al., 2013), carbon storage (e.g. Duarte et al., 2005), habitat extent (e.g. Irmler et al., 2002) and the wave attenuating capacity (Vuik et al., 2016) increase with an increasing extent of the salt marsh. The magnitude and variability of the ecosystem service can be quantified using the biogeomorphological model set up in this thesis, through which the value of intertidal ecosystems becomes more tangible. Moreover, the global contribution of intertidal ecosystems to coastal protection, can be assessed by extending knowledge from this thesis. In Chapter 1 national available bathymetrical and hydrodynamical data was combined with rules of thumb for vegetation presence, to calculate the wave attenuating capacity with SWAN (Simulating WAves Nearshore). A similar assessment can be applied worldwide, using datasets of the presence of salt marshes (Mcowen et al., 2017) and mangroves (Giri et al., 2011), hydrodynamics (e.g. Muis et al., 2016; Muis et al., 2017) and bathymetrical data (Weatherall et al., 2015). Once ecosystems are included in Nature Based Flood Defenses, a certain wave attenuating capacity of the ecosystem should be assumed. The salt marsh width should be monitored periodically (with an interval of weeks to months, depending on the temporal variation in hydrodynamic energy) to detect seaward growth, but most importantly landward retreat in an early stage. Online coupling field observations with model environments might contribute in predicting a retreating phase of the ecosystem in an early stage. Moreover, in estuaries with little accommodation space, this might be a prerequisite for adaptive management of Nature Based Flood Defenses.

References

Achete, F. M., van der Wegen, M., Roelvink, D., & Jaffe, B. (2016). Suspended sediment dynamics in a tidal channel network under peak river flow. *Ocean Dynamics, 66*(5), 703-718.10.1007/s10236-016-0944-0.

Adam, P. (2002). Saltmarshes in a time of change. *Environmental Conservation, 29*(1), 39-61.10.1017/S0376892902000048.

Allen, J. R., & Pye, K. (1992). *Saltmarshes: morphodynamics, conservation and engineering significance*: Cambridge University Press.

Allen, J. R. L. (2000). Morphodynamics of Holocene salt marshes: a review sketch from the Atlantic and Southern North Sea coasts of Europe. *Quaternary Science Reviews, 19*(12), 1155-1231.http://dx.doi.org/10.1016/S0277-3791(99)00034-7.

Andersen, T. J. (2001). Seasonal Variation in Erodibility of Two Temperate, Microtidal Mudflats. Estuarine, *Coastal and Shelf Science, 53*(1), 1-12.http://dx.doi.org/10.1006/ecss.2001.0790.

Andersen, T. J., Lund-Hansen, L. C., Pejrup, M., Jensen, K. T., & Mouritsen, K. N. (2005). Biologically induced differences in erodibility and aggregation of subtidal and intertidal sediments: a possible cause for seasonal changes in sediment deposition. *Journal of Marine Systems, 55*(3–4), 123-138.https://doi.org/10.1016/j.jmarsys.2004.09.004.

Andersen, T. J., Pejrup, M., & Nielsen, A. A. (2006). Long-term and high-resolution measurements of bed level changes in a temperate, microtidal coastal lagoon. *Marine Geology, 226*(1), 115-125.http://dx.doi.org/10.1016/j.margeo.2005.09.016.

Anderson, K., Westoby, M. J., & James, M. R. (2019). Low-budget topographic surveying comes of age: Structure from motion photogrammetry in geography and the geosciences. *Progress in Physical Geography: Earth and Environment, 43*(2), 163-173.10.1177/0309133319837454.

Anderson, M. E., & Smith, J. M. (2014). Wave attenuation by flexible, idealized salt marsh vegetation. *Coastal Engineering, 83*, 82-92.https://doi.org/10.1016/j.coastaleng.2013.10.004.

Austen, I., Andersen, T. J., & Edelvang, K. (1999). The Influence of Benthic Diatoms and Invertebrates on the Erodibility of an Intertidal Mudflat, the Danish Wadden Sea. *Estuarine, Coastal and Shelf Science, 49*(1), 99-111.http://dx.doi.org/10.1006/ecss.1998.0491.

Bakker, J. P., Esselink, P., Dijkema, K. S., van Duin, W. E., & de Jong, D. J. (2002). Restoration of salt marshes in the Netherlands. *Hydrobiologia, 478*(1), 29-51.10.1023/a:1021066311728.

Bakker, W. T., & Vrijling, J. K. (1980). Probabilistic Design of Sea Defences. *Coastal Engineering 1980* (pp. 2040-2059).

Balke, T., Bouma, T. J., Horstman, E. M., Webb, E. L., Erftemeijer, P. L. A., & Herman, P. M. J. (2011). Windows of opportunity: thresholds to mangrove seedling establishment on tidal flats. *Mar. Ecol. Prog. Ser., 440*, 1-9.http://dx.doi.org/10.3354/meps09364.

Balke, T., Stock, M., Jensen, K., Bouma, T. J., & Kleyer, M. (2016). A global analysis of the seaward salt marsh extent: The importance of tidal range. *Water Resources Research, 52*(5), 3775-3786.10.1002/2015WR018318.

Balke, T., Webb, E. L., van den Elzen, E., Galli, D., Herman, P. M. J., & Bouma, T. J. (2013). Seedling establishment in a dynamic sedimentary environment: a conceptual framework using mangroves. *Journal of Applied Ecology, 50*(3), 740-747.10.1111/1365-2664.12067.

Baptist, M. J. (2005a). Biogeomorphology. In M. L. Schwartz (Ed.), *Encyclopedia of coastal science*. Dordrecht, The Netherlands: Springer.

Baptist, M. J. (2005b). *Modelling floodplain biogeomorphology*: DUP Science.

Baptist, M. J., Dankers, P., Cleveringa, J., Sittoni, L., Willemsen, P., Elschot, K., . . . Hendriks, M. (2019a). *A large-scale field experiment on salt marsh construction in the Ems estuary, the Netherlands*. Paper presented at the RCEM, Auckland, New Zealand.

Baptist, M. J., Gerkema, T., van Prooijen, B. C., van Maren, D. S., van Regteren, M., Schulz, K., . . . van Puijenbroek, M. E. B. (2019b). Beneficial use of dredged sediment to enhance salt marsh development by applying a 'Mud Motor'. *Ecological Engineering, 127*, 312-323.https://doi.org/10.1016/j.ecoleng.2018.11.019.

Baptist, M. J., Penning, W. E., Duel, H., Smits, A. J. M., Geerling, G. W., Van der Lee, G. E. M., & Van Alphen, J. S. L. (2004). Assessment of the effects of cyclic floodplain rejuvenation on flood levels and biodiversity along the Rhine River. *River Research and Applications, 20*(3), 285-297.10.1002/rra.778.

Barbier, E. B., Hacker, S. D., Kennedy, C., Koch, E. W., Stier, A. C., & Silliman, B. R. (2010). The value of estuarine and coastal ecosystem services. *Ecological Monographs, 81*(2), 169-193.10.1890/10-1510.1.

Barbier, E. B., Koch, E. W., Silliman, B. R., Hacker, S. D., Wolanski, E., Primavera, J., ... Cramer, L. A. (2008). Coastal ecosystem-based management with nonlinear ecological functions and values. *science, 319*(5861), 321-323.

Bearman, J. A., Friedrichs, C. T., Jaffe, B. E., & Foxgrover, A. C. (2010). Spatial Trends in Tidal Flat Shape and Associated Environmental Parameters in South San Francisco Bay. *Journal of coastal Research, 26*(2), 342-349, 348.

Belliard, J.-P., Toffolon, M., Carniello, L., & D'Alpaos, A. (2015). An ecogeomorphic model of tidal channel initiation and elaboration in progressive marsh accretional contexts. *Journal of Geophysical Research: Earth Surface, 120*(6), 1040-1064.10.1002/2015jf003445.

Bendoni, M., Mel, R., Solari, L., Lanzoni, S., Francalanci, S., & Oumeraci, H. (2016). Insights into lateral marsh retreat mechanism through localized field measurements. *Water Resources Research, 52*(2), 1446-1464.10.1002/2015wr017966.

Berends, K. D., Scheel, F., Warmink, J. J., de Boer, W. P., Ranasinghe, R., & Hulscher, S. J. M. H. (2019). Towards efficient uncertainty quantification with high-resolution morphodynamic models: A multifidelity approach applied to channel sedimentation. *Coastal Engineering, 152*, 103520.https://doi.org/10.1016/j.coastaleng.2019.103520.

Best, Ü. S. N., Van der Wegen, M., Dijkstra, J., Willemsen, P. W. J. M., Borsje, B. W., & Roelvink, D. J. A. (2018). Do salt marshes survive sea level rise? Modelling wave action, morphodynamics and vegetation dynamics. *Environmental Modelling & Software, 109*, 152-166.https://doi.org/10.1016/j.envsoft.2018.08.004.

Bomers, A., Schielen, R. M. J., & Hulscher, S. J. M. H. (2019a). Application of a lower-fidelity surrogate hydraulic model for historic flood reconstruction. *Environmental Modelling & Software, 117*, 223-236.https://doi.org/10.1016/j.envsoft.2019.03.019.

Bomers, A., Schielen, R. M. J., & Hulscher, S. J. M. H. (2019b). The influence of grid shape and grid size on hydraulic river modelling performance. *Environmental Fluid Mechanics*.10.1007/s10652-019-09670-4.

Bomers, A., van der Meulen, B., Schielen, R. M. J., & Hulscher, S. J. M. H. (2019c). Historic Flood Reconstruction With the Use of an Artificial Neural Network. *Water Resources Research, 55*(11), 9673-9688.10.1029/2019wr025656.

Booij, N., Ris, R. C., & Holthuijsen, L. H. (1999). A third-generation wave model for coastal regions: 1. Model description and validation. *Journal of Geophysical Research: Oceans, 104*(C4), 7649-7666.10.1029/98JC02622.

Borsje, B. W. (2012). *Biogeomorphology of coastal seas.* (PhD thesis).

Borsje, B. W., de Vries, M. B., Bouma, T. J., Besio, G., Hulscher, S. J. M. H., & Herman, P. M. J. (2009). Modeling bio-geomorphological influences for offshore sandwaves. *Continental Shelf Research, 29*(9), 1289-1301.https://doi.org/10.1016/j.csr.2009.02.008.

Borsje, B. W., van Wesenbeeck, B. K., Dekker, F., Paalvast, P., Bouma, T. J., van Katwijk, M. M., & de Vries, M. B. (2011). How ecological engineering can serve in coastal protection. *Ecological Engineering, 37*(2), 113-122.http://dx.doi.org/10.1016/j.ecoleng.2010.11.027.

Bouma, T. J., De Vries, M. B., Low, E., Peralta, G., Tánczos, I. C., van de Koppel, J., & Herman, P. M. J. (2005). Trade-offs related to ecosystem engineering: a case study on stiffness of emerging macrophytes. *Ecology, 86*(8), 2187-2199.doi:10.1890/04-1588.

Bouma, T. J., van Belzen, J., Balke, T., van Dalen, J., Klaassen, P., Hartog, A. M., . . . Herman, P. M. J. (2016). Short-term mudflat dynamics drive long-term cyclic salt marsh dynamics. *Limnology and Oceanography, 61*(6), 2261-2275.10.1002/lno.10374.

Bouma, T. J., van Belzen, J., Balke, T., Zhu, Z., Airoldi, L., Blight, A. J., . . . Herman, P. M. J. (2014). Identifying knowledge gaps hampering application of intertidal habitats in coastal protection: Opportunities & steps to take. *Coastal Engineering, 87*, 147-157.http://dx.doi.org/10.1016/j.coastaleng.2013.11.014.

Bouma, T. J., van Duren, L. A., Temmerman, S., Claverie, T., Blanco-Garcia, A., Ysebaert, T., & Herman, P. M. J. (2007). Spatial flow and sedimentation patterns within patches of epibenthic structures: Combining field, flume and modelling experiments. *Continental Shelf Research, 27*(8), 1020-1045.http://dx.doi.org/10.1016/j.csr.2005.12.019.

Bouma, T. J., Vries, M. B. D., & Herman, P. M. J. (2010). Comparing ecosystem engineering efficiency of two plant species with contrasting growth strategies. *Ecology, 91*(9), 2696-2704.10.1890/09-0690.1.

Braat, L., van Dijk, W., Pierik, H. J., van de Lageweg, W., Bruckner, M., Wagner-Cremer, F., & Kleinhans, M. G. (2019). Tidal bar accretion by mudflat sedimentation.

Bretschneider, C., Krock, H., Nakazaki, E., & Casciano, F. (1986). *Roughness of typical Hawaiian terrain for tsunami run-up calculations: A users manual*, JKK Look Lab. Rep (Report).

Broekx, S., Smets, S., Liekens, I., Bulckaen, D., & De Nocker, L. (2011). Designing a long-term flood risk management plan for the Scheldt estuary using a risk-based approach. *Natural Hazards, 57*(2), 245-266.10.1007/s11069-010-9610-x.

Brooks, H., Möller, I., Carr, S., Chirol, C., Christie, E., Evans, B., . . . Royse, K. (2020). Resistance of salt marsh substrates to near-instantaneous hydrodynamic forcing. *Earth Surface Processes and Landforms*.10.1002/esp.4912.

Callaghan, D. P., Bouma, T. J., Klaassen, P., van der Wal, D., Stive, M. J. F., & Herman, P. M. J. (2010). Hydrodynamic forcing on salt-marsh development: Distinguishing the relative importance of waves and tidal flows. *Estuarine, Coastal and Shelf Science, 89*(1), 73-88.http://dx.doi.org/10.1016/j.ecss.2010.05.013.

Campbell, A. D., & Wang, Y. (2020). Salt marsh monitoring along the mid-Atlantic coast by Google Earth Engine enabled time series. *PLoS ONE, 15*(2), e0229605.10.1371/journal.pone.0229605.

Cao, H., Zhu, Z., Balke, T., Zhang, L., & Bouma, T. J. (2018). Effects of sediment disturbance regimes on Spartina seedling establishment: Implications for salt marsh creation and restoration. *Limnology and Oceanography, 63*(2), 647-659.10.1002/lno.10657.

Cao, H., Zhu, Z., Herman, P. M. J., Zhang, L. Q., Yuan, L., & Bouma, T. J. (In preparation). Species-specific clonal expansion traits of pioneer marsh plants in response to geomorphic constrains.

Cao, H., Zhu, Z., James, R., Herman, P. M. J., Zhang, L., Yuan, L., & Bouma, T. J. (2019). Wave effects on seedling establishment of three pioneer marsh species: survival, morphology and biomechanics. *Annals of Botany, 125*(2), 345-352.10.1093/aob/mcz136.

Chapple, D., & Dronova, I. (2017). Vegetation Development in a Tidal Marsh Restoration Project during a Historic Drought: A Remote Sensing Approach. *Frontiers in Marine Science, 4*(243).10.3389/fmars.2017.00243.

Chen, Y., Thompson, C. E. L., & Collins, M. B. (2012). Saltmarsh creek bank stability: Biostabilisation and consolidation with depth. *Continental Shelf Research, 35*, 64-74. https://doi.org/10.1016/j.csr.2011.12.009.

Cheong, S.-M., Silliman, B., Wong, P. P., van Wesenbeeck, B., Kim, C.-K., & Guannel, G. (2013). Coastal adaptation with ecological engineering. Nature Clim. *Change, 3*(9), 787-791.10.1038/nclimate1854.

Chmura, G. L., Anisfeld, S. C., Cahoon, D. R., & Lynch, J. C. (2003). Global carbon sequestration in tidal, saline wetland soils. *Global Biogeochemical Cycles, 17*(4).10.1029/2002GB001917.

Coops, H., Geilen, N., Verheij, H. J., Boeters, R., & van der Velde, G. (1996). Interactions between waves, bank erosion and emergent vegetation: an experimental study in a wave tank. *Aquatic Botany, 53*(3), 187-198.https://doi.org/10.1016/0304-3770(96)01027-3.

Corenblit, D., Baas, A. C. W., Bornette, G., Darrozes, J., Delmotte, S., Francis, R. A., ... Steiger, J. (2011). Feedbacks between geomorphology and biota controlling Earth surface processes and landforms: A review of foundation concepts and current understandings. *Earth-Science Reviews, 106*(3–4), 307-331.http://dx.doi.org/10.1016/j.earscirev.2011.03.002.

Corenblit, D., Gurnell, A. M., Steiger, J., & Tabacchi, E. (2008). Reciprocal adjustments between landforms and living organisms: Extended geomorphic evolutionary insights. *CATENA, 73*(3), 261-273.https://doi.org/10.1016/j.catena.2007.11.002.

Costa, M. B., Araújo, M., Araújo, T. C., & Siegle, E. (2016). Influence of reef geometry on wave attenuation on a Brazilian coral reef. *Geomorphology, 253*, 318-327.

Costanza, R., d'Arge, R., Groot, R. d., Farber, S., Grasso, M., Hannon, B., ... Paruelo, J. (1998). The value of the world's ecosystem services and natural capital.

Cox, R., Wadsworth, R. A., & Thomson, A. G. (2003). Long-term changes in salt marsh extent affected by channel deepening in a modified estuary. *Continental Shelf Research, 23*(17), 1833-1846.http://dx.doi.org/10.1016/j.csr.2003.08.002.

Crooks, S., Herr, D., Tamelander, J., Laffoley, D., & Vandever, J. (2011). Mitigating climate change through restoration and management of coastal wetlands and near-shore marine ecosystems: challenges and opportunities.

D'Alpaos, A., Lanzoni, S., Marani, M., & Rinaldo, A. (2007). Landscape evolution in tidal embayments: Modeling the interplay of erosion, sedimentation, and vegetation dynamics. *Journal of Geophysical Research: Earth Surface, 112*(F1). doi:10.1029/2006JF000537.

D'Alpaos, A., & Marani, M. (2016). Reading the signatures of biologic–geomorphic feedbacks in salt-marsh landscapes. *Advances in Water Resources, 93*, 265-275. https://doi.org/10.1016/j.advwatres.2015.09.004.

Dahdouh-Guebas, F., Mathenge, C., Kairo, J. G., & Koedam, N. (2000). Utilization of mangrove wood products around mida creek (Kenya) amongst subsistence and commercial users. *Economic Botany, 54*(4), 513-527.10.1007/bf02866549.

Damme, S. V., Struyf, E., Maris, T., Ysebaert, T., Dehairs, F., Tackx, M., . . . Meire, P. (2005). Spatial and temporal patterns of water quality along the estuarine salinity gradient of the Scheldt estuary (Belgium and The Netherlands): results of an integrated monitoring approach. *Hydrobiologia, 540*(1), 29-45.10.1007/s10750-004-7102-2.

Damveld, J. H., Borsje, B. W., Roos, P. C., & Hulscher, S. J. M. H. (2020). Biogeomorphology in the marine landscape: Modelling the feedbacks between patches of the polychaete worm Lanice conchilega and tidal sand waves. *Earth Surface Processes and Landforms*(45), 2572– 2587.10.1002/esp.4914.

Danish Hydraulic Institute. (2016). *MIKE 21 & MIKE 3 Flow Model FM Hydrodynamic Module: Short description* (Report).

Darwin, C. (1892). *The formation of vegetable mould through the action of worms: with observations on their habits* (Vol. 37): Appleton.

Day Jr, J. W., Scarton, F., Rismondo, A., & Are, D. (1998). Rapid deterioration of a salt marsh in Venice Lagoon, Italy. *Journal of coastal Research*, 583-590.

Day, J. W., Psuty, N. P., & Perez, B. C. (2000). The Role of Pulsing Events in the Functioning of Coastal Barriers and Wetlands: Implications for Human Impact, Management and the Response to Sea Level Rise. In M. P. Weinstein & D. A. Kreeger (Eds.), *Concepts and Controversies in Tidal Marsh Ecology* (pp. 633-659). Dordrecht: Springer Netherlands.

De Groot, R., Brander, L., van der Ploeg, S., Costanza, R., Bernard, F., Braat, L., . . . van Beukering, P. (2012). Global estimates of the value of ecosystems and their services in monetary units. *Ecosystem Services, 1*(1), 50-61.http://dx.doi.org/10.1016/j.ecoser.2012.07.005.

De Kruif, A. C. (2001). *Bodemdieptegegevens van het Nederlandse Kustsysteem. Beschikbare digitale data en een overzicht van aanvullende analoge data* (Report).

de Vet, P. L. M., van Prooijen, B. C., Colosimo, I., Ysebaert, T., Herman, P. M. J., & Wang, Z. B. (2020). Sediment Disposals in Estuarine Channels Alter the Eco-Morphology of Intertidal Flats. *Journal of Geophysical Research: Earth Surface, 125*(2), e2019JF005432.10.1029/2019jf005432.

de Vriend, H. J., van Koningsveld, M., Aarninkhof, S. G. J., de Vries, M. B., & Baptist, M. J. (2015). Sustainable hydraulic engineering through building with nature. *Journal of Hydro-environment Research, 9*(2), 159-171.https://doi.org/10.1016/j.jher.2014.06.004.

Deegan, L. A., Johnson, D. S., Warren, R. S., Peterson, B. J., Fleeger, J. W., Fagherazzi, S., & Wollheim, W. M. (2012). Coastal eutrophication as a driver of salt marsh loss. *Nature, 490*, 388.10.1038/nature11533.

Deltares. (2015). *User manual DELFT3D-FLOW* (Report).

Deltares. (2019a). *D-Flow Flexible Mesh User Manual* (Report).

Deltares. (2019b). D-Morphology User Manual.

Deltares. (2019c). *D-Waves User Manual* (Report).

Dijkema, K. s., van Duin, W. E., Nicolai, A., Frankes, J., Jongerius, H., Keegstra, H., & Swierstra, J. (2009). *Monitoring en beheer van de kwelderwerken in Friesland en Groningen 1960-2007* (Report).

Donnelly, J. P., Cleary, P., Newby, P., & Ettinger, R. (2004). Coupling instrumental and geological records of sea-level change: Evidence from southern New England of an increase in the rate of sea-level rise in the late 19th century. *Geophysical Research Letters, 31*(5).10.1029/2003GL018933.

Doody, J. P. (2004). 'Coastal squeeze'— an historical perspective. *Journal of Coastal Conservation, 10*(1), 129-138.http://dx.doi.org/10.1652/1400-0350(2004)010[0129:CSAHP]2.0.CO;2.

Doody, J. P. (2007). *Saltmarsh conservation, management and restoration* (Vol. 12): Springer Science & Business Media.

Doody, J. P. (2013). Coastal squeeze and managed realignment in southeast England, does it tell us anything about the future? *Ocean & Coastal Management, 79*, 34-41. http://dx.doi.org/10.1016/j.ocecoaman.2012.05.008.

Duarte, C. M., Dennison, W. C., Orth, R. J. W., & Carruthers, T. J. B. (2008). The Charisma of Coastal Ecosystems: Addressing the Imbalance. *Estuaries and Coasts, 31*(2), 233-238.10.1007/s12237-008-9038-7.

Duarte, C. M., Losada, I. J., Hendriks, I. E., Mazarrasa, I., & Marbà, N. (2013). The role of coastal plant communities for climate change mitigation and adaptation. *Nature Climate Change, 3*, 961.10.1038/nclimate1970.

Duarte, C. M., Middelburg, J. J., & Caraco, N. (2005). Major role of marine vegetation on the oceanic carbon cycle. *Biogeosciences, 2*(1), 1-8.10.5194/bg-2-1-2005.

Emanuel, K. (2005). Increasing destructiveness of tropical cyclones over the past 30 years. *Nature, 436*(7051), 686-688.10.1038/nature03906.

EurOtop, I. (2016). *Manual on wave overtopping of sea defences and related structures: An overtopping manual largely based on European research, but for worldwide application* (Report).

Fagherazzi, S. (2014). Coastal processes: Storm-proofing with marshes. *Nature Geosci, 7*(10), 701-702.10.1038/ngeo2262.

Fagherazzi, S., & Furbish, D. J. (2001). On the shape and widening of salt marsh creeks. *Journal of Geophysical Research: Oceans, 106*(C1), 991-1003.10.1029/1999jc000115.

Fagherazzi, S., Kirwan, M. L., Mudd, S. M., Guntenspergen, G. R., Temmerman, S., D'Alpaos, A., . . . Clough, J. (2012). Numerical models of salt marsh evolution: Ecological, geomorphic, and climatic factors. *Reviews of Geophysics, 50*(1).10.1029/2011rg000359.

Fagherazzi, S., Mariotti, G., Wiberg, P. L., & McGlathery, K. J. (2013). Marsh Collapse Does Not Require Sea Level Rise. *Oceanography, 26*(3), 70-77.

Folmer, E., Dekinga, A., Holthuijsen, S., Van der Meer, J., Mosk, D., Piersma, T., & van der Veer, H. (2017). *Species distribution models intertidal benthos: tools for assessing e impact of physical and morphological drivers o benthos and birds in the Wadden Sea* (Report).

Ford, H., Garbutt, A., Ladd, C., Malarkey, J., & Skov, M. W. (2016). Soil stabilization linked to plant diversity and environmental context in coastal wetlands. *Journal of Vegetation Science, 27*(2), 259-268.10.1111/jvs.12367.

Francalanci, S., Bendoni, M., Rinaldi, M., & Solari, L. (2013). Ecomorphodynamic evolution of salt marshes: Experimental observations of bank retreat processes. *Geomorphology, 195*, 53-65.https://doi.org/10.1016/j.geomorph.2013.04.026.

Freeman, A. M., Jose, F., Roberts, H. H., & Stone, G. W. (2015). Storm induced hydrodynamics and sediment transport in a coastal Louisiana lake. *Estuarine, Coastal and Shelf Science, 161*, 65-75.https://doi.org/10.1016/j.ecss.2015.04.011.

French, M. N., Krajewski, W. F., & Cuykendall, R. R. (1992). Rainfall forecasting in space and time using a neural network. *Journal of Hydrology, 137*(1), 1-31.https://doi.org/10.1016/0022-1694(92)90046-X.

Friedrichs, C. T. (2011). 3.06 - Tidal Flat Morphodynamics: A Synthesis *Treatise on Estuarine and Coastal Science* (pp. 137-170). Waltham: Academic Press.

Friedrichs, C. T., Cartwright, G. M., & Dickhudt, P. J. (2008). Quantifying benthic exchange of fine sediment via continuous, noninvasive measurements of settling velocity and bed erodibility. *Oceanography, 21*(4), 168-172.

Friess, D. A., Krauss, K. W., Horstman, E. M., Balke, T., Bouma, T. J., Galli, D., & Webb, E. L. (2012). Are all intertidal wetlands naturally created equal? Bottlenecks, thresholds and knowledge gaps to mangrove and saltmarsh ecosystems. *Biological reviews, 87*, 346-366.http://dx.doi.org/10.1111/j.1469-185X.2011.00198.x.

Gautier, C., & Groeneweg, J. (2012). *Achtergrondrapportage hydraulische belasting voor zee en estuaria* (Report).

Gedan, K. B., Kirwan, M. L., Wolanski, E., Barbier, E. B., & Silliman, B. R. (2011). The present and future role of coastal wetland vegetation in protecting shorelines: answering recent challenges to the paradigm. *Climatic Change, 106*(1), 7-29.10.1007/s10584-010-0003-7.

Gedan, K. B., Silliman, B. R., & Bertness, M. D. (2009). Centuries of Human-Driven Change in Salt Marsh Ecosystems. *Annual Review of Marine Science, 1*(1), 117-141.10.1146/annurev.marine.010908.163930.

Gersonius, B., Ashley, R., Pathirana, A., & Zevenbergen, C. (2013). Climate change uncertainty: building flexibility into water and flood risk infrastructure. *Climatic Change, 116*(2), 411-423.10.1007/s10584-012-0494-5.

Giri, C., Ochieng, E., Tieszen, L. L., Zhu, Z., Singh, A., Loveland, T., . . . Duke, N. (2011). Status and distribution of mangrove forests of the world using earth observation satellite data. *Global Ecology and Biogeography, 20*(1), 154-159.10.1111/j.1466-8238.2010.00584.x.

Grabowski, R. C., Droppo, I. G., & Wharton, G. (2011). Erodibility of cohesive sediment: The importance of sediment properties. *Earth-Science Reviews, 105*(3), 101-120. https://doi.org/10.1016/j.earscirev.2011.01.008.

Green, M. O., & Coco, G. (2014). Review of wave-driven sediment resuspension and transport in estuaries. *Reviews of Geophysics, 52*(1), 77-117.10.1002/2013RG000437.

Groeneweg, J., & Van Nieuwkoop, J. (2015). SWAN's underestimation of long wave penetration into coastal systems.

Harmsworth, G. C., & Long, S. P. (1986). An assessment of saltmarsh erosion in Essex, England, with reference to the Dengie Peninsula. *Biological Conservation, 35*(4), 377-387.https://doi.org/10.1016/0006-3207(86)90095-9.

Hinde, H. P. (1954). The Vertical Distribution of Salt Marsh Phanerogams in Relation to Tide Levels. *Ecological Monographs, 24*(2), 209-225.doi:10.2307/1948621.

Horstman, E. M., Dohmen-Janssen, C. M., Bouma, T. J., & Hulscher, S. J. M. H. (2015). Tidal-scale flow routing and sedimentation in mangrove forests: Combining field data and numerical modelling. *Geomorphology, 228*(0), 244-262.http://dx.doi.org/10.1016/j.geomorph.2014.08.011.

Horstman, E. M., Dohmen-Janssen, C. M., Narra, P. M. F., van den Berg, N. J. F., Siemerink, M., & Hulscher, S. J. M. H. (2014). Wave attenuation in mangroves: A quantitative approach to field observations. *Coastal Engineering, 94*, 47-62.http://dx.doi.org/10.1016/j.coastaleng.2014.08.005.

Houser, C. (2010). Relative Importance of Vessel-Generated and Wind Waves to Salt Marsh Erosion in a Restricted Fetch Environment. *Journal of coastal Research, 26*(2 (262)), 230-240.10.2112/08-1084.1.

Hu, Z., Lenting, W., van der Wal, D., & Bouma, T. J. (2015a). Continuous monitoring bed-level dynamics on an intertidal flat: Introducing novel, stand-alone high-resolution SED-sensors. *Geomorphology, 245*, 223-230.http://dx.doi.org/10.1016/j.geomorph.2015.05.027.

Hu, Z., van Belzen, J., van der Wal, D., Balke, T., Wang, Z. B., Stive, M., & Bouma, T. J. (2015b). Windows of opportunity for salt marsh vegetation establishment on bare tidal flats: The importance of temporal and spatial variability in hydrodynamic forcing. *Journal of Geophysical Research: Biogeosciences, 120*(7), 1450-1469.10.1002/2014JG002870.

Hu, Z., Wang, Z. B., Zitman, T. J., Stive, M. J. F., & Bouma, T. J. (2015c). Predicting long-term and short-term tidal flat morphodynamics using a dynamic equilibrium theory. *Journal of Geophysical Research: Earth Surface, 120*(9), 1803-1823.10.1002/2015JF003486.

Hu, Z., Willemsen, P. W. J. M., Borsje, B. W., Wang, C., Wang, H., van der Wal, D.,... Bouma, T. J. (2020a). High resolution bed level change and synchronized biophysical data from 10 tidal flats in northwestern Europe. *Earth Syst. Sci. Data Discuss., 2020*, 1-19.10.5194/essd-2020-78.

Hu, Z., Yao, P., van der Wal, D., & Bouma, T. J. (2017). Patterns and drivers of daily bed-level dynamics on two tidal flats with contrasting wave exposure. *Scientific Reports, 7*(1), 7088.10.1038/s41598-017-07515-y.

Hu, Z., Zhou, J., Wang, C., Wang, H., He, Z., Peng, Y., . . . Bouma, T. J. (2020b). A Novel Instrument for Bed Dynamics Observation Supports Machine Learning Applications in Mangrove Biogeomorphic Processes. *Water Resources Research*, e2020WR027257. 10.1029/2020wr027257.

Hughes, A. L. H., Wilson, A. M., & Morris, J. T. (2012). Hydrologic variability in a salt marsh: Assessing the links between drought and acute marsh dieback. *Estuarine, Coastal and Shelf Science, 111*, 95-106.https://doi.org/10.1016/j.ecss.2012.06.016.

Hunt, S., Bryan, K. R., & Mullarney, J. C. (2015). The influence of wind and waves on the existence of stable intertidal morphology in meso-tidal estuaries. *Geomorphology, 228*, 158-174.https://doi.org/10.1016/j.geomorph.2014.09.001.

IPCC. (2014). *Climate Change 2014: Synthesis Report. Contribution of Working Groups I, II and III to the Fifth Assessment Report of the Intergovernmental Panel on Climate Change* (Report).

Irmler, U., Heller, K., Meyer, H., & Reinke, H.-D. (2002). Zonation of ground beetles (Coleoptera: Carabidae) and spiders (Araneida) in salt marshes at the North and the Baltic Sea and the impact of the predicted sea level increase. *Biodiversity & Conservation, 11*(7), 1129-1147.10.1023/A:1016018021533.

Janssen, S., Van Tatenhove, J. P. M., Otter, H., & Mol, A. (2014). Greening Flood Protection—An Interactive Knowledge Arrangement Perspective. *Journal of Environmental Policy and Planning*.10.1080/1523908X.2014.947921.

Kabat, P., Fresco, L. O., Stive, M. J. F., Veerman, C. P., van Alphen, J. S. L. J., Parmet, B. W. A. H., ... Katsman, C. A. (2009). Dutch coasts in transition. *Nature Geoscience, 2*(7), 450-452.10.1038/nge0572.

Kernkamp, H. W. J., Van Dam, A., Stelling, G. S., & de Goede, E. D. (2011). Efficient scheme for the shallow water equations on unstructured grids with application to the Continental Shelf. *Ocean Dynamics, 61*(8), 1175-1188.10.1007/s10236-011-0423-6.

King, S. E., & Lester, J. N. (1995). The value of salt marsh as a sea defence. *Marine Pollution Bulletin, 30*(3), 180-189.https://doi.org/10.1016/0025-326X(94)00173-7.

Kirby, R. (2000). Practical implications of tidal flat shape. *Continental Shelf Research, 20*(10–11), 1061-1077.http://dx.doi.org/10.1016/S0278-4343(00)00012-1.

Kirwan, M. L., Guntenspergen, G. R., D'Alpaos, A., Morris, J. T., Mudd, S. M., & Temmerman, S. (2010). Limits on the adaptability of coastal marshes to rising sea level. *Geophysical Research Letters, 37*(23).10.1029/2010GL045489.

Kirwan, M. L., & Megonigal, P. (2013). Tidal wetland stability in the face of human impacts and sea-level rise. *Nature, 504*, 53-60.http://dx.doi.org/10.1038/nature12856.

Kirwan, M. L., & Murray, A. B. (2007). A coupled geomorphic and ecological model of tidal marsh evolution. *Proceedings of the National Academy of Sciences, 104*(15), 6118-6122.10.1073/pnas.0700958104.

Kirwan, M. L., Temmerman, S., Skeehan, E. E., Guntenspergen, G. R., & Fagherazzi, S. (2016). Overestimation of marsh vulnerability to sea level rise. *Nature Clim. Change, 6*(3), 253-260.http://dx.doi.org/10.1038/nclimate2909.

Knutson, P. L., Brochu, R. A., Seelig, W. N., & Inskeep, M. (1982). Wave damping inSpartinaalterniflora marshes. *Wetlands, 2*(1), 87-104.10.1007/BF03160548.

Knutson, T. R., McBride, J. L., Chan, J., Emanuel, K., Holland, G., Landsea, C., . . . Sugi, M. (2010). Tropical cyclones and climate change. *Nature Geoscience, 3*(3), 157-163.10.1038/nge0779.

Kogut, T., & Weistock, M. (2019). Classifying airborne bathymetry data using the Random Forest algorithm. *Remote Sensing Letters, 10*(9), 874-882.10.1080/2150704X.2019.1629710.

Kolker, A. S., Goodbred, S. L., Hameed, S., & Cochran, J. K. (2009). High-resolution records of the response of coastal wetland systems to long-term and short-term sea-level variability. *Estuarine, Coastal and Shelf Science, 84*(4), 493-508.https://doi.org/10.1016/j.ecss.2009.06.030.

Ladd, C. J. T., Duggan-Edwards, M. F., Bouma, T. J., Pagès, J. F., & Skov, M. W. (2019). Sediment Supply Explains Long-Term and Large-Scale Patterns in Salt Marsh Lateral Expansion and Erosion. *Geophysical Research Letters, 46*(20), 11178-11187.10.1029/2019gl083315.

Le Hir, P., Monbet, Y., & Orvain, F. (2007). Sediment erodability in sediment transport modelling: Can we account for biota effects? *Continental Shelf Research, 27*(8), 1116-1142.http://dx.doi.org/10.1016/j.csr.2005.11.016.

Leckebusch, G. C., & Ulbrich, U. (2004). On the relationship between cyclones and extreme windstorm events over Europe under climate change. *Global and Planetary Change, 44*(1), 181-193.https://doi.org/10.1016/j.gloplacha.2004.06.011.

Lesser, G. R., Roelvink, J. A., van Kester, J. A. T. M., & Stelling, G. S. (2004). Development and validation of a three-dimensional morphological model. *Coastal Engineering, 51*(8–9), 883-915.http://dx.doi.org/10.1016/j.coastaleng.2004.07.014.

Lin, N., Emanuel, K., Oppenheimer, M., & Vanmarcke, E. (2012). Physically based assessment of hurricane surge threat under climate change. *Nature Climate Change, 2*, 462.10.1038/nclimate1389.

Marani, M., D'Alpaos, A., Lanzoni, S., & Santalucia, M. (2011). Understanding and predicting wave erosion of marsh edges. *Geophysical Research Letters, 38*(21).10.1029/2011gl048995.

Marijs, K., & Parée, E. (2004). *Nauwkeurigheid vaklodingen Westerschelde en monding: "de praktijk"* (Report).

Mariotti, G., & Canestrelli, A. (2017). Long-term morphodynamics of muddy backbarrier basins: Fill in or empty out? *Water Resources Research, 53*(8), 7029-7054.10.1002/2017wr020461.

Mariotti, G., & Carr, J. (2014). Dual role of salt marsh retreat: Long-term loss and short-term resilience. *Water Resources Research, 50*(4), 2963-2974.10.1002/2013wr014676.

Mariotti, G., & Fagherazzi, S. (2010). A numerical model for the coupled long-term evolution of salt marshes and tidal flats. *Journal of Geophysical Research: Earth Surface, 115*(F1).10.1029/2009JF001326.

Mariotti, G., & Fagherazzi, S. (2013). Critical width of tidal flats triggers marsh collapse in the absence of sea-level rise. *Proceedings of the National Academy of Sciences, 110*(14), 5353.10.1073/pnas.1219600110.

Maris, T., Cox, T., Temmerman, S., De Vleeschauwer, P., Van Damme, S., De Mulder, T.,... Meire, P. (2007). Tuning the tide: creating ecological conditions for tidal marsh development in a flood control area. *Hydrobiologia, 588*(1), 31-43.

Maza, M., Lara, J. L., Losada, I. J., Ondiviela, B., Trinogga, J., & Bouma, T. J. (2015). Large-scale 3-D experiments of wave and current interaction with real vegetation. Part 2: Experimental analysis. *Coastal Engineering, 106*, 73-86.https://doi.org/10.1016/j.coastaleng.2015.09.010.

Mazda, Y., Magi, M., Kogo, M., & Hong, P. (1997). Mangroves as a coastal protection from waves in the Tong King delta, Vietnam. *Mangroves and Salt Marshes, 1*(2), 127-135.10.1023/A:1009928003700.

Mazik, K., Smith, J. E., Leighton, A., & Elliott, M. (2007). Physical and biological development of a newly breached managed realignment site, Humber estuary, UK. *Marine Pollution Bulletin, 55*(10), 564-578.https://doi.org/10.1016/j.marpolbul.2007.09.017.

McKee, K. L., & Patrick, W. H. (1988). The relationship of smooth cordgrass (Spartina alterniflora) to tidal datums: A review. *Estuaries, 11*(3), 143-151.10.2307/1351966.

McLoughlin, S. M., Wiberg, P. L., Safak, I., & McGlathery, K. J. (2015). Rates and Forcing of Marsh Edge Erosion in a Shallow Coastal Bay. *Estuaries and Coasts, 38*(2), 620-638.10.1007/s12237-014-9841-2.

Mcowen, C. J., Weatherdon, L. V., Bochove, J.-W. V., Sullivan, E., Blyth, S., Zockler, C., ... Fletcher, S. (2017). A global map of saltmarshes. *Biodiversity Data Journa*l, 5.10.3897/BDJ.5.e11764.

Méndez, F. J., & Losada, I. J. (2004). An empirical model to estimate the propagation of random breaking and nonbreaking waves over vegetation fields. *Coastal Engineering, 51*(2), 103-118.https://doi.org/10.1016/j.coastaleng.2003.11.003.

Möller, I. (2006). Quantifying saltmarsh vegetation and its effect on wave height dissipation: Results from a UK East coast saltmarsh. *Estuarine, Coastal and Shelf Science, 69*(3), 337-351.http://dx.doi.org/10.1016/j.ecss.2006.05.003.

Möller, I., Kudella, M., Rupprecht, F., Spencer, T., Paul, M., van Wesenbeeck, B. K., . . . Schimmels, S. (2014). Wave attenuation over coastal salt marshes under storm surge conditions. *Nature Geosci, 7*(10), 727-731.10.1038/ngeo2251.

Möller, I., & Spencer, T. (2002). Wave dissipation over macro-tidal saltmarshes: Effects of marsh edge typology and vegetation change. *Journal of coastal Research*, 506-521.10.2112/1551-5036-36.sp1.506.

Morris, J. T., Porter, D., Neet, M., Noble, P. A., Schmidt, L., Lapine, L. A., & Jensen, J. R. (2005). Integrating LIDAR elevation data, multi-spectral imagery and neural network modelling for marsh characterization. *International Journal of Remote Sensing, 26*(23), 5221-5234.10.1080/01431160500219018.

Morris, J. T., Sundareshwar, P. V., Nietch, C. T., Kjerfve, B., & Cahoon, D. R. (2002). Responses of coastal wetlands to rising sea level. *Ecology, 83*(10), 2869-2877.http://dx.doi.org/10.1890/0012-9658(2002)083[2869:ROCWTR]2.0.CO;2.

Muis, S., Verlaan, M., Nicholls, R. J., Brown, S., Hinkel, J., Lincke, D., . . . Ward, P. J. (2017). A comparison of two global datasets of extreme sea levels and resulting flood exposure. *Earth's Future, 5*(4), 379-392.10.1002/2016ef000430.

Muis, S., Verlaan, M., Winsemius, H. C., Aerts, J. C. J. H., & Ward, P. J. (2016). A global reanalysis of storm surges and extreme sea levels. *Nature Communications, 7*, 11969.10.1038/ncomms11969.

Murray, A. B., Knaapen, M. A. F., Tal, M., & Kirwan, M. L. (2008). Biomorphodynamics: Physical-biological feedbacks that shape landscapes. *Water Resources Research, 44*(11).10.1029/2007WR006410.

Narayan, S., Beck, M. W., Wilson, P., Thomas, C. J., Guerrero, A., Shepard, C. C., . . . Trespalacios, D. (2017). The Value of Coastal Wetlands for Flood Damage Reduction in the Northeastern USA. *Scientific Reports, 7*(1), 9463.10.1038/s41598-017-09269-z.

Nelder, J. A. (1961). The Fitting of a Generalization of the Logistic Curve. *Biometrics, 17*(1), 89-110.10.2307/2527498.

Nelson, J. L., & Zavaleta, E. S. (2012). Salt Marsh as a Coastal Filter for the Oceans: Changes in Function with Experimental Increases in Nitrogen Loading and Sea-Level Rise. *PLoS ONE, 7*(8), e38558.10.1371/journal.pone.0038558.

Nepf, H. M. (1999). Drag, turbulence, and diffusion in flow through emergent vegetation. *Water Resources Research, 35*(2), 479-489.10.1029/1998WR900069.

Neumann, B., Vafeidis, A. T., Zimmermann, J., & Nicholls, R. J. (2015). Future Coastal Population Growth and Exposure to Sea-Level Rise and Coastal Flooding - A Global Assessment. *PLoS ONE, 10*(3), e0118571.10.1371/journal.pone.0118571.

Oorschot, M. v., Kleinhans, M., Geerling, G., & Middelkoop, H. (2016). Distinct patterns of interaction between vegetation and morphodynamics. *Earth Surface Processes and Landforms, 41*(6), 791-808.10.1002/esp.3864.

Partheniades, E. (1965). Erosion and deposition of cohesive soils. *Journal of the Hydraulics Division, 91*(1), 105-139.

Paul, M., & Amos, C. L. (2011). Spatial and seasonal variation in wave attenuation over Zostera noltii. *Journal of Geophysical Research: Oceans, 116*(C8).10.1029/2010JC006797.

Peckham, S. D., Hutton, E. W. H., & Norris, B. (2013). A component-based approach to integrated modeling in the geosciences: The design of CSDMS. *Computers & Geosciences, 53*, 3-12.https://doi.org/10.1016/j.cageo.2012.04.002.

Poppema, D. W., Willemsen, P. W. J. M., de Vries, M. B., Zhu, Z., Borsje, B. W., & Hulscher, S. J. M. H. (2019). Experiment-supported modelling of salt marsh establishment. *Ocean & Coastal Management, 168*, 238-250.https://doi.org/10.1016/j.ocecoaman.2018.10.039.

Pringle , A. W. (1995). Erosion of a cyclic saltmarsh in Morecambe Bay, North-West England. *Earth Surface Processes and Landforms, 20*(5), 387-405.10.1002/esp.3290200502.

Pye, K. (1995). Controls on Long-term Saltmarsh Accretion and Erosion in the Wash, Eastern England. *Journal of coastal Research, 11*(2), 337-356.

Rahman, H., Sherren, K., & van Proosdij, D. (2019). Institutional Innovation for Nature-Based Coastal Adaptation: Lessons from Salt Marsh Restoration in Nova Scotia, Canada. *Sustainability, 11*(23), 6735.

Raju, M. M., Srivastava, R. K., Bisht, D. C. S., Sharma, H. C., & Kumar, A. (2011). Development of Artificial Neural-Network-Based Models for the Simulation of Spring Discharge. *Advances in Artificial Intelligence, 2011*, 686258.10.1155/2011/686258.

Reed, A. S. (2001). Rates and Processes of Marsh Shoreline Erosion in Rehoboth Bay, Delaware, U.S.A. *Journal of coastal Research, 17*(3), 672-683.

Reed, D., van Wesenbeeck, B., Herman, P. M. J., & Meselhe, E. (2018). Tidal flat-wetland systems as flood defenses: Understanding biogeomorphic controls. *Estuarine, Coastal and Shelf Science, 213*, 269-282.https://doi.org/10.1016/j.ecss.2018.08.017.

Riethmüller, R., Heineke, M., Kühl, H., & Keuker-Rüdiger, R. (2000). Chlorophyll *a* concentration as an index of sediment surface stabilisation by microphytobenthos? *Continental Shelf Research, 20*(10), 1351-1372.https://doi.org/10.1016/S0278-4343(00)00027-3.

Ris, R. C., Holthuijsen, L. H., & Booij, N. (1999). A third-generation wave model for coastal regions: 2. Verification. *Journal of Geophysical Research: Oceans, 104*(C4), 7667-7681.10.1029/1998JC900123.

Rodell, M., Houser, P. R., Jambor, U., Gottschalck, J., Mitchell, K., Meng, C.-J.,... Toll, D. (2004). The Global Land Data Assimilation System. *Bulletin of the American Meteorological Society, 85*(3), 381-394.10.1175/bams-85-3-381.

Roelvink, J. A. (2006). Coastal morphodynamic evolution techniques. *Coastal Engineering, 53*(2), 277-287.https://doi.org/10.1016/j.coastaleng.2005.10.015.

Ruessink, G., & Roelvink, J. A. (2000). *Validation of On-line Mud Transport within Delft3DFLOW* (Report).

Rupprecht, F., Möller, I., Evans, B., Spencer, T., & Jensen, K. (2015). Biophysical properties of salt marsh canopies — Quantifying plant stem flexibility and above ground biomass. *Coastal Engineering, 100*, 48-57.https://doi.org/10.1016/j.coastaleng.2015.03.009.

Rupprecht, F., Möller, I., Paul, M., Kudella, M., Spencer, T., van Wesenbeeck, B. K., . . . Schimmels, S. (2017). Vegetation-wave interactions in salt marshes under storm surge conditions. *Ecological Engineering, 100*, 301-315.https://doi.org/10.1016/j.ecoleng.2016.12.030.

Scheres, B., & Schüttrumpf, H. (2019). *Enhancing the Ecological Value of Sea Dikes. Water, 11*(8), 1617.

Schuerch, M., Spencer, T., Temmerman, S., Kirwan, M. L., Wolff, C., Lincke, D., . . . Brown, S. (2018). Future response of global coastal wetlands to sea-level rise. *Nature, 561*(7722), 231-234.10.1038/s41586-018-0476-5.

Schuerch, M., Vafeidis, A., Slawig, T., & Temmerman, S. (2013). Modeling the influence of changing storm patterns on the ability of a salt marsh to keep pace with sea level rise. *Journal of Geophysical Research: Earth Surface, 118*(1), 84-96.10.1029/2012jf002471.

Schwarz, C., Gourgue, O., van Belzen, J., Zhu, Z., Bouma, T. J., van de Koppel, J., . . . Temmerman, S. (2018). Self-organization of a biogeomorphic landscape controlled by plant life-history traits. *Nature Geoscience, 11*(9), 672-677.10.1038/s41561-018-0180-y.

Schwarz, C., Ye, Q. H., van der Wal, D., Zhang, L. Q., Bouma, T., Ysebaert, T., & Herman, P. M. J. (2014). Impacts of salt marsh plants on tidal channel initiation and inheritance. *Journal of Geophysical Research: Earth Surface, 119*(2), 385-400.10.1002/2013jf002900.

Seijffert, J. W., & Philipse, L. (1991). Resistance of Grassmat to Wave Attack. *Coastal Engineering 1990* (pp. 1662-1674).

Shepard, C. C., Crain, C. M., & Beck, M. W. (2011). The Protective Role of Coastal Marshes: A Systematic Review and Meta-analysis. *PLoS ONE, 6*(11), e27374.10.1371/journal.pone.0027374.

Short, A. (1991). Macro-meso tidal beach morphodynamics: an overview. *Journal of coastal Research*, 417-436.

Siemes, R., Borsje, B. W., Daggenvoorde, R., & Hulscher, S. (2020). Artificial Structures Steer Morphological Development of Salt Marshes: A Model Study. *Journal of Marine Science and Engineering, 8*, 326.10.3390/jmse8050326.

Silinski, A., van Belzen, J., Fransen, E., Bouma, T. J., Troch, P., Meire, P., & Temmerman, S. (2016). Quantifying critical conditions for seaward expansion of tidal marshes: A transplantation experiment. *Estuarine, Coastal and Shelf Science, 169*, 227-237.http://dx.doi.org/10.1016/j.ecss.2015.12.012.

Silliman, B. R., van de Koppel, J., McCoy, M. W., Diller, J., Kasozi, G. N., Earl, K., . . . Zimmerman, A. R. (2012). Degradation and resilience in Louisiana salt marshes after the BP–Deepwater Horizon oil spill. *Proceedings of the National Academy of Sciences, 109*(28), 11234.10.1073/pnas.1204922109.

Singh Chauhan, P. P. (2009). Autocyclic erosion in tidal marshes. *Geomorphology, 110*(3), 45-57.https://doi.org/10.1016/j.geomorph.2009.03.016.

Small, C., & Nicholls, R. J. (2003). A global analysis of human settlement in coastal zones. *Journal of coastal Research*, 584-599.

Smith, G. M., Seijffert, J. W. W., & Meer, J. W. v. d. (1995). Erosion and Overtopping of a Grass Dike Large Scale Model Tests. *Coastal Engineering 1994* (pp. 2639-2652).

Smits, A. J. M., Nienhuis, P. H., & Saeijs, H. L. F. (2006). Changing Estuaries, Changing Views. *Hydrobiologia, 565*(1), 339-355.10.1007/s10750-005-1924-4.

Smolders, S., João Teles, M., Leroy, A., Maximova, T., Meire, P., & Temmerman, S. (2020). Modeling Storm Surge Attenuation by an Integrated Nature-Based and Engineered Flood Defense System in the Scheldt Estuary (Belgium). *Journal of Marine Science and Engineering, 8*(1), 27.

Soetaert, K., Petzoldt, T., & Setzer, R. (2010). Solving Differential Equations in R: Package deSolve. *Journal of Statistical Software*, 33.10.18637/jss.v033.i09.

Soulsby, R. (1997). *Dynamics of marine sands: a manual for practical applications*: Thomas Telford.

Spalding, M. D., McIvor, A. L., Beck, M. W., Koch, E. W., Möller, I., Reed, D. J., . . . Woodroffe, C. D. (2014). Coastal Ecosystems: A Critical Element of Risk Reduction. *Conservation Letters, 7*(3), 293-301.10.1111/conl.12074.

Spencer, T., Brooks, S. M., Evans, B. R., Tempest, J. A., & Möller, I. (2015). Southern North Sea storm surge event of 5 December 2013: Water levels, waves and coastal impacts. *Earth-Science Reviews, 146*, 120-145.https://doi.org/10.1016/j.earscirev.2015.04.002.

Spencer, T., Möller, I., Rupprecht, F., Bouma, T. J., van Wesenbeeck, B. K., Kudella, M., ... Schimmels, S. (2016). Salt marsh surface survives true-to-scale simulated storm surges. *Earth Surface Processes and Landforms, 41*(4), 543-552.10.1002/esp.3867.

Staats, N., de Deckere, E. M. G. T., de Winder, B., & Stal, L. J. (2001). Spatial patterns of benthic diatoms, carbohydrates and mud on a tidal flat in the Ems-Dollard estuary. *Hydrobiologia, 448*(1), 107-115.10.1023/a:1017545204214.

Stal, L. J. (2010). Microphytobenthos as a biogeomorphological force in intertidal sediment stabilization. *Ecological Engineering, 36*(2), 236-245.https://doi.org/10.1016/j.ecoleng.2008.12.032.

Suchrow, S., & Jensen, K. (2010). Plant Species Responses to an Elevational Gradient in German North Sea Salt Marshes. *Wetlands, 30*(4), 735-746.10.1007/s13157-010-0073-3.

Suzuki, T., & Arikawa, T. (2010). *Numerical analysis of bulk drag coefficient in dense vegetation by immersed boundary method* (Vol. 1).

Suzuki, T., Zijlema, M., Burger, B., Meijer, M. C., & Narayan, S. (2012). Wave dissipation by vegetation with layer schematization in SWAN. *Coastal Engineering, 59*(1), 64-71. http://dx.doi.org/10.1016/j.coastaleng.2011.07.006.

Syvitski, J. P. M., Kettner, A. J., Overeem, I., Hutton, E. W. H., Hannon, M. T., Brakenridge, G. R., ... Nicholls, R. J. (2009). Sinking deltas due to human activities. Nature Geosci, 2(10), 681-686.http://www.nature.com/ngeo/journal/v2/n10/suppinfo/ngeo629_S1.html.

Taal, M., Meersschaut, Y., & Liek, G. J. (2015). *Understanding the tides crucial for joint management of the Scheldt Estuary*. Paper presented at the IAHR World Congres, The Hague, The Netherlands.

Tambroni, N., & Seminara, G. (2012). A one-dimensional eco-geomorphic model of marsh response to sea level rise: Wind effects, dynamics of the marsh border and equilibrium. *Journal of Geophysical Research: Earth Surface, 117*(F3).10.1029/2012jf002363.

Temmerman, S., Bouma, T. J., Govers, G., Wang, Z. B., De Vries, M. B., & Herman, P. M. J. (2005). Impact of vegetation on flow routing and sedimentation patterns: Three-dimensional modeling for a tidal marsh. *Journal of Geophysical Research: Earth Surface, 110*(F4), F04019.http://dx.doi.org/10.1029/2005JF000301.

Temmerman, S., Bouma, T. J., Van de Koppel, J., Van der Wal, D., De Vries, M. B., & Herman, P. M. J. (2007). Vegetation causes channel erosion in a tidal landscape. *Geology, 35*(7), 631-634.10.1130/g23502a.1.

Temmerman, S., Govers, G., Wartel, S., & Meire, P. (2004). Modelling estuarine variations in tidal marsh sedimentation: response to changing sea level and suspended sediment concentrations. *Marine Geology, 212*(1), 1-19.https://doi.org/10.1016/j.margeo.2004.10.021.

Temmerman, S., Meire, P., Bouma, T. J., Herman, P. M. J., Ysebaert, T., & De Vriend, H. J. (2013). Ecosystem-based coastal defence in the face of global change. *Nature, 504*(7478), 79-83.10.1038/nature12859.

Temmink, R. J. M., Christianen, M. J. A., Fivash, G. S., Angelini, C., Boström, C., Didderen, K., ... van der Heide, T. (2020). Mimicry of emergent traits amplifies coastal restoration success. *Nature Communications, 11*(1), 3668.10.1038/s41467-020-17438-4.

The Royal Netherlands Meteorological Institute (KNMI). (2020). Windrozen van de Nederlandse hoofdstations. Retrieved from https://www.knmi.nl

Thoms, M. C., & Parsons, M. (2002). Eco-geomorphology: an interdisciplinary approach to river science. *International Association of Hydrological Sciences, Publication, 276*, 113-119p.

Tolhurst, T. J., Black, K. S., Shayler, S. A., Mather, S., Black, I., Baker, K., & Paterson, D. M. (1999). Measuring the in situ Erosion Shear Stress of Intertidal Sediments with the Cohesive Strength Meter (CSM). *Estuarine, Coastal and Shelf Science, 49*(2), 281-294. https://doi.org/10.1006/ecss.1999.0512.

Tonelli, M., Fagherazzi, S., & Petti, M. (2010). Modeling wave impact on salt marsh boundaries. *Journal of Geophysical Research: Oceans, 115*(C9).

Torio, D. D., & Chmura, G. L. (2013). Assessing Coastal Squeeze of Tidal Wetlands. *Journal of coastal Research*, 1049-1061.http://dx.doi.org/10.2112/JCOASTRES-D-12-00162.1.

Tsujimoto, T. (1999). Fluvial processes in streams with vegetation. *Journal of Hydraulic Research, 37*(6), 789-803.10.1080/00221689909498512.

Turner, R. E. (2011). Beneath the Salt Marsh Canopy: Loss of Soil Strength with Increasing Nutrient Loads. *Estuaries and Coasts, 34*(5), 1084-1093.10.1007/s12237-010-9341-y.

Turner, R. K., Burgess, D., Hadley, D., Coombes, E., & Jackson, N. (2007). A cost–benefit appraisal of coastal managed realignment policy. *Global Environmental Change, 17*(3), 397-407.https://doi.org/10.1016/j.gloenvcha.2007.05.006.

Valiela, I., Bowen, J. L., & York, J. K. (2001). Mangrove Forests: One of the World's Threatened Major Tropical Environments. *BioScience, 51*(10), 807-815.10.1641/0006-3568(2001)051[0807:mfootw]2.0.co;2.

Van Damme, S., Ysebaert, T., Meire, P., & Van den Berg, E. (1999). *Habitatstructuren, waterkwaliteit en leefgemeenschappen in het Schelde-estuarium* (Report).

van der Wal, D., & Pye, K. (2004). Patterns, rates and possible causes of saltmarsh erosion in the Greater Thames area (UK). *Geomorphology, 61*(3), 373-391.https://doi.org/10.1016/j.geomorph.2004.02.005.

van der Wal, D., Pye, K., & Neal, A. (2002). Long-term morphological change in the Ribble Estuary, northwest England. *Marine Geology, 189*(3), 249-266.https://doi.org/10.1016/S0025-3227(02)00476-0.

Van der Wal, D., Van Dalen, J., Willemsen, P., Borsje, B. W., & Bouma, T. (In preparation). Continuous versus episodic lateral saltmarsh cliff erosion from high resolution SED sensors and terrestrial laser scans.

Van der Wal, D., Wielemaker-Van den Dool, A., & Herman, P. M. J. (2008). Spatial patterns, rates and mechanisms of saltmarsh cycles (Westerschelde, The Netherlands). *Estuarine, Coastal and Shelf Science, 76*(2), 357-368.http://dx.doi.org/10.1016/j.ecss.2007.07.017.

Van Eerden, M. R., Drent, R. H., Stahl, J., & Bakker, J. P. (2005). Connecting seas: western Palaearctic continental flyway for water birds in the perspective of changing land use and climate. *Global Change Biology, 11*(6), 894-908.10.1111/j.1365-2486.2005.00940.x.

van Hulzen, J. B., van Soelen, J., & Bouma, T. J. (2007). Morphological variation and habitat modification are strongly correlated for the autogenic ecosystem engineerSpartina anglica (common cordgrass). *Estuaries and Coasts, 30*(1), 3-11.10.1007/bf02782962.

van Maren, D. S., van Kessel, T., Cronin, K., & Sittoni, L. (2015). The impact of channel deepening and dredging on estuarine sediment concentration. *Continental Shelf Research, 95*, 1-14.https://doi.org/10.1016/j.csr.2014.12.010.

van Wesenbeeck, B. K., Mulder, J. P. M., Marchand, M., Reed, D. J., de Vries, M. B., de Vriend, H. J., & Herman, P. M. J. (2014). Damming deltas: A practice of the past? Towards nature-based flood defenses. *Estuarine, Coastal and Shelf Science, 140*, 1-6. https://doi.org/10.1016/j.ecss.2013.12.031.

Van Wesenbeeck, B. K., Van De Koppel, J., Herman, P. M. J., & Bouma, T. J. (2008). Does scale-dependent feedback explain spatial complexity in salt-marsh ecosystems? *Oikos, 117*(1), 152-159.doi:10.1111/j.2007.0030-1299.16245.x.

Van de Koppel, J., Van der Wal, D., Bakker, J. P., & Herman, P. M. J. (2005). Self-Organization and Vegetation Collapse in Salt Marsh Ecosystems. *The American Naturalist, 165*(1), E1-E12.doi:10.1086/426602.

Viles, H. A. (1988). *Biogeomorphology*. Oxford, UK: Blackwell.

Vrijling, J. K. (2001). Probabilistic design of water defense systems in The Netherlands. *Reliability Engineering & System Safety, 74*(3), 337-344.https://doi.org/10.1016/S0951-8320(01)00082-5.

Vuik, V., Borsje, B. W., Willemsen, P. W. J. M., & Jonkman, S. N. (2019). Salt marshes for flood risk reduction: Quantifying long-term effectiveness and life-cycle costs. *Ocean & Coastal Management, 171*, 96-110.https://doi.org/10.1016/j.ocecoaman.2019.01.010.

Vuik, V., Jonkman, S. N., Borsje, B. W., & Suzuki, T. (2016). Nature-based flood protection: The efficiency of vegetated foreshores for reducing wave loads on coastal dikes. *Coastal Engineering, 116*, 42-56.http://dx.doi.org/10.1016/j.coastaleng.2016.06.001.

Vuik, V., Suh Heo, H. Y., Zhu, Z., Borsje, B. W., & Jonkman, S. N. (2018a). Stem breakage of salt marsh vegetation under wave forcing: A field and model study. *Estuarine, Coastal and Shelf Science, 200*, 41-58.https://doi.org/10.1016/j.ecss.2017.09.028.

Vuik, V., van Vuren, S., Borsje, B. W., van Wesenbeeck, B. K., & Jonkman, S. N. (2018b). Assessing safety of nature-based flood defenses: Dealing with extremes and uncertainties. *Coastal Engineering, 139*, 47-64.https://doi.org/10.1016/j.coastaleng.2018.05.002.

Walters, B. B., Rönnbäck, P., Kovacs, J. M., Crona, B., Hussain, S. A., Badola, R., ... Dahdouh-Guebas, F. (2008). Ethnobiology, socio-economics and management of mangrove forests: A review. *Aquatic Botany, 89*(2), 220-236.https://doi.org/10.1016/j.aquabot.2008.02.009.

Wamsley, T. V., Cialone, M. A., Smith, J. M., Atkinson, J. H., & Rosati, J. D. (2010). The potential of wetlands in reducing storm surge. *Ocean Engineering, 37*(1), 59-68. https://doi.org/10.1016/j.oceaneng.2009.07.018.

Wang, H., van der Wal, D., Li, X., van Belzen, J., Herman, P. M. J., Hu, Z., ... Bouma, T. J. (2017). Zooming in and out: Scale dependence of extrinsic and intrinsic factors affecting salt marsh erosion. *Journal of Geophysical Research: Earth Surface, 122*(7), 1455-1470.10.1002/2016JF004193.

Watts, C. W., Tolhurst, T. J., Black, K. S., & Whitmore, A. P. (2003). In situ measurements of erosion shear stress and geotechnical shear strength of the intertidal sediments of the experimental managed realignment scheme at Tollesbury, Essex, UK. *Estuarine, Coastal and Shelf Science, 58*(3), 611-620.https://doi.org/10.1016/S0272-7714(03)00139-2.

Weatherall, P., Marks, K. M., Jakobsson, M., Schmitt, T., Tani, S., Arndt, J. E., ... Wigley, R. (2015). A new digital bathymetric model of the world's oceans. *Earth and Space Science, 2*(8), 331-345.10.1002/2015ea000107.

Whelchel, A. W., Reguero, B. G., van Wesenbeeck, B., & Renaud, F. G. (2018). Advancing disaster risk reduction through the integration of science, design, and policy into eco-engineering and several global resource management processes. *International Journal of Disaster Risk Reduction*. https://doi.org/10.1016/j.ijdrr.2018.02.030.

Wiberg, P. L., Fagherazzi, S., & Kirwan, M. L. (2020). Improving Predictions of Salt Marsh Evolution Through Better Integration of Data and Models. *Annual Review of Marine Science, 12*(1), 389-413.10.1146/annurev-marine-010419-010610.

Widdows, J., Blauw, A., Heip, C., Herman, P., Lucas, C., Middelburg, J., . . . Verbeek, H. (2004). Role of physical and biological processes in sediment dynamics of a tidal flat in Westerschelde Estuary, SW Netherlands. *Marine Ecology Progress Series, 274*, 41-56.

Widdows, J., & Brinsley, M. (2002). Impact of biotic and abiotic processes on sediment dynamics and the consequences to the structure and functioning of the intertidal zone. *Journal of Sea Research, 48*(2), 143-156.https://doi.org/10.1016/S1385-1101(02)00148-X.

Wiegman, N., Perluka, R., Oude Elberink, S., & Vogelzang, J. (2005). *Vaklodingen: de inwintechnieken en hun combinaties. Vergelijking tussen verschillende inwintechnieken en de combinaties ervan* (Report).

Willemsen, P. W. J. M., Borsje, B. W., Hulscher, S. J. M. H., Van der Wal, D., Zhu, Z., Oteman, B., ... Bouma, T. J. (2018). Quantifying Bed Level Change at the Transition of Tidal Flat and Salt Marsh: Can We Understand the Lateral Location of the Marsh Edge? *Journal of Geophysical Research: Earth Surface, 123*(10), 2509-2524. doi:10.1029/2018JF004742.

Willemsen, P. W. J. M., Borsje, B. W., Vuik, V., Bouma, T. J., & Hulscher, S. J. M. H. (2020). Field-based decadal wave attenuating capacity of combined tidal flats and salt marshes. *Coastal Engineering, 156*, 103628.https://doi.org/10.1016/j.coastaleng.2019.103628.

Willemsen, P. W. J. M., Horstman, E. M., Borsje, B. W., Friess, D. A., & Dohmen-Janssen, C. M. (2016). Sensitivity of the sediment trapping capacity of an estuarine mangrove forest. *Geomorphology, 273*, 189-201.https://doi.org/10.1016/j.geomorph.2016.07.038.

Willemsen, P. W. J. M., Smits, B. P., Borsje, B. W., Herman, P. M. J., Dijkstra, J. T., Bouma, T. J., & Hulscher, S. J. M. H. (submitted). Modelling biophysical response of decadal salt marsh development.

Williams, R. D., Brasington, J., & Hicks, D. M. (2016). Numerical Modelling of Braided River Morphodynamics: Review and Future Challenges. *Geography Compass, 10*(3), 102-127.10.1111/gec3.12260.

Yang, S.-l., Ding, P.-x., & Chen, S.-l. (2001). Changes in progradation rate of the tidal flats at the mouth of the Changjiang (Yangtze) River, China. *Geomorphology, 38*(1), 167-180.https://doi.org/10.1016/S0169-555X(00)00079-9.

Yang, S. L., Shi, B. W., Bouma, T. J., Ysebaert, T., & Luo, X. X. (2012). Wave Attenuation at a Salt Marsh Margin: A Case Study of an Exposed Coast on the Yangtze Estuary. *Estuaries and Coasts, 35*(1), 169-182.10.1007/s12237-011-9424-4.

Zhang, K., Liu, H., Li, Y., Xu, H., Shen, J., Rhome, J., & Smith III, T. J. (2012). The role of mangroves in attenuating storm surges. *Estuarine, Coastal and Shelf Science, 102*, 11-23.

Zhang, R. S., Shen, Y. M., Lu, L. Y., Yan, S. G., Wang, Y. H., Li, J. L., & Zhang, Z. L. (2004). Formation of Spartina alterniflora salt marshes on the coast of Jiangsu Province, China. *Ecological Engineering, 23*(2), 95-105.https://doi.org/10.1016/j.ecoleng.2004.07.007.

Zhou, Z., Yang, Y., & Chen, B. (2018). Estimating Spartina alterniflora fractional vegetation cover and aboveground biomass in a coastal wetland using SPOT6 satellite and UAV data. *Aquatic Botany, 144*, 38-45.https://doi.org/10.1016/j.aquabot.2017.10.004.

Zhu, Z., van Belzen, J., Zhu, Q., van de Koppel, J., & Bouma, T. J. (2020a). Vegetation recovery on neighboring tidal flats forms an Achilles' heel of saltmarsh resilience to sea level rise. *Limnology and Oceanography, 65*(1), 51-62.10.1002/lno.11249.

Zhu, Z., Vuik, V., Visser, P. J., Soens, T., van Wesenbeeck, B., van de Koppel, J., ... Bouma, T. J. (2020b). Historic storms and the hidden value of coastal wetlands for nature-based flood defence. *Nature Sustainability*.10.1038/s41893-020-0556-z.

Zhu, Z., Yang, Z., & Bouma, T. J. (2019). Biomechanical properties of marsh vegetation in space and time: effects of salinity, inundation and seasonality. *Annals of Botany*.10.1093/aob/mcz063.

Publications

Peer-reviewed journal papers

1 **Willemsen, P.W.J.M.**, Smits, B.P., Borsje, B.W., Herman, P.M.J., Dijkstra, J.T., Bouma, T.J., Hulscher, S.J.M.H. (submitted). Modelling decadal salt marsh development: variability of the salt marsh extent under influence of waves and sediment availability.

2 Hu, Z., **Willemsen, P.W.J.M.**, Borsje, B.W., Wang, C., Wang, H., Van der Wal, D., Zhu, Z., Oteman, B., Vuik, V., Evans, B., Möller., I., Belliard, J-P., Van Braeckel, A., Temmerman, S., Bouma ,T.J. (2020). Synchronized high-resolution bed-level change and biophysical data from ten marsh-mudflat sites in northwestern Europe. *Earth System Science Data*,. https://doi.org/10.5194/essd-2020-78

3 **Willemsen, P.W.J.M.**, Borsje, B.W., Vuik, V., Bouma, T.J., Hulscher, S.J.M.H. (2020). Field-based decadal wave attenuating capacity of combined tidal flats and salt marshes. *Coastal Engineering, 156*. https://doi.org/10.1016/j.coastaleng.2019.103628

4 Vuik, V., Borsje, B.W., **Willemsen, P.W.J.M.**, Jonkman, S.N. (2019). Salt marshes for flood risk reduction: Quantifying long-term effectiveness and life-cycle costs. *Ocean and Coastal Management, 171*, 96-110. https://doi.org/10.1016/j.ocecoaman.2019.01.010

5 Baptist, M.J., Gerkema, T., Van Prooijen, B.C., Van Maren, D.S., Van Regteren, M., Schulz, K., Colosimo, I., Vroom, J., Van Kessel, T., Grasmeijer, B., **Willemsen, P.**, Elschot, K., de Groot, A.V., Cleveringa, J., Van Eekelen, E.M.M., Schuurman, F., De Lange, H.J., Van Puijenbroek, M.E.B. (2019). Beneficial use of dredged sediment to enhance salt marsh development by applying a 'Mud Motor'. *Ecological Engineering, 127*, 312-323. https://doi.org/10.1016/j.ecoleng.2018.11.019

6 Poppema, D.W., **Willemsen, P.W.J.M.**, de Vries, M.B., Zhu, Z., Borsje, B.W., & Hulscher, S.J. (2019). Experiment-supported modelling of salt marsh establishment. *Ocean & Coastal Management, 168*, 238-250. https://doi.org/10.1016/j.ocecoaman.2018.10.039

7 Taillardat, P., **Willemsen, P.W.J.M.**, Marchand, C., Friess, D.A., Widory, D., Baudron, P., Truong, V.V., NguyEn, T-N., Ziegler, A.D. (2018). Assessing the contribution of porewater discharge in carbon export and CO2 evasion in a mangrove tidal creek (Can Gio, Vietnam). *Journal of hydrology, 563*, 303-318. https://doi.org/10.1016/j.jhydrol.2018.05.042

8 Best, Ü.S.N., Van der Wegen, M., Dijkstra, J., **Willemsen, P.W.J.M.**, Borsje, B.W., & Roelvink, D.J.A. (2018). Do salt marshes survive sea level rise? Modelling wave action, morphodynamics and vegetation dynamics. *Environmental modelling & software, 109*, 152-166. https://doi.org/10.1016/j.envsoft.2018.08.004

9 **Willemsen, P.W.J.M.**, Borsje, B.W., Hulscher, S.J.M.H., Van Der Wal, D., Zhu, Z., Oteman, B., Evans, B., Möller, I., Bouma, T. J. (2018). Quantifying Bed Level Change at the Transition of Tidal Flat and Salt Marsh: Can We Understand the Lateral Location of the Marsh Edge? *Journal of geophysical research. Earth surface, 123*, 2509–2524. https://doi.org/10.1029/2018JF004742

10 **Willemsen, P.W.J.M.**, Horstman, E.M., Borsje, B.W., Fries, D.A., Dohmen-Janssen, C.M., 2016. Sensitivity of the sediment trapping capacity of an estuarine mangrove forest. *Geomorphology, 273*, pp 189-201. https://doi.org/10.1016/j.geomorph.2016.07.038

Professional articles

1 De Vries, B., Van Puijenbroek, M., **Willemsen, P.W.J.M.**, Coumou, L., Dankers, P.. (2020). Proeftuin voor ontwikkeling kwelder voor de kust van Delfzijl. *Land + Water*, Juli 2020.

2 Vuik, V., Jonkman, S.N., **Willemsen, P.W.J.M.**, Borsje, B.W., Janssen, S.K.H., Hermans, L.M., Bouma, T.J. (2019). Voorlanden voor hoogwaterbescherming. *H2O: tijdschrift voor watervoorziening en waterbeheer*, September 2019.

3 Poppema, D., **Willemsen, P.W.J.M.**, Borsje, B.W., De Vries, M., Zhu, Z., Dankers, P., Hulscher, S.J.M.H. (2018). Naar een grondiger begrip van vegetatievestiging. *H2O: tijdschrift voor watervoorziening en waterbeheer*, Januari 2018.

Conference abstracts and presentations

1. Hendriks, M., Dankers, P., Cleveringa, J., Sittoni, L., **Willemsen, P.W.J.M.**, Elschot, K., Van Puijenbroek, M., Baptist, M.J. (2020). A large-scale field experiment on salt marsh construction. NCK-days 2020.

2 Baptist, M.J., Dankers, P., Cleveringa, J., Sittoni, L., **Willemsen, P.W.J.M.**, Elschot, K., Van Puijenbroek, M.E.B., Hendriks, M. (2019). A large-scale field experiment on salt marsh construction in the Ems estuary, the Netherlands. 95-95 11th River, Coastal and Estuarine Morphodynamics Symposium, RCEM 2019, Auckland, New Zealand.

3 **Willemsen, P.W.J.M.**, Borsje, B.W., Vuik, V., Bouma, T.J., & Hulscher, S. J. (2019). Decadal wave attenuating capacity of foreshores under extreme wave conditions. AGU Fall Meeting 2019, San Francisco, USA. *Oral presentation*.

4 Smits, B., **Willemsen, P.W.J.M.**, Odink, S.J., Borsje, B.W., Hulscher, S.J.M.H., Dijkstra, J.T., & Herman, P.M. (2019). Process-Based Biogeomorphologic Modelling of the Establishment and Survival of Salt Marshes Under Changing Abiotic Conditions. AGU Fall Meeting 2019, San Francisco, USA.

5 Borsje, B., **Willemsen, P.W.J.M.**, & Hulscher, S. (2018). Vegetated foreshores as coastal protection strategy: coping with uncertainties and implementation. *Coastal Engineering Proceedings, 1*(36), 7. ICCE 2018, Baltimore USA.

6 **Willemsen, P.W.J.M.**, Borsje, B.W., Bouma, T., & Hulscher, S.J.M.H. (2018). The salt marsh/mudflat transition - All about stress. NCK symposium Hydro-morphodynamic research in the Western Scheldt estuary, Delft, Netherlands. *Oral presentation.*

7 **Willemsen, P.W.J.M.**, Borsje, B.W., Bouma, T., Hu, Z., & Hulscher, S.J.M.H. (2018). Modelling bio-physical processes for long-term tidal mudflat dynamics. *ECSA 57*, Perth, Australia. *Oral presentation*.

8 **Willemsen, P.W.J.M.**, Borsje, B.W., Bouma, T.J., Hu, Z., & Hulscher, S.J.M.H. (2018). Seasonal wind and biota drive tidal mudflat dynamics. 83-83. NCK-Days 2018, Haarlem, Netherlands. *Poster presentation*.

9 **Willemsen, P.W.J.M.**, Borsje, B.W., Bouma, T.J., Van der Wal, D., Hulscher, S.J.M.H. (2017). Assessing salt marsh stability for flood risk reduction: characterizing salt-marsh mudflat transitions. CERF 2017, Providence, Rhode Island, USA. *Oral presentation*.

10 **Willemsen, P.W.J.M.**, Borsje, B.W., Zhu, Z., Otemans, B., Van der Wal, D., Bouma, T.J., Hulscher, S.J.M.H., 2017. Seasonality in morphological behaviour at the interface of salt marshes and tidal flats using high temporal resolution field data. NCK-days 2017, Den Helder, The Netherlands, 35. *Oral presentation*.

11 Best, U.S.N., Van der Wegen, M., Dijkstra, J., Borsje, B.W., Roelvink, D., **Willemsen, P.W.J.M.** (2017). Modelling sea level rise impact on salt marsh/mangrove-mudflat morphodynamics. NCK-days 2017, Den Helder, The Netherlands.

12 **Willemsen, P.W.J.M.**, Borsje, B.W., Bouma, T.J., Hulscher, S.J.M.H., 2016. Long-term landscape evolution of the coupled system of vegetated marshes and bare intertidal flats explained by hydrodynamic and ecological field data. ECSA 56, Bremen, Germany. *Oral presentation*.

13 **Willemsen, P.W.J.M.**, Borsje, B.W., Vuik, V., Janssen, S.K.H., Bouma, T.J., Hulscher, S.J.M.H., 2016. Long-term biogeomorphological behavior of coupled bare intertidal flats and vegetated foreshores. NCK-days 2016, Ouddorp, The Netherlands. *Poster presentation*.

14 **Willemsen, P.W.J.M.**, Vermaas, T., Hulscher, S.J.M.H., 2014. Morphological development of the Ameland inlet/Boschplaat in the Dutch Wadden Sea. NCK-Days 2014, Delft, The Netherlands, 78. *Poster presentation*.

Datasets

1 Hu, Z., **Willemsen, P.W.J.M.**, Borsje, B.W., Wang, C., Wang, H., Van der Wal, D., Zhu, Z., Oteman, B.F., Vuik, V., Evans, B., Möller, I., Belliard, J., van Braeckel, A., Temmerman, S., Bouma, T.J. (2020). High resolution bed level change and synchronized biophysical data from 10 tidal flats in northwestern Europe. *4TU.Centre for Research Data*. https://doi.org/10.4121/uuid:4830dbc2-84b8-46f9-99a3-90f01ab5b923

2 **Willemsen, P.W.J.M.**, Borsje, B.W., Vuik, V., Bouma, T.J., Hulscher, S.J.M.H. (2020). Data presented in the paper: "Field-based decadal wave attenuating capacity of combined tidal flats and salt marshes". *4TU.Centre for Research Data*. https://doi.org/10.4121/uuid:4c25347f-f71e-466b-be3c-1fe8f8d8784c

3 **Willemsen, P.W.J.M.**, Borsje, B.W., Hulscher, S.J.M.H., Van der Wal, D., Zhu, Z., Evans, B., Bouma, T., Möller, I. (2018). Data presented in the paper "Quantifying bed level change at the transition of tidal flat and salt marsh: can we understand the lateral location of the marsh edge?". *4TU.Centre for Research Data*. https://doi.org/10.4121/uuid:c0be318c-9858-4a05-a546-782e29b4abef

Awards

1 NCK research movie prize: BE-SAFE movie (2019)

2 Top downloaded paper 2018-2019: Quantifying Bed Level Change at the Transition of Tidal Flat and Salt Marsh: Can We Understand the Lateral Location of the Marsh Edge? On of the most read in Journal of Geophysical Research: Earth Surface (2019)

3 De Breed Kreiken Innovatiebeurs (2016)

About the author

Pim Willemsen was born in Zevenaar, the Netherlands, on April 7th 1991. After moving to Enschede, Pim entered the Civil Engineering program at the University of Twente in 2010. He obtained his Bachelor's degree in 2013 and Master's degree in 2015. The latter was obtained with a Master's thesis on the topic: sensitivity of the sediment trapping capacity of an estuarine mangrove forest, a combined field observational and numerical modelling study. He then joined the Marine & Fluvial Systems group of the University of Twente and the department of Estuarine & Delta Systems at NIOZ to pursue his PhD degree. His PhD research was part of the larger BE SAFE consortium (NWO): Bio-Engineering for Safety using vegetated foreshores. This multi-disciplinary research combined ecology, biogeomorphology, safety and governance. His doctoral thesis was focused on biogeomorphological dynamics of salt marshes and how these dynamics affect the contribution of salt marshes to flood defense. Besides working on his doctoral thesis, Pim was employed by Deltares as researcher/consultant from 2016. At Deltares, he aimed at combining knowledge from research in more applied projects, such as the Slibmotor near Koehoal and the Marconi salt marsh in Delfzijl. In the past 5 years, Pim collaborated with many researchers on dynamics in salt marshes and mangroves: on field observations in mangroves in Singapore and Vietnam with researchers from the National University of Singapore and Vietnam National University Ho Chi Minh City and on observations in salt marshes with researchers from Sun Yat-sen University. He also visited the NEPF Environmental fluid mechanics lab at MIT. Moreover, part of his PhD work was in collaboration with Deltares. He was also actively involved in education in several MSc courses of the Water Engineering and Management department. He also supervised nine MSc graduation projects, of which some results were published in journal papers, professional papers and presented at international conferences. Following his PhD defense in January 2020, Pim will continue to work as a researcher at the University of Twente and researcher/consultant at Deltares.